

# University of Wollongong - Research Online

## Thesis Collection

Title: Development and characterisation of polyaniline - carbon nanotube conducting composite fibres

Author: Vahid Mottaghitalab

Year: 2006

Repository DOI:

### Copyright Warning

You may print or download ONE copy of this document for the purpose of your own research or study. The University does not authorise you to copy, communicate or otherwise make available electronically to any other person any copyright material contained on this site.

You are reminded of the following: This work is copyright. Apart from any use permitted under the Copyright Act 1968, no part of this work may be reproduced by any process, nor may any other exclusive right be exercised, without the permission of the author. Copyright owners are entitled to take legal action against persons who infringe their copyright. A reproduction of material that is protected by copyright may be a copyright infringement. A court may impose penalties and award damages in relation to offences and infringements relating to copyright material.

Higher penalties may apply, and higher damages may be awarded, for offences and infringements involving the conversion of material into digital or electronic form.

**Unless otherwise indicated, the views expressed in this thesis are those of the author and do not necessarily represent the views of the University of Wollongong.**

Research Online is the open access repository for the University of Wollongong. For further information contact the UOW Library: [research-pubs@uow.edu.au](mailto:research-pubs@uow.edu.au)

*University of Wollongong Thesis Collections*

*University of Wollongong Thesis Collection*

---

*University of Wollongong*

*Year 2006*

---

Development and characterisation of  
polyaniline - carbon nanotube conducting  
composite fibres

Vahid Mottaghitalab  
University of Wollongong

Mottaghitalab, Vahid, Development and characterisation of polyaniline - carbon nanotube conducting composite fibres, PhD thesis, School of Mechanical, Materials and Mechatronic Engineering, University of Wollongong, 2006. <http://ro.uow.edu.au/theses/491>

This paper is posted at Research Online.

<http://ro.uow.edu.au/theses/491>

## **NOTE**

This online version of the thesis may have different page formatting and pagination from the paper copy held in the University of Wollongong Library.

## **UNIVERSITY OF WOLLONGONG**

### **COPYRIGHT WARNING**

You may print or download ONE copy of this document for the purpose of your own research or study. The University does not authorise you to copy, communicate or otherwise make available electronically to any other person any copyright material contained on this site. You are reminded of the following:

Copyright owners are entitled to take legal action against persons who infringe their copyright. A reproduction of material that is protected by copyright may be a copyright infringement. A court may impose penalties and award damages in relation to offences and infringements relating to copyright material. Higher penalties may apply, and higher damages may be awarded, for offences and infringements involving the conversion of material into digital or electronic form.

**DEVELOPMENT AND CHARACTERISATION OF  
POLYANILINE - CARBON NANOTUBE CONDUCTING  
COMPOSITE FIBRES**

A thesis submitted in fulfillment of the  
requirements for the award of the degree

**DOCTOR OF PHILOSOPHY**

From

**UNIVERSITY OF WOLLONGONG**



by

**VAHID MOTTAGHITALAB**

**(B.Sc. Chemical Engineering; M.Sc. Polymer Engineering)**

**School of Material, Mechanical and Mechatronic Engineering**

JUNE 2006



*IN THE NAME OF ALLAH, THE MOST GRACIOUS, THE MOST MERCIFUL*

*This thesis is dedicated to:*

*My wife: Mahin*

*My son: Amir Reza*

*For their love, support and patience  
and my Mother for her encouragement,  
especially in memory of my father  
and*

*To My Brothers*

## THESIS CERTIFICATION

---

I, Vahid Mottaghitalab, declare that this thesis, submitted in fulfillment of the requirements for the award of Doctor of Philosophy, in the School of Material, Mechanical and Mechatronic Engineering, Faculty of Engineering, University of Wollongong, is wholly my own work unless otherwise referenced or acknowledged. The thesis was completed under the supervision of Prof. Geoffery. M. Spinks and Prof. Gordon. G. Wallace and has not been submitted for qualification at any other academic institution.

Vahid Mottaghitalab

JUNE 2006

## ACKNOWLEDGMENTS

---

The author would like to express his sincere gratitude to Prof. Geoffery. M. Spinks for his supervision, encouragement, guidance and inspiration provided during the course of this research. I would also like to express my sincere thanks to Prof. Gordon. G. Wallace for his advice, encouragement and critical review of several aspects of this study and providing the necessary facilities.

The author also wishes to express his sincere thanks for helpful contributions made by the following professionals during the period of this study:

Dr Peter Innis for his very helpful technical collaboration, Dr Chee O Too for supportive role in preparation of experimental requirement and safety , Dr Syed Ashraf for synthesis of exclusive ionic liquids, Dr Phil Whitten for his impressive comments and suggestions.

I also deeply appreciate from Dr Simon Moulton and Dr Violteta Misoska helpful assistance in electron microscopy.

I also gratefully acknowledge helpful assistance of the students at the Intelligent Polymer Research Institute, Scott Mc Govern, Dr George Tsekouras, Yanzhe Wu and Dr Binbin Xi who always enthusiastically shared their excellent ideas and allocated valuable time for removing of obstacles.

Special thanks also to Mehrdad Bahrami for running of actuation tests and Dr C.Y .Wang for achievement of the experiment in battery tests. I would like to address the administrative help and support of Phil Smugreski.

I also would like to thank academic staff in the School of Materials, Mechanical and Mechatronic Engineering, especially Chris Lukey and David Wexler for their laboratory

assistance and also, Nick Mackie and Greg Tillman for their kind assistance in electron microscopy .

The author also would like to appreciate Mr Steve Cooper and Mr Peter Sarah in science workshop who their enthusiasm for assisting of students was enormous.

The author wishes to thank Dr Saied Sotanian and Dr Jossip Hovart for their contributions in transport measurement tests. The assistance provided by the Faculty of Engineering, University of Wollongong is also appreciated.

I would also like to acknowledge with sincere appreciation, the financial support of the Ministry of Science, Research and Technology of the Islamic Republic of Iran and University of Guilan.

Most importantly, I would like to express my deepest thanks to me and my wife parents and members of our family in IRAN who have provided continued support throughout this study and indeed for our my entire life. This study would not have been finished without support, encouragement of my wife and son.

## **PUBLICATIONS**

---

### **Published Paper:**

1. **V. Mottaghitalab**, G. M. Spinks and G. G. Wallace, The influence of carbon nanotubes on mechanical and electrical properties of polyaniline fibres, Synthetic Metals, 152, **(2005)**, 77-80.
2. G. M. Spinks, **V. Mottaghitalab**, M. Bahrami-Samani, P. G. Whitten and G. G. Wallace, Carbon Nanotube Reinforced Polyaniline Composite Fibres for High Strength Artificial Muscles, Advanced Materials, 18, (2006), 637.

### **In Press**

1. **V. Mottaghitalab**, B. Xi, G. M. Spinks and G. G. Wallace, Polyaniline Fibres Containing Single Walled Carbon Nanotubes: Enhanced Performance Artificial Muscles, Synthetic. Metals. **(2006)**.
2. **V. Mottaghitalab**, G. M. Spinks and G. G. Wallace, The development and characterization of polyaniline - single walled nanotube composite fibres using 2-acrylamido-2 methyl -1-propane sulfonic acid (AMPSA) through one step wet spinning process, Polymer, **(2006)**.

### **Submitted to Journals:**

1. C. Y. Wang, **V. Mottaghitalab**, C. O. Too, G. M. Spinks and G. G. Wallace, Investigation of Polyaniline fibre as battery material in ionic liquid, Journal of power source, **(2006)**.

3. B. Xi, V.T. Truong, **V. Mottaghitalab**, P. Whitten, G. M. Spinks, G. G. Wallace, “ Actuation behavior of polyaniline films and tubes prepared by the phase inversion technique”, Submitted , Smart Mater. and Struct.(2005)

### **Conference papers:**

1. **V. Mottaghitalab**, B. Xi, G. M. Spinks and G. G. Wallace, “The influence of carbon nanotubes on mechanical, electrical and electrochemical properties of polyaniline fibre”, ICSM, Wollongong, Australia, **2004**, Session: Electronic Fibres and Other Unconventional Substrates.
2. **V. Mottaghitalab**, B. Xi, G. M. Spinks and G. G. Wallace, Polyaniline-single wall nanotube composite fibre: opportunities and challenges, Umist, Manchester, UK, **(2004)**, session 7a-Nanostructured fibres I.
3. **V. Mottaghitalab**, G. M. Spinks and G. G. Wallace, A. R. Wilson, Polyaniline-nanotube multifunctional fibre: capabilities toward the manufacturing of smart fabric, 5648, SPIE, Sydney, Australia, **(2004)**.385-396.
4. G. M. Spinks, **V. Mottaghitalab**, Binbin Xi, P. Whitten, G. Wallace, S. J. Kim, S. R. Shin and S. I. Kim, Carbon Nanotube Reinforcement of Conducting Polymers and Hydrogels for High Strength Actuators, MRS Fall Meeting, W6.2/V7.2, Boston , MA ,USA, **(2005)**.
5. G. Spinks, B. Xi, T. Campbell, P. Whitten, **V. Mottaghitalab**, M. Bahrami Samani and G. G. Wallace, In pursuit of high-force/high-stroke conducting polymer actuators (Invited Paper), Proceedings of SPIE-The International Society for Optical Engineering, 5759,(2005), 314-321.

6. G. G. Wallace, **V. Mottaghitalab**, S. E. Moulton and a. G. M. Spinks., Synthesis and properties of organic, electronically conducting fibres: a platform for electronic textiles, Fr C3.2, Queenstown, New Zealand, **(2005)**.
8. B. Xi, V.-T. Truong, **V. Mottaghitalab**, P. Whitten, G. M. Spinks and G. G. Wallace, Ed: S. F. Al-Sarawi, Actuation behaviour of polyaniline films and tubes prepared by phase inversion technique, 5649, SPIE, Sydney, Australia, **(2005)**.436-444.

**Manuscript in preparation:**

1. **Vahid Mottaghitalab**, Philip G. Whitten, Geoffrey M. Spinks and Gordon G. Wallace , Nanotube orientation and load transfer in Polyaniline /Single Walled Carbon Nanotube Composite Fibre
2. **V. Mottaghitalab**, B. Xi, G. M. Spinks and G. G. Wallace, The study of electrical behavior of PANi- AMPSA fibre filled with CNTs: the enhanced metallic transport,

## ABSTRACT

---

The present study describes methods for development and characterization of conducting electroactive polymer (CEP) fibre consisting of polyaniline (PAni) and single walled carbon nanotubes (SWNTs) which have potential applications as electronic devices to form building blocks of electronic textiles. The conducting composite fibres of PAni-SWNT were developed respectively using two steps (acid doping after fibre spinning) and one step methods (doping during preparation of spinning solution). The effectiveness of nanotube inclusion for improvement of mechanical, electrical and electrochemical properties was studied in each method. During development of the fibres, techniques such as UV-Vis-NIR, Raman spectroscopy, Dynamic light scattering and viscometry were used to characterise the quality of dispersion and spinning solutions. It has been shown that the N,N'-dimethyl propylene urea (DMPU) and dichloro acetic acid (DCAA) as solvents respectively for PAni in base and salt form are able to effectively disperse the pristine SWNTs to reach percolation level. The addition of nanotubes changes the rheological behavior of neat PAni spinning solution from a Newtonian to non-Newtonian shear thinning fluid based on power law regime which reflects nanotube-nanotube and/or nanotube-polymer physical entanglement. Several techniques including DMA, DSC, SEM, TEM, FIB, Raman spectroscopy, CV and four point probe electrical conductivity measurement were employed to characterize the various properties of the solid fibre. In both, one step or two steps methods, fibres containing SWNTs have superior tensile strength and elastic modulus compared with neat PAni fibre. The inclusion of SWNTs to PAni, however, decreases the elongation at break. These outcomes directly can be



attributed to physical and/or chemical interfacial interaction between well distributed SWNTs bundles and the PANi matrix. The addition of nanotubes to the PANi matrix also increases the electrical conductivity and enhances the electrochemical redox process. However, the two step method was found to have some problem include low spinning rate, low flexibility and low conductivity and insufficient charge transfer along the fibre to be working electrode. These disadvantages were diminished by faster spinning of PANi-ES/2-acrylamido-2 methyl -1-propane sulfonic acid (AMPSA)/SWNT using the one step process with more than 5 times stretching ratio. An electronic conductivity percolation threshold of  $\sim 0.35$  % w/w SWNTs was determined with fibres possessing electronic conductivity up to  $\sim 750 \text{ Scm}^{-1}$ . The well defined electrochemical window for neat PANi-ES/AMPSA fibre and its composite containing SWNT either in aqueous or ionic liquid electrolyte, with wider electrochemical window, confirms the ease of charge transport through a new conduction path for the fibre formed from salt structure, which was enhanced by addition of nanotubes. The ultimate tensile strength, elastic modulus and elongation at break of PANi-ES/AMPSA/SWNT fibres containing 0.76 % w/w nanotubes respectively were obtained  $255 \pm 32 \text{ Mpa}$ ,  $7.3 \pm 0.4 \text{ GPa}$  and  $4 \pm 1$  % compared with  $170 \pm 22 \text{ MPa}$ ,  $3.4 \pm 0.4 \text{ GPa}$  and  $9 \pm 3$  % for PANi-ES/AMPSA fibre. The quantitative analysis of nanotube orientation and detection of load transfer from matrix to nanotubes were investigated in PANi-ES/AMPSA/SWNT composite fibre using Raman spectroscopy. It has been found that thermal stretching of as spun fibre mostly orients the nanotubes in a range of about  $\pm 30^\circ$  versus fibre axis which extremely increase the Herman orientation factor from 0.02 for as spun fibre to 0.43 for the 5x drawn fibre. Moderate orientation and Raman shift about  $90\text{-}130 \text{ cm}^{-1}$  in D\* band of SWNT also can

be correlated to effective but not perfect load transfer between PANi matrix and nanotubes. The result of temperature dependent electrical conductivity data was shown that the higher conductivity of PANi-ES/AMPSA/SWNT composite fibre compared to neat PANi-ES/AMPSA fibre also can be described by improvement of the metallic property in the crystalline areas and boosting of the metallic disorder contribution in amorphous area. The consequence of improvement of mechanical, electrical and electrochemical properties were a benefit for applying of PANi/ES-AMPSA fibre and its composite having SWNT in applications as actuator, power source and sensor. While the fibres showed great promise as actuators, their response as batteries and temperature/humidity sensors was limited. The significant improvement was observed in actuator strength in excess of 100 MPa and work-per-cycle of over 300 kJ/m<sup>3</sup> through the incorporation of small amounts of SWNTs as reinforcement in the PANi matrix. This performance is 3 times higher than previously produced conducting polymer actuators and exceeds skeletal muscle in terms of stress generation by 300 times. PANi-ES/AMPSA/SWNT exhibited a higher charge/discharge capacity (12.4/11.2 mAhg<sup>-1</sup>) compared with the neat PANi-ES/AMPSA (4.5/4.1 mAhg<sup>-1</sup>). All the results show that solid polyaniline fibre can be used directly as electrode in ionic liquid of EMI.TFSI for wearable power source system. However its current performance is still well below conventional rechargeable battery systems. PANi fibre and its SWNT composite showed a nonlinear response with some delay to temperature signals. The PANi fibre incorporated with SWNTs showed lower sensitivity to change in humidity pulse compared with neat PANi fibre. This behavior has good opportunity for application in conducting yarn that

needs the lowest variability in conductivity for transferring of electrical signal but clearly is not favored for sensing of humidity.

## Abbreviations

Ch	Chiral vector
MWNT	multi wall carbon nanotubes
$n$	Power law index
NIBS	Non invasive backscattering
NIR	near infra red
NMP	N- methyl pyrrolidinone
$n_R$	The solvent refractive index
Nylon	11 - poly $\omega$ -aminoundecanoyl
ODF	Orientation distribution function
PAN	Polyacrylonitrile
PAni	Polyaniline
PBO	Poly butyl oxide
PGB	Pernigraniline base
Pi (cos $\theta$ )	The Legendre polynomial of degree i
$\langle P_2(\cos\theta) \rangle$	The average amount of $P_2(\cos\theta)$
$\langle P_4(\cos\theta) \rangle$	The average amount of $P_4(\cos\theta)$
POT	polyoctylthiophene
PPMS	Physical property measurement system
PPy	Polypyrrole
Psi	Pound per square inch
PT	Polythiophene
PVA	Poly vinyl alcohol
Q	volumetric flow rate (cm <sup>3</sup> /min)
R	Resistance(ohm)
RBM	Resonance breathing mode
S	Cross sectional area of fibre (cm <sup>2</sup> )
SEM	Scanning electron microscopy

SWNT	single wall carbon nanotubes
$S\sigma$	the critical exponent at percolation
T	Temperature (K, °C)
TEM	Transmission electron microscopy
T <sub>g</sub>	glass transition temperature (°C)
TGA	Thermogravimetric analysis
TM	Tangential mode (G band)
TPa	Tera pascal
T <sub>t</sub> and T <sub>s</sub>	tunneling parameters for transport model(K)
V	Voltage (V, mV)
V <sub>d</sub>	Drawing velocity (m/min)
V <sub>i</sub>	Injection rate (g/min)
V <sub>t</sub>	Take up velocity (m/min)
$\alpha$	Chiral angle
$\gamma$	Shear rate (s <sup>-1</sup> )
$\delta_b$	Tensile strength at break (MPa)
$\epsilon_{c,m,f}$	Expected actuator strain of composite, matrix or filler
$\epsilon_b$	Elongation at break (%)
$\eta$	Viscosity (mPa.s=cP)
$\eta_0$	Zero shear viscosity (mPa.s=cP)
$\theta$	The scattering angle of laser beam
$\theta^\circ$	The angle between nanotubes and fibre axis
$\lambda_2$ and $\lambda_4$	The arbitrary parameter of orientation function
$\lambda_o$	The vacuum wavelength of the laser
$\rho$	Density (g/cm <sup>3</sup> )
$\rho_i$	Resistivity of a portion either amorphous or crystalline
$\sigma$	Conductivity (S/cm)
$\phi$	Spin draw ratio
$\phi_{th}$	Thermal draw ratio

$\psi$	The angle between the polarization plane and the fibre axis
$v_i$	Volume fraction of component i
$\omega$	SWNTs mass fraction in the solid fibre
$\omega_1$	The contribution of metallic resistivity in bulk resistivity
$\omega_2$	The contribution of nonmetallic resistivity in bulk resistivity
$\omega_c$	critical weight percentage of SWNT at percolation
$\omega_p$	weight fraction of polymer with regards to solvents

## **Table of Content**

---

<b>DEDICATION .....</b>	<b>II</b>
<b>CERTIFICATION.....</b>	<b>III</b>
<b>ACKNOWLEDGMENTS.....</b>	<b>IV</b>
<b>PUBLICATIONS.....</b>	<b>VI</b>
<b>ABSTRACT.....</b>	<b>IX</b>
<b>ABBREVIATIONS.....</b>	<b>XIII</b>
<b>LIST OF FIGURES .....</b>	<b>XXVI</b>
<b>LIST OF TABLES.....</b>	<b>XXXVIII</b>
<b>LIST OF SCHEMES.....</b>	<b>XLII</b>

### ***1. CHAPTER ONE.....1***

#### **General Introduction**

1.1. Introduction .....	2
1.2. Motivation.....	2
1.3. The aims of the project.....	9
1.4. References.....	12

### ***2. CHAPTER TWO.....17***

#### **Literature Review**

2.1. The chemical structure of Polyaniline.....	18
2.1.1. The solubility of polyaniline.....	20
2.1.2. Aggregation and gel formation of polyaniline solution.....	21

2.1.3.	The solubility of PANi doped with sulfonic acid in organic acid.....	24
2.2.	Carbon Nanotubes.....	26
2.2.1.	Discovery.....	26
2.2.2.	Structure of carbon nanotubes.....	28
2.2.3.	The physical properties of SWNTs.....	29
2.2.3.1.	Aspect ratio.....	29
2.2.3.2.	Mechanical properties .....	30
2.2.3.3.	Electrical properties.....	31
2.2.4.	Properties and applications of self assembled SWNT material.....	32
2.2.5.	SWNT-CEP composites.....	33
2.3.	Wet spinning of Polyaniline (PANi).....	35
2.3.1.	General description of the wet spinning process.....	35
2.3.2.	A literature review for PANi fibre formation.....	37
2.4.	References.....	44

### ***3. CHAPTER THREE.....52***

#### **General Experimental Techniques**

3.1.	Introduction.....	53
3.2.	Preparation of spinning solution using ex-situ approach.....	54
3.3.	Characterisation of spinning solution.....	56
3.3.1.	Elemental analysis.....	56
3.3.2.	Dynamic Light Scattering (DLS).....	56
3.3.2.1.	Theoretical background.....	56



3.3.2.2.	Sample preparation.....	57
3.3.2.3.	The measurement description.....	58
3.3.3.	Viscometry.....	59
3.3.4.	UV-Vis and UV-Vis- NIR spectroscopy.....	60
3.4.	General description of spinning process.....	61
3.4.1.	Spinning apparatus.....	61
3.4.2.	Drawing.....	63
3.5.	Techniques for characterisation of solid fibre.....	65
3.5.1.	Four probe electrical conductivity.....	65
3.5.2.	Cyclic voltammetry.....	66
3.5.3.	Dynamic mechanical analysis.....	68
3.5.3.1.	Stress-strain (Mechanical test) in strain rate mode.....	68
3.5.3.2.	Creep mode.....	69
3.5.3.3.	Viscoelasticity test.....	70
3.5.4.	Differential scanning calirometry.....	71
3.5.5.	Raman spectroscopy.....	71
3.5.6.	Scanning Electron Microscopy.....	72
3.5.7.	Transmission electron Microscopy.....	74
3.6.	References.....	75
<b>4.</b>	<b>CHAPTER FOUR.....</b>	<b>76</b>

**Development and Characterisation of Polyaniline (Leucoemeraldine base) / Single Walled Carbon Nanotubes Composite Fibre Prepared Using a Two Step Process**

4.1.	Introduction.....	77
4.2.	Experimental.....	78
4.2.1.	Materials and reagents.....	78
4.2.2.	Instrumentation.....	78
4.2.3.	Comparison of the ability of NMP and DMPU to disperse SWNTs.....	79
4.2.4.	Influence of polyaniline addition on the degree of SWNT aggregation...	80
4.2.5.	Use of DMPU for dispersing SWNTs at higher concentrations.....	80
4.2.6.	Preparation of spinning solution.....	80
4.2.7.	The fibre spinning process.....	81
4.2.7.1.	Effect of coagulation bath composition.....	82
4.2.7.2.	Effect of take up velocity.....	82
4.2.8.	Effect of CNT content.....	82
4.2.9.	Post spinning treatments.....	83
4.3.	Results and discussions.....	83
4.3.1.	The characterisation of SWNTs.....	83
4.3.1.1.	Elemental analysis.....	83
4.3.1.2.	Raman spectroscopy of the bulk SWNTs.....	84
4.3.2.	Characterisation of SWNT dispersions.....	85
4.3.2.1.	UV-visible – NIR spectroscopy.....	85
4.3.2.2.	Dynamic Light Scattering.....	88
4.3.2.3.	Viscosity of SWNT/DMPU dispersions.....	91
4.3.3.	Viscometry of PANi-(LEB)-SWNT-DMPU spinning solution.....	92
4.3.4.	The effect of fibre spinning parameters on PANi/SWNT morphology.....	98

4.3.4.1. Influence of solvent in the coagulation bath on morphology of as spun fibre.....	99
4.3.4.2. The influence of take up velocity on morphology.....	100
4.3.5. Thermal transition temperatures in as spun fibre.....	102
4.3.6. Thermal stretching.....	103
4.3.7. Mechanical properties of thermally stretched PAni/SWNT fibres.....	105
4.3.8. Flexibility of PAni/SWNT composite fibres.....	111
4.3.9. Raman spectroscopy of PAni/SWNTs composite fibres.....	112
4.3.10. Electrical properties of PAni/SWNTs fibres.....	116
4.3.10.1. Electrical properties of PAni/SWNTs fibres before acid doping..	117
4.3.10.2. Electrical properties of PAni/SWNTs fibres after acid doping....	120
4.3.11. Cyclic voltammetry of PAni/SWNTs composite fibres.....	121
4.4. Conclusions.....	123
4.5. References.....	126

## **5. CHAPTER FIVE.....130**

### **Development and Characterisation of PAni/SWNTs Composite Fibres Using 2-Acrylamido-2 Methyl -1-Propane Sulfonic Acid and a One Step Wet Spinning Process.**

5.1 Introduction.....	131
5.2 Experimental.....	132
5.2.1 Materials and Reagents.....	132

5.2.2	Instrumentation.....	132
5.2.3	Characterisation of SWNT dispersions.....	136
5.2.3.1	DCAA versus DMPU as solvent.....	136
5.2.3.2	Influence of AMPSA on degree of SWNT aggregation.....	136
5.2.3.3	Ability of DCAA to disperse higher concentration of SWNT....	137
5.2.4	Preparation of composite spinning solutions.....	137
5.2.5	The fibre spinning process.....	139
5.3	Results and discussion.....	140
5.3.1	SWNTs dispersions.....	140
5.3.1.1	UV-Vis– NIR spectroscopy of SWNT dispersions.....	140
5.3.1.2	Influence of AMPSA on degree of SWNT aggregation in DCAA.....	141
5.3.1.3	Effect of sonication time on SWNTs agglomeration in DCAA...	143
5.3.1.4	Effect of SWNT concentration on aggregation of SWNTs in DCAA .....	145
5.3.2	Characterisation of spinning solutions.....	147
5.3.2.1	Determination of suitable PAni/AMPSA composition.....	147
5.3.2.2	Viscometry of PAni-ES/AMPSA/SWNTs-DCAA spinning solutions.....	149
5.3.3	Preparation and characterisation of composite fibres .....	151
5.3.3.1	Morphological properties of PAni-ES/AMPSA/SWNT as spun fibres.....	151

5.3.3.2	Morphological properties of thermally stretched PANi-ES/AMPSA/SWNT.....	153
5.3.4	The mechanical properties of composite fibres.....	156
5.3.5	Thermal analysis of the PANi-ES/AMPSA/SWNT composite fibres.....	160
5.3.6	Electrical conductivity of PANi-ES/AMPSA-SWSNT composite fibres.....	164
5.3.7	Raman spectroscopy of PANi-ES/AMPSA/SWNTs fibres.....	166
5.3.8	Cyclic Voltammetry.....	171
5.3.8.1	Cyclic voltammetry of PANi-ES/AMPSA/SWNTs composite fibres in HCl(aq).....	172
5.3.8.2	Cyclic voltammetry of PANi-ES/AMPSA/SWNTs composite fibres in ionic liquid electrolyte.....	173
5.4	Conclusions.....	178
5.5	References.....	180

## **6. CHAPTER SIX. ....184**

### **The Understanding Of the Mechanism of Strength Increase in the PANi-ES/AMPSA/ SWNT Composite Fibre**

6.1.	Introduction.....	185
6.2.	Experimental.....	186
6.2.1.	Materials.....	186
6.2.2.	Instrumentation.....	186
6.3.	Results and discussion.....	187

6.3.1. SWNTs orientation.....	187
6.3.2. Load transfer Mechanism.....	200
6.4. Conclusion.....	203
6.5 References.....	205

## **7. CHAPTER SEVEN.....207**

### **Charge Transport Regime in the PAni-ES/AMPSA/SWNT Composite Fibre**

7.1. Introduction.....	208
7.2. Experimental.....	210
7.2.1. Material.....	210
7.2.2. Sample preparation .....	210
7.2.3. Instrumental.....	211
7.3. Results and discussion.....	211
7.3.1. Electrical transport analysis.....	211
7.3.2. Heterogeneous model.....	215
7.4. Conclusion.....	222
7.5. References.....	224

## **8. CHAPTER EIGHT.....226**

### **The Preliminary Studies into Applications of PAni-ES/AMPSA/SWNT Fibres**

8.1. Introduction.....	227
------------------------	-----

8.1.1.	Actuators: recent development and general requirement.....	227
8.1.2.	PAni fibre electrode for application in rechargeable battery.....	229
8.1.3.	Sensitivity to temperature and humidity.....	230
8.2.	Experimental.....	231
8.2.1.	The actuation tests.....	231
8.2.1.1.	Materials and reagents.....	231
8.2.1.2.	Instrumentation.....	232
8.2.2.	Electrode material for rechargeable battery.....	233
8.2.2.1.	Materials and reagents.....	233
8.2.2.2.	Fabrication of polymer electrode.....	233
8.2.2.3.	Electrochemical characterisation.....	233
8.2.3.	Tests for sensitivity to change of temperature and humidity.....	234
8.2.3.1.	Material and reagents.....	234
8.2.3.2.	Instrumentation.....	235
8.3.	Results and discussion.....	236
8.3.1.	Actuation behavior.....	236
8.3.2.	Performance of PAni-ES/AMPSA and its composite containing SWNTs fibres as electrode material in rechargeable battery.....	243
8.3.2.1.	Charge/discharge characteristics.....	243
8.3.2.2.	Cycle life.....	245
8.3.3.	Performance of PAni-ES/AMPSA fibres with and without SWNTs as humidity and temperature sensors.....	246
8.3.3.1.	Sensitivity to temperature.....	246

8.3.3.2. Sensitivity to relative humidity (% R.H.).....	248
8.4. Conclusions.....	250
8.5. References.....	252
<b>9. CHAPTER NINE.....</b>	<b>256</b>

***General Conclusion***



## LIST OF FIGURES

---

<b>Figure 1.1.</b> U.S. Smart and Interactive Textile market by application segment, 2003-2009 (\$ Millions) .....	8
<b>Figure 1.2.</b> The architecture of electronic textile based on component and function.....	9
*****	
<b>Figure 2.1.</b> The tubular structure of graphene layers of SWNT.....	27
<b>Figure 2.2.</b> Different arrangements of nanotubes (●) semiconducting (n,0) or (m,n) (○) metallic (n,n) or (m,n) [ $n-m = 3q$ ], q is integer.....	28
<b>Figure 2.3.</b> Schematic of the experimental setup used to make CNT fibres.....	33
<b>Figure 2.4.</b> Schematic showing the set up used for wet spinning of fibres.....	36
*****	
<b>Figure 3.1.</b> Schematic of sonication unit for dispersion of nanotubes in the solvent.....	55
<b>Figure 3.2.</b> The schematic of blending unit for mixing of PANi and SWNT dispersion...	56
<b>Figure 3.3.</b> Schematic diagram showing the measurement position for (a) small, weakly scattering samples and for (b) concentrated, opaque samples.....	57
<b>Figure 3.4.</b> The picture of spinning line apparatus has been used in this study (a) whole apparatus (b) pressure vessel (c) take up and drawing roller (d) spinneret...	62
<b>Figure 3.5.</b> The experimental set up used for cyclic voltammetry (a) cell set up (b) instrumental set up.....	67
<b>Figure 3.6.</b> The SEM pictures obtained using (a) Hitach- S900 from internal microstructure (b) Leica 440 from circular cross section.....	73

<b>Figure 3.7.</b> The images obtained from a sample of polyaniline fibre from different angle using FIB.....	74
*****	
<b>Figure 4.1.</b> Raman spectrum of bulk SWNTs ( $\lambda_{exc}=632.8$ nm).....	84
<b>Figure 4.2.</b> UV-Vis NIR spectra of SWNT (0.01% w/w) in (a) DMPU and (b) NMP after 2hrs sonication (A, B, C: refer to table 4.4).....	86
<b>Figure 4.3.</b> Hydrodynamic diameter distribution of SWNT bundles in DMPU for different sonication times (triangle) 30 min (square) 60 min (circle) 120 min.....	88
<b>Figure 4.4.</b> Affect of standing time on the stability of SWNT dispersions and influence of PANi on stability of SWNT dispersion in (a) SWNT- DMPU (0.01 % w/w) (b) SWNT (0.01 % w/w)-PANi (0.01 % w/w) in DMPU. Photograph was taken 6 hr after sonication. Arrows indicate large agglomerates.....	89
<b>Figure 4.5.</b> Hydrodynamic diameter distribution of SWNTs in DMPU (0.01 % w/w) with (square) and without (inverted triangle) PANi. The distribution immediately after sonication is represented by filled symbols while the distribution measured 60 min after sonication was stopped is shown by unfilled symbols. ....	90
<b>Figure 4.6.</b> The size distribution of SWNTs bundle in DMPU for different concentrations of ( $\Delta$ ) 0.05 % w/w, ( $\square$ ) 0.10 % w/w and ( $\square$ ) 0.20 % w/w.....	91
<b>Figure 4.7.</b> Viscometry of SWNT (0.2 % w/w) in DMPU dispersions after different sonication times (a) 30 min, (b) 60 min and (c) 120 min.....	92

<b>Figure 4.8.</b> Variation of viscosity of spinning solution of PAni (LEB) 10% w/w in DMPU containing (a) 0.00 % (b) 0.05 % (c) 0.10 % or (d) 0.20 % (w/w) of SWNT with regard to solvent. Shear rate = $1 \text{ s}^{-1}$ .....	93
<b>Figure 4.9.</b> Variation in viscosity of spinning solution based on PAni (LEB) 10 % w/w in DMPU containing (a) 0.00 % (b) 0.05 % (c) 0.10 % (d) 0.20 % (w/w) SWNT with regards to solvent, at different shear rates.....	95
<b>Figure 4.10.</b> Viscosity versus SWNTs content at different shear rate.....	97
<b>Figure 4.11.</b> Cross sectional SEMs of PAni (a, b) and PAni/SWNTs (2.0 % w/w SWNTs (c, d) into a coagulation baths containing (a,c) 10 % w/w NMP in water or ( b, d) water using take up velocity of 2 m/min. Scale bar 30 $\mu\text{m}$ .....	100
<b>Figure 4.12.</b> Cross sectional SEMs of PAni/SWNT fibres spun using different take up velocities for PAni(a, b) PAni/SWNTs containing 2 % w/w SWNT( c, d). Take up velocities were 3 m/min (a, c) or 6 m/min (b, d). Scale bar is 30 $\mu\text{m}$ (a,c) and 10 $\mu\text{m}$ (b, d).....	101
<b>Figure 4.13.</b> DSC thermal analysis curve of neat as spun polyaniline (LEB) fibre under a N <sub>2</sub> atmosphere first cycle (thick line); second (reheat) cycle (thin line) .....	102
<b>Figure 4.14.</b> SEM micrographs of PAni/SWNTs fibres after thermal stretching containing (a) 0.0 %, (b) 0.5 %, (c) 1.0 % and (d) 2.0 % (w/w) SWNTs with respect to PAni.....	104
<b>Figure 4.15.</b> Stress strain curves of PAni/SWNTs composite fibres with varying SWNTs content, before doping ( thick lines) and after doping for 24 hrs in MSA(thin	

lines). (a,a')Neat PAni, (b,b') PAni/SWNT (0.5 % w/w) (c,c') PAni/SWNT (1.0 % w/w) (d,d') PAni/SWNT( 2.0 % w/w).....	106
<b>Figure 4.16.</b> SEM images showing a typical cross sectional surface of (a) neat PAni (b) PAni/ SWNT (2.0 % w/w).....	108
<b>Figure 4.17.</b> SEMs of PAni/SWNTs composite fibres under flexural load with SWNTs of (a) 0.0 % w/w (b) 0.5 % w/w(c) 1.0 % w/w (d) 2.0 % w/w.....	111
<b>Figure 4.18.</b> Enhanced Raman Spectra (before doping) of (a) neat SWNTs, (e) neat PAni and PAni/SWNTs fibres with varying SWNT content (b) 0.5 %w/w (c) 1.0% w/w, (d) 2.0% w/w ( $\lambda_{exc}=632.8$ ).....	112
<b>Figure 4.19.</b> The schematic illustrating the interaction of SWNTs with PAni through the quinoid rings of latter.....	114
<b>Figure 4.20.</b> Enhanced Raman Spectra(after doping in MSA solution for 24 hrs following by drying at 100 °C) of (a) neat SWNTs (e) neat PAni and PAni/SWNTs with varying SWNTs content (b) 0.5 % w/w, (c) 1.0 % w/w, (d) 2.0 % w/w.....	115
<b>Figure 4.21.</b> The percolative behavior of SWNTs as filler in PAni matrix before doping .....	118
<b>Figure 4.22.</b> The Log-Log plot of conductivity vs reduced weight fraction of SWNTs. ....	118
<b>Figure 4.23.</b> The EPR spectra of PAni/SWNTs composite fibres before doping containing varying amounts of SWNTs. (a) 0.0 % w/w (b)0.5 %w/w, (c) 1.0 % w/w and (d) 2.0 % w/w.....	119

<b>Figure 4.24.</b> Cyclic voltametry of (a) neat PAni fibre (b) PAni/ SWNTs (2 % w/w) composite fibre. Scan rate= 50 mVs <sup>-1</sup> , electrolyte: 1.0 M HCl (aq).....	123
*****	
<b>Figure 5.1.</b> First step of FIB milling: labeling of working area.....	134
<b>Figure 5.2.</b> Second step of FIB milling: (a) Pt deposition and (b) milling of sloping trenches.....	134
<b>Figure 5.3.</b> Third step: reduction of thickness of thin film.....	135
<b>Figure 5.4.</b> Fourth step of FIB milling: (a) Further thinning of the lamella and (b) cutting of holding edges.....	135
<b>Figure 5.5.</b> Final step of FIB milling: (a) transfer of the thin film on a TEM grid using a micro robot (b) Schematic indicating a micro robot machine.....	136
<b>Figure 5.6.</b> UV-Vis NIR spectra of SWNT (0.01 % w/w) in (a) DCAA after 30 min sonication (b) DCAA-AMPSA (2 % w/w) after 30 min sonication and (c) DMPU after 2 hrs sonication.....	141
<b>Figure 5.7.</b> Influence of AMPSA concentration (% w/w) in DCAA on hydrodynamic diameter distribution of SWNT dispersions (0.05 % w/w). (□) 0 % w/w (□) 1 % w/w (□) 2 % w/w. The results were obtained 30 min after samples preparation.....	142
<b>Figure 5.8.</b> Hydrodynamic diameter of SWNTs (0.05 % w/w ) in DCAA with (□) and without (□) AMPSA (2 % w/w). Hydrodynamic diameters immediately after sonication are indicated by the filled symbols; while those measured 60 min after sonication was stopped are indicated by the unfilled symbols.....	143

**Figure 5.9.** Influence of sonication time on homogeneity of SWNTs dispersion as gauged by fluctuation of viscosity versus shear rate. The dispersion contained 0.060 % w/w SWNT and 2 %w/w AMPSA relative to the DCAA solvent.  
.....144

**Figure 5.10.** Average hydrodynamic diameter of SWNT dispersions for 5 repetitive experiments using either 10 min or 30 min sonication time. The dispersion contained 0.060 % w/w SWNT and 2 %w/w AMPSA relative to the DCAA solvent.....145

**Figure 5.11.** Influence of SWNTs concentration in DCAA/AMPSA solution on hydrodynamic diameter (□) 0.030 %w/w (□) 0.045 %w/w (□) 0.060 %w/w (□) 0.090 %w/w.....146

**Figure 5.12.** Viscosity vs. shear rate for SWNTs dispersion in DCAA containing 2 % w/w AMPSA for various SWNT loadings from 0.00% w/w to 0.09 % w/w.  
.....147

**Figure 5.13.** Influence of SWNTs content on viscosity of PAni-ES/AMPSA/SWNT solution versus shear rate. The total concentration of PAni and AMPSA was 11.5 % w/w.....149

**Figure 5.14.** Time before gelation indicated by sharp rise in viscosity for (a)neat PAni-ES/AMPSA and (b) PAni-ES/AMPSA/SWNT (0.090 % w/w) SWNT spinning solutions. Shear rate =1 s<sup>-1</sup>.....151

**Figure 5.15.** Typical SEM micrographs of as-spun fibres of (a) neat PAni-ES/AMPSA (b) PAni-ES/AMPSA/SWNT 0.76 %w/w.....152

<b>Figure 5.16.</b> Typical SEM micrographs of 5x thermally stretched fibre of (a) PAni-ES/AMPSA (b) PAni-ES/AMPSA/SWNT (0.76 % w/w).scale bar is 10 $\mu$ m	153
<b>Figure 5.17.</b> SEM micro graph of the PAni-ES/AMPSA/SWNT (0.76 %w/w)(a) side wall (b) cross section parallel to fibre axis.	154
<b>Figure 5.18.</b> TEM micrographs of thin film obtained by FIB milling, showing SWNTs dispersion within an PAni-ES/AMPSA matrix for (a) neat PAni-ESAMPSA (b) PAni-ES/AMPSA/SWNTs (0.76 %w/w SWNT	155
<b>Figure 5.19.</b> The typical stress – strain curve of PAni-ES/AMPSA fibre and its composites with different SWNT contents ( D fibre= $50\pm 20$ $\mu$ m, strain rate= $500$ $\mu$ m /min).	157
<b>Figure 5.20.</b> Strain recovery behavior of (□) neat PAni-ES/AMPSA fibre (□) PAni-ES/AMPSA/SWNT (0.76 % w/w) with cyclical application and removal of a 40 mN force.	158
<b>Figure 5.21.</b> SEM micrographs of full knots of (a) PAni-ES/AMPSA (b) PAni-ES/AMPSA/SWNT (0.76% w/w). SEM micrographs of 16 ply twisted fibre of PAni-ES/AMPSA/SWNT (0.76 % w/w) fibre with (c) S shaped twisting (d) Z shaped twisting. The number of twist per inch was 36.	159
<b>Figure 5.22.</b> (a)DSC thermogram of 5x drawn fibre (a) PAni-ES/AMPSA (b) PAni-ES/AMPSA/SWNT (0.76 %w/w). (b) The DSC thermogram for the first and second cycles of 5X drawn PAni-ES/AMPSA/SWNT	161

<b>Figure 5.23.</b> (A) Storage modulus (B) the $\tan\delta$ (Loss modulus/Storage modulus) vs temperature curves for (a) PANi-ES/AMPSA and (b) PANi-ES/AMPSA - SWNTs (0.76 % w/w).....	163
<b>Figure 5.24.</b> Influence of SWNTs content on the electrical conductivity of PANi-ES/AMPSA/SWNTs fibres.....	164
<b>Figure 5.25.</b> log–log plot of electrical conductivity vs reduced mass fraction.....	165
<b>Figure 5.26.</b> Enhanced Raman spectra ( $\lambda_{exc} = 632.8$ nm) obtained for PANi-ES/AMPSA/SWNTs obtained containing various amounts of SWNTs (a) 0.00 % w/w (b) 0.26 % w/w (c) 0.38 % w/w (d) 0.5 %w/w (e)0.76 % w/w and (f) SWNT bucky paper.....	167
<b>Figure 5.27.</b> Enhanced Raman spectra ( $\lambda_{exc} = 632.8$ ) of neat PANi-ES/AMPSA (a) before deprotonation, (b) 3 hr after deprotonation and (c) 6 hr after deprotonation (d) Raman spectrum of PANi(EB).Arrow indicates the transition from the protonated ES form to the deprotonated EB form.....	170
<b>Figure 5.28.</b> Enhanced Raman spectra ( $\lambda_{exc} = 632.8$ ) of (a) Neat PANi-ES/AMPSA fibre before deprotonation, (b) Neat PANi-ES/AMPSA after 6 hrs deprotonation (c) PANi-ES/AMPSA/SWNT (0.76 % w/w) before deprotonation and (d) PANi-ES/AMPSA/SWNT (0.76 % w/w) after 24 hrs deprotonation.....	171
<b>Figure 5.29.</b> CV characterization of (a) PANi-ES/AMPSA fibre (b) PANi-ES/AMPSA /SWNTs fibre 0.76 % w/w (b) in 1.0 M HCl (aq) electrolyte. 10 th cycle shown for each CV. Scan rate 10 mV/s. (L=10 mm, D= 70 $\mu$ m).....	172
<b>Figure 5.30.</b> CV characterisation of fibres made of (a) PANi-ES/AMPSA/SWNT and (b) PANi-ES/AMPSA/SWNT (0.76 %w/w) in EMI.TFSI. potential cycled in	



range of ( $\pm 1.5$ ), scan rate 50 mV/s, under 10 mN Load. (L=10 mm, D=70  $\mu\text{m}$ ).....175

**Figure 5.31.** Comparison of the electrochemical stability of (a,b) PAni-ES/AMPSA and (c,d) PAni-ES/AMPSA/SWNT (0.76 % w/w) over potential ranges of (a,c)  $\pm 1.5$  and  $\pm 2$  V (b,d).....177

**Figure 5.32.** CV characterisation of the PAni-ES/AMPSA/SWNT fibre illustrating electrochemical stability over 30 successive cycles. scan rate 50 mV/s, under 10 mN Load. Potential cycled in range of ( $\pm 2.0$ ).....178

\*\*\*\*\*

**Figure 6.1.** Demonstration of SWNTs coordination (xyz) in PAni-ES/AMPSA-SWNTs composite fibre (XYZ coordinates) and the fibre arrangement in reference frame of the Raman sample stage (x'y'z' coordinates).....187

**Figure 6.2.** The Raman spectra under VV and VH configuration,  $\psi$  = the angle between fibre axis and polarization plane (a) PAni-ES/AMPSA fibre (5x drawn fibre) for  $\psi=0^\circ$  and  $90^\circ$ . VV configuration (b) PAni-ES/AMPSA-SWNT (0.76 % w/w) composite fibre (as spun) VV configuration (c) PAni-ES/AMPSA-SWNT (0.76 % w/w) composite fibre (5x drawn) VV configuration.(d) PAni-ES/AMPSA-SWNT (0.76 % w/w) composite fibre (5x) VH configuration. From top to bottom, the angle between fibre axis and polarization plane is  $0^\circ$ ,  $30^\circ$ ,  $45^\circ$ ,  $60^\circ$ ,  $75^\circ$  and  $90^\circ$ .....189

**Figure 6.3.** The Raman spectra under VV and VH configuration for RBM band,  $\psi$  = the angle between fibre axis and polarization plane (a) PAni-ES/AMPSA fibre

(5x drawn fibre) for $\psi=0^\circ$ and $90^\circ$ . VV configuration (b) PAni-ES/AMPSA-SWNT (0.76 % w/w) composite fibre (5x) VH configuration .....	191
<b>Figure 6.4.</b> The comparison of $I_{vv}(\psi^\circ)/I_{vv} 0^\circ$ versus $\psi$ in tangential mode (TM) and resonance breathing mode (RBM) modes for this work and references ....	192
<b>Figure 6.5.</b> The orientation distribution function of SWNT in PAni-ES/AMPSA-SWNT (0.76 %w/w) composite fibres constructed with the orientation parameters, $\langle P_2(\cos\theta) \rangle$ and $\langle P_4\cos(\theta) \rangle$ listed in Table 6.1 .....	197
<b>Figure 6.6.</b> Effect of mechanical strain on the frequency shift of D* band of SWNTs incorporated in PAni-Es/AMPSA matrix. (dashed line) before applying strain (solid line) after applying 3 % strain.....	200
<b>Figure 6.7.</b> The Raman shift of D* peak of nanotube under axial tension for two sample of SWNT (0.76 %w/w) in the PAni.....	201
<b>Figure 6.8.</b> Mechanical versus spectroscopic stress – strain curve.....	202
*****	
<b>Figure 7.1.</b> Crystalline regions separated by disordered regions constitutes the heterogeneous morphology in composite fibre.....	209
<b>Figure 7.2.</b> The temperature dependence conductivity for PAni-ES/AMPSA fibre and their composite containing 0.25% and 0.76 %w/w SWNT.....	212
<b>Figure 7.3.</b> Log-Log plot of reduced activation energy (W) vs. temperature ( $\square$ ) PAni-Es-AMPSA ( $\Delta$ ) PAni-Es-AMPSA-SWNT (0.25 % w/w) ( $\square$ ) PAni-Es-AMPSA-SWNT (0.76 % w/w).....	213

<b>Figure 7.4.</b> The resistance arrangement in the proposed model of charge transport described in equation 7.1.....	215
<b>Figure 7.5.</b> The fitting quality of experimental data and proposed model and residual amount of least square of fitting calculation.....	219
*****	
<b>Figure 8.1.</b> Experimental set-up for actuation test in isotonic mode.....	232
<b>Figure 8.2.</b> Schematic shows the experimental set up used for measurement of resistance across the fibres for measurement of resistance in different humidity.....	236
<b>Figure 8.3.</b> The typical isotonic actuation data as a function of scanning potential in 1.0 M HCl at scan rate of 5 mV/s. Simultaneous demonstration of linear strain and cyclic voltammogram in one cycle for (a) Neat PAni-ES/AMPSA (b) PAni – ES/AMPSA/SWNT (0.76 % w/w)1 under 10 mN load.....	237
<b>Figure 8.4.</b> Isotonic strains measured during cyclic voltammetry in 1M HCl at 5 mV/s between -0.2 and 0.5V (vs. Ag/AgCl reference). Open and filled symbols show the results from two separate samples. Square symbols are for neat PAni-ES/AMPSA fibres and circles are for SWNT-reinforced fibre.....	239
<b>Figure 8.5.</b> Cyclic voltammograms showing current density (I) for potential (E) scans between -0.2V and +0.5V (vs. Ag/AgCl) in 1M HCl at 5 mV/s: a) neat PAni-ES/AMPSA and b) PAni-ES/AMPSA -SWNT fibres.....	242
<b>Figure 8.6.</b> Charge/discharge curves of PAni –ES/AMPSA or PAni-ES/AMPSA/SWNT (0.76 % w/w) fibres (a) PAni-ES/AMPSA fibre charges (b) PAni-ES/AMPSA fibre	

discharges(c) PANi –AMPSA-SWNT (0.76 % w/w) charges(d) PANi –ES/AMPSA-SWNT (0.76 % w/w) discharges.....	244
<b>Figure 8.7.</b> Cycle life of (a) PANi-ES/AMPSA (b) PANi-ES/AMPSA/SWNT fibres...	245
<b>Figure8.8.</b> The sensitivity of normalized resistivity versus (a) temperature by scan rate( 3 °C/min) at constant humidity for (b)Neat PANi-ES/AMPSA (c) PANi-ES/AMPSA-SWNT.....	247
<b>Figure 8.9</b> (a) Pulse in relative humidity at constant temperature. The variation of normalised resistance( $R/R_0$ ) for (b) PANi-ES/AMPSA fibre and (c) PANi-ES/AMPSA /SWNT composite versus humidity pulse change .....	249
*****	
<b>Figure 9.1.</b> The comparison of tensile strength versus elongation at break of PANi –CNT fibre with commercial yarns.....	261
<b>Figure 9.2.</b> The comparison of elastic modulus versus elongation at break of PANi –CNT fibre with commercial yarns.....	261

## LIST OF TABLES

---

<b>Table 2.1.</b> The solubility and conductivity of PANi cast from some typical protonic acids and solvents.....	26
<b>Table 2.2.</b> Different chirality based on chiral angle .....	29
<b>Table 2.3.</b> Typical mechanical properties of SWNTs compared with metals and carbon fibre.....	30
<b>Table 2.4.</b> The mechanical and electrical properties of SWNT in the form of bucky paper (mat) and fibres.....	32
<b>Table 2.5.</b> The mechanical and electrical properties of neat PANi fibre produced by the two step process.....	37
<b>Table 2.6.</b> The mechanical and electrical properties of PANi fibre processed from one step process.....	40
<b>Table 2.7.</b> The mechanical properties data of some synthetic and natural fibre .....	41
<b>Table 2.8.</b> The electrical and mechanical properties of composite of PANi and thermoplastic polymer.....	42
*****	
<b>Table 3.1.</b> Viscosity ranges and spindles.....	60
*****	
<b>Table 4.1.</b> Formulation of PANi (LEB)/SWNT-DMPU composite spinning solutions .....	81
<b>Table 4.2.</b> Elemental analysis of purified SWNTs prepared by Hipco@CNI(PO257).....	84

<b>Table 4.3.</b> Vibrational modes observed for Raman scattering in SWNTs .....	85
<b>Table 4.4.</b> Electronic transitions reported for dispersed SWNTs and their occurrence in different solvents.....	87
<b>Table 4.5.</b> Power law coefficients and exponents for PAni solution with different SWNT content in DMPU.....	96
<b>Table 4.6.</b> The typical diameters, deniers and densities of thermally stretched 2x drawn PAni/SWNT fibre containing different amounts of SWNTs.....	105
<b>Table 4.7.</b> Influence of SWNTs loading on mechanical properties of PAni/SWNTs fibres before acid doping.....	107
<b>Table 4.8.</b> Influence of SWNTs loading on mechanical properties of PAni/SWNT fibres after doping with MSA for 24 hr.....	107
<b>Table 4.9.</b> The effective elastic modulus of SWNT bundles embedded in undoped and doped PAni matrix.....	110
<b>Table 4.10.</b> Assignment of enhanced Raman spectra bands.....	113
<b>Table 4.11.</b> Influence of drying temperature on four point probe conductivity of 2x PAni/SWNTs fibres (2X) with varying SWNT content after acid doiping .....	120
*****	
<b>Table 5.1.</b> Range of PAni and AMPSA contents used to prepare PAni-ES/AMPSA solutions in DCAA for fibre spinning. 20 g of DCAA was used for each. .....	137

<b>Table 5.2.</b> Amount of PANi (EB), AMPSA and SWNTs used for the preparation of PANi-ES/AMPS/SWNTs spinning solution (each solution made up in 20 g DCAA solvent.....	138
<b>Table 5.3.</b> Summary of observations made during attempts to spin fibres from mixures “S1” to “S4”(refer Table 5.1).....	148
<b>Table 5.4.</b> The power law index and consistency index for samples containing different amounts of SWNTs.....	150
<b>Table 5.5.</b> The mechanical properties of PANi-ES/AMPSA fibre and its composites with different SWNT contents.....	157
<b>Table 5.6.</b> The influence of SWNT loading on four point probe conductivity of 5xdrawn fibre of PANi/AMPSA.....	165
<b>Table 5.7.</b> The assigned frequencies originated from PANi-ES/AMPSA and its SWNTs composite.....	168
<b>Table 5.8.</b> The chemical structure of the ionic liquids 1-butyl-3-methyl imidazolium tetrafluoroborate (BMI.BF <sub>4</sub> ) and ethyl methyl imidazolium bis (trifluoro methane sulfonyl) imide (EMI.TFSI).....	174

\*\*\*\*\*

<b>Table 6.1.</b> The polarized Raman scattering intensity ratio of TM and RBM bands in VV configuration ( $\theta=0^\circ$ , $90^\circ$ ) versus VH configuration at $\theta=0^\circ$ for as-spun and 5x drawn fibres of PANi-Es/AMPSA-SWNT (0.76 % w/w). Orientation order parameters are listed for construction of orientation distribution function....	196
--	-----

<b>Table 6.2.</b> The comparison of predicted elastic modulus from rule of mixture and experimental value.....	199
--	-----

\*\*\*\*\*

<b>Table 7.1.</b> The conductivity parameters for PANi-ES/AMPSA fibre and its SWNT composite fibre.....	214
---	-----

<b>Table 7.2.</b> The sensitivity of the model to the initial starting values for the fitting.....	217
--	-----

<b>Table 7.3.</b> The fitting parameters presented in equation 7.2 for different samples.....	220
---	-----

<b>Table 7.4.</b> The contribution of metallic resistivity in bulk resistivity and the metallic disorder in amorphous resistivity.....	221
--	-----

\*\*\*\*\*

<b>Table 8.1.</b> The description of aqueous solution required for preparation of different relative humidity in the conductivity chamber.....	235
--	-----

<b>Table 8.2.</b> Measured and calculated properties of PANi-ES/AMPSA-SWNT fibre composites.....	241
--	-----

\*\*\*\*\*

<b>Table 9.1.</b> The comparison of one step and two steps methods by considering economical and safety issues.....	266
---	-----

<b>Table 9.2.</b> The hazardous identification of non similar material used in one step and two steps methods.....	267
--	-----



## LIST OF SCHEME

---

<b>Scheme 1.1.</b> The schematic of the selection of conducting polymers.....	3
*****	
<b>Scheme 2.1.</b> (a)A general scheme for polymerisation of Aniline (b) different oxidation state of PANi .....	18
<b>Scheme 2.2.</b> Interconversions between different forms of polyaniline .....	19
<b>Scheme 2.4.</b> The chemical structure of DMPU and NMP.....	21
<b>Scheme 2.5.</b> Hydrogen bonding between PANi (EB) to DMPU.....	21
<b>Scheme 2.6.</b> The interaction of LEB chain with carbonyl group of DMPU.....	23
<b>Scheme 2.7.</b> Some of sulfonic acid dopants used for one step PANi fibre processing.....	25
*****	
<b>Scheme 5.1.</b> Polaronic (semiquinoid), bipolaronic and oxidized unit of PANi.....	169
<b>Scheme 5.2.</b> The mechanism of electrochemical switching of PANi-ES/AMPSA between ES-LEB oxidation states in EMI.TFSA.....	176

# ***CHAPTER ONE***

General Introduction

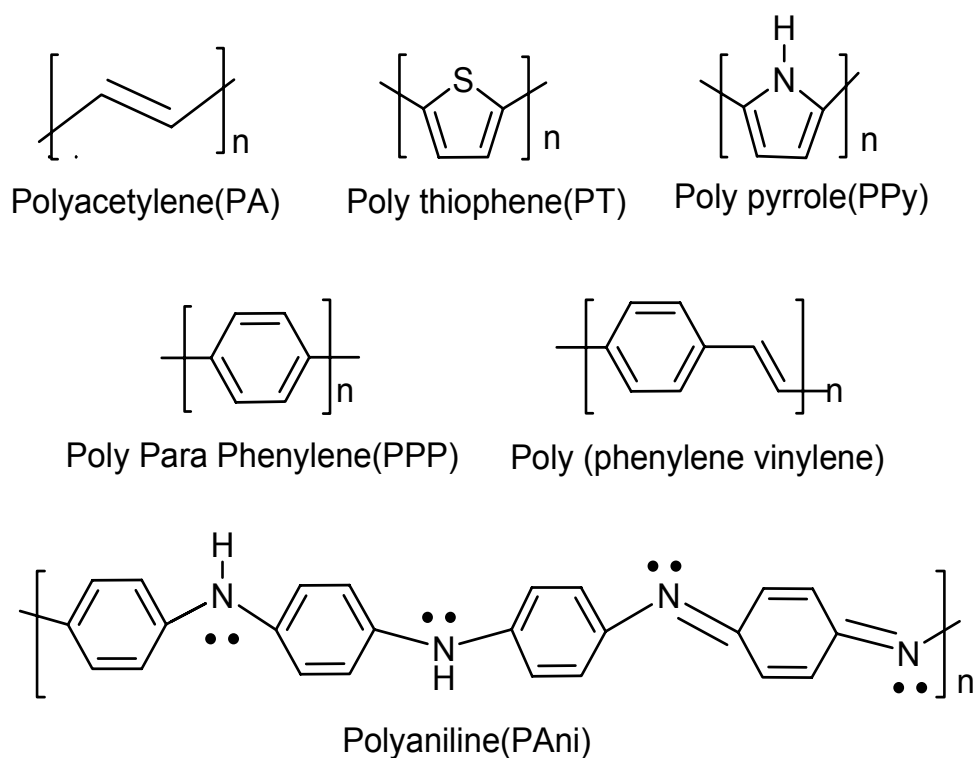
## **1.1. Introduction**

This chapter provides an introduction to the content of this thesis and the research conducted for this study on the development and characterisation of composite conducting electroactive fibres using smart materials including polyaniline (PAni) and single walled carbon nanotubes (SWNTs). First, the motivation behind this research is given, along with a general description of the physical properties and chemical structure of key materials. Next, the overall objective of this study and selected approaches are described. The final section of the chapter is an outline of this entire document, with a brief summary of each chapter.

## **1.2. Motivation**

Smart materials are one of frontier technologies in engineering and manufacturing. A smart material is capable of recognising appropriate environmental stimuli, processing the information arising from the stimuli, and responding to it in an appropriate manner and time frame [1]. Depending on changes in some external conditions such as temperature, pH, electric and magnetic field, their properties (mechanical, electrical, appearance), structure, composition and functions is altered within a specific regime and designed for specific performance. Examples of smart materials include piezoelectric, electro-strictive and magneto-strictive materials which are capable of changing their size in response to either an electric or magnetic field. Furthermore, the change in shape in response to heat or cold in shape of memory alloys or changing of optical properties when a voltage applies in electro chromic materials can be included as smart materials. In parallel with the recognition of these functionalities in a range of metallic and non metallic materials, the discovery of conducting electroactive polymers (CEPs) has revolutionised the concept

of a smart material because of their specific electrical property, electrochemical activity and wide range of forms in which they are available [2]. Conducting polymers are conjugated polymers with alternating single and double bonds in the backbone and a delocalised  $\pi$ -electron structure [1-3]. Numerous conducting polymers (Scheme 1.1) have been prepared and studied due to their potential use in wide range of applications.



**Scheme 1.1.** The chemical structures of a selection of conducting polymers

The evolution of the conducting polymers through delocalisation of  $\pi$ - electrons occurs through doping of localized structure. In completely conjugated system, the delocalisation makes the  $\pi$  electrons freely mobile over the entire length of the molecules. Despite the availability of a charge carrier, the conductivity of their pristine forms is not high. At this

hypothetical zero doping level, the polymer is neutral and its band structure is that of a standard semiconductor. Removal of one electron from the CPs chain produces a polaron. The polaron has a structure with a single positive charge delocalized over monomer units. Whenever the entire CP chain saturated with polaron, the bipolaron structure commence to form by removal of one additional electron and with further removal from valence/conduction band. At very high doping levels,( i.e. a maximum 50 % in PANi or 35 % in polypyrrole), the individual biopolaron states coalesce into bipolaron bands. At high dopant concentrations, the bipolarons, which are spinless, can become mobile under application of the electric field, thus giving rise to the high conductivity observed in CEPs. If one were able to achieve even higher doping, the two bipolaron bands would gradually broaden producing metal like conduction. [3, 4].

The electroactive behavior of the conducting polymer is unique because it is an example of a redox polymer reaction which is accompanied by a change in the electrical properties from an insulator to a conductor involving both electron and ion transport [5, 6]. Oxidation yields a charged polymer with incorporated anions, however, during the reduction, electro-neutrality is maintained either by expulsion of these anions or by incorporation of cations [7]. When a sufficient negative potential is applied to the polymer, the anions are expelled (electrochemical undoping), thus reducing it to the neutral state. Conversely, when a positive potential is applied to oxidise the neutral form the anions are taken up (electrochemical doping).

Besides the conductivity and electroactivity of conducting polymers, the ability to produce them in different forms is critical for practical applications. Most CEPs are insoluble specifically in the conductive form due to inherent delocalised  $\pi$  electronic

structures which induce high polarizability and a rigid polymer backbone [2]. High electronic polarizability leads to a large inter-chain  $\pi$ - $\pi$  attraction (dispersive force) which favors aggregation rather than solvation. Different routes have been explored for rendering an intractable polymer soluble in certain solvents. A well established method is the inclusion of solubilising monomeric structure along the polymer chain. It may induce steric consequences that reduce the ability of the polymer to form delocalised  $\pi$  electron density over the chain. It is likely to produce interruption to charge carrying thus reducing the level of conductivity [8].

Polyaniline (PAni), however, shows a very broad range of solubility in organic or non-organic solvents which is desirable for film formation or fibre spinning process [9-13]. The conductivity in PAni is related to the specific planar head to tail chemical structure. The ability to directly spin conducting PAni fibres from its solution is of particular interest in the present study.

The chemical properties of PAni make it very useful for use in sensors. It has been widely employed as gas [14], pH [15], humidity [16] and temperature sensors [17-21]. Sensor applications utilise the ability of PAni to change its electrical properties during reaction with various redox agents (dopants) or in response to moisture, heat, smell volatiles, taste soluble chemicals as well as applied strain or tension. The calibration of change in electrical conductivity to change in environmental stimulus is easily achieved when using conducting polymers as sensors.

The practical applications of PAni in electrochemical devices often requires electrochemical doping/undoping process, i.e. removal or addition of an electron to the polymer chain followed by the provision of a counter ion to balance the resulting charge

difference. For example, polymeric rechargeable batteries [19, 22-25] based on PANi powder as the cathodic electrode coupled with a Lithium electrode have been developed. The battery can be reversibly charged or discharged through the oxidation and reduction of PANi.

Another useful example of PANi electrochemistry is the application that involves conversion of electrical energy into mechanical energy (electrochemical actuators) [9, 26-30]. The actuation process is associated with insertion and expulsion of ions causing reversible expansion and contraction in size during the doping and dedoping of PANi.

Single walled carbon nanotubes (SWNTs) are hexagonal graphene sheets of carbon atoms in an  $sp^2$  configuration rolled-up into a cylindrical form with diameters as small as 1-4 nanometer and with a large aspect ratio [31, 32]. SWNTs have interesting properties, such as high mechanical strength [33, 34], flexibility [35], high electrical conductivity [36] and very high charge storage capability [37-39].

These remarkable mechanical and electrical properties exhibited by SWNTs have encouraged researchers to study SWNTs– polymer composites [40-44]. In this regards, composites of  $\pi$ -conjugated polymers and SWNTs are of great interest in terms of the novel electronic interaction between these two elements and the mechanical reinforcement of the polymer by SWNTs [40, 42, 45-47].

Conducting and electroactive materials have special interest if they can form flexible fibres. Examples, include wet spinning of pristine conducting polymer [48-50], wet or melt spinning composites of conducting polymer and insulating polymers [49, 51-53], wet spinning of pristine SWNT fibres [54-56] and coating of synthetic yarns with conducting polymers [57]. The development of these material was mostly responsible for the

emergence of a new class of textiles that can interact with the environment and respond to external stimulus[58-61].

This new area of study has been called “electronic textiles” (E-textiles) and has introduced new applications in diverse areas including medicine [62-64], clothing for military use [63, 65], devices to help people with disabilities [66], rehabilitation or sports injuries (e.g. rehabilitation glove and smart knee sleeve) [67] and entertainments [68]. The E-textiles with synonym names such as smart and interactive textiles (SMITs), Smart Fabrics and interactive textiles (SFIT) or smart fabric, are a new segment in the global textile industry. To date, the U.S. military has been leader in developing E-textile technologies and applications for such areas as body armor, artificial muscles, biochemical hazard protection, physiological status monitoring, location and embedded communications and computing [69]. Many of these technologies also have potential civilian and commercial applications. Indeed, the commercial sector has been ahead of the military in commercialising E-textile technologies. Figure 1.1 demonstrates the distribution of values of shipment in different sections. The U.S. market for smart and interactive textiles is valued at an estimated \$64.4 million in 2003 and is expected to rise at an AAGR (average annual growth rate) of 36 % to \$299.3 million in 2009. Most of the market comprises the consumer products that include low-tech items. Military, biomedical, and vehicle safety and comfort applications also are expected to grow rapidly.



**Figure 1.1.** U.S. Smart and Interactive Textile Market by application segment, 2003-2009 (\$ Millions) [69].

The architecture of smart fabrics is fundamentally based on replacing threads with flexible conducting filament in a fabric to provide a platform for consolidation of electronic components including sensors, actuators, signal processors, fibrous power source and data transfer elements (Fig 1.2). Integration of electronic components into textiles can be achieved by miniaturization of electronic components and attachment to textiles. Mostly the current E-textiles employ metallic based conducting fibre and micro electronic devices which are interconnected by soldering, gluing and encapsulation of joints. These current versions use integrated wiring and carrying devices that add bulk and weight to the garments making them uncomfortable for daily use. These items are also expensive with respect to maintenance and user safety [68].

Component	Sensor	Network	Processor	Actuator	Power
Function	Sensing biometric and environmental data and user command	Transmitting data Internally Externally	Calculating and storing of data	Responding to external or internal stimulus	Supplying energy

**Figure 1.2.** The architecture of electronic textile based on component, function

Incorporation of electronic devices into flexible textiles may be improved by development of organic based inherently conductive fibres with electronic functionalities. Such fibres would have physical properties similar to and/or compatible with more conventional textile fibres. The “smart” material characteristics of these fibres will allow for the development of textiles that will be able to measure and self-regulate, through active feedback, the environmental conditions of their immediate surroundings.

It has been proposed that the employment of PANi and SWNTs for fabrication of smart, conducting and electroactive composite fibres creates opportunities that could result in new applications in smart structures. These considerations provide the motivation for studying the electrical, mechanical and electrochemical properties of composites of PANi/SWNT alongside the investigation of their promising application as actuator, battery and sensor.

### 1.3. The aims of the project

The overall aim of the project is to examine means for developing composite fibres consisting of PANi reinforced with SWNTs and characterisation of the electrical,

mechanical and electrochemical properties of such fibres. In addition, the actuation performance, in particular, and preliminary evaluation of the performance of composite fibres as sensors or battery material will be introduced.

The outline of project includes a literature review of background knowledge (Chapter 2), and a description of general experimental techniques (Chapter 3), applied for the manufacturing, characterisation and evaluation of PANi-SWNT composite fibres. The other chapters comprise the following topics:

- 1) Two approaches to the production of composite fibres (i.e. one step and two step) have been applied in this work. The spinning solution has been prepared using an ex-situ process in both one step and two step approaches. The disperseability of SWNT in solvents of PANi has been studied in term of homogeneity and particle size using dynamic light scattering technique. The composite fibres developed in one step and the two step approaches have been manufactured using wet spinning processes followed by several chemical and thermal steps (Chapters 4, 5).
- 2) Various experimental techniques such as dynamic mechanical analysis (DMA in three mode: Strain rate, creep, and viscoelastic), four probe electrical conductivity, differential scanning calirometry (DSC). Raman spectroscopy, scanning electron microscopy (SEM), transmission electron microscopy (TEM) and cyclic voltammetry (CV) have been employed for the characterisation of the fibres which will be described in chapters 4, 5, 6 and 7. In addition, chapter 6 more specifically concentrates on the mechanism of load transfer from matrix (PANi) to filler (SWNTs) using polarised Raman spectroscopy. Chapter 7 also mainly focused on charge transport regime via the measurement of electrical transport behavior of the

composites over a wide range of temperatures using physical property measurement system (PPMS).

- 3) In chapter 8 the actuation performance of PANi and PANi/SWNT fibres will be compared. Moreover, some preliminary results will be presented for the PANi/SWNT fibre as an electrode in ionic liquid electrolyte or application in all polymer rechargeable battery. Then the response of the fibres to changes in humidity and temperature will be analyzed to introduce their capability as fibrous sensors.
- 4) In the final section of the manuscript, the results obtained from different parts will be summarised.

## 1.4. References

- [1] G. G. Wallace, G. M. Spinks and P. R. Teasdale, Conductive electroactive polymers, Technomic Publication, Pennsylvania, (1997), P.154.
- [2] M. Angelopoulos, in Handbook of conducting polymers, "Conducting polymers in microelectronics", Marcel Dekker, New York, (1997), 921-945.
- [3] J. L. Bredas and G. B. Street, Acc. Chem.Res. 18 (1985) 309-315.
- [4] P. Chandrasekhar, Conducting polymers, Fundamentals and Applications, Kluwer Academic Publishers Group, Massachusetts, (1999).
- [5] T. Shimidzu, A.Ohtani, T.Iyoda and K. Honda, J. Electroanal. Chem. 224 (1987) 123-125.
- [6] F. Diaz, J. I. Catillo, J. A. Logan and W.-Y. Lee, J. Electroanal. Chem. 129 (1981) 115-132.
- [7] K. Doblhofer and K. Rajeshwar, in Hand book of conducting polymers, "Electrochemistry of conducting polymer", Marcel Dekker, Newyork, (1998), 531-589.
- [8] J. R. Reynolds and M Pomereantz, in Electroresponsive Molecular and Polymeric Systems," Processable electronically conducting polymers", Marcel Dekker Inc, New york, (1991), 187-256.
- [9] G. M. Spinks, G. G. Wallace, L. Liu and D. Zhou, Macromolecular Symposia. 192 March (2003) 161-169.
- [10] A. P. Chacko, S. S. Hardaker, B. Huang and R. V. Gregory, Mat. Res. Soc. Symp. Proc. 413 (1996) 503-511.
- [11] A. P. Chacko, S. S. Hardaker, R. V. Gregory and R. J. Samuels, Synth. Met. 84 (1997) 41-44.
- [12] A. Dong, X. Jing, W. Wang and Z. Feng, Chinese J. Polym. Sci. (English Edition). 13 (1995) 347-352.
- [13] R. Jain and R. V. Gregory, Synth. Met. 74 (1995) 263-266.
- [14] P. S. Barker, C. Di Bartolomeo, A. P. Monkman, M. C. Petty and R. Pride, Sensors & Actuators B-Chemical. (1995) 451-453.

- 
- 
- [15] S. T. McGovern, G. M. Spinks and G. G. Wallace, *Sensors & Actuators B-Chemical*. 107 (2005) 657-665.
- [16] J. N. Barisci, T. W. Lewis, G. M. Spinks, C. O. Too and G. G. Wallace, *J. Intell. Mater. Sys. Struc.* 9 (1999) 723-731.
- [17] A. Guadarrama, M. L. Rodriguez-Mendez, J. A. de Saja, J. L. Rios and J. M. Olias, *Sensors & Actuators B-Chemical*. 69 (2000) 276-282.
- [18] J.-S. Huh, H. R. Hwang, J. G. Roh, D. D. Lee and J.-O. Lim, *Mater. Res. Soc. Symp- Proc.* 698 (2002) 95-100.
- [19] S. Taguchi and T. Tanaka, *Journal of Power Sources*. v 20 (1987) 249-252.
- [20] Q. Fang, D. G. Chetwynd, J. A. Convington, C.-S. Toh and J. W. Gardner, *Sensors & Actuators B-Chemical*. 84 (2002) 66-71.
- [21] M. Ferreira, A. Riul Jr, K. Wohnrath, F. J. Fonseca, O. N. Oliveira Jr and L. H. C. Mattoso, *Anal. Chem.* 75 (2003) 953-955.
- [22] L. Yang, W. Qiu and Q. Liu, *Solid State Ionics*. 86-88 (1996) 819-824.
- [23] T. Nakajima and T. Kawagoe, *Synth. Met.* 28 (1989) 629-638.
- [24] N. Li, J. Y. Lee and L. H. Ong, *J. Appl. Electrochem.* 22 (1992) 512-516.
- [25] F. Goto, K. Abe, K. Okabayashi, T. Yoshida and H. Morimoto, *Journal of Power Sources*. 20 (1987) 243-248.
- [26] R. H. Baughman, *Synth. Met.* 78 (1996) 339-353.
- [27] P. Chiarelli, D. De Rossi, A. Della Santa and A. Mazzoldi, *Polymer Gels & Networks*. 2 (1994) 289-297.
- [28] A. S. Hutchison, T. W. Lewis, S. E. Moulton, G. M. Spinks and G. G. Wallace, *SPIE. Proc.* 3669 (1999) 242-253.
- [29] T. W. Lewis, L. A. P. Kane-Maguire, A. S. Hutchison, G. M. Spinks and G. G. Wallace, *Synth. Met.* 102 (1999) 1317-1318.
- [30] A. D. Santa, D. De Rossi and A. Mazzoldi, *Smart Mater.Struc.* 6 (1997) 23-34.
- [31] M. S. Dresselhaus, G. Dresselhaus, A. Jorio, A. G. Souza Filho and R. Saito, *Carbon*. 40 (2002) 2043-2061.
- [32] R. Saito, G. Dresselhaus and M. S. Dresselhaus., *Physical Properties of Carbon Nanotubes*, Imperial College Press, London, (1998), P.35.
- [33] M. M. J. Treacy, T. W. Ebbesen and J. M. Gibson, *Nature*. 381 (1996) 678-681.

- 
- [34] J. P. Salvetat, J. M. Bonard, N. H. Thomson, A. J. Kulik, L. Forro, W. Benoit and L. Zuppiroli, *Appl. Phys. A.* 69 (1999) 255-60.
- [35] M. S. Dresselhaus, G. Dresselhaus, P. C. Eklund and R. Saito, *Physics world.* 10 (1997) 12.
- [36] T. W. Ebbesen, H. J. Lezec, H. Hiura, J. W. Bennett, H. F. Ghaemi and T. Thio, *Nature.* 382 (1996) 54-56.
- [37] K. H. An, W. S. Kim, Y. S. Park, J. M. Moon, D. J. Bae, S. C. Lim, Y. S. Lee and Y. H. Lee, *Adv. Func. Mater.* 11 (2001) 387-392.
- [38] K. H. An, K. K. Jeon, J. K. Heo, S. C. Lim, D. J. Bae and Y. H. Lee, *J. Electrochem. Soc.* 149 (2002) A1058-A1068.
- [39] K. Liang, A. Chen, W. Zhou and W. Wang, *Tien Tzu Hsueh Pao/Acta Electronica Sinica.* 30 (2002) 621-623.
- [40] H. Ago, K. Petritsch, M. S. P. Shaffer, A. H. Windle and R. H. Friend, *Adv. Mater.* 11 (1999) 1281-1285.
- [41] D. T. Colbert, *Plastics, Additives & Compounding.* 5 (2003) 18-25.
- [42] M. Hughes, G. Z. Chen, M. S. P. Shaffer, D. J. Fray and A. H. Windle, *Mater. Res. Soc. Symp- Proc.* 703 (2002) 553-558.
- [43] S. Kumar, T. D. Dang, F. E. Arnold, A. R. Bhattacharyya, B. G. Min, X. Zhang, R. A. Vaia, C. Park, R. H. Hauge, R. E. Smalley, S. Ramesh, P. A. Willis and W. Wade Adams, *Macromolecules.* 35 (2002) 9039-9043.
- [44] E. Kymakis, I. Alexandou and G. A. J. Amaratunga, *Synth. Met.* 127 (2002) 59-62.
- [45] I. Musa, M. Baxendale, G. A. J. Amaratunga and W. Eccleston, *Synth. Met.* 102 (1999) 1250.
- [46] V.-T. Truong, M. Tahhan, G. M. Spinks and G. G. Wallace, *Proceedings of SPIE - The International Society for Optical Engineering.* 4935 (2002) 26-31.
- [47] Q. Xiao and X. Zhou, *Electrochimica Acta.* 48 (2003) 575-580.
- [48] J. Zhou, G. Tzamalís, N. A. Zaidi, N. P. Comfort and A. P. Monkman, *J. Mater. Sci.* 36 (2001) 3089-3095.
- [49] C. H. Hsu, H. Shih, S. Subramoney and A. J. Epstein, *Synth. Met.* 101 (1999) 677-680.

- 
- 
- [50] D. Yang and B. R. Mattes, *Synth. Met.* 129 **(2002)** 249-260.
- [51] C.-H. Hsu, P. Vaca-Segonds and A. J. Epstein, *Synth. Met.* 41 **(1991)** 1005-1008.
- [52] R. Hirase, M. Hasegawa and M. Shirai, *J. Appl. Polym. Sci.* 87 **(2002)** 1073-1078.
- [53] P. Passiniemi, J. Laakso, H. Osterholm and M. Pohl, *Synth. Met.* 84 **(1997)** 775-776.
- [54] A. B. Dalton, S. Collins, Joselito Razal, Edgar Munoz, V. H. Ebron, B. G. Kim, Jonathan N. Coleman, J. P. Ferraris and R. H. Baughman, *J. Mater. Chem.* 14 **(2004)** 1-3.
- [55] B. Vigolo, A. Penicaud, C. Coulon, C. Sauder, R. Pailier, C. Journet, P. Bernier and P. Poulin, *Mater. Res. Soc. Symp. Proc.* 633 **(2001)** A1211-A1219.
- [56] P. Poulin, B. Vigolo and P. Launois, *Carbon.* 40 **(2002)** 1741-1749.
- [57] B. Kim, V. Koncar, E. Devaux, C. Dufour and P. Viallier, *Synth. Met.* 146 **(2004)** 167-174.
- [58] E. M. Genies, C. Petrescu and L. Olmedo, *Synth. Met.* 41 **(1991)** 665-668.
- [59] P. Yam, *Scientific American.* 273 **(1995)** 82-87.
- [60] A. Ramaratnam and N. Jalili, *Proceedings of SPIE - The International Society for Optical Engineering Smart Structures and Materials - Electroactive Polymer Actuators and Devices (EAPAD).* 5385 **(2004)** 349-356.
- [61] A. Dhawan, T. K. Ghosh, A. M. Seyam and J. Muth, *Mater. Res. Soc. Symp. Proc.* 736 **(2002)** 67-72.
- [62] D. Marculescu, R. Marculescu, N. H. Zamora, P. Stanley-Marbell, P. K. Khosla, S. Park, S. Jayaraman, S. Jung, C. Lauterbach, W. Weber, T. Kirstein, D. Cottet, J. Grzyb, M. Jones, G. Tröster, T. Martin and Z. Nakad, *Proc. IEEE.* 91 **(2003)** 1995-2018.
- [63] E. Fussell, *Intech.* 50 **(2003)** 32-34.
- [64] M. Catrysse, R. Puers, C. Hertleer, L. Van Langenhove, H. Van Egmond and D. Matthys, *Sensors & Actuators A-Physical.* 114 **(2004)** 302-311.
- [65] K. Roncone, *Journal of the Minerals Metals & Materials Society.* 56 **(2004)** 31-33.
- [66] L. E. Dunne, S. Brady, B. Smyth and D. Diamond, *Journal of neuroengineering and rehabilitation.* 2 **(2005)** 4.



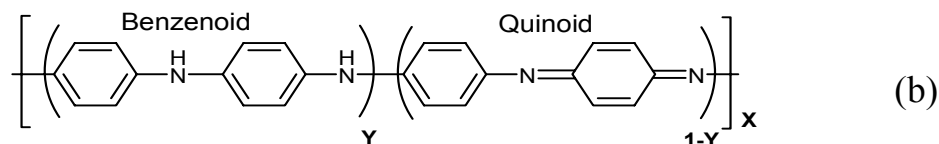
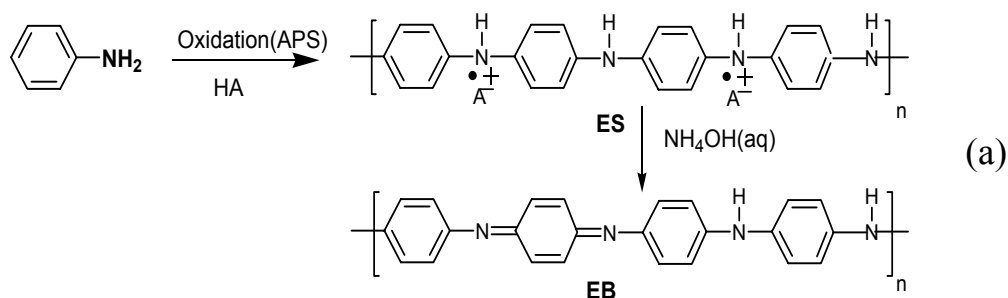
- [67] G. M. Spinks, G. G. Wallace, L. Liu and D. Zhou, Mater. Res. Soc. Symp - Proceedings. 698 (**2002**) 5-16.
- [68] D. Marculescu, R. Marculescu and P. K. Khosla, Proceedings - Design Automation Conference, IEEE. cat. n 02ch37324 (**2002**) 175-180.
- [69] B. C. Company, Smart Fabrics and Interactive Textiles: A Global Market Opportunity Assessment, BCC, Inc., (**2003**).

# ***CHAPTER TWO***

Literature Review

## 2.1. The chemical structure of Polyaniline

Polyaniline (PAni) in the emeraldine salt (ES) form can be synthesised by the oxidation of aniline monomer either by using an appropriate chemical oxidant (i.e ammonium per sulphate (APS)) or electrochemical oxidation in acidic media. In order to produce the emeraldine base form (EB) of the PAni, the process is followed by dedoping of the green ES form using a basic compound (i.e.  $\text{NH}_4\text{OH}$  (aq)) [1-3]. (Scheme 2.1(a))



$Y=0.5$  Emeraldine base (EB)

$Y=1$  Leucoemeraldine base (LEB)

$Y=0$  Pernigraniline base (PGB)

**Scheme 2.1.** (a) A general scheme for polymerisation of Aniline (b) different oxidation state of PAni

The structure of each repeating unit of PAni tetramer contains benzenoid diamine and/or quinoid diimine segments which are present based on the extent of reduction or oxidation. The extent of reduction of the repeating unit of PAni is represented by the Y index as indicated in the chemical structure (Scheme 2.1.b), where X is the degree of

polymerisation.  $Y$  varies between  $Y=1$  for leucoemeraldine base (LEB) to  $Y=0$  for pernigraniline base (PGB) while  $Y=0.5$  corresponds to the emeraldine base (EB). The conductivity of PANi depends both on the oxidation state of the polymer and the degree of protonation, which is characterised by the proton doping level [4]. The maximum conductivity occurs when PANi is protonated at a doping level of 50 %. During the chemical or electrochemical doping process, the PANi (EB) can be doped to the highly conducting PANi (ES) state which consists of amine ( $-NH-$ ) and imine ( $=N-$ ) sites in equal proportion. The imine sites are protonated in preference to give the bipolaron (dication salt) form (Scheme 2.2).

**Scheme 2.2.** Interconversions between different forms of polyaniline [5].

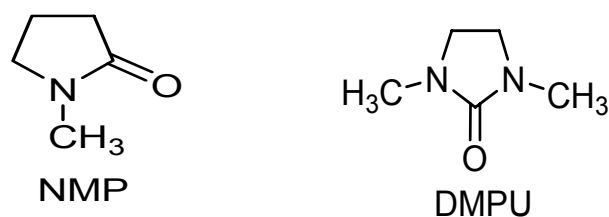
PAni can be switched between different states by the addition of acids and bases that protonate and deprotonate the base sites in tandem with the gain or loss of electrons. These reactions lead to the complex relationship of states that is shown in Scheme 2.2. The electrochemical oxidation or reduction results in a variety of switching paths depending on the pH of the solution. The very critical dependence of the polymer oxidation state to pH of the solution can be seen from Scheme 2.2. For example the LEB form of PAni can be changed to ES upon exposure to acidic solutions ( $1 < \text{pH} < 4$ ), followed by further oxidation. In the mean time, doping process from LEB to ES can be directly conducted by exposing to a lower pH acidic solution ( $\text{pH} < 1$ ).

In solutions of pH greater than 4, PAni loses its electroactivity entirely because the ES form does not form in this PH range. These reversible switches between different oxidation states can be easily observed by cyclic voltammetry when the voltage is cycled in the range of -0.2 V to 1.0 V (vs. Ag/AgCl as reference electrode)[6, 7].

### 2.1.1. The solubility of polyaniline

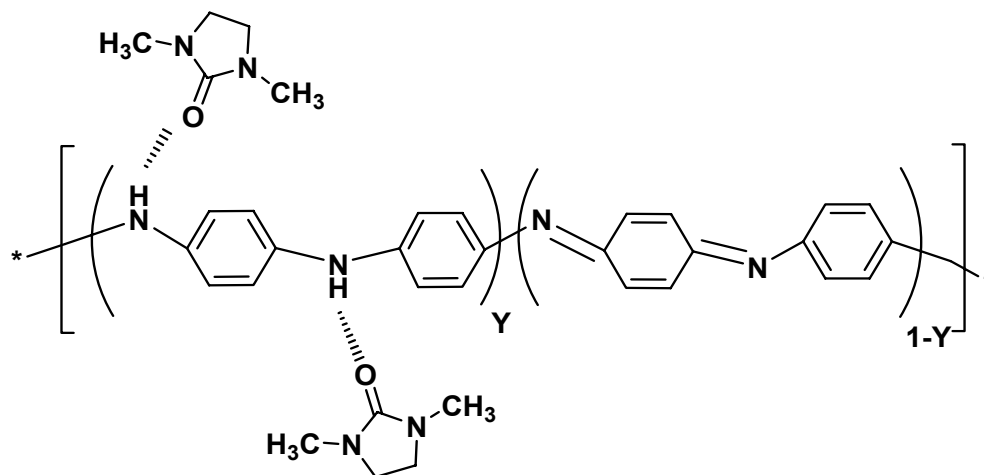
Several methods have been reported to dissolve PAni in the doped (ES) or undoped (EB, LEB) states without changing the molecular structure. Angelopoulos and co-workers reported that the emeraldine base form of PAni is soluble in N- methyl pyrrolidinone (NMP) [5]. More efficient solubility in N,N'-dimethyl propylene urea (DMPU) [8] has been achieved for the EB and LEB oxidation states compared with NMP, according to higher solubility parameters and intrinsic viscosity [8-10]. NMP and DMPU (Scheme 2.3) are both polar solvents with a high dielectric constant and are classified as polar aprotic (dissolving power without hydrogen attached to oxygen or nitrogen) and a Lewis base

solvent. They show a high degree of free electron availability ( $\beta$ ) without hydrogen donicity ( $\Pi^*$ ) [11, 12].



**Scheme 2.3.** The chemical structure of DMPU and NMP

Hydrogen bonding interaction between the amine group of the tetramer repeating unit in PAni (EB) and the carbonyl group of the polar aprotic solvent is responsible for the solubility of EB (Scheme 2.4).



**Scheme 2.4.** Hydrogen bonding between PAni (EB) to DMPU.

### 2.1.2. Aggregation and gel formation of PAni solution

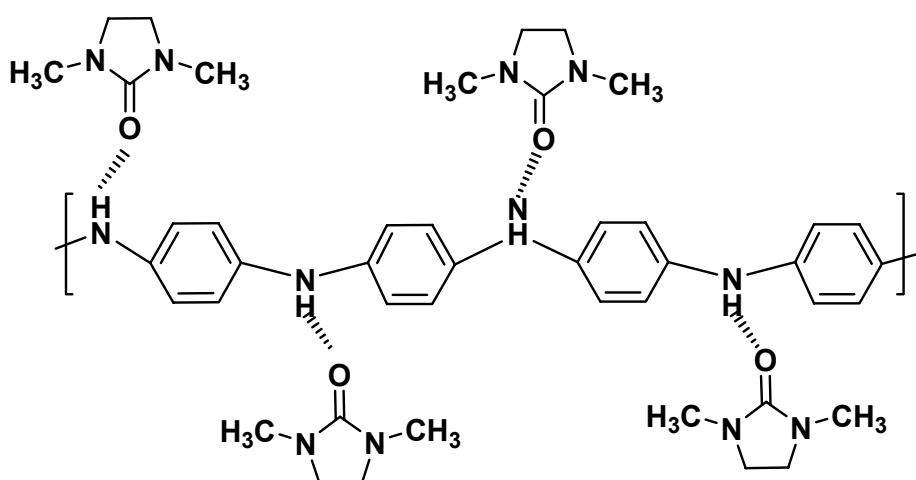
Extrusion methods for fibre manufacturing based on solution processing of PAni in the EB form are loaded with difficulties associated with the instability of the solution at high concentrations. Rapid gelation occurs during a short period of time at both higher

concentration and/or molecular weight of EB in these polar solvents. If the polymer solute concentration is less than 5 % w/w ( which is suitable for film processing), then the development of hydrogen bonding through the interaction of amine and imine groups respectively, in quinoid and benzenoid ring of EB is less likely to occur due to the increased spacing between chains (see Scheme 2.4). However, beyond 5 % w/w, the polymer chains then become more closely spaced, which leads to aggregation and development of a strong, physically cross linked, three dimensional gel network in short periods of time. In this instance, the polymer amine nitrogens, which are not associated with solvent molecules, reform interchain hydrogen bonds with the nearest neighboring imine nitrogen. Gelation will thus develop very rapidly in the more concentrated EB solutions. Jain et.al. [10] have shown that the tendency for gel formation in NMP due to poorer polymer–solvent interaction and stronger polymer–polymer interaction is more than observed in DMPU. A 10 % w/w solution of PANi in NMP gels within 60 min whereas a 17.5 % w/w solution in DMPU did not show any change in viscosity over 400 min. These observations suggest that DMPU is a better solvent compared to NMP for PANi (EB).

PAni fibres have been spun from DMPU with reasonable mechanical properties, but, the reproducibility in spinning solution preparation (14 % w/w) and the instability of spinning solution during the spinning process created serious obstacles for the scaling up of the process [13]. Moreover, for high molecular weight polymers, the use of DMPU alone is not able to inhibit gel formation [14]. In this situation, to achieve a solution that does not gel two different methodologies have been reported. Both methods are based on the removing of the effect of the imine group by using a reducing agent [13] or blocking of

the nitrogen in the imine group by gel inhibitors [14]. The former method is explained since it has been used in the present study.

A reducing agent such as phenyl hydrazine has been employed to change the oxidation state of PANi from EB to LEB. As a result the imine nitrogens are converted to amines in the fully reduced form of PANi. The linkage between the carbonyl group of DMPU and the amine group of PANi (LEB) was illustrated in Scheme 2.5.



**Scheme 2.5.** The interaction of LEB chain with carbonyl group of DMPU

The viscoelastic properties of a solution of 14 % w/w of PANi (EB) and PANi (LEB) in DMPU have been characterised by oscillatory shear rheometry [13]. For the solution of PANi (EB)/ DMPU the storage modulus increased significantly with time indicating a development of elastic interactions leading to the formation of a network structure. Meanwhile, with same PANi content, the LEB form shows a higher loss modulus versus storage modulus during the experiment indicating that formation of an elastic gel was prevented.

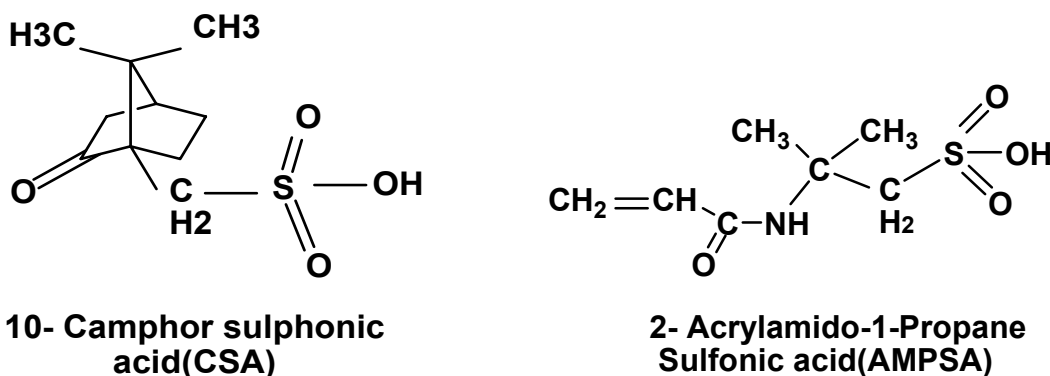


### 2.1.3. The solubility of PANi doped with sulfonic acid in organic acid

PAni (EB) can also be processed from solution if it is functionalised by sulfonic acid to render the resulting PANi complex soluble in organic acids. Cao and co-workers [15] studied the effect of different alkyl groups in dopants  $H^+(M^--R)$  on the solubility of PANi in organic solvents. The counter ion species ( $M^--R$ ) contains a functional group R that was chosen to be compatible with nonpolar or moderately polar organic liquid, and  $M^-$  represent the sulfate anion ( $SO_3^-$ ) group. Utilising functionalised protonic acids with a variety of R groups, results in different levels of solubility in organic solvents and also a range of conductivity values [16]. In addition, the molar ratio of counter ion to the PANi tetramer unit is a critical parameter. According to MacDiarmid [17], for fully protonated PANi a numerical amount of 0.5 should be chosen for the mole ratio of  $H^+$ / PANi tetramer unit. Moreover, it was discovered that various combinations of counterions and solvents could significantly affect the polymer chain conformation and morphology through the specific molecular interactions, and this can drastically modify the electronic properties of PANi [18, 19].

Usually the charged polymer chains are polar in nature, and the polarity of the counterion and solvent play crucial roles in the chain conformation. For instance, in the presence of a combination of camphor sulfonic acid (CSA) in m-cresol or 2-acrylo-amido-1-propane sulfonic acid (AMPSA) (See Scheme 2.6) in dichloroacetic acid (DCAA), the PANi chains tend to form the extended chain conformation [18, 19]. In contrast, the PANi chain in EB and LEB form in solvents like DMPU and NMP tends to coil up [20]. Organic solvents that can dissolve the fully protonated conducting PANi salt, can be divided into two groups [16]. The first group includes substances with strong hydrogen

bonding group, such as cresols, dimethyl sulphoxide (DMSO), NMP, or dichloro acetic acid (DCAA). The second group comprises those solvent without or with weak hydrogen bonding ability such as toluene, xylene, chlorobenzene.



**Scheme 2.6.** Some of sulfonic acid dopants used for one step PANi fibre processing.

Fully protonated PANi can be dissolved in these solvents only by combination with an excess of the same or a different functionalised protonic acid [15]. Table 2.1 demonstrates the performance of some of typical protonic acids and selected solvents on the solubility and conductivity of processed films. The selection of the proper acid and solvent for the acid processing route to fibre formation must first consider those that give a solution with appropriate rheological properties.

The performance of CSA and AMPSA is considerably better than DBSA with respect to higher solubility of PANi using formers dopants in organic acids. Moreover the extended chain in PANi induced by AMPSA or CSA counter ion is preferred in order to induce a highly oriented conducting fibre.

**Table 2.1.** The solubility and conductivity of PANi cast from some typical protonic acids and solvents.

## **2.2. Carbon Nanotubes**

### **2.2.1. Discovery**

A tubular form of Buckminster fullerence was discovered in 1990 [22]. These are capped at each end, for example, by the two hemispheres of C<sub>60</sub>, connected by a straight segment of tube, with only hexagonal units in its structure. Originally called 'buckytubes', they are now more commonly referred to as single wall carbon nanotubes (SWNTS) [23, 24] ( Figure 2.1).

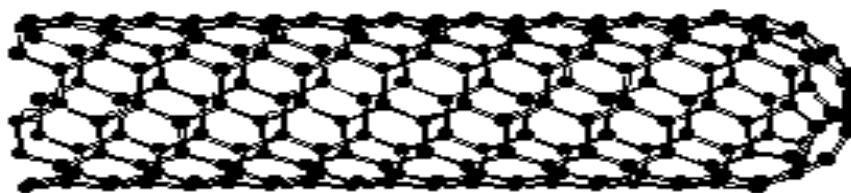


**Figure 2.1.** The tubular structure of graphene layer of SWNT.

Richard Smalley and his group at Rice University (TX) pioneered a laser ablation technique to produce SWNTs. In this process, a quartz tube is heated to approximately 1200 °C in a furnace. Within the furnace, an argon flow at sub-atmospheric pressure is maintained. The tube contains a block of graphite compressed with small amounts of a transition metal catalyst. The laser is used to vaporise the graphite. The nanotubes nucleate in the vapor phase, coalesce, get carried away by the flowing argon and condense downstream on the cooler walls of the quartz tube. The felt-like material, when scraped off the wall, contains single wall nanotubes mixed with graphite and metal particles. Metals such as cobalt and iron are essential catalysts in the production of SWNTs. Smalley's group also developed a high-pressure carbon monoxide (HiPco) process to produce SWNT from gas-phase reactions of iron pentacarbonyl in carbon monoxide at high pressures (10 - 100 atm). The HiPco process is a relatively clean process, i.e., SWNT is obtained with less graphitic deposits and amorphous carbon compared with other method. In the HiPco process, carbon monoxide mixed with a small amount of iron pentacarbonyl ( $\text{Fe}(\text{CO})_5$ ) is heated to produce SWNT. The products of thermal decomposition of  $\text{Fe}(\text{CO})_5$  react to produce iron clusters in gas phase. These metal clusters serve as nuclei upon which SWNT nucleate and grow. Many purification steps, including acid treatment and thermal annealing under different atmosphere, are applied to raw SWNT to reduce the iron content and amorphous carbon [25].

### 2.2.2. Structure of carbon nanotubes

To understand the structure of nanotubes, we start from the structure of graphite which consists of a layer of carbon atoms arranged in a honeycomb structure (see Fig 2.2). These honeycomb layers are stacked on top of each other. During the formation of graphite,  $sp^2$  hybridisation takes place where three hybrid  $sp^2$  orbitals are formed at  $120^\circ$  to each other within a plane. The in-plane bond, referred to as the  $\sigma$ -bond is a strong covalent bond that strongly binds the atoms in the plane. The remaining  $\pi$ -bond is out of plane (perpendicular to the plane) and much weaker than the in-plane bond. A carbon nanotube is formed when one single layer of graphite is wrapped onto itself and the resulting edge joined. The structure of a nanotube can be defined using a chiral vector  $C_h$  and a chiral angle  $\alpha$  as shown in Figure 2.2.

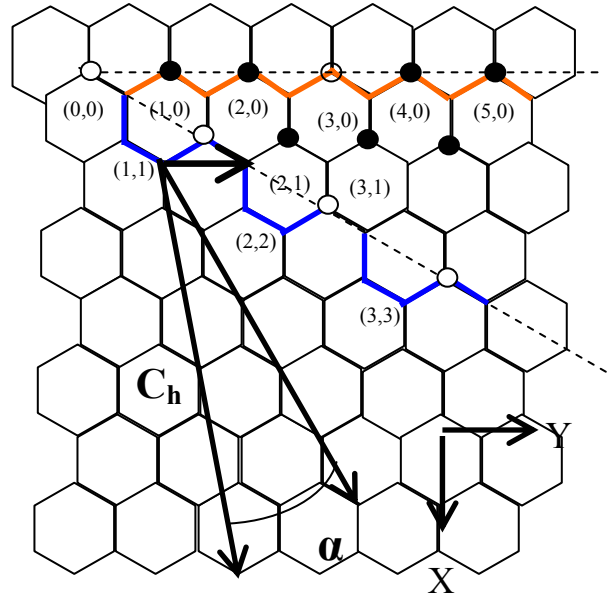


**Figure 2.2.** Different arrangements of nanotubes (●) semiconducting  $(n,0)$  or  $(m,n)$   
 (○) metallic  $(n,n)$  or  $(m,n)$  [  $n-m = 3q$  ],  $q$  is integer

The chiral vector can be defined as a linear combination of base vectors  $\mathbf{a}$  and  $\mathbf{b}$  of the basic hexagon,  $C_h = n\mathbf{a} + m\mathbf{b}$ , with  $m$  and  $n$  being integers. The roll-up vector is

perpendicular to the axis of the nanotube. Referring to Figure 2.2 and Table 2.2, three different types of nanotubes including armchair, zigzag and chiral are defined by the values of  $m$  and  $n$ . It has been shown that the  $(n,m)$  indices can be employed for measurement of the nanotube diameter, the chiral angle, the electronic energy bands and the density of electronic states [26].

**Table 2.2.** Different chirality based on chiral angle [26].

### **2.2.3. The physical properties of SWNTs**

#### **2.2.3.1. Aspect ratio**

According to different characterisation methods, it has been shown that SWNTs typically have a diameter in the range of 1- 4 nm and aspect ratio of  $10^4$ - $10^5$  which can produce a very high surface area in the range of  $\approx 1500 \text{ m}^2/\text{kg}$  [27]. The high aspect ratio of SWNT provides percolation (connected networks) at much lower loadings compared with other carbon fillers. According to literature the percolation level of SWNTs is one and two orders of magnitude lower than Multi wall carbon nanotubes (MWNT), and carbon fibres [28, 29] respectively. In principle, the reinforcement of a polymer matrix depends on the interaction between the filler and the host polymer. Therefore a higher interfacial surface area at lower loadings is an inherent advantage for SWNTs.

### 2.2.3.2. Mechanical properties

The structure of SWNTs provides their unique mechanical properties. The fundamental atomic forces consist of strong  $\sigma$ -bonding and  $\pi$ -bonding forces of C=C bonds to produce their exceptional mechanical properties [26].

It has been shown theoretically and experimentally that SWNTs have the greatest stiffness, both in tension and in bending, of any known fibre [30, 31]. Experimental data on the stress-strain relationship is difficult for very thin SWNT. However, Treacy and co-workers [32] obtained the Young's Modulus of isolated SWNTs by measuring the amplitude of their intrinsic thermal vibrations using transmission electron microscopy. Moreover, the measurement of the elastic modulus of SWNTs has been achieved by atomic force microscopy [33]. Table 2.3 shows the typical mechanical properties of different type of nanotubes compared with other strong materials. The comparison between mechanical properties of SWNTs, carbon fibre and metals demonstrate the promising application of SWNTs in manufacturing of light and tough materials.

**Table 2.3.** Typical mechanical properties of SWNTs compared with metals and carbon fibre

---

<sup>1</sup> density

<sup>2</sup> Young's Modulus

<sup>3</sup> Strength

The combination of stiffness and toughness make SWNTs the strongest known fibres in tension - around 100 times stronger than high-strength steel at one-sixth the weight. These are very important properties when considers the use of SWNT in composite material for reinforcement of the mechanical properties of the host matrix.

### 2.2.3.3. Electrical properties

Carbon in a planar graphene sheet is bonded in such a way that one electron per carbon atom is liberated to move freely, rather than stay near its 'home' atom. This is the situation in metals, where some electrons are not bound to their donor atom, but can easily be pulled in different directions under the influence of an electric field [45]. The quantum mechanics of graphene results in a semi-metal, a situation where the in-plane conductivity is only moderate and similar to that of a poorly conducting metal, such as lead. However, when rolled into a perfect tube, carbon-carbon bonds that are perpendicular to the tube axis (as in the armchair tube shown in Figure 2.2) are formed. The resulting electronic structure becomes that of a true metal, like copper or gold. Other ways of rolling up the graphene sheet produce semi-conducting tubes with such a small gap that at a few degrees above absolute zero they have high conductivity; yet others are similar to silicon in their conductivity [46-48]. The metallic behavior occurs when the valence band intersects / touches the conduction band and in SWNTs this condition occurs when  $(n-m = 3q)$ , where  $n$  and  $m$  are the integers which satisfy the tube structure and  $q$  is an integer.

According to this, the armchair tube  $(m,m)$ , mostly shows metallic behavior and zig-zag  $(m,0)$  or chiral SWNTs may show metallic or semi conducting behavior [26]. The latter behaves dominantly as a semiconductor, while, it will have metallic conduction if  $n-m$



would be a multiple of 3 [26, 49]. The metallic chirality may result in an exceptional electrical conductivity (5000 S/cm) [50].

#### **2.2.4. Properties and applications of self assembled SWNT material**

The mechanical properties (stiffness, strength and toughness), electrical properties (semi conducting or metallic behavior), very high aspect ratio and surface area of SWNT materials as compared to other material allow many applications in the form of bucky paper or continues filament. Examples include the application of SWNTs in actuators [51, 52], sensors [53-55], batteries or super capacitors [56-58] and electronic fibres [59-61].

Bucky paper is obtained by filtration of nanotube dispersions using positive or negative pressure [52]. Poulin and colleagues also reported the wet spinning of a SWNT (aq) dispersion into a PVA coagulation bath [62, 63] (Figure 2.3). Baughman and co-workers in a separate study produced mechanically the best ever known organic functional fibre [59]. The mechanical and electrical properties of selected bucky papers and fibres are shown in Table 2.4.

**Table 2.4.** The mechanical and electrical properties of SWNT in the form of bucky paper (mat) and fibres

It can be seen that the bucky papers shows very high conductivity but poor mechanical properties compared with SWNT fibres. PVA is essential for fibre formation but

adversely influences on the conductivity. In spite of reasonable mechanical and electrical properties of the nanotube fibre, the low solidification rate (slow counter diffusion of PVA and surfactant) resulted in a low spinning rate (100 cm/ min) which is a major challenge for commercial production.

**Figure 2.3.** Schematic of the experimental setup used to make nanotube fibres [66].

### 2.2.5. SWNT-CEP composites

The combination of carbon nanotubes with polymers offers many advantages not only to reinforce the physical properties of the host polymer but also to introduce new electronic properties based on morphological modification or electronic interaction between the two components [67-69]. In particular, the combination of carbon nanotubes with  $\pi$ -conjugated polymers (i.e. CEP polymers) is of interest because their  $\pi$ -conjugation enables the polymers to be used as an active material for application in a variety of electronic devices. In CEP/SWNT composites, it has been suggested that either the polymer functionalises the SWNTs [70], or the CEPs are doped with SWNTs [71], charge transfer occurs between the two constituents. For example, addition of SWNTs increases the strength and conductivity of polypyrrole (PPy) [72] as well as the electrical capacitance

[73]. The addition of SWNTs to polyoctylthiophene (POT) has been shown to enhance the conductivity by 5 orders of magnitude with an 11% percolation threshold [74].

Composites of PAni and SWNTs in the form of films [75] or pellets [76] have been prepared by employing of both MWNT [77-79] and SWNT [70, 75] through in-situ [70, 75, 79-82] and ex-situ [70, 83] processes. The ex-situ process includes blending of PAni in a SWNT dispersion or dispersion of SWNT in a PAni solution. However, the polymerisation of aniline in the presence of a SWNT dispersion either chemically [76] or electrochemically [81] is classified as an in-situ process. In another in-situ approach, it has been shown that aniline is capable of dispersing SWNT through formation of a donor-acceptor complex [84] and the monomer can then be chemically [85] or electrochemically [75] polymerised to form PAni/SWNT composite. Cochet et. al. [78] have shown that the resistivity of PAni at room temperature is less than MWNTs. However, the transport properties of the highly filled (50 % w/w) composites obtained by bulk oxidative polymerisation exhibit a one order of magnitude decrease in resistivity as compared to neat PAni through site selective interaction between the quinoid ring of PAni and MWNT. In addition, a weaker temperature dependency of the resistivity was observed in the PAni/SWNT composite compared with neat PAni. Similarly, the composite produced by emulsion polymerisation resulted in a network including PAni and SWNTs that form a new conduction path [76]. As a consequence, a one order of magnitude increase in conductivity has been observed by the addition of 4 % w/w SWNTs. The improvement of conductivity by addition of nanotubes has been also confirmed by other researchers. Huang and his colleagues [75, 85] claimed that the composites prepared from SWNT – aniline solution ( 8 % w/w versus weight of aniline ) via chemical or electrochemical

polymerisation shows a one order of magnitude increase in conductivity compared with the reference polymer. In addition, the higher electroactivity observed over neat PANi films coincide with the promotion in protonation with a doping effect of SWNTs on PANi. The improvement of conductivity has also been observed in the composites generated by ex-situ processes. The measured electrical characteristics of the film processed from a solution of PANi-MWNT (1 % w/w) indicate that the conductivity of the PANi/SWNT composite are nearly an order of magnitude higher than those of the neat PANi. Moreover, the physical characterisation of these composites by thermo gravimetric analysis, tensile testing, dynamic thermal mechanical analysis measurements indicate that the PANi-MWNT composite is more mechanically and thermally stable than neat PANi.

The published literature contains examples of different routes for synthesising and characterising of PANi/SWNTs composites. However, the selection of the optimised method for material preparation and the protocols used for manufacturing of composite fibres needs further attention and is addressed in this study.

## **2.3. Wet spinning of Polyaniline (PANi)**

### **2.3.1. General description of the wet spinning process**

Spinning from solutions is applied in the case of those polymers which do not form a viscose melt but can be dissolved in high enough concentration in suitable solvents. When a polymer is soluble in a volatile solvent (e.g. ether, acetone, tetrahydrofuran ) a dry spinning procedure is applied. The other fundamental method of spinning from solution, wet spinning is applied to polymers which do not melt and dissolve only in non volatile solvents [86]. The set up for a commercial wet spinning process is shown in Figure 2.4.

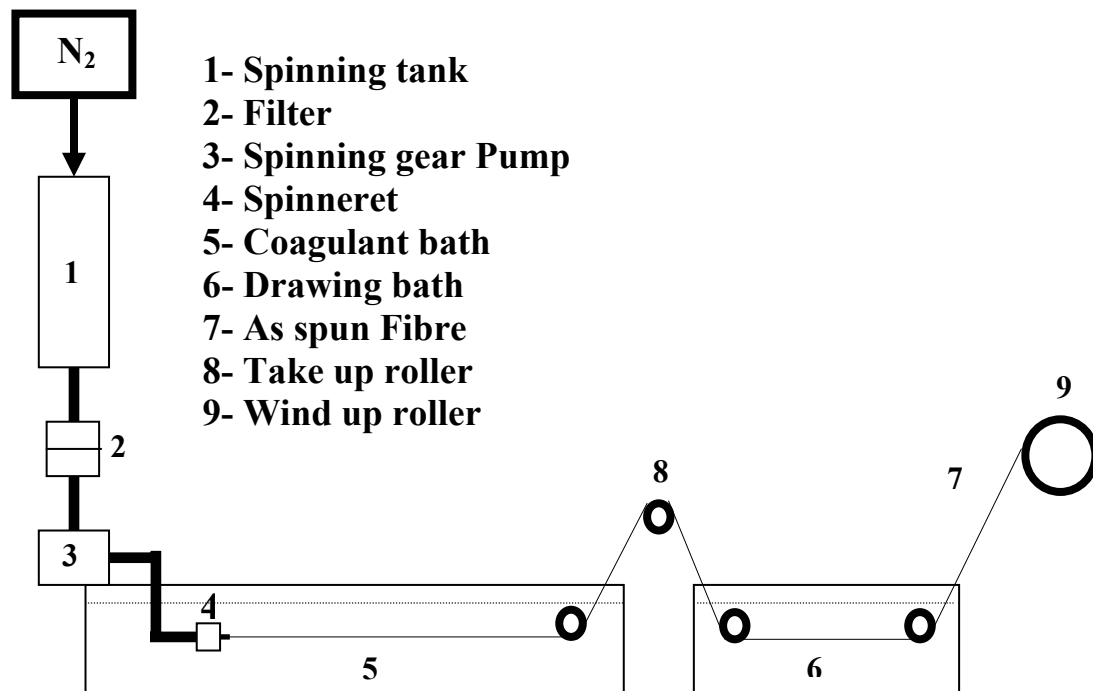


**Figure 2.4.** Schematic showing the set up used for wet spinning of fibres

Wet spinning consists of the extrusion of polymer solution into a liquid bath containing low molecular weight substances miscible with the solvent but that do not dissolve the polymer. In this coagulation bath, the polymer is precipitated from the solution, and a solid ‘gel filament’ containing considerable amounts of solvent and coagulating agent is formed. Solidification occurs because of the exchange of solvent and non-solvent. The solvent diffuses out of the extrudate into the bath, and a non-solvent diffuses from the bath into the extrudate. The polymer precipitates as a gel initially at the extrudate-coagulant interface but progressively throughout the extrudate. The final structure of the fibres arises through counter diffusion processes involving solvent and non solvent occurring during membrane formation [87]. The coagulated filaments pass over a guide toward driven rollers. The steps after coagulation vary according to the product but typically include washing, stretching and drying. The optimisation of process variables such as solvent/ non solvent pairs,

polymer concentration and molecular weight composition of polymer solution (i.e. fillers and additives) , residence time in the coagulation bath, dimension of spinneret , take up and wind up velocity or stretch applied during spinning must all be considered. Extensive research has been conducted with the goal of producing high tenacity, conductive, electro-active, homogenous and reproducible PANi fibres using the wet spinning process [87-102].

### 2.3.2. A literature review for PANi fibre formation

PAni fibres has been produced using either a two step [13, 88, 93, 99, 103-105] or one step process [98, 101]. In the two step process concentrated PANi solutions in the form of EB [93] or LEB [13] have been prepared by using gel inhibitors such as 2-methyl aziridine (2-MA) [103], 4-methyl piperidine, (4-MP) [106] and pyrrolidine [93] or reducing agents such as phenyl hydrazine [13] in N-methyl pyrrolidinone (NMP) or dimethyl propylene urea (DMPU) respectively. Fibres have subsequently been spun from these solutions.

**Table 2.5.** The mechanical and electrical properties of neat PANi fibre produced by the two step process.

---

<sup>4</sup> Fibre process is designated as: polyaniline form/solvent, post process

<sup>5</sup> Phenyl hydrazine has been used as reducing agent

<sup>6</sup> Methane Sulphonic acid

The fibres were successively doped with acid to render them conductive. The best results reported in the literatures are represented in Table 2.5. This data reveals the following facts that can be used in the optimisation of processes:

1) The increasing in mechanical strength of the fibres processed from LEB/DMPU is accompanied with a decrease in conductivity. Electrical conductivities for the LEB/DMPU fibres after oxidation and doping gave values of 150 S/Cm which is lower than that observed for EB/DMPU fibres (350 S/cm).

Gregory. et al. [88] stated that this inverse relationship is due to the presence of micro voids in the fibres with the density of the LEB/DMPU fibre is being twice that of the EB/DMPU materials. It has been claimed that the presence of microvoids in EB fibres causes weaker mechanical properties and facilitates diffusion of dopants resulting in higher conductivities. Less voids generate lower conductivity for LEB fibre and higher mechanical properties. It is worth noting that the dopants that have been used for the two samples are different. However, in reference [88] the role of dopant has been ignored and the higher conductivity was attributed solely to micro voids. Micro voids also cause facile dedoping through removing of volatile dopant. Wang et.al. [103] reported that Benzene Phosphinic acid (BPA) is a more efficient dopant than HCl and achieves higher conductivity due to reduced volatility. In addition, results of other studies [107, 108] emphasised that doping the fibre with inorganic acids (HCl) embrittles the fibre as a result of reduced cohesion force between polymer chains. In contrast doping with organic acid

---

<sup>7</sup> Solution also contained a 2- MA as Gel inhibitor

<sup>8</sup> Benzene Phosphinic acid

(acetic acid, benzene phosphinic acid,  $\text{MeSO}_3\text{H}$ ) may produce better mechanical and electrical properties [88].

2) Acid doping raises conductivity but is detrimental to mechanical properties. The tensile strength of both LEB/DMPU and EB/DMPU fibres decreased more than 50% after acid doping.

3) The processing of PANi fibres from EB/NMP/2-MA significantly decrease the conductivity compared with fibres produced from EB/DMPU without any gel inhibitor present. By contrast, the conductivity of PANi fibre doped with HCl processed from EB/NMP without gel inhibitor shows a conductivity in the range of 20 S/cm. Therefore the low conductivity obtained in the presence of the gel inhibitor can be attributed to a decrease in the degree of delocalisation along the polymer backbone.

The main problem in the fibre spinning process involves post doping. If the doping acid can diffuse into the fibre, to be effective as a dopant, then it is also possible for it to diffuse out again during storage or use. Secondly, in most cases a higher mechanical strength is associated with a denser fibre, so that, only doping of the fibre skin is achieved and dedoping readily occurs. In spite of these problems with the two step process, it has some advantages. These include the high stability of the spinning solution, ease of processing.

The doping of PANi before fibre formation (i.e. in solution form) should result in fibres with more ideal properties. Anderatta et.al. [90] employed concentrated sulfuric acid to produce conductive PANi fibre from protonated PANi solution. The PANi fibres obtained from these acidic processing systems exhibited very poor mechanical properties and moderate electrical conductivity (about 50 S/cm). Another alternative was borrowed from



the discovery by Cao et.al [109] by processing of PANi (ES), using sulfonic acids (see section 2.1.3). Using functionalised sulfonic acids such as CSA, PANi rendered to the doped PANi soluble in many new solvents such as m- cresol (refer to Table 2.1). It has been shown previously that [110] the use of functionalised sulfonic acids gives rise to high levels of crystallinity in the PANi, which directly correlates to a metallic electrical conductivity contribution in the material [111]. The as spun fibre obtained from anisotropic liquid crystalline PANi/ CSA/ m-Cresol solution has a brittle structure and weak mechanical properties but good electrical conductivity.

PAni fibre have also been fabricated directly in the emeraldine salt (ES) conductive form using dichloroacetic acid (DCAA) as solvent and 2- acrylamido-2-methyl-1-propane sulfonic acid (AMPSA) as dopant. Table 2.6 summarises the result obtained from mechanical and electrical conductivity tests.

**Table 2.6.** The mechanical and electrical properties of PANi fibre processed from one step method

However the AMPSA/ DCAA is a desirable dopant/ solvent alternative compared to the CSA/m-cresol system with both lower toxicity and greater processability. It has been observed that the as spun fibre of PAni/AMPSA/DCAA is highly flexible and can be drawn five times versus initial length due to the plasticising effect of AMPSA. That enables high orientation of the polymeric chain to obtain conductivity in the range of metallic material in the stretched form. These values are higher than can be obtained with the PAni/CSA/m-cresol formulation [21]. It has been shown that the ultimate tensile strength and elastic modulus of 5x drawn fibres of PAni/ AMPSA/DCAA fibre can be improved respectively to 97 MPa and 2 GPa by thermal stretching.

Despite having excellent conductivity, fibres spun from the PAni/AMPSA/DCAA, the mechanical properties are inferior to fibres obtained from EB/DMPU and LEB/DMPU fibres. Moreover, the mechanical properties of all these PAni fibres are inferior to natural or synthetic fibres applicable in the textile industry (See Table 2.5, 2.6 and 2.7).

**Table 2.7.** The mechanical properties data of some synthetic and natural fibre[113]

In this regard several studies have been conducted to produce composite fibres of PANi and common thermoplastic polymers such as poly- $\omega$ -aminoundecanoyl (Nylon 11) [114, 115], poly-phenylene terephthalamide (Kevlar) [99, 116] using wet spinning process. In both group of studies, concentrated  $H_2SO_4$  has been used as both solvent and dopant, however, the former requires post doping using dilute HCl to be conductive. The tensile strength and modulus of the PANi/Kevlar composite fibre are very high due to the presence of Kevlar, with highly oriented polymer chains, compared to PANi/nylon 11, with low compatibility of PANi as host polymer. These fibres may have promising applications in electrostatic charge dissipation or EMI shielding. However the conductivity is lower than that required for different applications in electronic devices (Table 2.8).

**Table 2.8.** The electrical and mechanical properties of composite of PANi and thermoplastic polymer

There is a need to introduce reinforcing filler that enhances the mechanical properties of PANi fibres while having a positive impact on their electronic properties. In this regard, the use of carbon nanotubes as a conductive reinforcement for PANi has been investigated here. The examples for reinforcement of mechanical and electrical property of matrices

using carbon nanotubes comprise PMMA/SWNT[117], PVA/SWNT[118], Epoxy/SWNT [119] composites as a film or PBO/SWNT [120] and PAN/SWNT as fibre [34]. The superposition of electrical, electrochemical and mechanical properties of neat PANi and SWNT potentially introduce this composite as multifunctional material for diverse applications.

## 2.4. References

- [1] I. D. Norris, L. A. P. Kane-Maguire and G. G. Wallace, *Macromolecules*. 31 (1998) 6529-6533.
- [2] F. Lux, *Polymer*. 35 (1994) 2915-2936.
- [3] E. M. Genies, A. Boyle, M. Lapkowski and C. Tsintavis, *Synth. Met.* 36 (1990) 139-182.
- [4] G. G. Wallace, G. M. Spinks and P. R. Teasdale, *Conductive electroactive polymers*, Technomic Publication, Pennsylvania, (1997), P.113.
- [5] M. Angelopoulos, G. E. Asturias, S. P. Ermer, E. M. S. A. Ray, A. G. MacDiarmid, M. Akhtar, Z. Kiss and A. J. Epstein, *Mol. Cryst. Liq. Cryst.* 160 (1988) 151-155.
- [6] S. N. Bhadani, M. K. Gupta and S. K. Sen Gupta, *Journal of Applied Polymer Science*. 49 (1993) 397-403.
- [7] M. Chakraborty, B. M. Mandal and D. C. Mukherjee, *Polymer International*. 54 (2005) 1158-1162.
- [8] A. P. Chacko, S. S. Hardaker, B. Huang and R. V. Gregory, *Mater. Res. Soc. Symp. Proc.* 413 (1996) 503-511.
- [9] L. W. Shacklette and C. C. Han, *Electrical, Optical, and Magnetic Properties of Organic Solid State Materials - Pittsburgh, PA, USA*. (1994) 157-166.
- [10] R. Jain and R. V. Gregory, *Synth. Met.* 74 (1995) 263-266.
- [11] M. H. Vandam, *Ind. Eng. Chem. Res.* 36 (1997) 4628-4638.
- [12] U. Mayer, V. Gutmann and W. Gerger, *Mater. Res. Chem.* 106 (1975) 1235.
- [13] A. P. Chacko, S. S. Hardaker, R. V. Gregory and R. J. Samuels, *Synth. Met.* 84 (1997) 41-44.
- [14] D. Yang and B. R. Mattes, *J. Polym. Sci. Part B-Polym. Phys.* 40 (2002) 2702-2713.
- [15] Y. Cao, P. Smith and A. J. Heeger, *Synth. Met.* 48 (1992) 91-97.
- [16] Y. Cao, J. Qiu and P. Smith, *Synth. Met.* 69 (1995) 187-190.
- [17] A. G. MacDiarmid, J.-C. Chiang, W. Huang, B. D. Humphery and N. L. D. Somasiri, *Mol. Cryst. Liq. Cryst.* 125 (1985) 309-318.

- 
- 
- [18] Y. Xia, A. G. MacDiarmid and A. J. Epstein, *Macromolecules*. 27 (**1994**) 7212-7217.
- [19] O. T. Ikkala, L. O. Pietila, L. Ahjopalo, H. Osterholm and P. J. Passiniemi, *J. Chem. Phys.* 103 (**1995**) 9855-9863.
- [20] W. Zheng, Y. Min, S-J.Lee, A.G.Macdiarmid, M.Angelopoulous, Y-H.Liao and A.J.Epstien, *Mater. Res. Soc. Symp. Proc.* 413 (**1996**) 535-540.
- [21] P. N. Adams, P. Devasagayam, S. J. Pomfret, L. Abell and A. P. Monkman, *J. Phys: Cond. Mater.* 10 (**1998**) 8293-8303.
- [22] S. Iijima, *Nature*. 354 (**1991**) 56-58.
- [23] D. S. Bethune, *Nature*. 363 (**1993**) 605-608.
- [24] S. Iijima and T. Ichihashi, *Nature*. 363 (**1993**) 603-605.
- [25] I. W. Chiang, B.E.Brinson, R.E.Smalley, J. L. Margrave and R.H.Hauge, *J. phys. Chem. B.* 105 (**2001**) 1157-1161.
- [26] R. Saito, G. Dresselhaus and M. S. Dresselhaus., *Physical Properties of Carbon Nanotubes*, Imperial College Press, London, (**1998**), P.207.
- [27] M. Cinke, J. Li, B. Chen, A. Cassell, L. Delzeit, J. Han and M. Meyyappan, *Chem. phys. Lett.* 365 (**2002**) 69-74.
- [28] k. Lozano, J. Bonilla-Rios and E. V. Barrera, *J. Appl. Polym. Sci.* 80 (**2000**) 1162-1172.
- [29] F. Du, R. C. Scogna, W. Zhou, S. Brand, J. E. Fischer and K. I. Winey, *Macromolecules*. 37 (**2004**) 9048-9055.
- [30] G. Overney, W. Zhong and D. Tomanek, *Z. Phys. D.* 27 (**1993**) 93-96.
- [31] B. I. Yakobson and R. E. Smalley, *Am. Sci.* 85 (**1997**) 324-338.
- [32] M. M. J. Treacy, T. W. Ebbesen and J. M. Gibson, *Nature*. 381 (**1996**) 678-680.
- [33] F. Y. Meng, S. F. Bradely, S. Arepalli and R. S. Ruoff, *Phys. Rev. Lett.* 84 (**2000**) 5552-5555.
- [34] V. Thaliyil, V. sreekumar, T. Li, B. G. Min, H. Guo, S. Kumar, R. H. hauge and R. E. Smalley, *Adv. Mater.* 16 (**2004**) 58-61.
- [35] D. D. L. Chung, *Carbon fiber composites*, Butterworth-Heinemann, Massachuset, (**1994**), P.29.

- 
- 
- [36] O. N. Senkov, D. B. Miracle and S. A. Firstov, *Metallic materials with High structural efficiency*, Kluwer Academic Publisher, MA, USA, (2004), P.152.
- [37] G.-H. Gao, T. Cagin and W. A. Goddard, *Nanotechnology*. 9 (1998) 184-191.
- [38] X. Zhou, J. J. Zhou and Z. C. Ou-Yang, *Phys. ReV. B*. 62, 13692-13696 (2000) 13692-13696.
- [39] B. I. Yakobson, C. J. Brabec, J. Bernholc and 1996, 2511-2514., *Phys. Rev. Lett.* 76 (1996) 2511-2514.
- [40] C. F. Cornwell and L. T. Wille, *Solid State Commun.* 101 (1997) 555-558.
- [41] E. Hernandez, C. Goze, P. Bernier and A. Rubio, *Phys. Rev. Lett.* (1998) 4502-4505.
- [42] J. P. Salvetat, A. J. Kulik, J. M. Bonard, G. Andrew, D. Briggs, T. Stockli, K. Motonier, S. Bonnamy, Francois Boguin, N. A. Burnham and L. Forro, *Adv. Mater.* 11 (1999) 161-165.
- [43] F. Li, H. M. Cheng, S. Bai, G. Su and M. S. Dresselhaus, *Appl. Phys. Lett.* 77 (2000) 3161-3.
- [44] M. F. Yu, O. Lourie, M. J. Dyer, K. Moloni, T. F. Kelly and R.S.Ruoff, *Science*. 287 (2000) 637-640.
- [45] M. S. Dresselhaus, G. Dresselhaus and P. C. Eklund, *Science of Fullerenes and Carbon Nanotubes*, Academic press, New York, (1996), .
- [46] M. S. Dresselhaus, G. Dresselhaus and R. Saito, *Phys. Rev. B*. 45 (1992) 6234.
- [47] N. Hamade, S. Sawada and A. Oshiyama, *Phys. Rev. Lett.* 68 (1992) 1579.
- [48] J. W. Mintmire, B. I. Dunlop and C. T. White, *Phys. Rev. Lett.* 68 (1992) 631.
- [49] R. S. Ruoff and D. C. Lorents, *Carbon*. 33 (1995) 925-930.
- [50] A. Thess, R. Lee, P. Nikolaev, H. Dai, P. Petit, J. Robert, C. Xu, Y. H. Lee, S. G. Kim, A. G. Rinzler, D. T. Colbert, G. E. Scuseria, D. Tománek, J. E. Fischer and R. E. Smalley, *Science*. 273 (1996) 483-487.
- [51] G. M. Spinks, G. G. Wallace, L. S. Fifield, L. R. Dalton, A. Mazzoldi, D. De Rossi, I. I. Khayrullin and R. H. Baughman, *Adv. Mater.* 14 (2002) 1728-1732.
- [52] R. H. Baughman, C. Cui, A. A. Zakhidov, Z. Iqbal, J. N. Barisci, G. M. Spinks, G. G. Wallace, A. Mazzoldi, D. De Rossi, A. G. Rinzler, O. Jaschinski, S. Roth and M. Kertesz, *Science*. 284 (1999) 1340-1344.

- 
- [53] S. Chopra, A. Pham, J. Gaillard and A. M. Rao, IEEE MTT-S International Microwave Symposium Digest. 2 (2002) 639-642 (IEEE cat n 02CH37278).
- [54] L. Dai, Proceedings of SPIE - The International Society for Optical Engineering. 4695 (2002) 237-244.
- [55] S. Ghosh, A. K. Sood and N. Kumar, Science. 299 (2003) 1042-1044.
- [56] J. Y. Lee, K. H. An, J. K. Heo and Y. H. Lee, J. Phys. Chem. B. 107 (2003) 8812-8815.
- [57] K. Liang, A. Chen, W. Zhou and W. Wang, Tien Tzu Hsueh Pao/Acta Electronica Sinica. 30 (2002) 621-623.
- [58] E. Frackowiak, K. Jurewicz, K. Szostak, S. Delpeux and F. Beguin, Fuel Processing Technology. 77 (2002) 213-219.
- [59] A. B. Dalton, S. Collins, Joselito Razal, Edgar Munoz, V. H. Ebron, B. G. Kim, Jonathan N. Coleman, J. P. Ferraris and R. H. Baughman, J.Mater.Chem. 14 (2004) 1-3.
- [60] E. Munoz, A. B. Dalton, S. Collins, M. Kozlov, J. Razal, J. N. Coleman, B. G. Kim, V. H. Ebron, M. Selvidge, J. P. Ferraris and R. H. Baughman, Adv. Eng. Mater. 6 (2004) 801-804.
- [61] B. Vigolo, P. Poulin, M. Lucas, P. Launois and P. Bernier, Appl. Phys.Lett. 81 (2002) 1210-1212.
- [62] P. launois, A.Marucci, B.Vigolo, p.Bernier, A.Derre and P.Poulin, J. Nanosci. and Nanotech. 1 (2001) 125-128.
- [63] P. Poulin, B. Vigolo and P. Launois, Carbon. 40 (2002) 1741-1749.
- [64] B. Vigolo, A. Pe'nicaud, Claude Coulon, C. d. Sauder, R. Paillet, C. Journet, P. Bernier and P. Poulin, Science. 290 (2000) 1331-1333.
- [65] J. N. Coleman, W. J. Blau, A. B. Dalton, E. M. oz, S. Collins, B. G. Kim, J. Razal, M. Selvidge, G. Vieiro and R. H. Baughman, Appl. Phys. Lett. 82 (2003) 1682-1684.
- [66] P. Poulin, B. Vigolo and P. Launoise, Carbon. 40 (2002) 1741-1749.
- [67] C. Stephan, T. P. Nguyen, M. Lamy de la Chapelle, S. Lefrant, C. Journet and P. Bernier, Synth. Met. 108 (2000) 139-149.
- [68] J. Wang and M. Musameh, Anal. Chem. 75 (2003) 2075-2079.



- 
- 
- [69] J. Zeng, B. Saltysiak, W. S. Johnson, D. A. Schiraldi and S. Kumar, *Composites Part B: Engineering*. 35 (2004) 245-249.
- [70] M. Baibarac, I. Baltog, S. Lefrant, J. Y. Mevellec and O. Chauvet, *Chem. Mater.* 15 (2003) 4149-4156.
- [71] H. Zengin, W. Zhou, J. Jin, R. Czerw, J. Smith, W. Dennis, L. Echegoyen, D. L. Carroll, S. H. Foulger and J. Ballato, *Adv. Mater.* 14 (2002) 1480-1483.
- [72] G. Z. Chen, M. S. P. Shaffer, D. Coleby, G. Dixon, W. Zhou, D. J. Fray and A. H. Windle, *Adv. Mater.* 12 (2000) 522-526.
- [73] M. Hughes, M. S. P. Shaffer, A. C. Renouf, C. Singh, G. Z. Chen, D. J. Fray and A. H. Windle, *Adv. Mater.* 14 (2002) 382-385.
- [74] E. Kymakis, I. Alexandou and G. A. J. Amaratunga, *Synth. Met.* 127 (2002) 59-62.
- [75] J. E. Huang, X. H. Li, J. C. Xu and H. L. Li, *Carbon*. 41 (2003) 2731-2736.
- [76] J. Deng, X. Ding, W. Zhang, Y. Peng, J. Wang, X. Long, P. Li and A. S. C. Chan, *Europ. Polym. J.* 38 (2002) 2497-2501.
- [77] S. R. C. Vivekchand, L. Sudheendra, M. Sandeep, A. Govindaraj and C. N. R. Rao, *J. Nanosci and Nanotech.* 2 (2002) 631-635.
- [78] M. Cochet, W. K. Maser, A. M. Benito, M. A. Callejas, M. T. Martinez, J. M. Benoit, J. Schreiber and O. Chauvet, *Chem. Comm.* (2001) 1450-1451.
- [79] T.-M. Wu, Y.-W. Lin and C.-S. Liao, *Carbon*. 43 (2005) 734-740.
- [80] W. Feng, X. D. Bai, Y. Q. Lian, J. Liang, X. G. Wang and K. Yoshino, *Carbon*. 41 (2003) 1551-1557.
- [81] M. Baibarac, I. Baltog, C. Godon, S. Lefrant and O. Chauvet, *Carbon*. 42 (2004) 3143-3152.
- [82] Y. Wang, X. Jing and J. Qiang, *Fuhe Cailiao Xuebao/Acta Materiae Compositae Sinica*. 21 (2004) 38-43.
- [83] P. C. Ramamurthy, A. M. Malshe, W. R. Harrell, R. V. Gregory, K. McGuire and A. M. Rao, *Solid-State Electronics*. 48 (2004) 2019-2024.
- [84] Y. Sun, S. R. Wilson and D. Schuster, *J. Am. Chem. Soc.* 123 (2001) 5348-5349.
- [85] X. H. Li, B. Wu, J. E. Huang, J. Zhang, Z. F. Liu and H. I. Li, *Carbon*. 41 (2002) 1670-1673.

- 
- 
- [86] A. Ziabicki, in *Fundamental of fiber formation*, "General Introduction", Wiley, New York, (1976), 35.
- [87] D. Yang, A. Fadeev, P. N. Adams and B. R. Mattes, *Proceedings of SPIE - The International Society for Optical Engineering*. 4329 (2001) 59-71.
- [88] A. P. Chacko, S. S. Hardaker and R. V. Gregory, *Polymer Preprints*. 37 (1996) 743-744.
- [89] A. Andreatta, Y. CAO, J. C. Chiang and A. J. Heeger, *Synth. Met.* 26 (1988) 383-389.
- [90] A. Andreatta, C. Yong, J. C. Chiang, A. J. Heeger and P. Smith, *Polymer Preprints*. 30 (1988) 149-150.
- [91] C. H. Hsu, J. D. Cohen and R. F. Tietz, *Synth. Met.* 59 (1993) 37-41.
- [92] R. V. Gregory *ANTEC Conference Proceedings*. 2 (1995) 1683-1687.
- [93] B. R. Mattes, H. L. Wang, D. Yang, Y. T. Zhou, W. R. Blumenthal and M. F. Hundeleys, *Synth. Met.* 84 (1997) 45-49.
- [94] E. M. Scherr, A. G. Macdiarmid, S. K. Manohar, J. G. Masters, Y. Sun, X. Tang, M. A. Druy, P. J. Glatkowski, V. B. Cajipe, J. E. Fischer, K. R. Cromack, M. E. Jozefowicz, J. M. Ginder, R. P. McCall and A. J. Epstein, *Synth. Met.* 41 (1991) 735-738.
- [95] K. Tzou and R. V. Gregory, *Synth. Met.* 55-57 (1993) 983-988.
- [96] A. P. Chacko, S. S. Hardaker and R. V. Gregory, *Polymer Preprint*. 38 (1997) 367-368.
- [97] B. R. Mattes, H.-L. Wang and D. Yang, *ANTEC Conference Proceedings*. 2 (1997) 1463-1467.
- [98] S. J. Pomfret, P. N. Adams, N. P. Comfort and A. P. Monkman, *Polymer*. 41 (2000) 2265-2269.
- [99] C. H. Hsu, H. Shih, S. Subramoney and A. J. Epstein, *Synth. Met.* 101 (1999) 677-680.
- [100] H.-L. Wang, R. J. Romero, B. R. Mattes, Y. Zhu and M. J. Winokur, *Journal of Polymer Science Part B-Polymer Physics*. 38 (2000) 194-204.
- [101] S. J. Pomfret, P. N. Adams, N. P. Comfort and A. P. Monkman, *Adv. Mater.* 10 (1998) 1351-1353.

- 
- 
- [102] J. Zhou, G. Tzamalidis, N. A. Zaidi, N. P. Comfort and A. P. Monkman, *J. Mater. Sci.* 36 **(2001)** 3089-3095.
- [103] H. L. Wang, R. J. Romero, B. R. Mattes, Y. Zhu and M. J. Winokur, *J. Polym. Sci. B-Polym. Phys.* 38 **(2000)** 194-204.
- [104] H. L. Wang, Y. Zhu, J. A. Valdez and B. R. Mattes, ANTEC, Conference Proceedings. Brookfield, CT. 2 **(1998)** 1346-1350.
- [105] B. R. Mattes, H. L. Huang and DaliYang, Materials Annual Technical Conference - ANTEC, Conference Proceedings. 2 **(1997)** 1463-1467.
- [106] I. D. Norris, A. G. Fadeev, J. perregrino and B. R. mattes, ICSM 2004 - Australia, Wollongong. **(2004)**.
- [107] C. H. Hsu and A. J. Epstein, *Synth Met.* 84 **(1997)** 51-54.
- [108] Y. Z. Wang, J. Joo, C. H. Hsu, J. P. Pouget and A. J. Epstein, *Macromolecules.* 27 **(1994)** 5871-5876.
- [109] Y. Cao, P. smith and A. J. Heager, *Synth. Met.* 3 **(1992)** 91.
- [110] L. Abell, P. N. Adams and A. Monkman, *Proceeding of SPE ANTEC.* **(1996)** 2991.
- [111] E. R. Holland, S. Pomfret, P. N. Adams and A. P. Monkman, *J Phys: Condens Matter.* 8 **(1996)** 2991.
- [112] C. H. Hsu and A. J. Epstein, *Journal of Engineering & Applied Science.* 2 **(1996)** 1353-1357.
- [113] W. E. Morton and J. W. S. Hearle, in *Physical properties of textile fibres, "Tensile properties"*, Textile Institute, Manchester [England], **(1993)**, .
- [114] Q. Zhang, X. Wang, D. Chen and X. Jing, *J. Appl. Polym. Sci.* 85 **(2002)** 1458-1464.
- [115] Q. Zhang, H. Jin, X. Wang and X. Jing, *Syntethic Metals.* 123 **(2001)** 481-485.
- [116] C.-H. Hsu, P. Vaca-Segonds and A. J. Epstein, *Synth. Met.* 41 **(1991)** 1005-1008.
- [117] R. Haggenmueller, H. H. Gommans, A. G. Rinzler, J. E. Fischer and K. I. Winey, *Chem. Phys. Lett.* 330 **(2000)** 219.
- [118] J. N. Coleman, M. Cadek, R. Blake, V. Nicolosi, K. P. Ryan, C. Belton, A. Fonseca, J. B. Nagy, Y. K. Gun'ko and W. J. Blau, *Adv. Func. Mater.* 14 **(2004)** 791-798.

- [119] Y. Ren, F. Li, H.-M. Cheng and K. Liao, Carbon. 41 (**2003**) 2177-2179.
- [120] S. Kumar, T. D. Dang, F. E. Arnold, A. R. Bhattacharyya, B. G. Min, X. Zhang, R. A. Vaia, C. Park, W. W. Adams, R. H. Hauge, R. E. Smalley, S. Ramesh and P. A. Willi, Macromolecules. 35 (**2002**) 9039.

# ***CHAPTER THREE***

General Experimental Techniques

### 3.1. Introduction

This chapter describes the general preparation and characterisation techniques that were employed in this thesis. The general steps utilised for preparation of composite fibres include:

- A. Preparation of spinning solution using ex-situ blending of Single walled carbon nanotubes (SWNTs) and polyaniline (PAni)
- B. Fibre formation of spinning solution to produce as spun fibre
- C. Thermal stretching and chemical treatment

The various techniques used to characterise the materials before and after fibre processing includes:

#### I. Techniques used in preparation of spinning solution

- a. Elemental analysis
- b. Dynamic light scattering
- c. Shear viscometry
- d. UV-Vis -NIR spectroscopy

#### II. Techniques used for characterisation of solid fibre

- a. The measurement of fibre diameter using optical microscopy.
- b. Determination of density and denier of produced fibres.
- c. Determination of electrical conductivity by four-probe method.
- d. Measurement of tensile mechanical properties.
- e. Cyclic voltammetry (CV).
- f. Identification of thermal transitions using differential scanning calorimetry (DSC).

- g. Dynamic mechanical analysis (DMA) to identify viscoelastic properties of composite fibres
- h. Raman spectroscopy for study of interaction between constituents, distribution of SWNT and load transfer mechanism using two modes including spot and mapping
- i. Scanning Electron Microscopy (SEM)
- j. Transmission electron Microscopy (TEM)
- k. Focused Ion beam milling for sectioning of composite fibre (FIB)

### **3.2. Preparation of spinning solution using ex-situ approach**

This step involved ultrasonication of SWNTs in the appropriate solvent followed by blending of the dispersion with the PANi. SWNTs in various forms (i.e. powder, pellet, bucky paper) in purified formulation were dispersed in different solvents for various times, depending on the procedure (i.e. one step or two step). It was shown that the time of sonication and transmitted ultrasonic energy to nanotubes are extremely effective on changing the geometry of nanotube and consequently reduce the effectiveness of nanotubes for reinforcing purpose[1]. A high power horn ultrasonicator (Sonics & Material Inc, 500 W) with adjustable time, power and pulsing program was employed to properly exfoliate and homogenously distribute the SWNTs in the solvent. A default power and pulsing program was used and the sonication time was optimised using dynamic light scattering and viscometry techniques. The glass vial containing SWNTs and solvent was maintained in the water bath to control the temperature rise which can be produced by ultrasonic energy. Figure 3.1 schematically shows the sonication unit used to obtain SWNT-solvent dispersion. The appropriate

amount of SWNTs was sonicated to prepare homogenous dispersions which were then transferred to a pressure vessel which includes a blade blender connected to overhead stirrer (Figure 3.2).

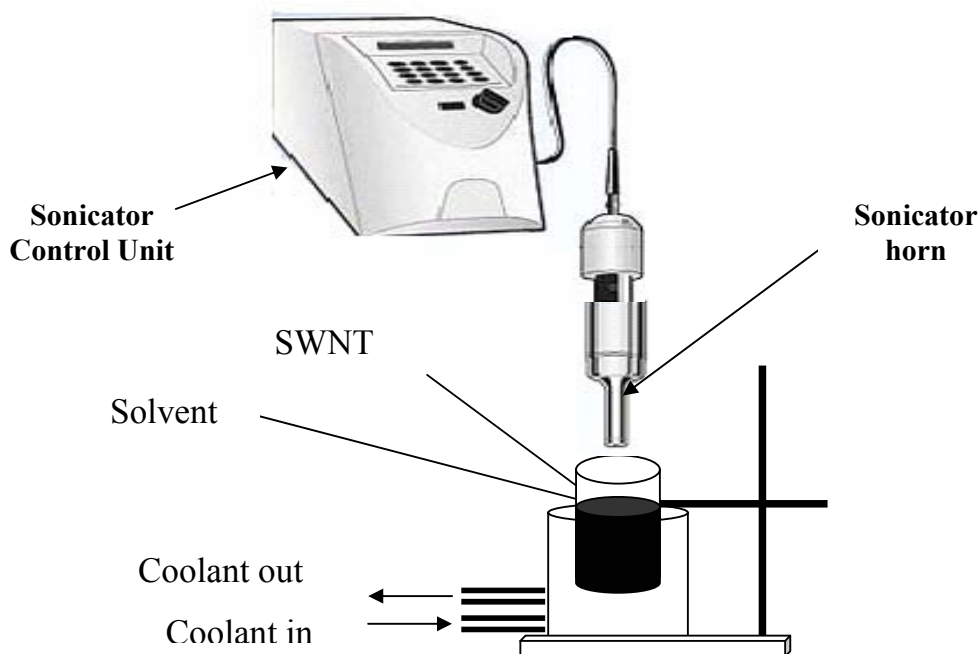


**Figure 3.1.** Schematic of sonication unit for dispersion of CNTs in the solvent.

Polyaniline (EB), (MW = 280000-300000, Santa Fe Science & Technology Inc.) was added to the SWNTs dispersion gradually to prohibit any agglomeration and the composite spinning solution was stirred for a specific period of time under  $N_2$  pressure. There are several parameters such as temperature of mixing, stirring rate and duration that should be controlled to produce highly spinnable solution. The experimental set up used for preparation of the PAni-SWNT solution is shown in Figure 3.2. Stirring of the solution produces thermal energy due to shear which amplifies the possibility of hydrogen bonding and gel formation. The shear rate can be controlled by rotation rate and the effect of shear build up on heat propagation is



controlled by a water bath. Finally, after obtaining a homogenous solution, deaeration under a dynamic vacuum ensured a bubble free solution that is necessary to prevent fibre breakage during spinning. The solution is filtered prior to spinning to remove any agglomeration.

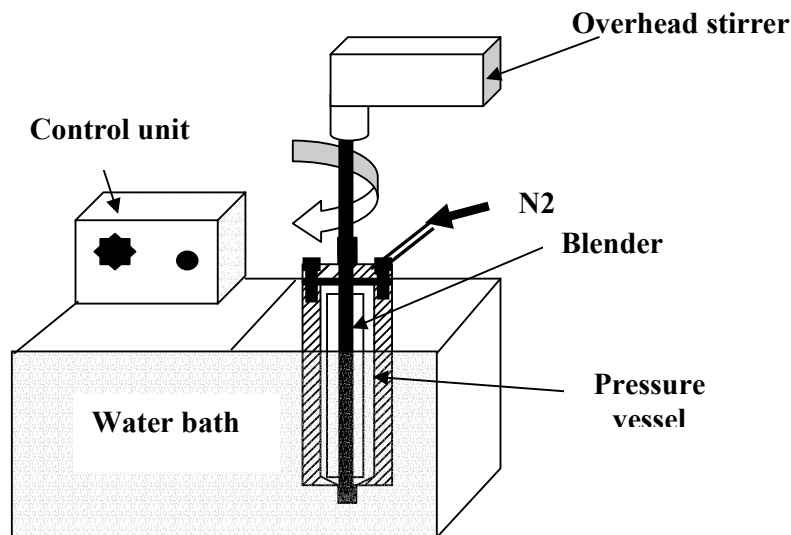


**Figure 3.2.** The schematic of blending unit for mixing of PANi and SWNT dispersion.

### 3.3. Characterisation of spinning solution

#### 3.3.1. Elemental analysis

SWNT samples were sent to Australian National University (ANU) for elemental analysis. The data presented are based on weight percent of each element.

#### 3.3.2. Dynamic Light Scattering (DLS)

##### 3.3.2.1. Theoretical background

Dynamic light scattering (DLS) is a routine method used for particle size measurements. DLS provides many advantages as a particle size analysis method that measures a large population of particles in a very short time period, with no

manipulation of the surrounding medium. Modern DLS instruments, notably the Zetasizer Nano System (Malvern Instruments, Southborough, MA), can measure particle sizes by detection and analysis of scattered light when a 632 nm He /Ne laser beam incidents the dispersed particle. Furthermore the system uses the NIBS (non-invasive back scatter) technology where the optic system is not in contact with the sample. Back scatter is detected in this system and the measurement position can be changed automatically by software based on the concentration of the sample. NIBS technology reduces multiple scattering effects, because the laser beam does not have to travel through the entire sample. This means that higher concentrations of sample can be measured. Figure 3.3 shows a general schematic of the NIBS system. Contaminants such as dust particles within the dispersant scatter light mainly in the forward direction. Therefore, backscatter detection reduces the effects of dust.

**Figure 3.3.** Schematic diagram showing the measurement position for (a) small, weakly scattering samples and for (b) concentrated, opaque samples.[2]

#### **3.3.2.2. Sample preparation**

The tubes and the caps are first soaked for at least one hour in hot soap. Then they are rinsed thoroughly in water followed by acetone. In order to completely dry the tubes,

they are placed in an oven ( $T > 50\text{ }^{\circ}\text{C}$ ) over-night. The dispersion after long enough sonication was poured into the cube glass cuvette and placed in the sample holder and examined under the red laser beam of 632 nm (He/Ne). No further dilution and filtration has been carried out on the sample to achieve real condition of aggregates after sonication. For each experiment 10 measurements with 10 min delay were performed in order to study the stability and interaction of particles.

### 3.3.2.3. The measurement description

As a consequence of the particle motion, light scattered from the particle group will fluctuate with time. These intensity fluctuations are measured across a very short time interval and used to calculate correlation data as shown in equation 3.1( where  $t$  is start time, and  $\tau$  is delay time) [3, 4]. This delay is used to produce a correlation curve. From the correlation curve the particle diffusion coefficient is extracted based on the standard algorithm. The correlation curve can be fitted to a single exponential form as given in Equation. 3.1 where  $B$  is the baseline,  $A$  is the amplitude, and  $D$  is the translational diffusion coefficient. The scattering vector ( $q$ ) is defined by equation 3.2, where  $n$  is the solvent refractive index,  $\lambda_0$  is the vacuum wavelength of the laser, and  $\theta$  is the scattering angle.

$$G(\tau) = \int_0^{\infty} I(t)I(t + \tau)dt = B + Ae^{-2q^2D\tau} \quad \text{Equation 3-1}$$

$$q = \frac{4\pi n}{\lambda_0} \sin\left(\frac{\theta}{2}\right) \quad \text{Equation 3-2}$$

The particle radius obtained from curve fitting is defined as the hydrodynamic radius and is calculated using the Stokes-Einstein equation (Equation 3.3).

$$D(H) = \frac{kT}{3\pi\eta D} \quad \text{Equation 3-3}$$

$D(H)$  = Hydrodynamic diameter (nm)

$D$  = Translational diffusion coefficient ( $\text{m}^2/\text{s}$ )

$k$  = Boltzmann's constant ( $1.3806503 \times 10^{-23} \text{ m}^2 \text{ kg s}^{-2} \text{ K}^{-1}$ )

$T$  = Absolute temperature (K)

$\eta$  = Viscosity (mPa.s)

The radius derived from the translational diffusion coefficient is that of a hypothetical hard sphere that diffuses with the same speed as the particle under experiment. SWNTs are rod shape, so the size given by DLS is not meant to be an accurate dimension (i.e. length and diameter) but rather a relative measure of the degree of SWNT dispersion in the solvents used.

### 3.3.3. Viscometry

After preparation of the spinning solutions and before fibre spinning, viscometry was used to determine rheological properties. The break-up of a fluid jet is influenced by the ratio of the surface tension to the viscosity of the solutions. The higher the ratio, the more probable is the break up. The surface tension of organic polymers varies over a very short range (i.e. 20-80 dyn/cm) while viscosity changes over several order of magnitude depending on composition, molecular weight and the preparation condition used [5]. The magnitude of the zero shear viscosity,  $\eta_0$ , determines the ability to extrude a solution through spinneret channels to ensure production of long threads without breakage.

Viscometry in the shear mode has been measured in two formats, versus time in constant shear rate ( $\dot{\gamma} = 1 \text{ s}^{-1}$ ) and versus shear rate with a short time duration between

each shear rate step. The viscosity of the polymer solution was measured using a Brookfield viscometer (RV-DV II+) using spindle DIN 85-87. The DIN Adapter Accessory (DAA) is a cylindrical spindle geometry that conforms to the DIN 53019 specification. Three spindles and three chambers are provided. The DIN chambers fits into a flow jacket so that precise temperature control can be achieved when a circulating temperature bath is used. The stirring action of the rotating spindle, plus the small sample volume helps to keep the temperature gradient across the sample to a minimum value. The viscometer was equipped with software (Rheocalc 2.4) to collect, store data and allow it to be plotted or analyzed. The DV-II+ PRO with variable speed capability from 0.01 to 200 rpm can continuously display viscosity (cP or mPa·s), temperature (°C or °F), shear rate, shear stress, % torque. The data is reliable when % torque is in the range of 10-100%.

**Table 3.1.** Viscosity ranges and spindles.

Viscosity Range (cP)		
Spindle 85 Minimum - Maximum	Spindle 86 Minimum - Maximum	Spindle 87 Minimum – Maximum
6 - 5000	36.5 - 10,000	121.3 - 150,000

#### 3.3.4. UV-Vis and UV-Vis- NIR spectroscopy

Ultra violet Shimadzu 1601 and Cary 5000 spectrophotometers were employed to cover the wavelength range of 190-1100 and 175 to 3000 respectively. The scanning speed varies between 60 nm/min -3200 nm/min. The photometric range in absorbance mode can be changed between 0.5 to 3.99 ABS (arbitrary unit). Before starting the experiment pure solvent is placed in the sample compartment and the base line

correction automatically is carried out by the instrument. Each sample was filtered using a syringe filter 0.45  $\mu\text{m}$  pore size (Milipore) before spectra were obtained.

### **3.4. General description of spinning process**

#### **3.4.1. Spinning apparatus**

The fibre spinning apparatus is illustrated in Figure 3.4. In order to simplify the ease of operation, the spinning solution is pressurised in the same pressure vessel which was used for its preparation. The inner surface of the pressure vessel was smoothly polished to be used as a cylinder for moving of a piston to drive the material. The spinning solution contained in the pressure vessel is pushed through two stages of stainless steel filter (400 $\mu\text{m}$  and then 200  $\mu\text{m}$ , Millipore) using  $\text{N}_2$  pressure and then passed through an in-line tube with diameter 1mm to deliver the solution to the spinneret head. The filtered spinning solution then passes through a single hole spinneret (with  $L/D = 4$  and  $D = 250 \mu\text{m}$ ) and finally to the coagulation baths. According to the literature the lower the diameter of the spinneret and the higher number of hole in spinneret, better the mechanical property obtained [5]. However, here a diameter of 250  $\mu\text{m}$  and a one hole spinneret was selected for ease of usual maintenance. For homogenous and steady state flow in the spinneret, the aspect ratio (the ratio of length and diameter of spinneret) of 1-5 has been recommended for fibre spinning based on boundary layer theory [6]. In this study the flow rate has been fixed in each experimental setup using the control of  $\text{N}_2$  pressure. The length of the first and second bath is 2m and 1m respectively. In the first coagulation bath solution solidifies and the emerging fibre was taken up on the first bobbin ( $D = 2.5 \text{ cm}$ ). Then the semi-

solid fibre was passed through the second bath guided by smoothly rotating PVC rollers and collected using a linear velocity that was twice that used as the first bobbin.

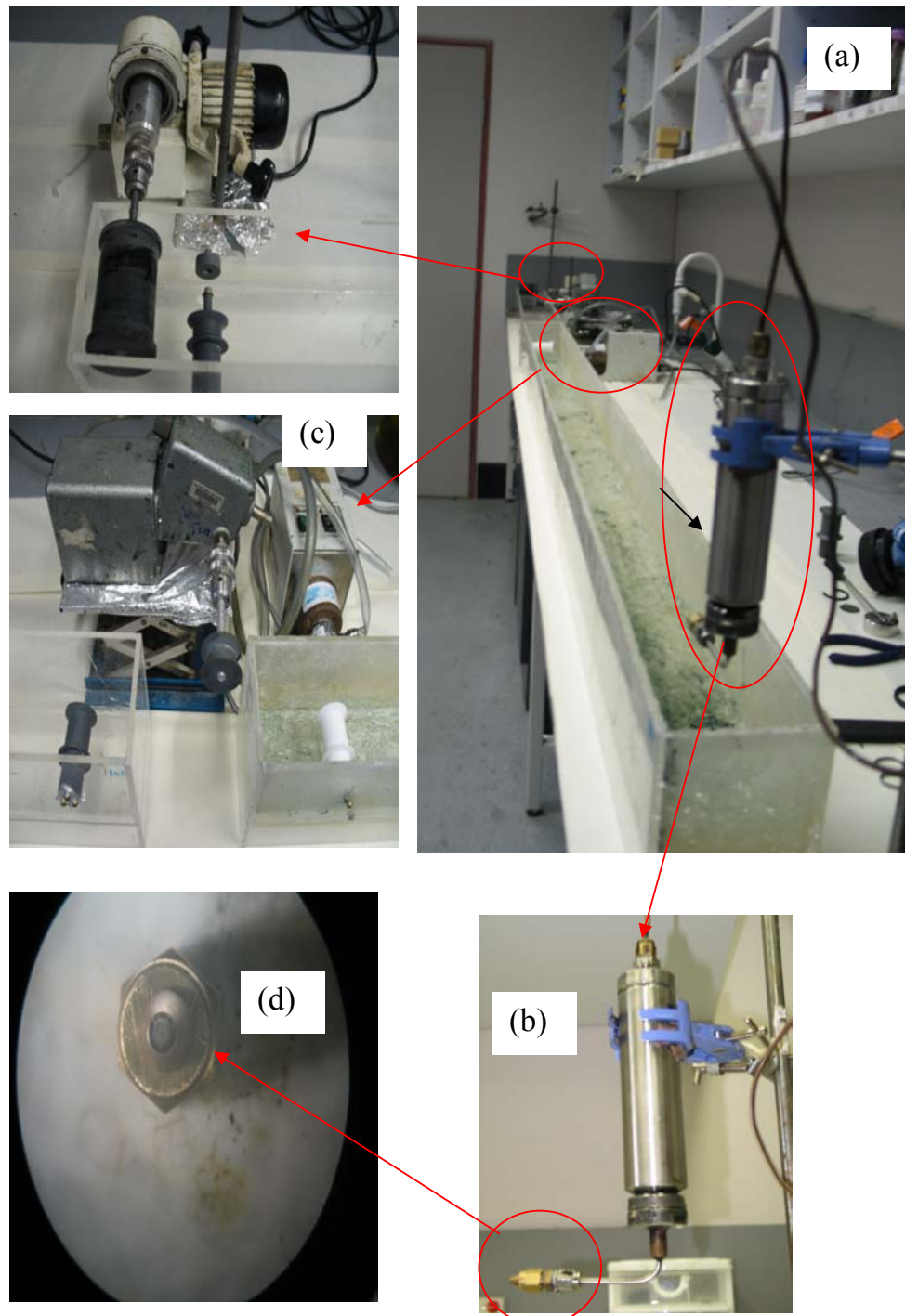


**Figure 3.4.** The picture of spinning line apparatus has been used in this study (a) whole apparatus (b) pressure vessel (c) take up and drawing roller (d) spinneret

### 3.4.2. Drawing

As-spun fibres normally exhibit low tensile strength, high irreversible deformability, low elastic modulus and low electrical conductivity. The stretching of as spun fibres is accompanied with extension and orientation of polymer chains along the fibre axis with a concomitant improvement in electrical and mechanical properties. In this work drawing was performed in three steps:

1. Taking up of the as spun fibre on first bobbin
2. Cold (one step) or hot (two step) drawing between first and second bobbin
3. Thermal drawing of fibre collected on second bobbin in higher temperature.

The first and second step was accomplished continuously; however, the final step was carried out in a separate operation. The adjustment of injection rate ( $V_i$ ), take up velocity ( $V_t$ ), drawing velocity ( $V_d$ ) or spin draw ratio ( $\phi_s = V_d / V_t$ ) and thermal draw ratio ( $\phi_{th}$ ) determine the fineness and diameter of as spun fibre. The fineness of the fibre is characterised by the denier value which shows the mass of 9000 meter of yarn in gram. If a steady state flow of polymer with density of  $\rho_s$  (g/cm<sup>3</sup>), weight fraction of  $\omega_p$ , volumetric flow rate of  $Q$  (cm<sup>3</sup>/min) would be injected from a spinneret with diameter of  $D$  (mm), then following formula demonstrate the denier of the fibre.

$$Denier = \frac{Q \times \rho \times \omega_p}{V_t \times \phi_s \times \phi_{th}} \times 9000 \quad \text{Equation 3-4}$$

The maximum take up velocity of threads attaining the lowest porosity is a critical parameter which varies as a function of coagulation rate. A higher coagulation rate means shorter solidification path or shorter time required for the solidification boundary to reach the centre of the forming fibre ( $t_R$ ). This time is a function of



spinneret diameter, concentration of solvent in phases, diffusion coefficients and the length of the coagulation bath. For a definite formulation of spinning solution, the maximum concentration of solvent in the coagulation bath can be experimentally found based on skin formation of a long and continuous thread without breakage. Then, a range of take up speeds should be examined to find the proper take up velocity to obtain proper  $t_R$  and produce a non porous solid.

The fibre collected on the first bobbin has plenty of solvent that acts as a plasticiser producing a semisolid fibre. The fibre readily stretches between the first and second bobbins to a specific spin draw ratio. The higher the spin draw ratio, the more oriented and the thinner the fibre that can be obtained. The final step of stretching is a critical step, because the final morphology will be determined during a thermal stretching process. Heating the fibres above the glass transition temperature ( $T_g$ ) allows drawing without plastic fracture or neck type deformation.  $T_g$  is measured by thermal analysis using either differential scanning calorimetry or dynamic mechanical analysis. The thermal drawing process involves stretching of the as-spun fibre to different extents across a soldering iron wrapped with Teflon tape. The temperature of the soldering iron was adjusted based on the glass transition temperature of as spun fibre. The  $T_g$  can be reduced by the presence of residual solvent in the un-drawn fibre. The physical and structural properties of drawn fibre extremely depend on the draw ratios ( $\phi_s$  and  $\phi_{th}$ ). Tensile strength ( $\delta_b$ ), Young's Modulus ( $E$ ), and yield stress ( $\delta_{y=0.2}$ ) increase monotonically with draw ratio; however breaking elongation ( $\epsilon_b$ ) decrease monotonically with increased draw ratio. In addition, a higher draw ratio decreases the porosity through collapsing of voids formed in solidification of the solution spun fibres and changes the sorptional properties.

### 3.5. Techniques for characterisation of solid fibre

#### 3.5.1. Four probe electrical conductivity

The conductivity of the conductive fibres was measured using the four point-probe technique. A homemade four probe electrical conductivity cell operated at constant humidity and temperature has been employed. The electrodes were circular pins with separation distance of 0.33 cm and fibres were connected to pins by silver paint (SPI). Between the two outer electrodes a constant DC current was applied by Potentiostat/Galvanostat model 363 (Princeton Applied Research). The generated potential difference between the inner electrodes along the current flow direction was recorded by digital multimeter 34401A(Agilent). The conductivity of the solid fibre with circular cross section can then be calculated according to the cross-sectional area of the fibre, DC current applied and the potential drop across the two inner electrodes.

$$\sigma = \frac{I \times L}{V \times S} \quad \text{Equation 3.5}$$

$\sigma$  = Conductivity (S/cm)

I= Current (mA)

V= Potential drop (mV)

L= The distance between inner electrode (cm)

S=Cross-sectional area (cm<sup>2</sup>)

The cross sectional area of the fibres can be calculated from following formula:

$$S = \frac{D}{900900 \times \rho} \quad \text{Equation 3.6}$$

D= denier (grams of 9000 m filament)

$\rho$ = density (g/cm<sup>3</sup>)

Denier of fibre filaments has been obtained by measurement of weight of different sample with specified length. The density has been measured by floating of samples in different liquid with a range of density from 0.7 and 1.6. Two miscible liquid such as hexane and carbon tetra chloride was selected because they have not any swelling effect on the fibre. The denier and diameter of fibre can also be employed to calculate the numerical amount of density from Equation 3.7 [7].

$$\rho(g/cm^3) = 141.37 \times \frac{\text{denier}}{D^2(\mu m)} \quad \text{Equation 3.7}$$

### 3.5.2. Cyclic voltammetry

Cyclic voltammetry is one of the most common electrochemical techniques, and is extensively used for electrochemical characterisation of conducting polymers. In general, CV involves the measurement of current at the working electrode as a function of applied potential. The resulting current-potential plot is the cyclic voltammogram. CV is the most effective and versatile electrochemical technique available for the study of redox systems. In this work, CV was used for characterisation of the conductive polymer fibres. A three electrode electrochemical cylindrical cell (15mm×50mm) equipped with a stopper was used for cyclic voltammetry tests. The fibre was the working electrode, an Ag/AgCl or Ag/Ag<sup>+</sup> reference electrode, respectively, was used for aqueous and ionic liquid electrolytes, and a Pt mesh counter electrode was employed. The sample fibre was connected to one end of a Pt wire using silver paint. When the silver paint had dried, the resistivity was checked to ensure efficient connection. After testing the connection point was covered by super glue or epoxy resin. The other end of the fibre was glued with super glue to a nonconductive wire. The Pt wire was passed through the stopper and mounted on the

bottom of the cell for connection to the potentiostat. The other end of the fibre, which was connected to the insulated wire, was attached to the lever arm for applying a 10 mN load to the fibre to keep it straight.

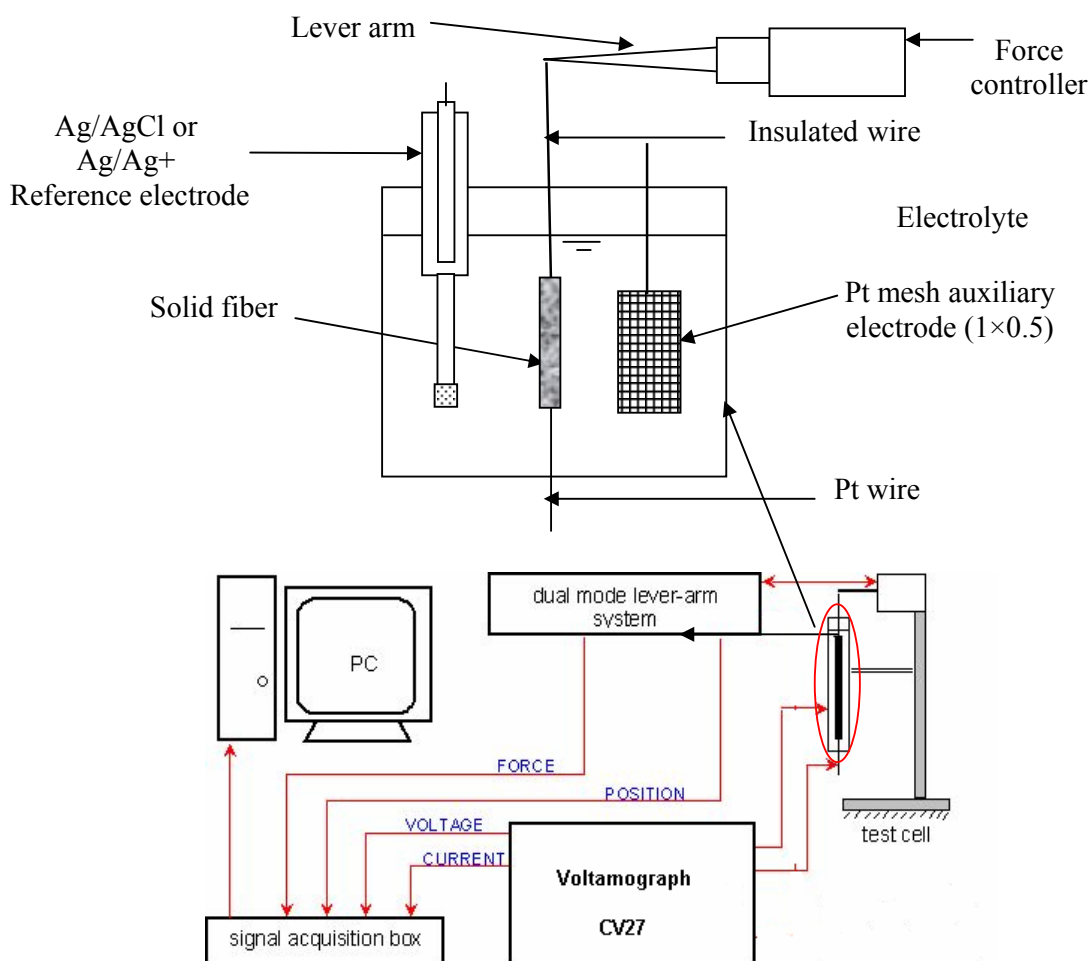


**Figure 3.5.** The experimental set up used for cyclic voltammetry (a) cell set up (b) instrumental set up

Constant force conditions were applied using a force/length controller (Aurora Scientific, Dual Mode Mode 1300B). The MacLab/4e ADI unit (signal acquisition box) has four analogue input channels that were used to record the voltage and current

generated by the voltamograms (CV27), and the force and position, which was measured by the lever-arm system. The input signals were then digitised and can be sampled at very high rates (up to 200 000Hz). The unit can also filter the signals if necessary, before passing them on to the computer. The resulting data was recorded on a personal computer using a software package known as Chart. Chart provides various options for processing and presenting the data; for example it allows the user to change the scaling or the sampling rate of the signal.

### **3.5.3. Dynamic mechanical analysis**

The dynamic mechanical analysis instrument model Q-800 (TA series) was employed to perform mechanical analysis in different modes. Before doing any tests the system was calibrated using a standard procedure:

**1-Clamp mass calibration** is performed to allow the instrument to compensate for the mass of a specific clamp.

**2- Clamp Zero calibration** is needed to determine the point of zero of the sample length.

**3-Compliance calibration** is used to measure the flexibility of a clamp and calibrates the instrument to that flexibility.

If calibration results are in the range defined by instrument, the system is ready to test the samples.

#### **3.5.3.1. Stress-strain (Mechanical test) in strain rate mode**

The strain rate mode was used to collect stress vs. strain data equivalent to that obtained from a universal testing machine (Instron). In this mode a sample is stretched at a specified strain or displacement rate until the sample breaks. The cross section of 10 samples of 10 mm gauge length has been measured using an optical microscope.

Both ends of fibre samples clamped using soft wood (Balsa) and super glue. The sample is stretched at a strain rate of 500  $\mu\text{m}/\text{min}$  until the sample breaks at 25 °C in a closed furnace. The test fails if the sample breaks from both ends.

In fibre technology to define stress/strain behavior units of N/tex or gpd based on density or denier of fibre are used. The specific tensile stress or elastic modulus based on N/tex or gpd ( gram per denier) can be defined using the following equations [7]:

$$\left( \frac{N}{\text{tex}} \right) = \frac{\text{Stress}(\text{GPa})}{\text{density}(\text{g/cm}^3)} \quad \text{Equation 3-8}$$

$$\text{gpd} = 11.3 \times \left( \frac{N}{\text{tex}} \right) \quad \text{Equation 3-9}$$

The slope of the portion of the curve where stress is linearly proportional to strain (elastic portion) is referred to Young's Modulus (E). The yield point is identified by crossing of a line with stress-strain curve, which is parallel to elastic portion at strain 0.2 % ( $\delta_{y=0.2}$ ). The highest stress the material can tolerate is characterised by ultimate tensile stress ( $\delta_b$ ) and the ultimate elongation at fracture is recognised as  $\epsilon_b$  (%).

### 3.5.3.2. Creep mode

In a creep experiment, a constant force (stress) is rapidly applied to the material and the resulting deformation (strain) is measured as a function of time. Creep compliance is calculated by dividing the time-dependent strain by the applied stress. After creep has occurred for a specified period of time, the stress is removed and the strain recovery of the sample is measured. A preliminary preload force is available for creep measurements ( 0.01 mN). This preload force ensures that the sample material is fully elongated (no slack). In all cases, the preload force should be limited to the minimum

force required to achieve the desired starting condition. Otherwise, it may affect the creep results. The stress applied during creep measurements can be a nominal value sufficiently large to ensure good deformation. Most creep experiments are carried out either at ambient temperature or at a temperature where sufficient creep occurs to enable comparisons between materials. The creep time is the time that the stress is applied to the material. The recovery time is the time after the applied stress is removed and the material is allowed to recover from the strain resulting during creep. Respectively a 10 and 20 minutes have been selected for creep time and recovery time.

#### **3.5.3.3. Viscoelasticity test**

Most real-world materials exhibit mechanical responses that are a mixture of viscous and elastic behavior known as viscoelastic. For a viscoelastic material, the complex modulus is defined as a function of loss modulus,  $E''$  (viscous portion) and storage modulus,  $E'$  (elastic portion). The tangent of the phase angle (The phase shift between stress and strain) is the ratio of the loss modulus to storage modulus ( $\tan \delta = E''/E'$ ). This ratio is a measure of the damping ability of a material.

In this mode, a constant frequency of 1 Hz with amplitude 20-50  $\mu\text{m}$  using a temperature ramp of 5  $^{\circ}\text{C}/\text{min}$  has been used to evaluate the viscoelastic response of a material by the observed changes in the storage and loss modulus. Determination of the  $T_g$  and other transitions of materials also is possible by recording of temperatures corresponds to sudden drop in storage modulus or peak points of the curves of loss modulus or  $\tan \delta$ .

#### **3.5.4. Differential scanning calorimetry**

Differential scanning calorimetry (DSC) was carried out using a Q-100 (TA series) instrument. DSC is a thermal analysis technique that measures the heat flow associated with transitions in materials as a function of time and temperature. Such measurements provide qualitative and quantitative information about physical and chemical transitions that involve endothermic or exothermic processes or changes in heat capacity. Typical measurements include, glass transition temperature ( $T_g$ ) in amorphous/semi-crystalline materials, melting point ( $T_m$ ), crystallisation temperature, cross linking or degradation temperature. Also the degree of crystallinity can be deduced from the enthalpy of fusion.

In a "heat flux" DSC, the sample material, encapsulated in a pan, and an empty reference pan sit on a thermoelectric disk surrounded by a furnace. As the temperature of the furnace is changed (usually by heating at a linear rate, 5-10 °C/min), heat is transferred to the sample and reference through the thermoelectric disk. The differential heat flow to the sample and reference is measured by thermocouples. Nonhermetic aluminum pans were used for all experiments in temperature range of 25-450 °C. The TA Instruments blue sample encapsulating press was used to seal samples in the DSC sample nonhermetic pan.

#### **3.5.5. Raman spectroscopy**

Raman spectroscopy has become an important analytical and research tool. It can be used for analysis and identification of molecular structures, effects of bonding, environment and stress on a sample in a broad range of materials including polymers and carbon nanomaterial. Raman spectroscopy is a light scattering technique and can be described as a process where a photon of light interacts with a sample to produce



scattered radiation of different wavelengths. Raman spectra were obtained with the JOBIN Yvon Horiba micro Raman spectrometer model HR800 which offers the very high optical efficiency necessary to detect signals of carbon nanotubes and conducting polymers. The spectra were collected with a spectral resolution of  $1.5 \text{ cm}^{-1}$  in the backscattering mode, using the 632.8 nm excitation line of a Helium/Neon laser. The nominal power of the laser polarised 500:1, was 20 mW. A Gaussian/ Lorentzian-fitting function was used to obtain band position and intensity. The incident laser beam was focused onto the specimen surface through a  $100 \times$  microscopic objective lens, forming a laser spot of approximately  $5 \text{ }\mu\text{m}$  in diameter, using a capture time of 50 s. The Raman signals were obtained with the half wave plate rotated at  $170^\circ$  with a confocal hole set at  $1100 \text{ }\mu\text{m}$  and the slit set at  $300 \text{ }\mu\text{m}$ .

In the present study Raman spectroscopy was also employed to determine degree of orientation of SWNTs in the composite fibres. Moreover, Raman spectroscopy is a powerful tool for the analysis of load transfer from matrix to nanotubes due to high sensitivity of Raman bands of SWNTs to applied load. The detail of these techniques will be described in Chapter 6.

### **3.5.6. Scanning Electron Microscopy**

The morphology and microstructure of the sample fibres prepared in this work have been investigated using SEM. The images obtained were recorded using a fully digital LEO Cambridge/Leica Stereoscan 440 scanning electron microscope with tungsten filament using 20 kV beam energy at the Department of Materials Engineering, University of Wollongong (Australia) In addition the Hitachi S-900 “in line” field emission scanning electron microscope has been employed at the Electron Microscopic unit of University of New South Wales (Australia) to be capable for

imaging at very high resolutions ( $\sim 0.5$  nm). The field emission gun provides a fine, but intense beam of electrons which can be used to obtain a meaningful signal of very fine detail on the specimen surface.

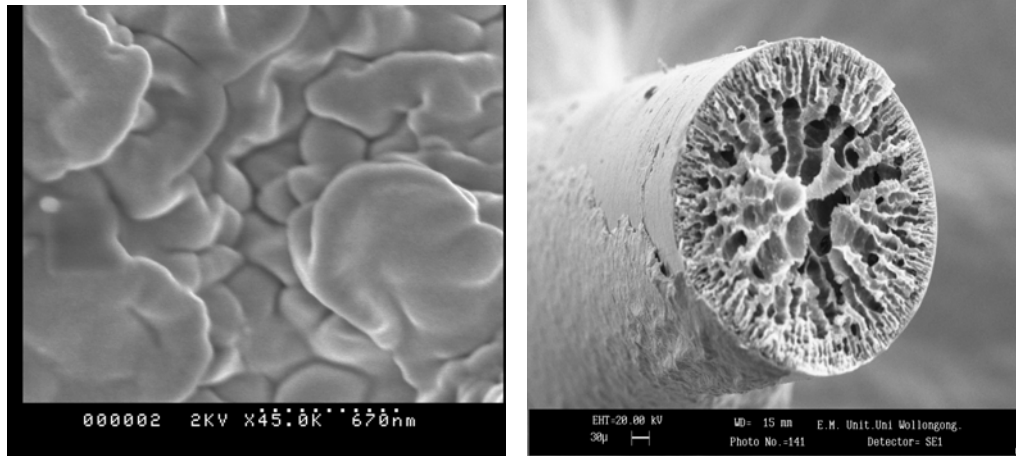


**Figure 3.6.** The SEM pictures obtained using (a) Hitach- S900 from internal microstructure (b) Leica 440 from circular cross section

SEM samples were sputter coated (35 mA for 20 Seconds under 200 mbar vacuum (Dynavac) with a thin layer of gold to make them sufficiently conductive. For side wall imaging, a small piece was cut from the fibre and mounted on a stub or small brass plate (11×5 mm) using conductive carbon tape or silver paint. To obtain a clear picture from a cross section, the fibre samples were broken using liquid N<sub>2</sub> to obtain a circular undamaged cross section

Alternatively, The XT Nova NanoLab 200 combines a dual beam high resolution focussed ion beam (Ga FIB) and a high resolution scanning electron microscope for nanomilling to prepare thin film ( $\sim 100$ nm) and imaging of internal structure of fibres. The FIB uses a fine, energetic beam of gallium ions that scan over the surface of a specimen. A sample picture obtained using XT –Nova after sectioning is given below.

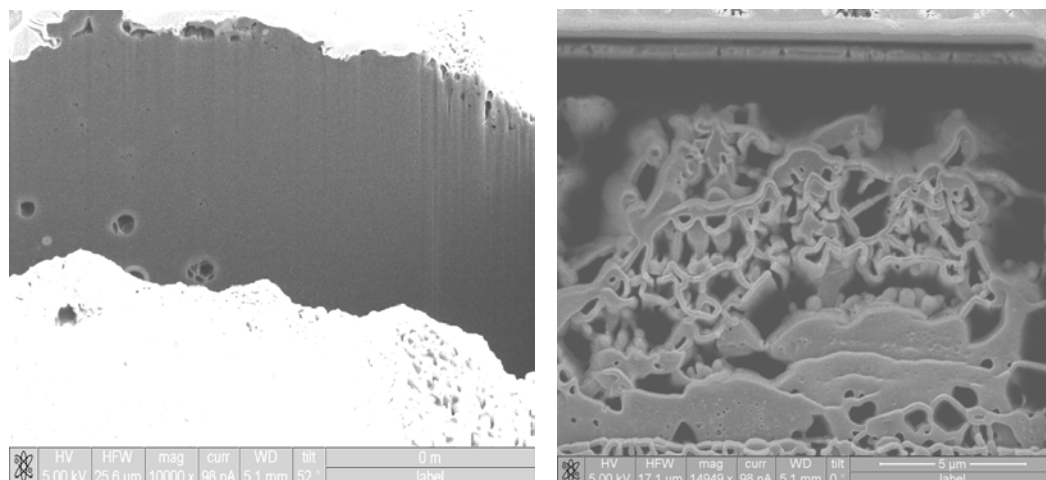


**Figure 3.7.** The images obtained from a sample of polyaniline fibre from different angle using FIB

### 3.5.7. Transmission electron Microscopy

The high resolution transmission electron microscopy (TEM) was conducted using Philips CM200. The Philips CM200 field emission gun transmission electron microscope (accelerating voltage of 200 KV) allows very high resolution images to be obtained from thin, electron transparent sections of materials. In addition, it has a SIS CCD camera for direct recording of digital images. The samples for TEM imaging are thin films which were prepared by FIB. The detail of preparation of thin film using FIB will be described in Chapter 5.

**3.6. References**

- [1] S. Badaire, P. Poulin, M. Maugey and C. Zakri, *Langmuir*. 20 **(2004)** 10367-10370.
- [2] M. Kaszuba, M. Connah and K. Mattison, High concentration particle size measurements using dynamic light scattering, *Lab plus international*, **(2004)**.
- [3] R. Pecora, *Dynamic Light Scattering: Applications of Photon Correlation Spectroscopy*, Plenum Press, **(1985)**.
- [4] K. Mattison, A. Morfesis and M. Kaszuba, *A Primer on Particle Sizing Using Dynamic Light Scattering*, American Biotechnology Laboratory, **(2003)**.
- [5] A. Ziabicki, in *Fundamental of fiber spinning*, "General theoritical fundamentals", Wiley, New York, **(1976)**, 13-147.
- [6] A. Ziabicki, in *Fundamental of fiber spinning*, "Wet and dry spinning", Wiley, New York, **(1976)**, 256-349.
- [7] W. E. Morton and J. W. S. Hearle, *Physical properties of textile fibres*, Textile Institute, Manchester ,UK, **(1993)**.

# **CHAPTER FOUR**

Development and Characterisation of  
Polyaniline (Leucoemeraldine base) –  
SingleWalled Nanotubes Composite  
Fibre Prepared Using a Two Step  
Process

### **4.1. Introduction**

The complementary mechanical and electrical properties of carbon nanotubes can be expected to enhance the properties of polyaniline (PAni) fibres. This chapter reports on the preparation and characterisation of PAni/ single walled carbon nanotubes (SWNT) composite fibres produced from PAni- leucoemeraldine base (LEB) solutions.

A key factor in developing of a polymer reinforced with carbon nanotube (CNTs) is the homogenous dispersion of the nanotubes in the polymer matrix. It is therefore essential to develop methods for effectively dispersing nanotubes in the spinning solution and to prevent their agglomeration through van der waals forces [1]. In other words, the formation of a homogenous fibre needs a homogenous and viscose solution. This requires the selection of a solvent suitable for both dissolution and dispersion of the nanotubes. The tendency of PAni in the LEB state to dissolve in polar aprotic solvents such as NMP and DMPU was described in detail in chapter two. Dispersion of CNTs in the viscose PAni solutions by either shear mixing or ultrasonication using a horn sonicator was investigated here. According to the literature, the minimum concentration of PAni required for fibre spinning using a take up mechanism is at least 10 % w/w and this produces a viscosity in the order of 1000 cP [2]. Ultrasonicators produce mechanical vibration using sound waves above 19 kHz. As the viscosity of material increases, the ability of an ultrasonicator to transmit the vibration decreases and consequently dispersion cannot be properly achieved. Therefore, the dispersion of CNTs in the solvent using ultrasonication followed by the addition of PAni in order to obtain a viscous solution was the protocol adapted in this work. This chapter focuses on the manufacturing of PAni (LEB)-SWNTs composite fibres from a spinning solution prepared through mixing of

SWNT dispersions with polyaniline in the reduced (LEB) form. In addition the mechanical, electrical and electrochemical properties of PAni (LEB)-SWNT composite fibres have been determined.

## **4.2. Experimental**

### **4.2.1. Materials and reagents**

Purified SWNTs prepared using the Hipco approach [3] were obtained from Carbon Nanotechnology Incorporated (CNI) in powder form (batch number PO257). Elemental analysis was used to determine the level of impurities including Fe particles.

PAni in the emeraldine base (EB) form with molecular weight of 280000-300000(g/mole) (trade name EB-300) was purchased from Santa Fe Science and Technology.

The 1,3-Dimethyl-3,4,5,6-Tetrahydro-2(1H)-Pyrimidinone (DMPU, 98 % ), N-methyl-2-pyrrolidinone (NMP, 99 %), Polyethylene glycol tert-octylphenyl ether known as TritonX-100 or TX-100 and phenyl hydrazine (99%) were supplied by Sigma Aldrich and used as received. Methane sulfonic acid (Sigma Aldrich, 99%) was used as acid dopant after dilution with Milli-Q water.

### **4.2.2. Instrumentation**

A Shimadzu 1601 and a Cary 5000 were employed for UV-Vis and UV-Vis-NIR spectroscopy respectively. Viscometry was carried out using a Brookfield viscometer (RV-DV II+) using spindle of Din 85-87. Size distribution was determined using a dynamic light scattering (zeta sizer model ZS (Malvern, UK)) with red laser 632 nm

(He/Ne). An optical microscope (Olympus) was used to find the average diameter of as spun and drawn fibres. A Leica scanning electron microscope (SEM) Lecia was employed to obtain cross sectional view of composite fibers based on the procedure described in section 3.5.6. Raman spectra were obtained using a JOBIN Yvon Horiba Raman spectrometer model HR800 in spot mode ( $\lambda_{exc}= 632.8$ ).

Mechanical tests were carried out using a dynamic mechanical analysis (DMA) instrument Q-800 (TA series) in strain rate mode to record the force -displacement data generated at constant temperature. Thermal studies were conducted using a differential scanning calorimeter (DSC) Q-100 (TA series).

The electrical conductivity of composite fibres was measured using the four point probe method. EChem software (ADI instruments) coupled with a potentiostat (Bioanalytical system CV27) and a Maclab (ADI instruments) were employed for cyclic voltammetry using the PAni fibre and its composite containing SWNT as working electrode.

Electron paramagnetic resonance (EPR) spectroscopy of solid PAni fibres was carried out using a Bruker EMX spectrometer. Equal masses of different samples were placed into a quartz tube and spectra recorded at room temperature at X wavebands (9.75 GHz).

#### **4.2.3. Comparison of the ability of NMP and DMPU to disperse SWNTs**

In this part SWNT bucky paper was used rather than raw powder because it was observed that [4] the bucky-paper made specifically from the Triton X-100 solution when redispersed in other dispersant and imaged by contact-mode atomic force microscopy (AFM) is very clean. A free standing SWNT paper was prepared from a purified SWNTs dispersion using methods published previously [4]. This involved sonication of purified



SWNTs (0.01 % w/w) in water with 0.5 % w/w TX-100 present as a nonionic surfactant. The bucky paper was then obtained by filtration of the dispersion through a 0.2  $\mu\text{m}$  Polytetrafluoro ethylene (PTFE) membrane filter (Millipore) followed by washing with water and methanol to drive off the surfactant and drying at 130 °C for 30 min. To investigate the effectiveness of the solvents under investigation, a 5 mg sample of the SWNT bucky paper was redispersed by sonication in 50 mL DMPU or NMP for 2 hrs.

#### **4.2.4. Influence of polyaniline addition on the degree of SWNT aggregation**

EB powder (5 mg) was added to SWNT-DMPU dispersion after 2hr sonication (prepared in section 4.2.3) while sonicating for a few seconds. The dispersions with and without PAni present were characterised by dynamic light scattering to show the influence of polyaniline on the stability of the dispersion.

#### **4.2.5. Use of DMPU for dispersing SWNTs at higher concentrations**

Appropriate amounts of SWNT paper were sonicated in 20 g of DMPU for 2 hrs to produce dispersions contains 0.05, 0.1, 0.2 or 0.25 % w/w SWNTs with respect to the weight of solvent. Dynamic light scattering and viscometry were employed to characterise these SWNT dispersions.

#### **4.2.6. Preparation of spinning solutions**

The procedure used for the preparation of the spinning solution was based on the method and formulation described in the literature for the LEB form of PAni [5] with some modifications. Table 4.1 shows the amount of materials used for preparation of various spinning solutions. The appropriate amounts of SWNT bucky paper were

sonicated in DMPU for different period of time at 60 °C to drive the SWNTs into solution. PAni (EB) powder was then added to the SWNT dispersion with a weight ratio of 1:1 with respect to SWNT while sonicating for a few seconds. In this time scale the sonication has not any harmful effect on structure and properties of PAni. PAni (EB) and phenyl hydrazine (30 % w/w vs EB) as reducing agent were added gradually over a 2 hrs period to SWNT–DMPU-PAni dispersions while mixing using an overhead stirrer at 40 R.P.M. in a water bath held at 0-5 °C. The spinning solution was stirred for another 2 hrs under the same conditions.

Finally, dynamic vacuum was applied to the pressure vessel to ensure a bubble free solution. This solution was then passed through a 400 µm filter and kept in the pressure vessel under very low N<sub>2</sub> pressure prior to fiber spinning.

**Table 4.1.** Formulation of PAni (LEB)-SWNT-DMPU composite spinning solutions

Test	PAni(EB) (g)	DMPU (g)	SWNT (mg)	SWNT/DMPU (% w/w )	Phenyl hydrazine(g)
1	2	20	0	0	0.66
2	2	20	10	0.05	0.66
3	2	20	20	0.1	0.66
4	2	20	40	0.2	0.66

#### 4.2.7. The fibre spinning process

The spinning solution was transferred to a N<sub>2</sub> pressure vessel, driven through a second filter (100 µm, Millipore), followed by a single hole spinneret (with L/D = 4 and D = 250 µm) and finally into the coagulation bath. The lengths of the first and second baths were 2 m and 1 m, respectively.

**4.2.7.1. Effect of coagulation bath composition**

10 % w/w PAni (LEB) spinning solution with and without SWNTs (0.2 % w/w) present were used. Different amounts of NMP namely 30, 20 and 10 % w/w, were mixed with water in order to find the appropriate amount of solvent for the coagulation bath to obtain the proper skin formation rate. The N<sub>2</sub> pressure was adjusted ~20 psi to fix the injection rate for the spinning process. In the first coagulation bath the spinning solution solidified and the emerging fibre was taken up to the first bobbin (D = 2.5 cm) at a linear velocity of 2 m/min. This semi-solid fibre was then passed through a second bath and collected using a linear velocity of 4 m/min on to the second bobbin (D = 5 cm) rotating in a water bath.

**4.2.7.2. Effect of take up velocity**

10 % w/w PAni (LEB) spinning solution with and without SWNTs (0.2 % w/w) present and a 10 % w/w NMP/Water coagulation bath were used to investigate the effect of take up velocity. Different take up velocities were used to find the optimum residence time in order to minimise the porosity of the fibres. The N<sub>2</sub> pressure was adjusted to ~ 20 psi to fix the injection rate for the spinning process. In the first coagulation bath the solution solidified and the emerging fibre was taken up on the first bobbin (D = 2.5 cm) at a linear velocity of 2 or 6 m/min. A second coagulation bath was not used for such experiment.

**4.2.8. Effect of CNT content**

Fibres with different SWNT contents, namely 0, 0.5, 1 and 2 % w/w (with respect to mass of PAni) were produced using a 10 % w/w NMP/water coagulation bath, an injection rate of 1.35-1.40 cm<sup>3</sup>/min (by applying an N<sub>2</sub> pressure of 20-80 Psi), a take up velocity of 2m/min on the first bobbin (D = 2.5 cm), and a spin draw ratio of 2 using a second bobbin.

Fibres were then kept for 2 hrs in a water bath at room temperature to reduce the solvent content and then for an additional 12 hr at room temperature in preparation for the hot drawing process. Before thermal stretching, the density, denier and diameter of fibres were measured using the methods described in Chapter 3.

#### **4.2.9. Post spinning treatments**

The drawing process involved stretching of the as-spun fibre 2-3 times across a soldering iron wrapped with Teflon tape. The appropriate temperature for the drawing was based on data obtained using by the DSC of composite fibres.

Complete removal of the residual solvent was carried out by extraction in a water bath for 24 hrs followed by drying in a vacuum oven at 50 °C for 12 hrs before doping. After complete drying, the stretched fibres were doped in MSA (1M) for 24 hrs as described previously [1, 6]. Treatment of LEB with acid converted the PAni to the ES form due to natural oxidation of the unstable LEB. After doping, fibres were dried at room temperature for at least 48 hrs before further characterisation to ensure water removal. To explore the effect of drying procedure on conductivity, fibers also were imposed to higher temperature (100 °C) in atmospheric pressure.

### **4.3. Results and discussions**

#### **4.3.1. The characterisation of SWNTs**

##### **4.3.1.1. Elemental analysis**

Even with purification, SWNTs were still shown to have some impurities primarily related to iron particles remaining from the metallic catalyst used during the growth

process. Table 4.2 shows the weight percent of elements within SWNTs as detected by elemental analysis. No attempts were made to further purify the SWNTs.

**Table 4.2.** Elemental analysis of purified SWNTs prepared by Hipco@CNI (PO257)

element	C	H	N	Fe
%w/w	90.44	0.43	0.10	8.59

#### 4.3.1.2. Raman spectroscopy of the bulk SWNTs

Raman spectra of bulk SWNTs were obtained, using a 632.8 nm excitation wavelength (Figure 4.1). Four prominent sets of peaks were observed in the low- ( $\sim 200\text{ cm}^{-1}$ , RBM [radial breathing mode]), moderate frequency ( $1600\text{ cm}^{-1}$ , G band, and  $1300\text{ cm}^{-1}$ , D band) and high-frequency ( $2600\text{ cm}^{-1}$ , D\* band) regions. These peaks are typical of SWNTs and their assignments are summarised in Table 4.3.

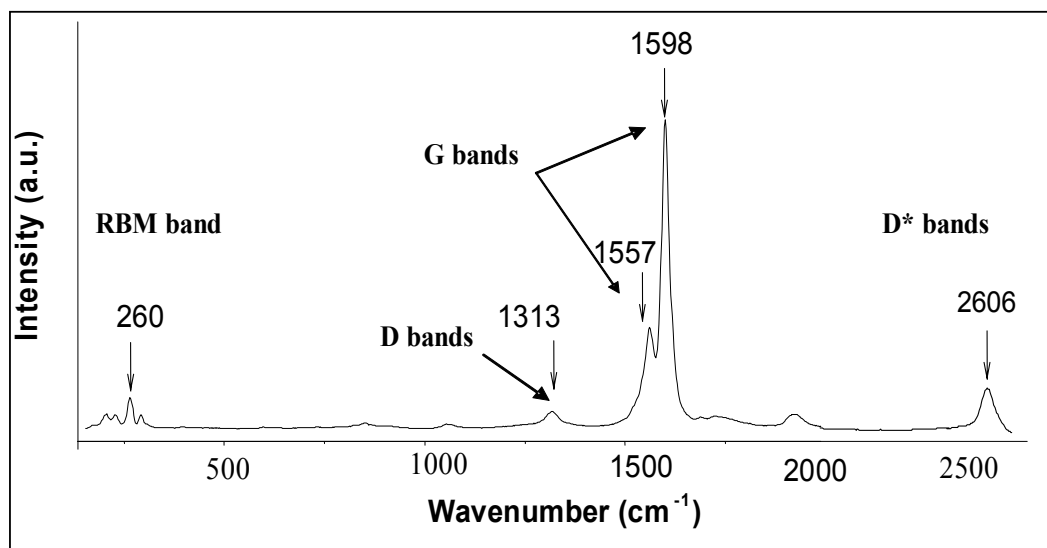


**Figure 4.1.** Raman spectrum of bulk SWNTs ( $\lambda_{\text{exc}}=632.8\text{ nm}$ )

**Table 4.3.** Vibrational modes observed for Raman scattering in SWNTs [7-11].

### 4.3.2. Characterisation of SWNT dispersions

#### 4.3.2.1. UV-visible – NIR spectroscopy

Previous studies [4, 12] have shown that strong absorption bands appear when methanol, dimethyl formamide (DMF) and NMP were used for dispersion of pristine SWNTs (refer to Table 4.4). As described in chapter two, NMP is a good solvent for PAni (EB), however, the solutions gel after a short time, making NMP unsuitable for fibre spinning. However, a more stable solution can be obtained from DMPU which has a high dielectric constant and is similar to NMP in term of its classification as a polar aprotic, Lewis base solvent. Compared to NMP, DMPU shows a higher degree of free electron availability ( $\beta$ )

---

<sup>§</sup> Raman shift is independent of laser excitation energy

without hydrogen donicity ( $\Pi^*$ ) [13, 14]. Since ( $\beta$ ) and ( $\Pi^*$ ) are key properties when determining the solvation of SWNTs [4], DMPU was tested for dispersing SWNTs . Figure 4.2 shows the more pronounced absorption bands obtained after dispersion of SWNT in DMPU compared to when NMP was used. A comparison of the peaks observed in this study with those reported in the literature is given in Table 4.4.

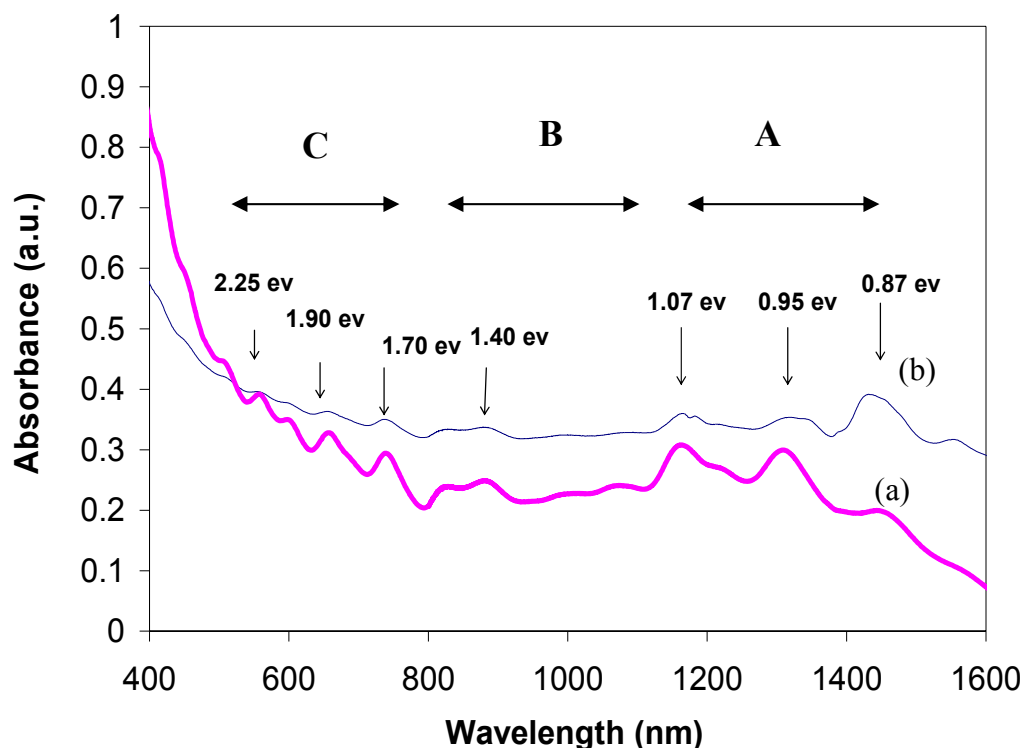


**Figure 4.2.** UV-Vis NIR spectra of SWNT (0.01% w/w) in (a) DMPU and (b) NMP after 2hrs sonication (A, B, C: refer to table 4.4)

SWNT dispersed in NMP and DMPU demonstrate several peaks between 0.8 and 2.5 eV related to the interband transitions between the van Hove singularities in the electronic density of states (DOS) of metallic and semiconducting tubes of a bulk sample of SWNTs [15]. The pronounced absorption bands observed in the UV-Vis-NIR are indicative of well

dispersed SWNTs. The bands observed at higher wavelength (1.40, 1.07, 0.95 and 0.87 eV) are attributed to transitions between DOS singularities in semi conducting tubes and bands observed at lower wavelength (2.25, 1.90 and 1.7 eV) can be attributed to the Fermi level transitions observed in metallic SWNTs. The bands observed at other wavelengths are attributed to the heterogeneity of the samples in terms of tube diameters and helicity [12, 15, 16]. The UV-Vis- NIR of SWNTs dispersed in DMPU shows all the same peaks as for SWNTs dispersed in NMP which has previously been shown to be a good dispersant for SWNTs. Slight differences in absorbance may be related to differences in the degree of exfoliation of SWNTs bundles that occur in the two solvents.

**Table 4.4.** Electronic transitions reported for dispersed SWNTs and their occurrence in different solvents.

*\* Results obtained in this study*



**4.3.2.2. Dynamic Light Scattering**

In general, the utilisation of SWNT initially requires their homogenous dispersion in a solvent or polymer matrix. Dynamic light scattering of SWNTs dispersions indicate that the hydrodynamic diameter of the nanotube bundles is between 150 and 400 nm after 30 min of sonication. After 60 min and 120 min sonication, the diameter was reduced to 100-200 nm and 20-80 nm, respectively (Figure 4.3).

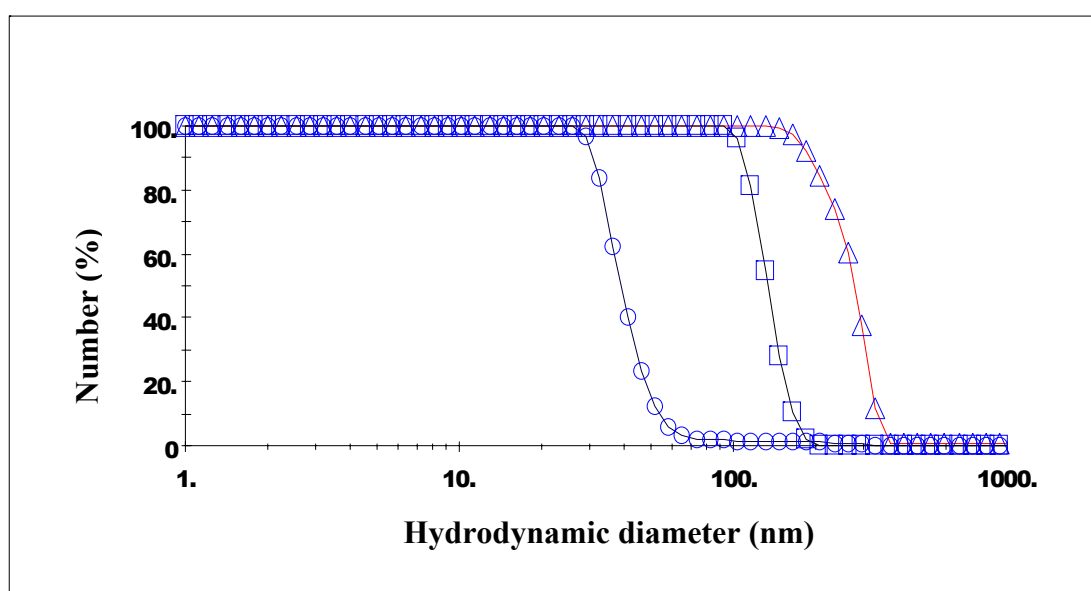


**Figure 4.3.** Hydrodynamic diameter distribution of SWNT bundles in DMPU for different sonication times (triangle) 30 min (square) 60 min (circle) 120 min.

The optimal mechanical reinforcement provided by SWNTs and any enhancement in charge transfer characteristics would be favored by the presence of long and thin bundles homogeneously exfoliated throughout the matrix [17]. Therefore, the selection of sonication time is based on a balance between the size of nanotubes and the homogeneity of the dispersion. The results presented in Figure 4.3 indicate that ultrasonication was an effective method for dispersing SWNTs in DMPU. However, SWNT bundles were found

to re-agglomerate upon standing after sonication, as shown in Figure 4.4 where large agglomerate particles are indicated by arrows. As shown in Figure 4.5, the size distribution of SWNT/DMPU dispersions show a considerable increase in hydrodynamic diameter when measured 60 minutes after sonication, compared with the sample measured immediately following sonication.

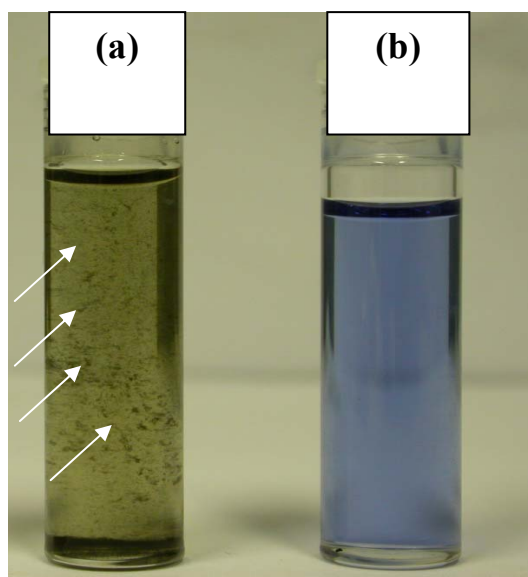


**Figure 4.4.** Affect of standing time on the stability of SWNT dispersions and influence of PAni on stability of SWNT dispersion in (a) SWNT- DMPU (0.01 % w/w) (b) SWNT (0.01 % w/w)-PAni (0.01 % w/w) in DMPU. Photograph was taken 6 hr after sonication. Arrows indicate large agglomerates.

The addition of PAni to the SWNT-DMPU dispersions was found to stabilise the exfoliated nanotubes and limit re-agglomeration. Figure 4.5 shows that the hydrodynamic diameter of the SWNTs immediately after sonication and in the presence of PAni was  $\sim 20$  nm compared with  $\sim 30$  nm when PAni was not added. When the size distributions were measured again 60 minutes after sonication, the hydrodynamic diameter with PAni

present had increased slightly to  $\sim 50$  nm, but had increased significantly to 100-800 nm when no PAni was present.

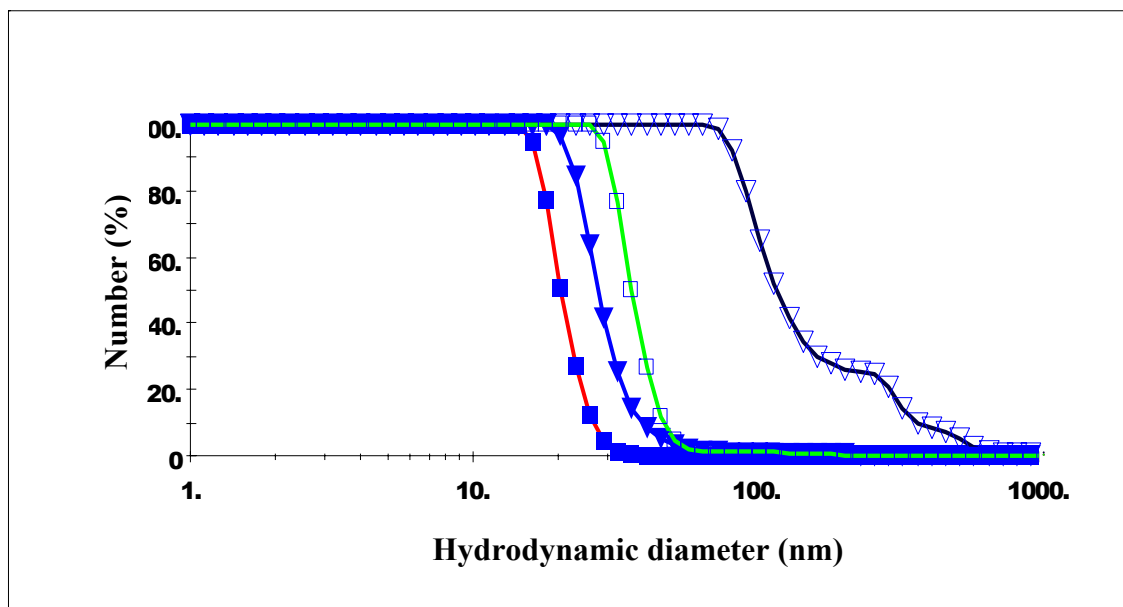


**Figure 4.5.** Hydrodynamic diameter distribution of SWNTs in DMPU (0.01 % w/w) with (square) and without (inverted triangle) PAni. The distribution immediately after sonication is represented by filled symbols while the distribution measured 60 min after sonication was stopped is shown by unfilled symbols.

The size distribution of SWNTs was found to depend on their concentration (Figure 4.6). Result showed that the range of the hydrodynamic diameter was between 20 nm and 50 nm for the dispersion containing 0.05 % w/w SWNT, while for dispersions containing 0.1 or 0.2 % w/w SWNT, higher ranges of hydrodynamic diameter between 40-100 nm and 100-200 nm were observed respectively. The maximum concentration of SWNTs that could be dispersed in the PAni containing DMPU solution was 0.2 % w/w. At 0.25 % w/w large agglomerates were observed visually, even after 2 hrs sonication.

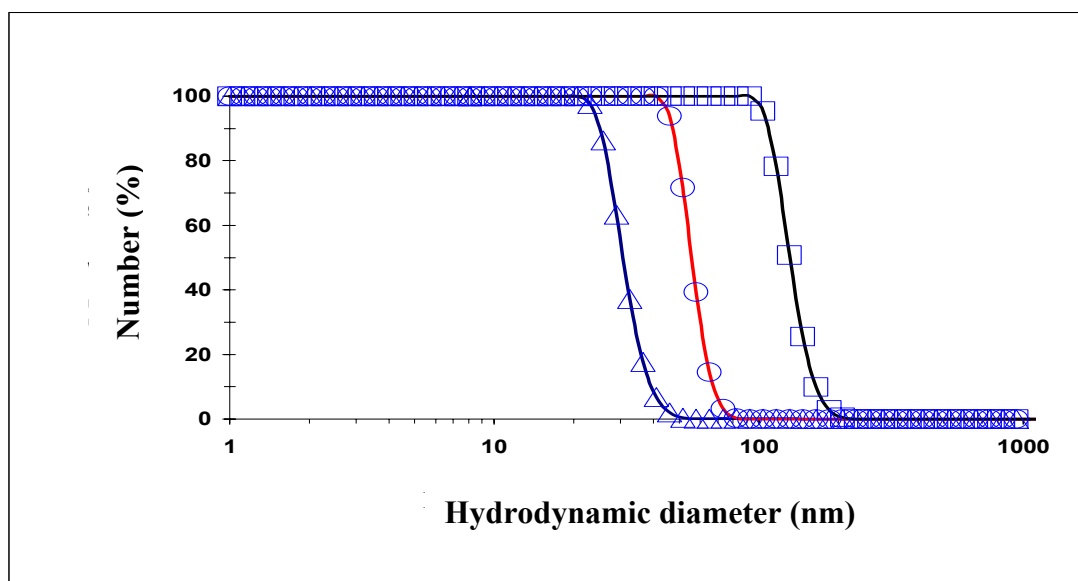


**Figure 4.6.** The size distribution of SWNTs bundle in DMPU for different concentrations of (Δ) 0.05 % w/w, (○) 0.10 % w/w and (□) 0.20 % w/w.

#### 4.3.2.3. Viscosity of SWNT/DMPU dispersions

The viscosity of the SWNT/DMPU dispersions as a function of shear rate was determined after different sonication times (Figure 4.7). The fluctuations in viscosity observed after 30 or 60 min sonication times were indicative of heterogeneity in the dispersion. The smooth curve observed after 120 min of sonication indicated homogeneity of dispersion. Note also that this dispersion had the lowest viscosity, which can be attributed to the smaller size of SWNTs bundles after longer sonication.

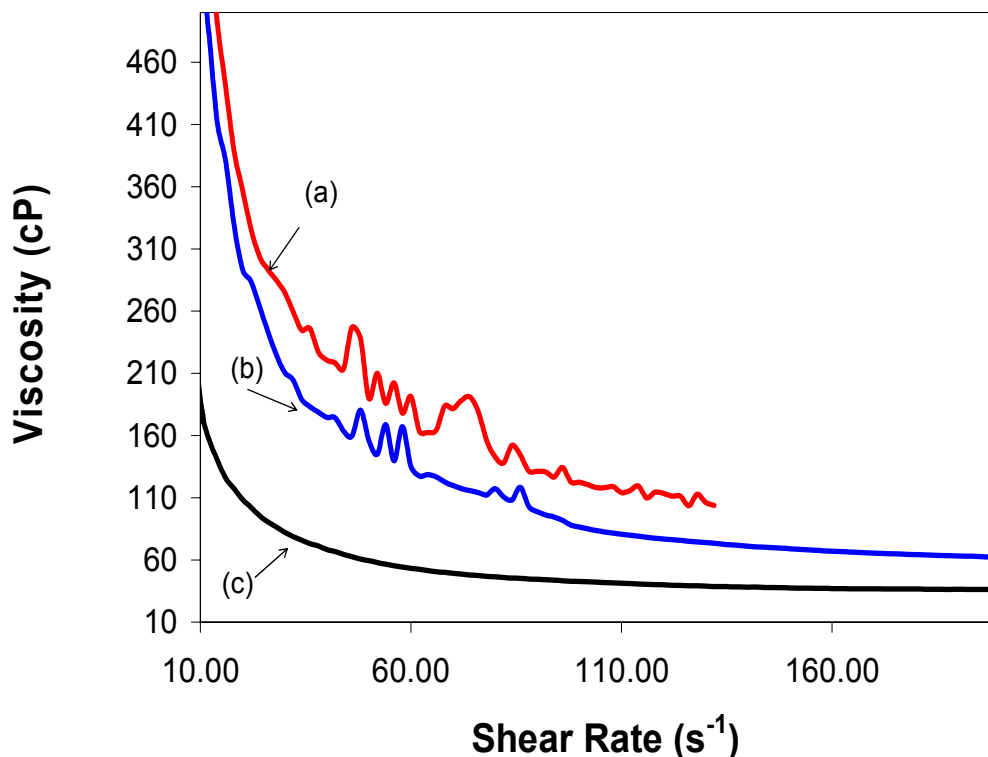


**Figure 4.7.** Viscometry of SWNT (0.2 % w/w) in DMPU dispersions after different sonication times (a) 30 min, (b) 60 min and (c) 120 min

#### 4.3.3. Viscometry of PAni-(LEB)-SWNT-DMPU spinning solution

The minimum concentration of PAni required to give the minimum viscosity for spinning is  $\sim 10$  % w/w [6] and so this concentration was used in this study as with varying SWNT concentration. Figure 4.8 shows the viscosity profile over time for PAni/SWNT solutions. The viscosity profile of samples with SWNTs has three distinct rheological regions labeled I, II and III. In contrast, solution without SWNTs showed little change in region I and exhibited only two rheological regions. The following will describe and identify the significance of the rheological regions I, II and III with respect to fiber spinning.

Region I was characterised by a decrease in viscosity with time. This region was not clearly identifiable in the neat PAni solution. The higher the SWNT content, the more pronounced the decrease in viscosity and the longer was the time to reach a stable viscosity.

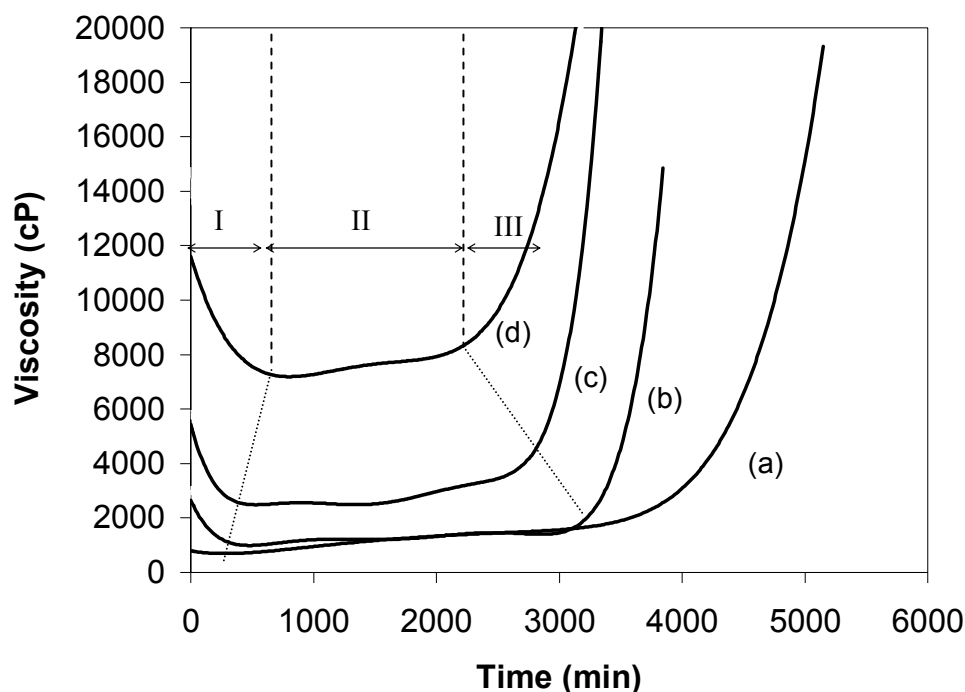


**Figure 4.8 .** Variation of viscosity of spinning solution of PAni (LEB) 10% w/w in DMPU containing (a) 0.00 % (b) 0.05 % (c) 0.10 % or (d) 0.20 % (w/w) of SWNT with regard to solvent. Shear rate =  $1 \text{ s}^{-1}$ .

Mattes and co-workers [18] observed a decreasing trend of viscosity over time (as in region I) for PAni (EB) (17-25 % w/w) in NMP. The authors claimed that a specific time was required for the formation of a complex between the EB and added gel inhibitor molecules (2- methyl aziridine). Due to the formation of such a complex, the interaction between EB molecules decreased and therefore, the solution viscosity decreased. It was

noted that, for higher concentrations of EB, more time needed to reach the plateau zone corresponding to region II and complete complex formation. In the present study, similar behavior was observed Figure 4.8 with the mixing of SWNTs with PAni. The higher the SWNT content, the higher the viscosity obtained and the longer the time required reaching the plateau zone. This behavior may be considered analogous to the behavior of highly concentrated PAni (EB)/2-methyl aziridin(2-MA) solution complex[18]. For all samples, it was observed that the viscosity reached a low value plateau after a certain time (region II). This region is the preferred window of time for wet spinning since the viscosity is stable. The time window of reach region II decreased from 4000 min for the neat PAni solution to 1500 min for the composite solution containing 0.20 % w/w SWNTs. In regard to the time width of region I, higher concentrations of SWNTs in PAni solutions led to an increase in region I since there is a greater probability to form entangled structures, so that longer time periods are needed to break up such structure.

The very sharp change in the slope of viscosity versus time in Figure 4.8 (region III) can be used to identify the gelation time [19]. Gelation is characterised by both a large increase in viscosity and by the development of an elastic network. Once gelation begins, the solutions are unsuitable for wet spinning. Gelation in PAni solutions is known to be caused by hydrogen bonding interactions between polymer chains that produce a 3D network [18]. The presence of SWNTs in the solution assists in the formation of such networks through strong interactions between the SWNT and the polymer chains. In fact, SWNTs have been previously shown to produce gels in polymer solutions that do not form gels in the absence of CNTs (e.g. polycarbonate with and without CNTs for same polymer concentrations [20]).

Figure 4.9 shows the viscosity of PAni/ SWNTs solutions taken from region II in Figure 4.8 versus shear rate. The viscosity at low shear rate is a meaningful criterion for processes such as film casting, however, for continuous fibre spinning, the effect of high shear at the orifice of the spinneret should be taken into account. As the SWNT content increases in this composite system, nanotube –nanotube interaction and nanotube-polymer interactions begin to dominate producing a higher viscosity, particularly at low shear rate. In addition solutions containing SWNTs showed a non-Newtonian shear thinning behaviour, whereas, the neat PAni solution shows only a very small dependence on the shear rate

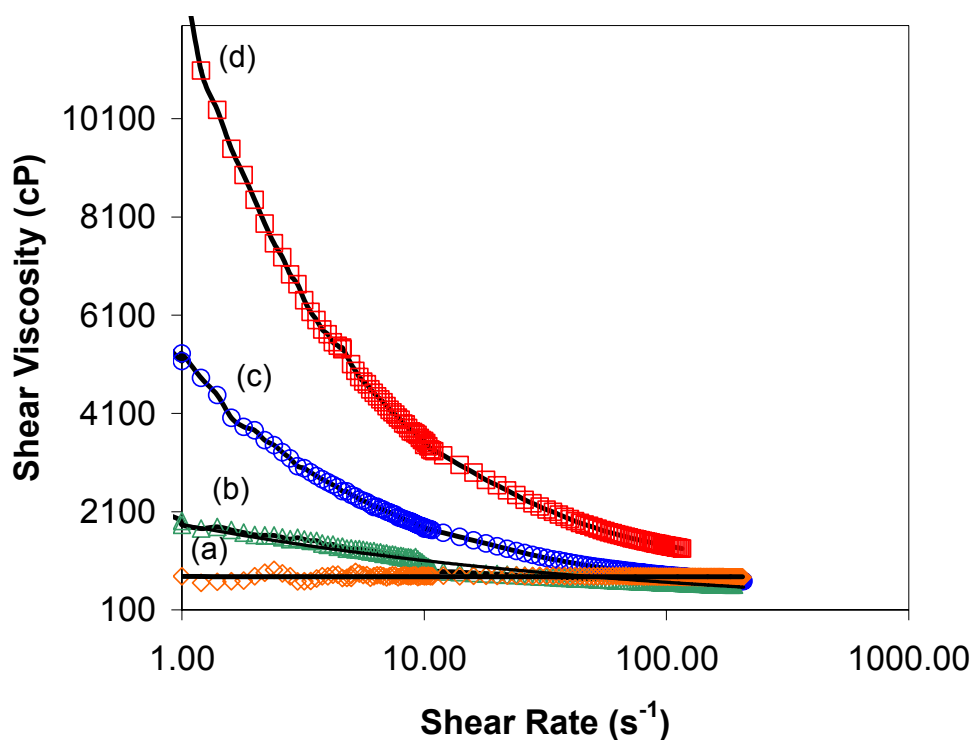


**Figure 4.9.** Variation in viscosity of spinning solution based on PAni (LEB) 10 % w/w in DMPU containing (a) 0.00 % (b) 0.05 % (c) 0.10 % (d) 0.20 % (w/w) SWNT with regards to solvent, at different shear rates.



Table 4.5 demonstrates the power law exponent and power law coefficient of the spinning solutions having different SWNT contents. The power law equation is:

$$\eta = K \dot{\gamma}^{n-1} \quad \text{Equation 4-1}$$

Where

$\eta$  = Viscosity (cP)

$\dot{\gamma}$  = Shear rate (1/s)

$K$  = Consistency index (cP)

$n$  = Flow index (power law exponent)

**Table 4.5.** Power law coefficients and exponents for PAni solution with different SWNT content in DMPU

% w/w SWNT/DMPU	0.00 %	0.05%	0.10%	0.20%
<b><i>K</i></b>	780	1838	4814	11935
<b><i>n</i></b>	0.99	0.78	0.61	0.52
<b>% of confidence</b>	95	95	96	98

The presence of SWNTs in the PAni solutions facilitated a greater entanglement of polymer chains through the strong interactions that form between the SWNTs and the PAni. Consequently, the viscosity at low shear rates was higher for solutions containing

more SWNTs (Figure 4.9). High shear mixing likely disrupt SWNT /polymer interactions, therefore reducing the viscosity. It was interesting to note that the viscosity of the PAni containing 0.05 % w/w or 0.10 % w/w SWNTs solutions was essentially the same as that of the neat PAni solution at high shear rates. For example, the PAni solution containing 0.20 % w/w SWNTs showed a viscosity similar to neat PAni at  $100 \text{ s}^{-1}$  shear rate. (Figure 4.10). Thus, the high shear rates used in the wet spinning process can virtually eliminate the effect of the SWNT-polymer interaction so that the viscosity becomes equivalent to the neat PAni solution.

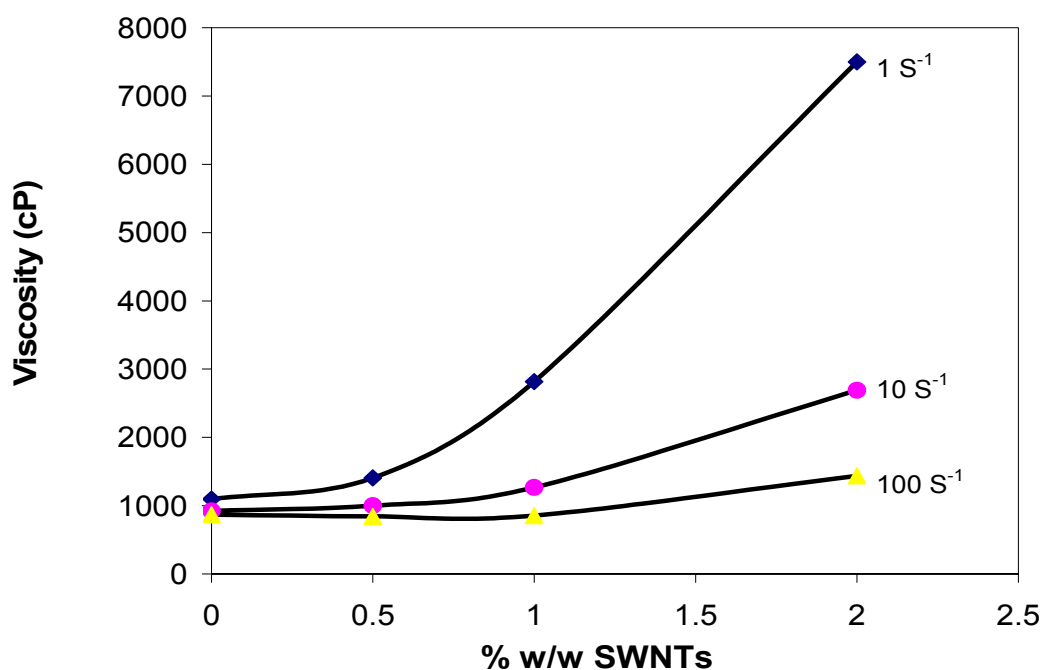


**Figure 4.10.** Viscosity versus SWNTs content at different shear rate

During fibre formation, the shear rate in the spinneret channel through unsteady Poiseuille flow can reach a range of  $10^4 - 10^6 \text{ s}^{-1}$  [21] depending on the dimensions of the spinneret,

the flow rate and the power law exponent. For shear thinning fluids, the effective viscosity at the spinneret can be many times less than the initial value and it may drop in the spinneret flow to even 1/10 to 1/30 of the initial zero shear viscosity [22]. This clearly indicated that the wet spinning conditions used in this study, the viscosity of PAni/SWNT solutions in the spinneret was essentially independent of SWNT content. This is an important observation, since the flow rate of each of the composite solution should be similar for a given injection rates. The plot of PAni/ SWNT solution viscosity against SWNTs content for various shear rates in Figure 4.10 illustrates this point.

#### **4.3.4. The effect of fibre spinning parameters on PAni/SWNT morphology**

For improved mechanical and electrical properties, it is desirable to reduce fibre porosity and to maximise alignment of SWNTs along the fibre axis. Several researchers have investigated the effect of polymer concentration, polymer molecular weight and temperature and formulation of the coagulation bath on the mechanical properties of wet spun fibres [19, 23]. The higher the molecular weight and the concentration of the polymer in the spinning solution, the lower the porosity in the resultant fibre [19]. It also has been shown that, the use of a higher coagulation bath temperature results in macrovoids that degrade the mechanical properties [19, 22]. In addition, it has been observed that addition of solvent into the coagulation bath decreases porosity through decreasing of the solvent –nonsolvent counter diffusion rate [19]. Finally, drawing of fibres can improve the mechanical properties through polymer chain alignment [24].

The following sections consider the effect of coagulation bath formulation and take up velocity on the morphology of PAni/SWNTs fibres.

**4.3.4.1. Influence of solvent in the coagulation bath on morphology of as spun fibre**

The addition of solvent into the coagulation bath is a common technique used to minimise macrovoid formation during the wet spinning of fibres. More dense fibres are produced because of the slower diffusion rate of the solvent out of the fibre into the non solvent, and also due to delays in the demixing of solvent and non solvent [25]. Different NMP/Water mixture compositions were prepared to find which formulation produced the minimum porosity in composite fibres prepared from 10 % w/w PAni (LEB) with or without SWNTs solutions. It was observed that for 30 % w/w NMP in water, the spinning line actually absorbs solvent from the coagulation bath and the fibre skin does not form at all. Decreasing the solvent content to 20 % w/w NMP in water increased the possibility of fibre formation; however the slow diffusion rate of solvent caused a very slow solidification rate so that a higher residence time was needed to produce cohesion high enough for proper handling of the fibres. In this case a very long coagulation bath or a very slow take up velocity would be required to remove the majority of the solvent from the nascent fibre. Such operating conditions were not feasible using our setup. Fibre solidification in a water based coagulation bath containing 10 % w/w NMP occurred at a faster rate and yielded fibers that could be readily handled. The cross sectional SEM of these fibres are shown in Fig 4.11-a, c. A coagulation bath of pure water resulted in very rapid skin formation and smooth surface fibres (Figure 4.11-b,d). However, these fibres showed much higher porosity after taking up from the first coagulation bath compared to fibres produced from the 10 % w/w NMP in water coagulation bath. Based on these observations, a 10 % w/w NMP in water solution was used in subsequent experiment.

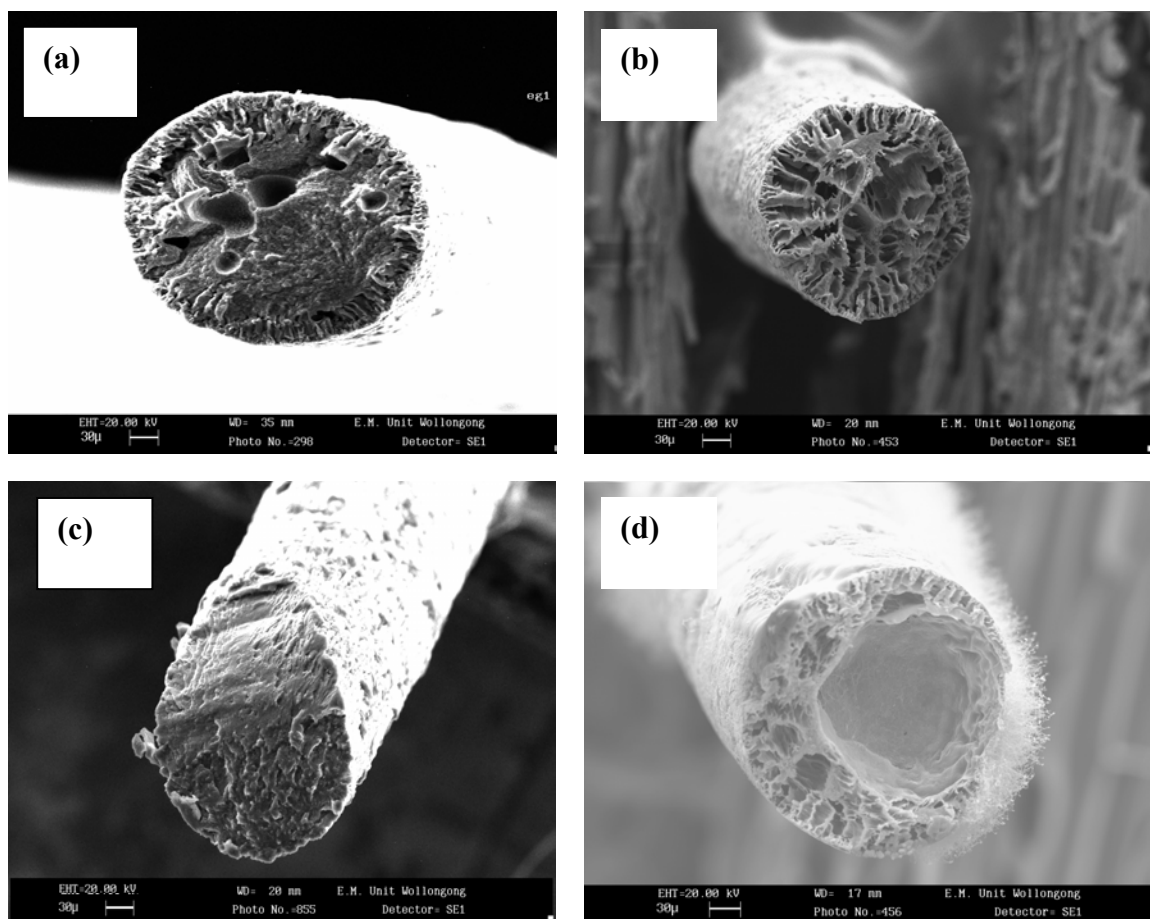


**Figure 4.11.** Cross sectional SEMs of PAni (a, b) and PAni/SWNTs (2.0 % w/w SWNTs (c, d) into a coagulation baths containing (a,c) 10 % w/w NMP in water or ( b, d) water using take up velocity of 2 m/min. Scale bar 30 µm.

#### 4.3.4.2. The influence of take up velocity on morphology

Using a 10 % w/w NMP in water coagulation bath, different take up velocities were examined using the same spinneret and the same spinning solution. The cross sectional SEMs in Figure 4.12 demonstrate the porosity of as spun fibres using take up velocities of 3 or 6 m/min. These take up velocities corresponded to residence time of 40 sec and 20 sec in coagulation bath respectively. It can be seen from Figure 4.12 that increasing the take up velocity resulted in higher porosity as a consequence of an incomplete

solidification process for residence times 1 min. Although the increased take up velocity resulted in smaller diameter, the prescribed residence time utilised did not seem to be sufficient for fibre skin formation and complete growth towards the core region. Based on these results, a take up velocity 2m/min was adjusted for fibre spinning to reach the minimum porosity in the given range of spinning solution viscosities.

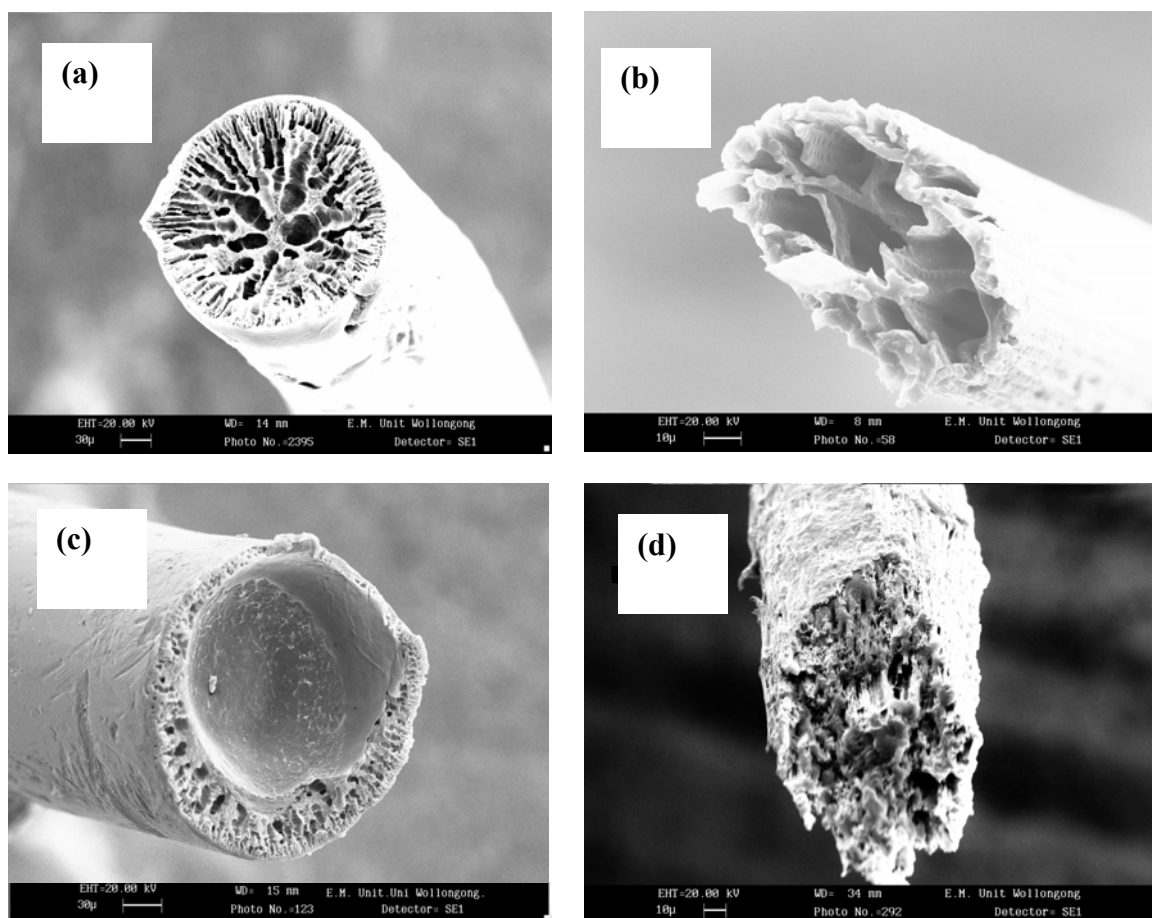


**Figure 4.12.** Cross sectional SEMs of PAni/SWNT fibers spun using different take up velocities for PAni(a, b) PAni/SWNTs containing 2 % w/w SWNT( c, d). Take up velocities were 3 m/min (a, c) or 6 m/min (b, d). Scale bar is 30  $\mu\text{m}$  (a,c) and 10  $\mu\text{m}$  (b, d)

### 4.3.5. Thermal transition temperatures in as spun fibre

The as-spun fibre after drawing may retain the capability to be further stretched at higher temperatures. The extent of stretching and the choice of thermal drawing temperature of as-spun fibres depend on the solvent /nonsolvent residual in the structure of the fibres [26]. The DSC thermogram of neat PAni (LEB) for two consecutive heat-cool cycles was recorded using a scan rate of 5 °C/min and is illustrated in Figure 4.13.

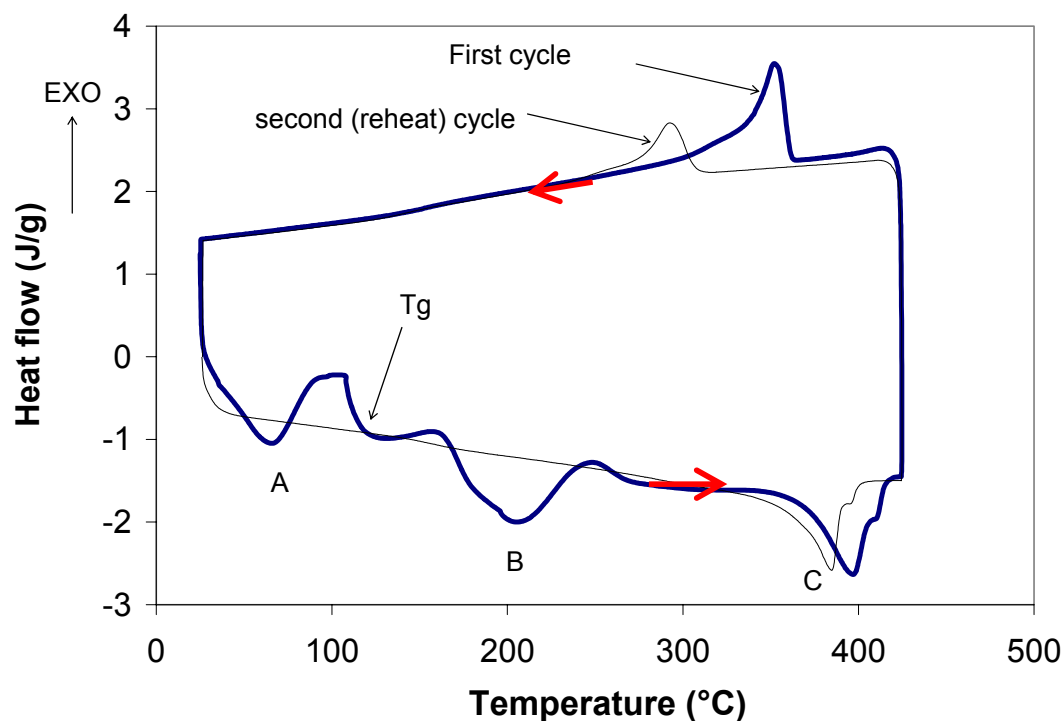


**Figure 4.13.** DSC thermal analysis curve of neat as spun polyaniline (LEB) fibre under a  $N_2$  atmosphere first cycle (thick line); second (reheat) cycle (thin line)

In the first cycle, the DSC curve shows two endotherms in temperature ranges of 50-100 °C (A) and 160-240 °C (B) most likely corresponding to the vaporisation of water and solvent (DMPU). Another endothermic peak was observed at ~ 400 °C (C). This peak is a consequence of thermal melting, since it also appeared in the second cycle at a similar

intensity, although it shifted slightly to 385 °C [27]. Crystallisation exotherms during the cooling cycles on the first and second cycles were observed in Figure 4.13 which can be attributed to the thermoplastic property of PAni in LEB oxidation state. These observations are in good agreement with previous studies for the LEB form of polyaniline [5]. Between the first (A) and second (B) endothermic peaks, a sudden drop in heat flow was clearly observed. The temperature corresponding to halfway between the onset (110.9 °C) and end (117°C) of the step/glass transition region represents the glass transition temperature ( $T_g$ ) which is  $\sim 110$  °C. This value is less than the reported  $T_g$  for annealed PAni (LEB) of 220 °C [27], presumably due to solvent/nonsolvent remaining in the fibre after the drying process used in this study. The solvent/nonsolvent mixture acts as a plasticiser during the stretching process and reduces the  $T_g$  of the polymer compared with the completely dry polymer [5].

In general, SWNTs increase  $T_g$  [28-30]. However, the effect of SWNTs on PAni/SWNT fibres was dominated by the influence of residual solvent/nonsolvent. As a result, the composite fibres containing different amounts of SWNTs were thermally stretched in a range of temperature similar to that used for neat PAni fibres.

#### **4.3.6. Thermal stretching**

The SEM micrographs presented in Figure 4.14 show the cross sectional morphology of the PAni/SWNT s with varying SWNT content following thermal stretching process. For solid fibres the nanotube content is described with respect to the weight of initial PAni (2 g). Thermal stretching created a considerable plastic flow in the PAni/SWNT composite fibres which reduced fibre diameter and porosity compared to when thermal stretching of fibres was not used (Figure 4.12.)



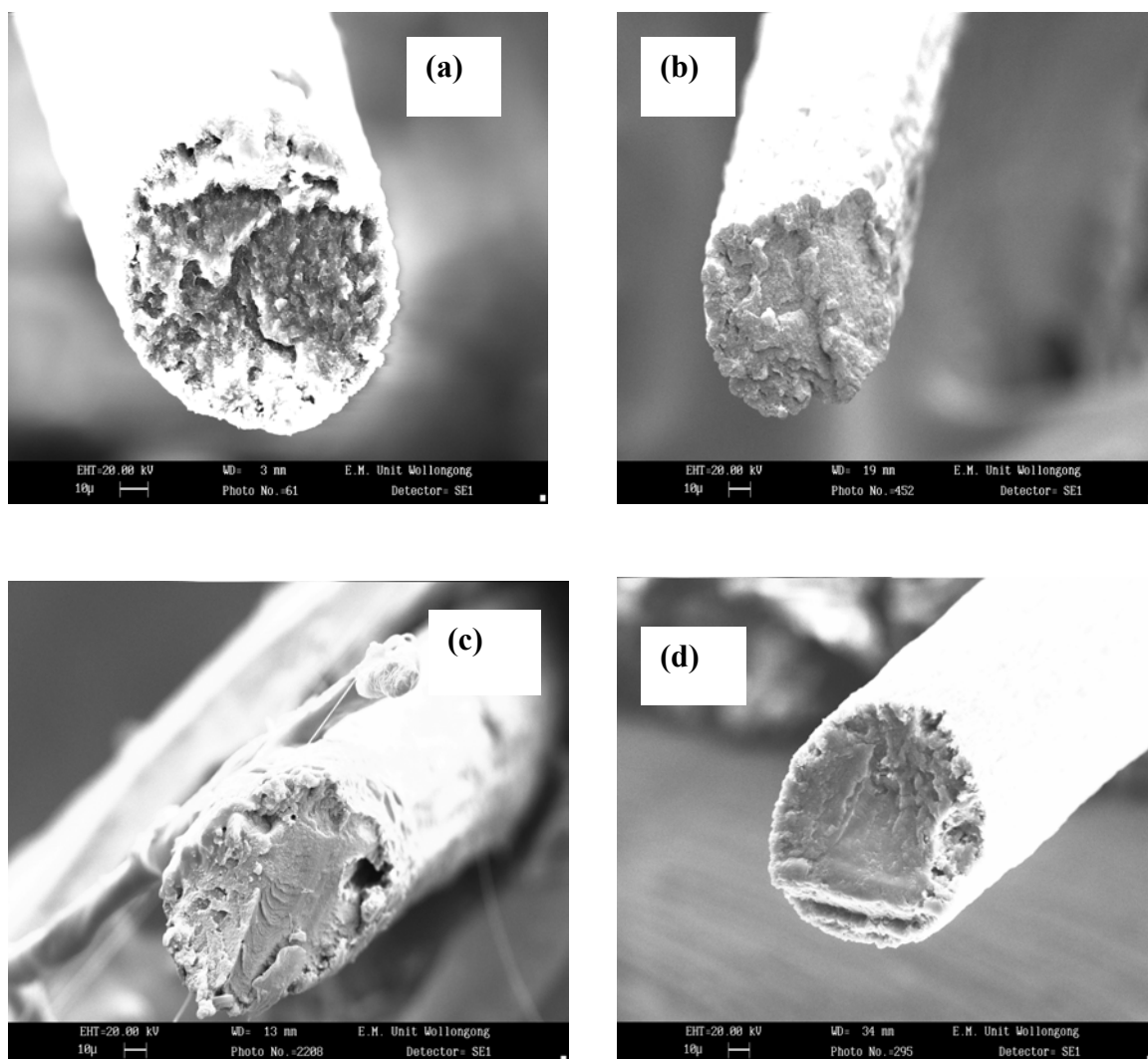


**Figure 4.14.** SEM micrographs of PANi/SWNTs fibres after thermal stretching containing (a) 0.0 %, (b) 0.5 %, (c) 1.0 % and (d) 2.0 % (w/w) SWNTs with respect to PANi

Table 4.6 shows that fibre diameters were reduced to between 85 -100  $\mu\text{m}$  (compared to  $\sim 210 \mu\text{m}$  in spun fibres) and the bulk densities were increased to between  $\sim 0.9\text{-}1.1 \text{ g/cm}^3$  (compared to  $\sim 0.7\text{-}1.0 \text{ g/cm}^3$  for as spun fibre)

**Table 4.6.** The typical diameters, deniers and densities of thermally stretched 2x drawn PAni/SWNT fibre containing different amounts of SWNTs

<b>% w/w SWNT</b>	<b>Denier</b>	<b>Diameter(<math>\mu\text{m}</math>)</b>	<b><math>\rho(\text{g}/\text{cm}^3)</math></b>
<b>0</b>	$65 \pm 10$	$100 \pm 10$	$0.91 \pm 0.15$
<b>0.5</b>	$55 \pm 15$	$85 \pm 5$	$1.0 \pm 0.10$
<b>1</b>	$70 \pm 10$	$95 \pm 5$	$1.1 \pm 0.10$
<b>2</b>	$60 \pm 10$	$100 \pm 5$	$1.0 \pm 0.10$

#### 4.3.7. Mechanical properties of thermally stretched PAni/SWNT fibres

The effect of SWNTs loading on the mechanical properties of composite PAni/SWNT fibres (2 X drawn) was investigated. Results of tensile stress-strain testing are shown in Figure 4.15. For undoped PAni, the addition of 2 % w/w SWNTs increased the yield stress by 100 %, tensile stress ( $\delta_b$ ) by 50 %, and Young's Modulus (E) by more than 200 %. A 30 % decrease in elongation at break ( $\epsilon_b$ ) was also observed. The data from the tensile testing of undoped PAni/SWNT fibres with varying SWNTs content summarised in Table 4.7. A common unit for reporting mechanical properties is the "gram per denier" (gpd) as defined in Chapter 3. The data in Table 4.7 has been converted to gpd using formula 3.15. After acid doping of PAni/SWNTs fibers with MSA (1 M) solution for a 24 hrs a 40 % decrease in the Young's modulus and a 25% decrease in tensile strength were observed for the fibre containing 2% w/w SWNTs. In comparison much higher decrease of 50% in Young's modulus and a 70 % in tensile strength occurred upon acid doping of neat PAni fibres.

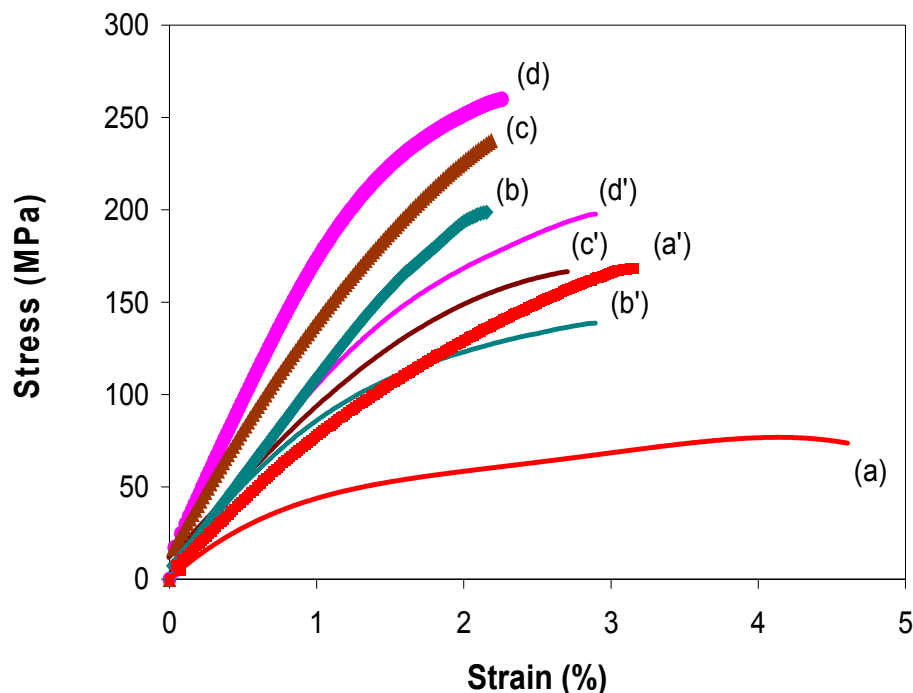


**Figure 4.15.** Stress strain curves of PAni/SWNTs composite fibres with varying SWNTs content, before doping ( thick lines) and after doping for 24 hrs in MSA(thin lines). (a,a')Neat PAni, (b,b') PAni/SWNT (0.5 % w/w) (c,c') PAni/SWNT (1.0 % w/w) (d,d') PAni/SWNT( 2.0 % w/w).

Presumably, the reduction in modulus and strength of fibres after acid doping was related to the introduction of charge and counter ions on the polymer in addition to the swelling that occurs during doping where by the swelling reduces the effective weight or volume fraction of the nanotubes. The smaller decreases in modulus and strength for composite PAni/SWNT fibres compared to neat PAni fibre further illustrates the efficient reinforcement produced by the SWNTs. Table 4.8 summarises the tensile testing data of PAni/SWNT fibres with varying SWNTs content after acid doping using MSA solution for 24 hrs.

**Table 4.7.** Influence of SWNTs loading on mechanical properties of PAni/SWNTs fibres before acid doping

% w/w SWNTs	$\sigma_{y=0.2}$		$\delta_b$		E		$\epsilon_b$ (%)
	(MPa)	gpd	(MPa)	gpd	GPa	gpd	
0	120 $\pm$ 27	1.5	168 $\pm$ 45	2.1	6.6 $\pm$ 0.4	82	3.1 $\pm$ 1.5
0.5	195 $\pm$ 5	2.1	198 $\pm$ 20	2.4	10.5 $\pm$ 1.8	111	2.1 $\pm$ 0.3
1.0	230 $\pm$ 15	2.4	236 $\pm$ 25	2.4	13.8 $\pm$ 2.7	142	2.1 $\pm$ 0.6
2.0	250 $\pm$ 38	2.6	260 $\pm$ 33	2.75	17.2 $\pm$ 1.3	183	2.2 $\pm$ 0.5

**Table 4.8.** Influence of SWNTs loading on mechanical properties of PAni/SWNT fibres after doping with MSA for 24 hr

% w/w SWNTs	$\sigma_{y=0.2}$		$\delta_b$		E		$\epsilon_b$ (%)
	(MPa)	gpd	(MPa)	gpd	(GPa)	gpd	
0	35 $\pm$ 8	0.434	45 $\pm$ 10	0.56	3.5 $\pm$ 0.5	25	4.6 $\pm$ 1.0
0.5	110 $\pm$ 7	1.155	138 $\pm$ 17	1.7	7.0 $\pm$ 1.8	93	3.1 $\pm$ 0.3
1.0	145 $\pm$ 15	1.4935	145 $\pm$ 20	1.6	9.4 $\pm$ 2.5	97	2.7 $\pm$ 0.5
2.0	165 $\pm$ 25	1.749	197 $\pm$ 30	2.1	10.5 $\pm$ 1.7	112	2.8 $\pm$ 0.5

As described above, thermal stretching improves the properties of PAni/SWNT fibres by collapsing the voids, producing lower porosity and alignment of polymer chain. The SEM images of the fracture surface of neat PAni fibre and PAni/SWNT (2 % w/w) further confirms the low porosity of the thermally stretched fibres (Figure 4.16). Since the porosity of PAni/SWNT fibres appears to be independent of SWNT content, other factors

must explain the significant improvement in mechanical properties when SWNT are added to the PAni matrix.

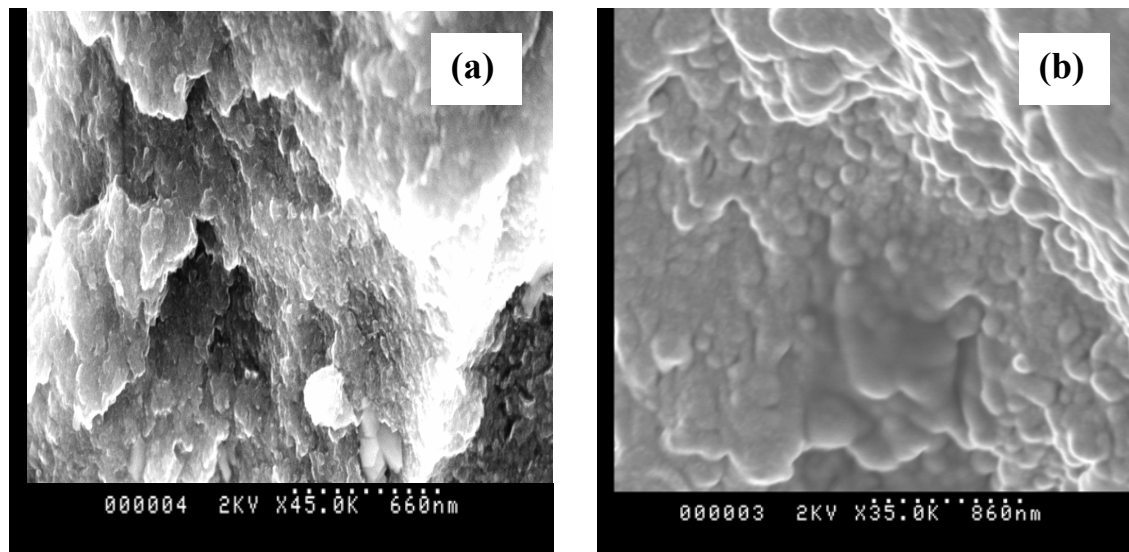


**Figure 4.16.** SEM images showing a typical cross sectional surface of (a) neat PAni (b) PAni/ SWNT (2.0 % w/w).

Improvement in the mechanical properties of polymers reinforced with SWNTs has been observed previously in several studies. Cadek and colleagues [29, 31] found that Young's Modulus increased by a factor of 1.8 at 1 % w/w SWNTs in poly vinyl alcohol (PVA). Such behavior has also been observed in the case of composite fibres such as the 50% improvement in elastic modulus of poly(p-phenylene benzobisoxazole)(PBO) reinforced with SWNT (10 % w/w) when compared to neat PBO [32], and increases in the tensile strength and elastic modulus by factors of 1.5 and 1.7 respectively by addition of 5 % w/w SWNTs to polyacrylonitrile (PAN) [33]. In the present study, the modulus of PAni fibres was observed to increase by a factor of  $\sim 2.5$  with the addition of 2.0 % w/w SWNTs which is significant when compared to previous studies of polymer composites with low

SWNT content [29, 31]. Theoretical basis for the improved mechanical properties of SWNT-reinforced PAni fibres is discussed below.

According to the Krenchel's rule of mixture, the elastic modulus of composites containing short length fillers can be represented as a function of the elastic modulus and volume fraction of constituents [34]:

$$E_C = E_{effNT} \nu_{NT} + (1 - \nu_{NT}) E_P \quad \text{Equation 4-2}$$

Where,  $E_C$  and  $E_P$  are the elastic modulus of composite and polymer matrix respectively.  $E_{effNT}$  is the effective modulus of elasticity of nanotubes and  $\nu_{NT}$  is the volume fraction of nanotubes. The value of  $\nu_{NT}$  can be obtained from the weight fraction of nanotubes ( $\omega_{NT}$ ) and densities of the nanotube and polyaniline fibres. These values are 1.3 [35] and ~0.9-1.0 (the calculated amount in previous section), respectively. According to the data given in Table 4.9 for the elastic modulus of the composite fibres and the volume fraction of nanotubes in the composite, the effective elastic modulus of nanotubes can be calculated based on equation (4.2). The effective elastic modulus of SWNTs ( $E_{effNTs}$ ) decreases from 970 GPa in the composite containing 0.5 % w/w to 641 GPa in the composite with 2 % w/w SWNT loading before doping. The  $E_{effNT}$  similarly decreases in nearly a similar fashion after doping. The weight and volume fraction after doping were calculated based on the weight of polymer and dopant (assuming 2 units of  $MSA^-$  dopant for every 4 aniline units within PAni).

**Table 4.9.** The effective elastic modulus of SWNT bundles embedded in undoped and doped PAni matrix

$\phi_{NT}$		$\nu_{NT}$		$E_C$ (GPa)		$E_{eff NTs}$ (GPa)	
before doping	after doping	before doping	after doping	before doping	after doping	before doping	after doping
0.0	0.0	0	0	6.6	3.5	-----	-----
0.5	0.4	0.004	0.003	10.5	7	970	1000
1.0	0.8	0.008	0.007	13.8	9.5	880	860
2.0	1.7	0.016	0.014	17	10.5	640	520

The Young's modulus of an individual SWNT varies in the range of 1.5 to ~5 TPa [36-38]. The effective SWNT modulus is lower than the ideal value because of the non-perfect orientation and bundling of the nanotubes along the fibre axis, which allows for inter-tube slippage[39]. The decreased effective modulus of SWNTs (Table 4.9) observed at higher SWNT content in the PAni/SWNT composite fibres suggests that the bundle size of SWNTs increases.

The mechanical properties of PAni/SWNT composite fibres reported in this study exceed those reported previously for neat PAni fibres[25]. The tensile strength of fibres produced from PAni (LEB) after doping [27] or PAni/AMPSA [25] are in the range of 95-169 MPa. For the PAni/SWNT fibres containing 2 % w/w SWNTs prepared in this study, the tensile strengths were 260 MPa (before doping) and 197 MPa (after doping). Moreover, the Young's Modulus of PAni/SWNT fibres was 17 GPa, much higher than PAni fibres produced in previous studies (2-7 GPa) [25, 27].

**4.3.8. Flexibility of PAni/SWNT composite fibres**

Flexibility is a prerequisite for the practical applications of fibres in the textile industry. The previous section showed that PAni/SWNTs composite fibres show improved tensile strength and elastic modulus, however also show low strain and little plastic deformation. Pure flexibility is a major obstacle in preparing twisted fibres and fibre bundles. The SEMs of PAni/SWNTs fibres with varying SWNT content in Figure 4.17 demonstrate the limited tolerance of composite fibres compared with neat PAni fibre under the flexural load applied by a simple knot.

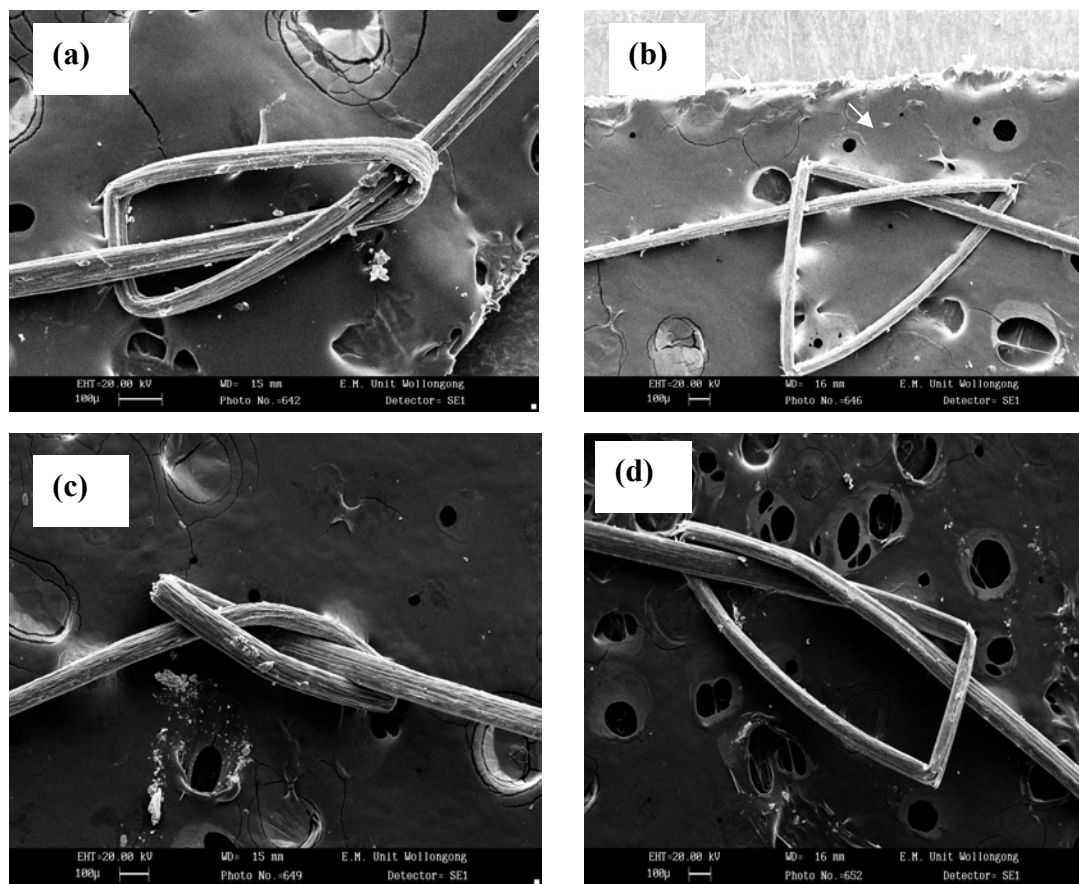


**Figure 4.17.** SEMs of PAni/SWNTs composite fibres under flexural load with SWNTs of

(a) 0.0 % w/w (b) 0.5 % w/w (c) 1.0 % w/w (d) 2.0 % w/w



### 4.3.9. Raman spectroscopy of PAni/SWNTs composite fibres

The interaction between PAni and SWNTs within PAni/SWNTs composite fibres before doping was investigated using Raman Spectroscopy (Figure 4.18).

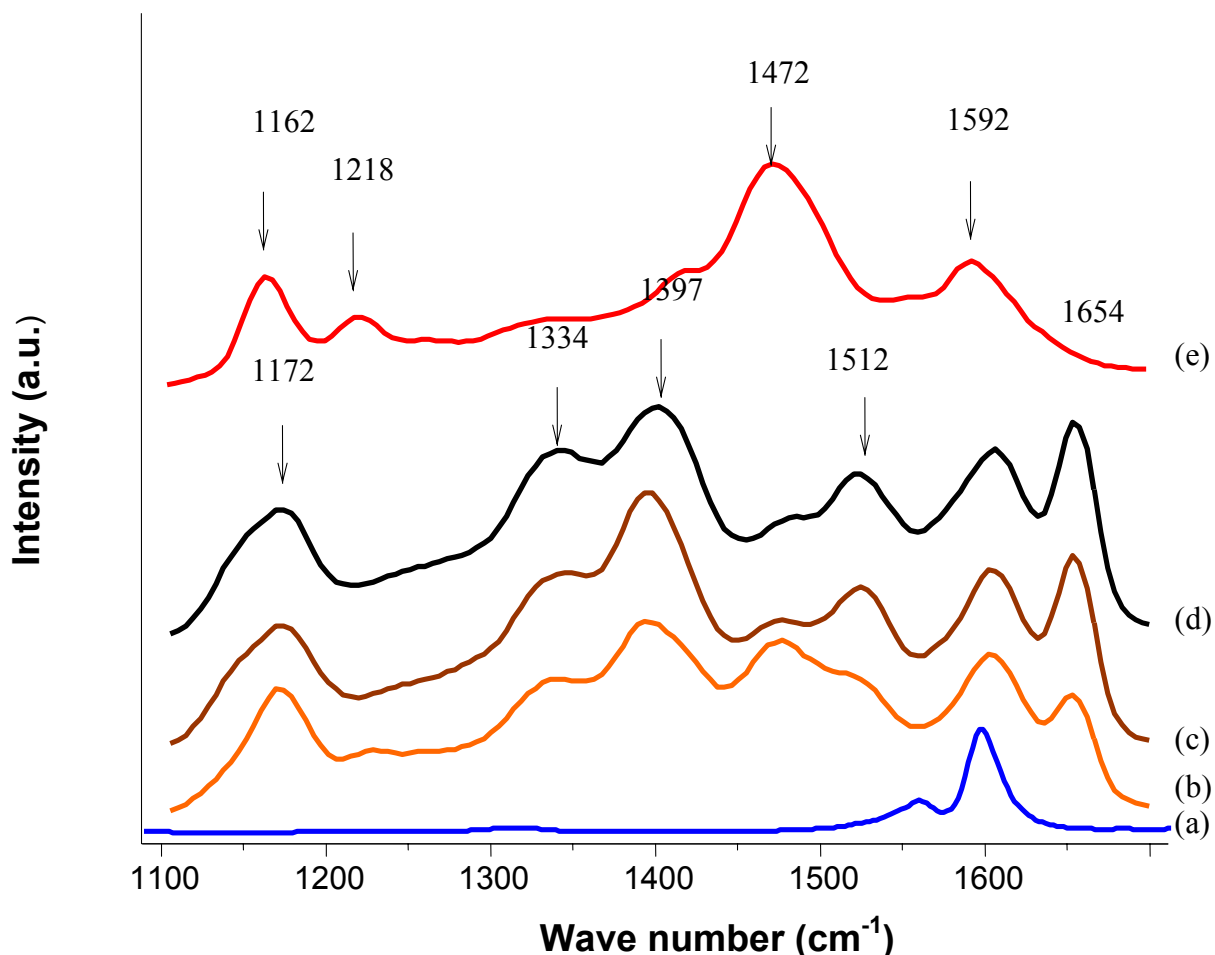


**Figure 4.18.** Enhanced Raman Spectra (before doping) of (a) neat SWNTs, (e) neat PAni and PAni/SWNTs fibres with varying SWNT content (b) 0.5 %w/w (c) 1.0% w/w, (d) 2.0% w/w ( $\lambda_{exc}=632.8$ ).

PAni Raman bands attributed to the quinoid ring (refer to Chapter 2) in the LEB state is fully reduced and should not be observed. However, LEB is a very unstable oxidation state and tends to switch to the emeraldine base (EB) form when the spinning solution is exposed to the atmosphere as evidenced visually by the appearance of the blue color. This

was confirmed in the Raman spectrum of neat PAni (Figure 4.18-e) which showed peak at  $1162\text{ cm}^{-1}$  and  $1472\text{ cm}^{-1}$  due to quinoid ring. Raman bands that may be observed for PAni are summarised in Table 4.10. The bands observed at  $1162\text{ cm}^{-1}$  and  $1472\text{ cm}^{-1}$  are attributed to C-H stretching and C=N stretching of the quinoid ring, respectively. The presence of the benzoid ring results in bands at  $1592\text{ cm}^{-1}$  corresponding to C=C stretching and  $1218\text{ cm}^{-1}$  attributed to C-N stretching [40-42].

**Table 4.10.** Assignment of enhanced Raman spectra bands

Raman shift( $\text{cm}^{-1}$ )	Assignment
1654, 1397	Ooxidised or deprotonated PAni segment
1592	C-C stretching of Benzoid ring
1512	N-H bending of bipolaronic structure
1472	C=N stretching of quinod ring
1337	C-N <sup>+</sup> stretching of bipolaron structure
1218	C-N stretching of Benzoid ring
1162	C-H stretching of quinoid ring
1173	C-H stretching of benzoid ring

When SWNTs were introduced into the PAni matrix the Raman spectra changed significantly. A decrease in intensity of the  $1472\text{ cm}^{-1}$  band (C=N stretching of quinoid ring) and an shift of the  $1162\text{ cm}^{-1}$  band (C-H stretching of quinoid ring) to  $1172\text{ cm}^{-1}$  band (C-H stretching of benzoid ring) were obvious(Figure 4.18(b-d)). It has been shown

that a decrease in the intensity of peaks assigned to the quinoid ring provides strong evidence for site selective interaction between the quinoid ring of PAni and SWNTs [43]. In fact, the  $\pi$ -bonded surface of SWNTs might interact strongly with conjugated structure of PAni especially through the quinoid ring. In fact, aromatic structures tend to interact with the plane of graphite surface via  $\pi$ - $\pi^*$  interaction [44] and such a  $\pi$  stacking interaction between PAni and SWNTs may likely be here. Schematic in Figure 4.19 illustrates the likely interaction between PAni and SWNTs, although the exact mechanism of doping is not fully understood. It is possible that functionalization of nanotubes during sonication provides the counter ion for the partially doped PAni

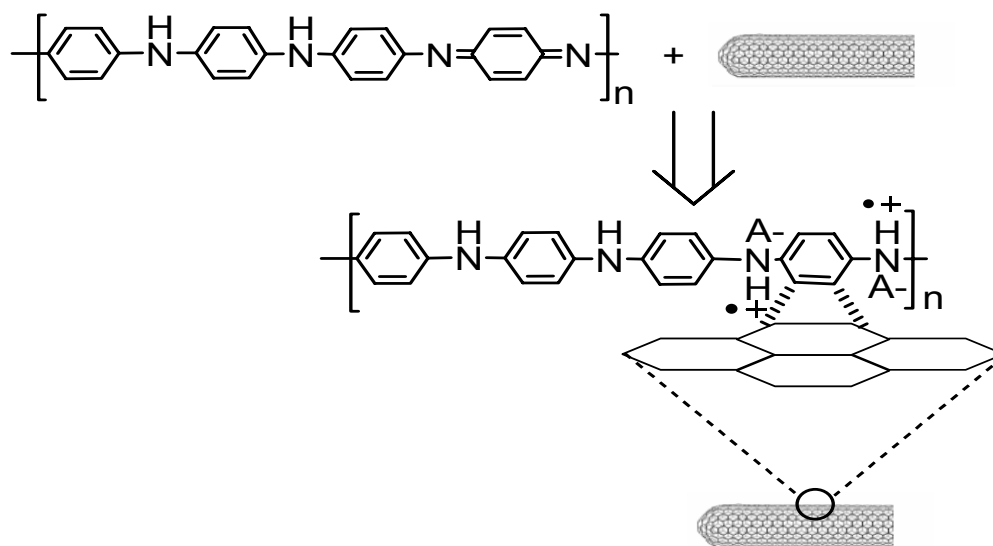


**Figure 4.19.** The schematic illustrating the interaction of SWNTs with PAni through the quinoid rings of latter.

It is worth noting that the up shift of the  $1162\text{ cm}^{-1}$  band to  $1172\text{ cm}^{-1}$  with increasing amounts of SWNTs indicated a transition towards the salt structure in the polymer [40-42]. In addition, the band at  $1334\text{ cm}^{-1}$  corresponding to  $\text{C-N}^+$  stretching of the radical

cation, is a Raman signature attributed to the of salt structure [41, 45] that was observed to grow in intensity with increasing SWNT content. Therefore, in the case of PAni/ SWNT fibres before doping, SWNTs play the role of a doping agent [44, 46], partially changing the base form of PAni to the salt form. The SWNTs appear to act as radical anion fragments interacting with positive charges induced on the PAni chain [44]. The emergence of bands at  $1397\text{ cm}^{-1}$  and  $1665\text{ cm}^{-1}$  in Figure 4.18 have not been reported in previous work on PAni/SWNT composites, presumably due to differences in the methods used for the processing of fibres ( e.g. coagulation, thermal stretching).

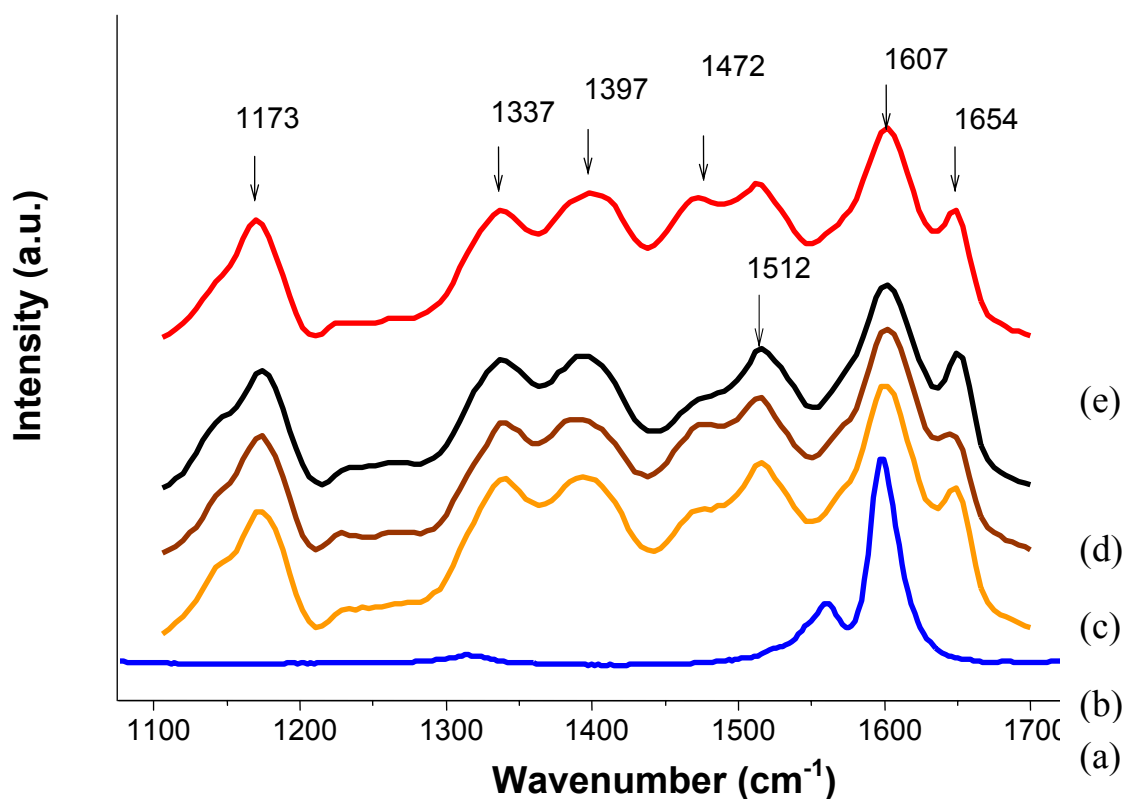


**Figure 4.20.** Enhanced Raman Spectra(after doping in MSA solution for 24 hrs following by drying at  $100\text{ }^{\circ}\text{C}$ ) of (a) neat SWNTs (e) neat PAni and PAni/SWNTs with varying SWNTs content (b) 0.5 % w/w, (c) 1.0 % w/w, (d) 2.0 % w/w

In regards to chemically doped PAni Colomban and coworkers [47] found that fibres of PAni Emeraldine salt (ES)-camphor sulphonic acid (CSA) and ES PAni doped with HCl have bands at  $1390\text{ cm}^{-1}$  and  $1650\text{ cm}^{-1}$  upon red light (647.1nm) excitation.

The  $1650\text{ cm}^{-1}$  band was assigned to the C=C stretching mode of the quinoid ring of a deprotonated PAni chain segment. In other studies [48, 49], the bands at  $1397\text{ cm}^{-1}$ , and  $1654\text{ cm}^{-1}$  appeared in the Raman spectra of doped PAni that had been heated in air. However, these bands were not observed in the spectrum of the PAni that had been sealed in a vacuum and heated, suggesting that these features came from a structure produced through oxidation of the polymer matrix resulted in a cross linked network [49]. The enhancement of peaks at  $1397\text{ cm}^{-1}$  and  $1654\text{ cm}^{-1}$  in PAni/SWNT fibres before doping Figure 4.18, therefore, can be firstly considered as evidence for the doping of PAni by SWNTs (similar spectra to those observed for ES form of PAni). Secondly, it suggests that SWNT to increase the possibility for the formation of a cross linked structure. The Raman spectra of PAni (ES) with and without SWNTs (Figure 4.20) are very similar except in the bands related to the interaction of PAni and SWNTs namely the decrease in intensity of the band at  $1475\text{ cm}^{-1}$  and the shift of the peak at  $1168\text{ cm}^{-1}$  to  $1173\text{ cm}^{-1}$ ). The prescribed peaks for PAni/SWNT fibre before doping increased in intensity after acid doping.

#### **4.3.10. Electrical properties of PAni/SWNTs fibres**

The potential interaction between highly delocalised  $\pi$ -electrons of SWNTs and the  $\pi$ -electrons of the polymer backbone of PAni increases the effective electron delocalisation and as a consequence may improve the conductivity of the host polymer. Specifically the enhancement of the  $1337\text{ cm}^{-1}$  band before doping of PAni (Figure 4.18) corresponded to

the C-N<sup>+</sup> stretching of the bipolaron structure, thereby forming a conductive way. Therefore the doping and interconnectivity of SWNTs may contribute to the formation of a conductive pathway in the PAni/SWNT composite before acid doping. The following section consider the electrical properties of the PAni/SWNTs composite fibres before and after acid doping.

#### **4.3.10.1. Electrical properties of PAni/SWNTs fibres before acid doping**

One of the great advantages of SWNTs over other conducting fillers is low critical concentration (known as percolation threshold [50]) required to achieve interconnection between filler particles. For instance, for carbon black a loading level of ~ 25 % w/w is required to achieve sufficient electrical conductivity in typical solution or melt-based system [51, 52]. Replacing carbon black with SWNTs leads to a significant lowering of the percolation threshold so that loading level of only 0.5 % w/w or less is sufficient for percolation to occur [53].

Four point probe electrical conductivities of 2x thermally stretched PAni fibres containing varying SWNTs contents before doping are shown in Figure 4.22. The fibre containing 2 % w/w SWNTs showed a 4 orders of magnitude increase in conductivity over undoped neat PAni fibre. The percolation behavior of a conductive filler can be used to correlate the conductivity of a composite to the critical concentration of filler at percolation threshold based on a power law regime[54].

$$\sigma = \sigma_0 (\omega - \omega_c)^S$$

**Equation 4-3**

Where  $\sigma$  is the electrical conductivity,  $\omega$  is the SWNTs mass fraction,  $\omega_c$  is the critical weight percentage at percolation threshold of the electrical conductivity and S is the

critical exponent. Data given in Figure 4.21 was fitted on Equation 4.3 and result was presented in Figure 4.22. It has been found that mass fraction of around 0.4 % w/w SWNTs was required to reach the percolation threshold for PAni/SWNTs composite fibres. This comparatively low amount is in good agreement with other polymer-conductive filler system that have shown a percolation threshold of 0.5 % w/w [55].

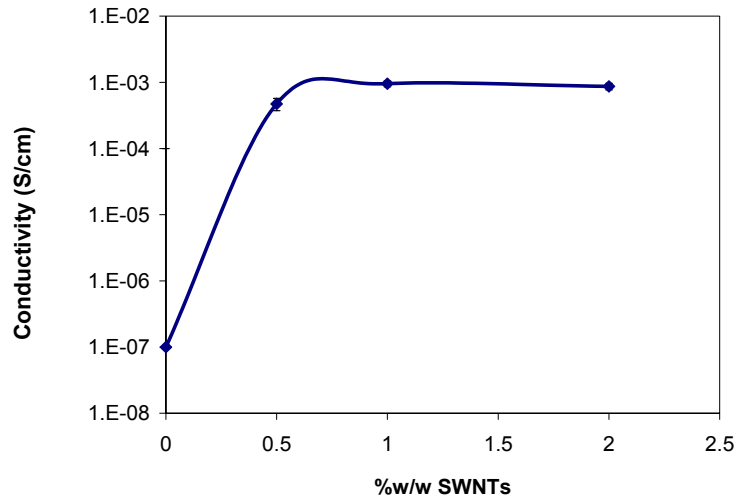


**Figure 4.21.** The percolative behavior of SWNTs as filler in PAni matrix before doping

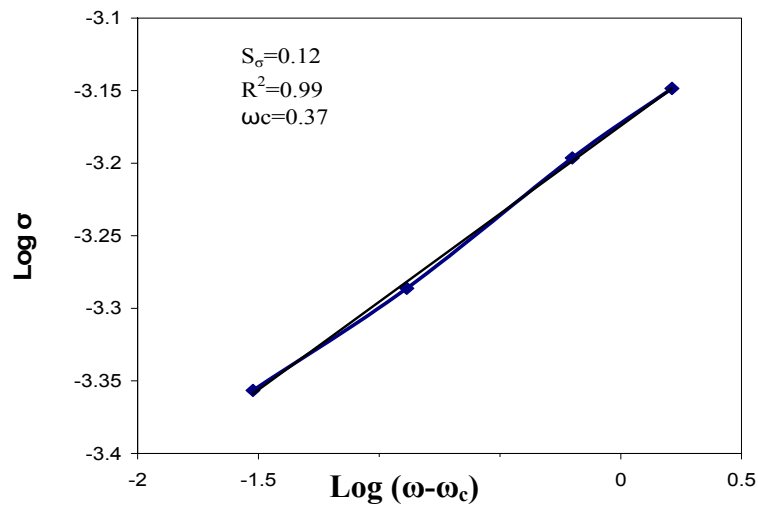


**Figure 4.22.** The Log-Log plot of conductivity vs reduced weight fraction of SWNTs.

The percolation threshold calculation above was confirmed by the enhancement of the Raman band at  $1336\text{ cm}^{-1}$  for PAni containing SWNTs before doping (Figure 4.18), which was assigned to the bipolaronic electronic structure. In addition to Raman spectroscopy evidence, electron paramagnetic resonance (EPR) spectroscopy revealed that the addition of SWNT to PAni increased the concentration of free radicals responsible for charge transport. Figure 4.23 shows the ESP spectra of PAni (LEB)/SWNT fibres containing varying amounts of SWNTs before doping. The ESR signal increased from zero for neat PAni fibres to higher levels with the addition of more SWNTs.

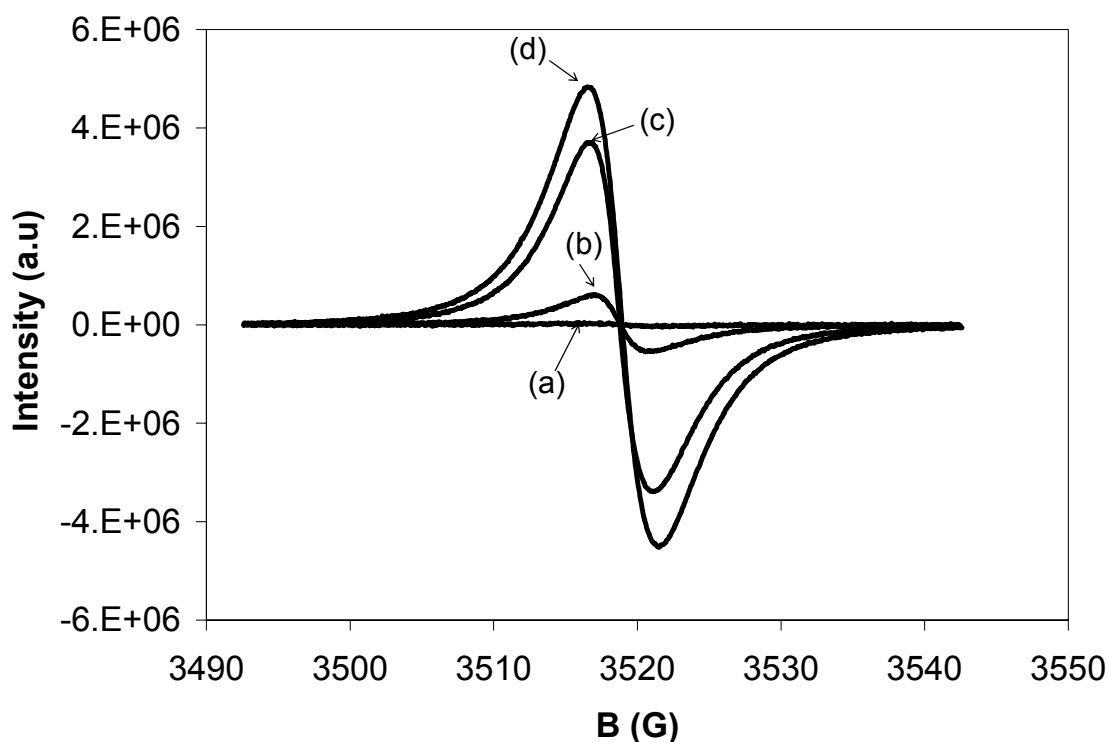


**Figure 4.23.** The EPR spectra of PAni/SWNTs composite fibres before doping containing varying amounts of SWNTs. (a) 0.0 % w/w (b) 0.5 % w/w, (c) 1.0 % w/w and (d) 2.0 % w/w



**4.3.10.2. Electrical properties of PAni/SWNTs fibres after acid doping**

Electrical conductivity of the PAni/SWNT composite fibres was measured after acid doping and following two different drying procedures (Table 4.11). After acid doping, fibre samples were dried initially at room temperature and at 100 °C. After drying at room temperature, the conductivity of PAni/SWNT fibres containing 2.0 w/w % SWNTs showed a 30 % increase relative to neat PAni fibres. In samples dried at room temperature the conductivity was probably dominated by the host doped PAni matrix. However, after drying at 100 °C, It was likely that the low molecular weight dopant MSA was removed by evaporation and that conductivity was mostly dominated by the presence of SWNTs. After drying at 100 °C, the conductivity of neat PAni was quite low ( $\sim 1$  S/cm) while the conductivity was increased 30 times upon addition of 2.0 % w/w SWNT. The low conductivity of neat PAni fibre after drying at 100 C can be attributed to deprotonation of the PAni segments through evaporation of the small dopants. The improvement of conductivity in PAni composites containing SWNTs could be attributed to the formation of a percolating network of SWNTs.

**Table 4.11.** Influence of drying temperature on four point probe conductivity of 2x PAni/SWNTs fibres (2X) with varying SWNT content after acid doping

% w/w SWNTs/PAni	Conductivity (S/cm)	
	Dried at 25°C	Dried at 100°C
0	$96 \pm 18$	$1.2 \pm 0.4$
0.5	$120 \pm 20$	$6.2 \pm 1.4$
1.0	$122 \pm 17.5$	$24.7 \pm 6.3$
2.0	$128 \pm 25$	$32.4 \pm 3.7$

Reported conductivities for 2x thermally stretched PAni (LEB) fibre [27] are ~150 S/cm after doping with HCl(1M) which is comparable to data obtained in this study.

The details of fibre processing are not completely clear in previous study [28], however, differences observed may be related to differences in the spinning process, measurement technique and /or treatment of the fibres after doping. Although the PAni (LEB)/ SWNT fibres produced in this study do not show appreciable advantage in conductivity compared with PAni(LEB) fibres reported in the literature, but they do show higher mechanical strength (  $\delta_b$ =200 MPa vs 160 MPa in [28] and E=10.5 GPa compared with 7 GPa in [28]) due to mainly to the inclusion of SWNTs.

#### **4.3.11. Cyclic voltammetry of PAni/SWNTs composite fibres**

Cyclic voltammetry (CV) was carried out on PAni/SWNTs composite fibres as part of the mechanical actuator testing (refer Chapter 8). The resistive nature of the fibres meant that poorly resolved CVs were obtained (not shown) since the applied potential decreased with distance from the point electrical contact. To improve the conductivity of fibres, very thin Pt layer was coated onto the fibres. Much improved CVs were obtained with the Pt covered fibres. Degradation and over oxidation of PAni occurs beyond 0.6 V after several cycle. However it is possible to observe the influence of nanotubes during first few cycles in the potential range of (-0.2)-(+1) V. In this range of the potential redox process cycles the PAni between the  $LEB \leftrightarrow ES \leftrightarrow PB$  oxidation states.

The influence of SWNTs on the electroactivity of Pt covered PAni fibres in 1M HCl aqueous solution is illustrated in Figure 4.24. It can be clearly seen that the addition of SWNTs enhanced the amplitude of the redox peaks, indicating a higher electroactivity

compared to neat PAni fibres. Peak potentials also shifted with the addition of SWNTs which can be attributed to interaction between PAni and SWNTs. According to the literature [56] the ratio between the amine and imine content can be determined by the applied electrochemical potential. At low potential ( $\sim +0.1$  volt) the imine concentration is low (Leucoemeraldine) and gradually increases to 50 % (emeraldine) at medium potential ( $\sim +0.4$  V) and then approach to 100% (nigraniline) at higher potential ( $\sim +0.7$  V) . Three oxidation peaks at +0.10 V, +0.42 V and 0.70 V were observed for samples containing SWNTs. Reduction peaks corresponding to the oxidation peaks at +0.42 V and +0.70 V were incorporated in a broad peak that composed of two unresolved peaks at +0.54 V and +0.22 V. The oxidation peak at +0.10 V showed no obvious reverse cathodic peak. In contrast, two non resolved oxidation peaks at +0.06 V and +0.64 V and one broad reduction peak at 0.46 V were observed in the CV of neat PAni fibre. Upon comparison of the peak potentials in Figure 4.24 it was revealed that addition of SWNTs to PAni results in easier electrochemical switching between leucoemeraldine, emeraldine and pernigraniline oxidation states compared to neat PAni. The more facile switching between oxidation states may be attributed to the interaction of the large  $\pi$  bonded surface of SWNTs with the conjugated structure of PAni via  $\pi$  stacking [57, 58] (see Figure 4.19). This increases the extent of electron delocalisation and results in improved charge transfer along the fibre axis. In addition the sharper electrochemical redox peaks in polyaniline fiber containing SWNT may be attributed to faster diffusion of ions through the fiber electrode. Ion diffusion in solid electrode is a complicated mass transfer process through porous media. Regarding to this, fiber density, skin quality and porosity should influence the ion diffusion rates. At the sub-micron scale the SEM observation from skin

and cross section ( Fig 4.16) did not show any significant difference between porosity of PAni fibers with and without nanotubes. Therefore, sharper redox peak in polyaniline fiber containing SWNT may be due to difference in porosity at the nanoscale.

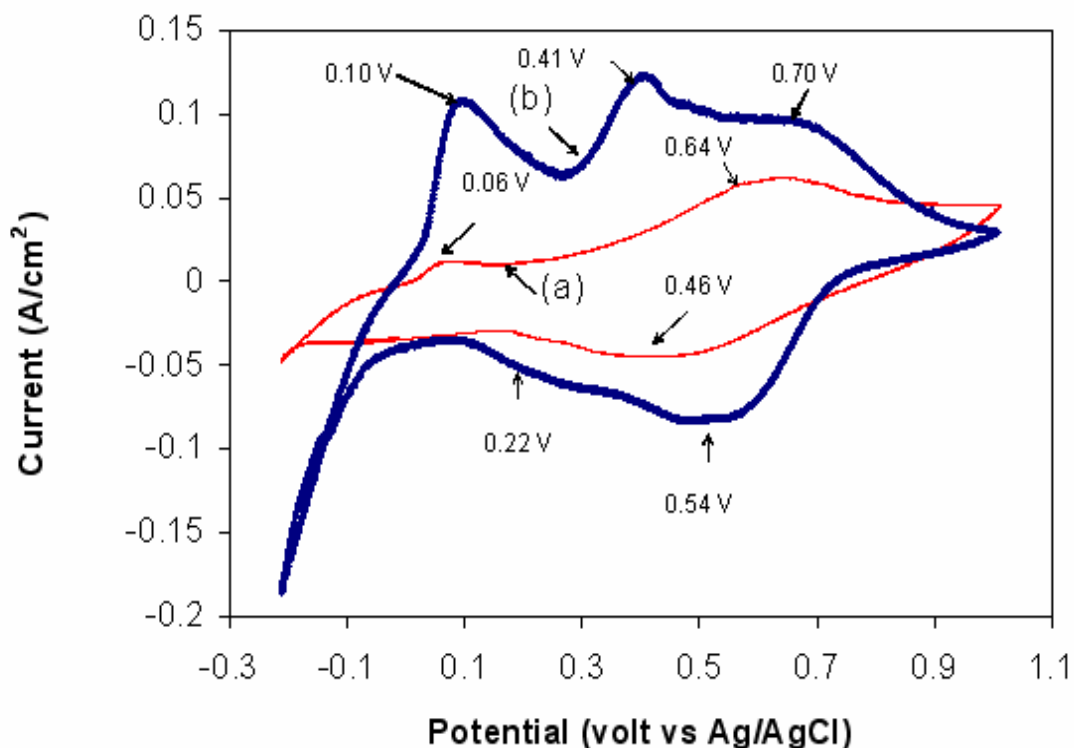


**Figure 4.24.** Cyclic voltammetry of (a) neat PAni fibre (b) PAni/ SWNTs (2 % w/w) composite fibre. Scan rate= 50 mVs<sup>-1</sup>, electrolyte: 1.0 M HCl (aq)

#### 4.4. Conclusions

PAni (LEB)/SWNTs composite fibres were produced using a wet spinning process. From a processing point of view, it was shown that the use of DMPU as solvent for PAni enables effective dispersion of the pristine SWNTs. This property was used to prepare a highly stable spinning solution containing PAni and SWNTs in concentration of 0.5, 1.0,

2.0 % w/w. Viscometry measurements results demonstrated a near 4 times increase in the viscosity with the addition of SWNTs, which reflected the physical entanglement between PAni chains and SWNTs bundles. Spinning solutions containing SWNTs did not show any tendency toward gel formation for at least 30 hrs. The rheological characteristics of solutions containing 10 % w/w PAni-LEB with up to 2 %w/w SWNTs in DMPU were found to be suitable for wet spinning. The fabrication of fibres with low porosities required the take up velocity to be limited to 2 m/min, which is quite low compared to commercial fibre spinning. Thermal stretching of the PAni/SWNT composite fibres gave fibres without macrovoids.

Fibres containing SWNTs showed superior mechanical, electrical and electrochemical properties compared with neat PAni fibres. Fibres containing 2.0 % w/w SWNTs demonstrated a 100 % increase in yield stress, a 50 % increase in tensile stress, a 240 % increase in Young's modulus (E) and a 30 % decrease in elongation at break compared with the neat PAni fibres. The dramatic increase in mechanical strength revealed efficient interfacial interaction between PAni and SWNTs. In spite of the superior mechanical strength of PAni/SWNT composite fibres, the low flexibility under bending stress is still a major disadvantage.

PAni/SWNT composite fibres showed higher electrical conductivities compared to neat PAni particularly for fibres dried at higher temperature. The conductivity of the PAni matrix was much reduced after drying at 100 °C and the SWNTs provided a more effective passage for conduction. Best results were obtained using room temperature drying. CV of neat PAni fibres and PAni/SWNT fibres containing 2.0 % w/w SWNTs (utilising a thin Pt coating for both to improve electrochemical response) revealed better

resolved redox peaks for the latter compared to former. The shifts in redox peaks with the addition of SWNTs indicated again interfacial interaction between PAni and SWNTs.

Major problems encountered here included low spinning rate and solidification rate, low flexibility and low conductivity and insufficient charge transfer along the naked fibre. To overcome these challenges, a switch toward processing of PAni/SWNTs fibres using emeraldine salt form of PAni through a one step process was investigated in the following chapter.

**4.5. References**

- [1] C. H. Hsu, J. D. Cohen and R. F. Tietz, *Synth. Met.* 59 (**1993**) 37-41.
- [2] K. Tzou and R. V. Gregory, *Synth. Met.* 55-57 (**1993**) 983-988.
- [3] I. W. Chiang, B. E. Brinson, A. Y. Huang, P. A. Willis, M. J. Bronikowski, J. L. Margrave, R. E. Smalley and R. H. Hauge, *J. Phys. Chem . B.* 105 (**2001**) 8297-8301.
- [4] K. D. Ausman, R. Piner, O. Lourie and R. S. Ruoff, *J. Phys. Chem. B.* 104 (**2000**) 8911-8915.
- [5] A. P. Chacko, S. S. Hardaker, R. V. Gregory and T. W. Hanks, *Polymer.* 39 (**1998**) 3289-3293.
- [6] A. P. Chacko, S. S. Hardaker and R. V. Gregory, *Polymer Preprints.* 37 (**1996**) 743-744.
- [7] R. Saito, G. Dresselhaus and M. S. Dresselhaus., *Physical Properties of Carbon Nanotubes*, Imperial College Press, London, (**1998**), .
- [8] R. A. Jishi, L. Venkataraman, M. S. Dresselhaus and G. Dresselhaus, *Chem. Phys. Lett.* 209 (**1993**) 77-82.
- [9] M. S. Dresselhaus, G. Dresselhaus, A. Jorio, A. G. Souza Filho and R. Saito, *Carbon.* 40 (**2002**) 2043-2061.
- [10] M. S. Dresselhaus and P. C. Eklund, *Adv. Phys.* 49 (**2000**) 705–814.
- [11] C. Thomsen and S. Reich, *Phys. Rev. Lett.* 85 (**2000**) 5214-5217.
- [12] O. Jost, A. A. Gorbunov, W. Pompe, T. Pichler, R. Friedlein, M. Knupfer, M. Reibold, H. D. Bauer, L. Dunsch, M. S. Golden and J. Fink, *J. Appl. Phys. Lett.* 75 (**1999**) 2217-2219.
- [13] U. Mayer, V. Gutmann and W. Gerger, *Mater. Res. chem.* 106 (**1975**) 1235.
- [14] M. H. Vandam, *Ind. Eng. Chem. Res.* 36 (**1997**) 4628-4638.
- [15] T. K. Pichler, M. Knupfer, M. S. Golden, J. Fink, A. Rinzler and R. E. Smalley, *Phys. Rev. Lett.* 80 (**1998**) 4729-4732.
- [16] T. W. Odom, J. L. Huang, P. Kim, M. Ouyang and C. M. Lieber, *J. Mater. Res.* 13 (**1998**) 2380-2388.
- [17] S. Badaire, P. Poulin, M. Maugey and C. Zakri, *Langmuir.* 20 (**2004**) 10367-10370.

- [18] D. Yang and B. R. Mattes, J. Polym. Sci.B-Polym. Phys. 40 **(2002)** 2702-2713.
- [19] D. Yang, A. Fadeev, P. N. Adams and B. R. Mattes, Proceedings of SPIE - The International Society for Optical Engineering. 4329 **(2001)** 59-71.
- [20] D. Zhou, G. G. Wallace, G. M. Spinks, L. Liu, R. Cowan, E. Saunders and C. Newbold, Synth. Met. 135-136 Apr 4 **(2003)** 39-40.
- [21] A. Ziabicki, in Fundamental of fiber spinning,"General theoritical fundamentals", Wiley, New York, **(1976)**, 13-147.
- [22] A. Ziabicki, in Fundamental of fiber spinning,"Wet and dry spinning", Wiley, New York, **(1976)**, 256-349.
- [23] H. L. Wang, R. J. Romero, B. R. Mattes, Y. Zhu and M. J. Winokur, J. Polym. Sci.B-Polym. Phys. 38 **(2000)** 194-204.
- [24] A. P. Chacko, S. S. Hardaker, B. Huang and R. V. Gregory, Mater. Res. Soc. Symp. Proc. 413 **(1996)** 503-511.
- [25] S. J. Pomfret, P. N. Adams, N. P. Comfort and A. P. Monkman, Polymer. 41 **(2000)** 2265-2269.
- [26] A. Ziabicki, in Fundamental of fiber formation,"Drawing", Wiley, New York, **(1976)**, 388-441.
- [27] A. P. Chacko, S. S. Hardaker and R. V. Gregory, Polymer Preprint. 38 **(1997)** 367-368.
- [28] S. Yang, J. R. Castilleja, E. V. Barrera and K. Lozano, Polymer Degradation & Stability. 83 **(2004)** 383-388.
- [29] M. Cadek, J. N. Coleman, V. Barron, K. Hedicke and W. J. Blau, Proceedings of SPIE - The International Society for Optical Engineering. 4876 **(2002)** 676-684.
- [30] C. Wei, D. Shrivastava and K. Choi, Nano Lett. 2. **(2002)** 647-650.
- [31] M. Cadek, J. N. Coleman, V. Barron, K. Hedicke and W. J. Blau, Appl. Phys. Lett. 81 **(2003)** 5123-5125.
- [32] S. Kumar, T. D. Dang, F. E. Arnold, A. R. Bhattacharyya, B. G. Min, X. Zhang, R. A. Vaia, C. Park, W. W. Adams, R. H. Hauge, R. E. Smalley, S. Ramesh and P. A. Willi, Macromolecules. 35 **(2002)** 9039.
- [33] V. Thaliyil, V. sreekumar, T. Li, B. G. Min, H. Guo, S. Kumar, R. H. hauge and R. E. Smalley, Adv. Mater. 16 **(2004)** 58-61.



- [34] H. Krenchel, Fibre Reinforcement, Akademisk Forlag, Copenhagen, (1964), .
- [35] P. Poulin, B. Vigolo and P. Launoise, Carbon. 40 (2002) 1741-1749.
- [36] R. S. Ruoff and D. C. Lorents, Carbon. 33 (1995) 925-930.
- [37] B. I. Yakobson, C. J. Brabec and J. Bernholc, Phys. Rev. Lett. 76 (1996) 2511-2514.
- [38] J. P. Lu, Phys. Rev. Lett. 79 (1997) 1297-1300.
- [39] J. Liu, Y. Lin, L. Liang, J. A. Voigt, D. L. Huber, Z. R. Tian, E. Coker, B. McKenzie and M. J. McDermott, Chemistry-A European Journal. 9 (2003) 604-611.
- [40] P. Colomban, S. Folch and A. Gruger, Macromolecules. 32 (1999) 3080-3092.
- [41] M. Cochet, G. Louarn, S. Quillard, J. P. Buisson and S. Lefrant, J. Raman. Spec. 31 (2000) 1041-1049.
- [42] M. Cochet, S. Quillard, J. P. Buisson, S. Lefrant and G. Louarn, Synth. Met. 101 (1999) 793-794.
- [43] M. Cochet, W. K. Maser, A. M. Benito, M. A. Callejas, M. T. Martinez, J. M. Benoit, J. Schreiber and O. Chauvet, Chem. Comm. (2001) 1450-1451.
- [44] M. Baibarac, I. Baltog, S. Lefrant, J. Y. Mevellec and O. Chauvet, Chem. Mater. 15 (2003) 4149-4156.
- [45] S. Quillard, G. Louarn, S. Lefrant and A. G. Macdiarmid, Phys. Rev. B. 50 (1994) 12496-12508.
- [46] H. Zengin, W. Zhou, J. Jin, R. Czerw, D. W. Smith Jr, L. Echegoyen, D. L. Carroll, S. H. Foulger and J. Ballato, Adv. Mater. 14 (2002) 1480-1483.
- [47] A. E. Khalki, A. Gruger and P. Colomban, Synth. Met. 139 (2003) 215-220.
- [48] J. E. Pereira da Silva, D. L. A. de Faria, S. I. Cordoba de Torresi and M. L. A. Temperini, Macromolecules. 33 (2000) 3077-3083.
- [49] G. M. Do Nascimento, J. E. Pereira da Silva, S. I. Cordoba de Torresi and M. L. A. Temperini, Macromolecules. 35 (2002) 121-125.
- [50] D. Stauffer and A. Aharony, Introduction to percolation theory, Taylor &Fransis, London, (1992), P.15.
- [51] M. Q. Zhang, G.YU, H.M.Zeng, H.B.Zhang and Y.H.Hou, Macromolecules. 31 (1998) 6724.

- [52] J.C.Grunlan, W.W.Gerberich and L.F.Francis, J. Mater. Res. 14 (1999) 4132.
- [53] J. C. Grunlan, A. R. Mehrabi, M. V. Bannon and J. L. Bahr, Adv. Mater. 16 (2004) 150-153.
- [54] S. Kirkpatrick, Rev.Mod. Phys. 45 (1973) 574.
- [55] F. Du, R. C. Scogna, W. Zhou, S. Brand, J. E. Fischer and K. I. Winey, Macromolecules. 37 (2004) 9048-9055.
- [56] P. Snauwaert, R. Lazzaroni, J. Riga, J. Verbist and D. Gonbeau, in Springer Series in Solid State Sciences, "Electronic Properties of Conjugated polymers", Springer, Berlin, (1989), 301–304.
- [57] H. Zengin, W. Zhou, J. Jin, R. Czerw, J. Smith, W. Dennis, L. Echegoyen, D. L. Carroll, S. H. Foulger and J. Ballato, Adv. Mater. 14 (2002) 1480-1483.
- [58] J. E. Huang, X. H. Li, J. C. Xu and H. L. Li, Carbon. 41 (2003) 2731-2736.

# **CHAPTER FIVE**

## **Development and Characterisation Of PAI/Single Walled Carbon Nanotubes Composite Fibres Using 2-Acrylamido-2 Methyl -1-Propane Sulfonic Acid and a One Step Wet Spinning Process**

## 5.1 Introduction

In Chapter 4, polymer fibres were readily produced from the insulating leucoemeraldine base (LEB) form of Polyaniline (PAni). These fibres were rendered conductive by doping using an aqueous acid (methane sulfonic acid) comprised of small anions. The main disadvantage was the adverse influence of the acid doping process on the mechanical properties of PAni fibres. Non uniform doping [1-6] and the possibility of dedoping through diffusion of small anions from the outer skin of the fibre [7] may causes heterogeneities in the fibre structure. Doping of PAni in solution, however, results in more homogenous doping and more uniform materials after subsequent casting [8]. Doping of PAni with sulfonic acids yields extended chain conformation, resulting in high electronic conductivity [9]. In this regard a number of studies that involve processing of PAni solutions blended with sulfonic acids in suitable solvent have been reported [7, 10]. The production of the electronically conductive emeraldine salt (ES) form of PAni fibre using 2-acrylamido-2 methyl -1-propane sulfonic acid (AMPSA) as the dopant acid and dichloroacetic acid (DCAA) as the solvent is the latest advance in this area [11].

This Chapter describes the preparation of a spinning solution for the processing of conductive electroactive PAni-ES/AMPSA/SWNTs composite fibres with high spinnability. The properties of spinning solutions and prepared fibres were characterised using a range of techniques including DLS, viscometry, UV-Vis-NIR, SEM, TEM, DSC, DMA, CV and Raman Spectroscopy.

## 5.2 Experimental

### 5.2.1 Materials and Reagents

PAni was obtained from Santa Fe Science and Technology (SFST) with an average molecular weight of 280,000 g/mol. Dichloroacetic acid (DCAA, Merck, 98 %) and 2-acrylamido-2-methyl-1-propane sulfonic acid (AMPSA, Aldrich, 99 %) were used without any further purification. Single wall carbon nanotubes (SWNTs, Hipco@CNI) were used as purchased and contained 8 % w/w iron residue as determined by elemental analysis (refer Chapter 4). The ionic liquid ethyl methyl imidazolium bis (trifluoromethane sulfonyl) imide (EMI.TFSI) was synthesised in our laboratories according to methods described elsewhere [12, 13].

### 5.2.2 Instrumentation

UV-Vis-NIR spectroscopy was carried out using a Cary 5000 spectrophotometer. The hydrodynamic diameter of SWNT bundles was measured using dynamic light scattering (ZS, Malvern, UK). The viscosity of SWNT dispersions and polymer solutions was recorded using a Brookfield viscometer (LV-DV II+) using a DIN spindle of 85 and 87 as a function of time or shear rate. A fully digital LEO Cambridge / Leica Stereoscan 440 Scanning Electron Microscope (SEM) with a tungsten filament using 20 kV beam energy was used for morphological studies of the composite fibres. Raman spectra were obtained using the Jobin Yvon Horiba model HR800 Raman spectrometer and were collected with a spectral resolution of  $1.5\text{ cm}^{-1}$  in the backscattering mode, using the 632.8 nm line of a He/Ne laser. The electrical conductivity of the composite fibres was measured using the four probe method as described in Chapter 3. More detailed description of the other information used in this Chapter follow below.

Dynamic mechanical analysis (DMA) was carried out using a Q-800 instrument (Thermal Analysis series). DMA results were under three different experimental modes. The strain rate mode was used to collect stress versus strain data equivalent to that obtained from a universal testing machine. For creep testing, a finite stress was instantaneously applied to the sample and held constant for 10 min. At the end of that period, the stress was removed instantaneously and the recovered strain monitored versus time. Viscoelastic behavior was characterised using DMA in constant frequency mode and the procedure described in Chapter 3.

A three electrode electrochemical cylindrical cell (15 mm diameter  $\times$  50mm height) equipped with a stopper was used for cyclic voltammetry (CV). The cell consisted of a fibre measuring 10 mm in length and  $\sim$  50-60  $\mu$ m in diameter as the working electrode, a Ag/AgCl or a Ag/Ag<sup>+</sup> reference electrode, for aqueous acid or ionic liquid electrolytes, respectively and a Pt mesh counter electrode. A constant load was applied to the sample to keep it straight.

Focused ion beam (FIB) milling has been achieved using a nanomilling (FEI company, The Netherlands) instrument model XT-NOVA in the Electron Microscope Unit of University of New South Wales. Fibre samples were fixed on a stub using silver paint and sputter coated with gold using Dynavac sputter coater. The samples were then placed in a vacuum chamber. The instrument equipped with software which comprises a step by step procedure known as “TEM Wizard” for preparation of thin film from specific samples. FIB milling provides locational precision of  $\sim$  1  $\mu$ m for preparing Transmission electron microscopy (TEM) samples. The following steps were performed to obtain a thin film:

- 1) Starting with sputter coated fibre ( Fig 5.1-a), two crosses were milled on either side of working area to enable image recognition and stage drift correction (Figure 5.1-b).

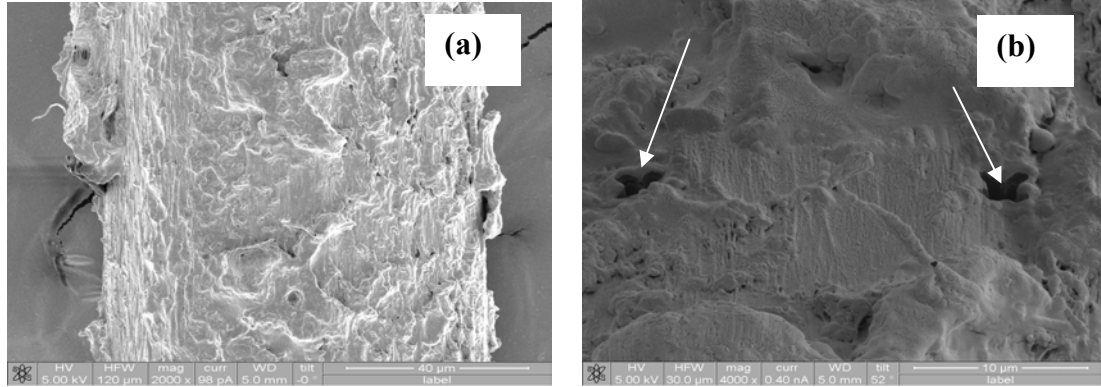


**Figure 5.1.** First step of FIB milling: labeling of working area

- 2) A 1 μm thick Pt bar( The marked area in Figure 5.2-a), was deposited to protect the working area from implantation damage and sputtering before a large beam current (5 nA) was used to mill sloping trenches (Figure 5.2-b)

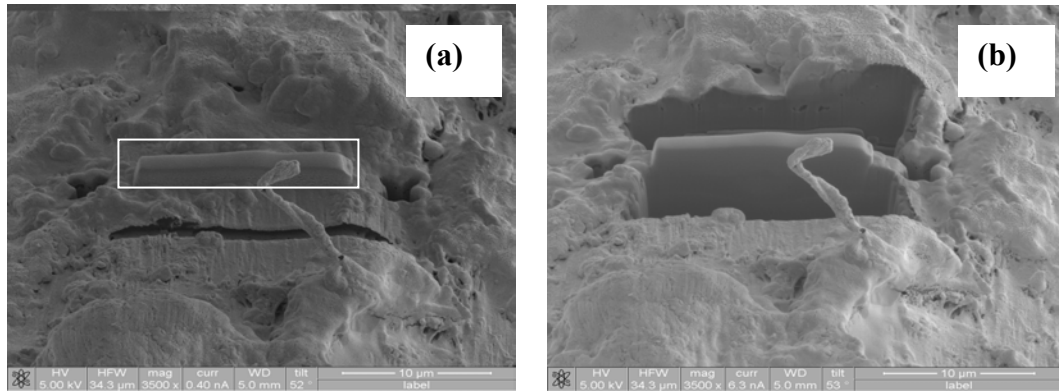


**Figure 5.2.** Second step of FIB milling: (a) Pt deposition and (b) milling of sloping trenches

- 3) Beam currents between 1-3 nA were used to reduce the thickness of the TEM lamella to 1  $\mu\text{m}$  before the sample was tilted by 45° and cuts made to partially free the lamella (Figure 5.3).

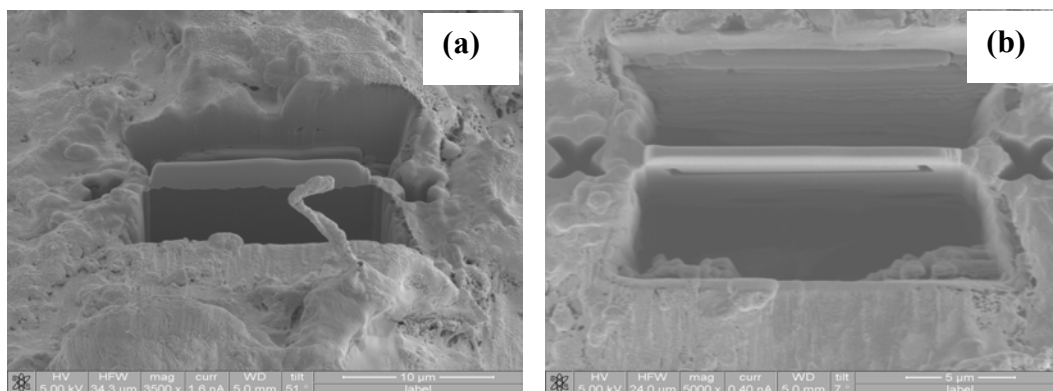


**Figure 5.3.** Third step: reduction of thickness of thin film

- 4) Lower beam currents were then used (300 & 100 pA) to thin the lamella further and finally create a near electron transparent region in the centre. Further thinning of the lamella can be performed using beams of lower current and diameter (50 pA or less). Finally the lamella is freed by making cuts at the holding edges (Figure 5.4).

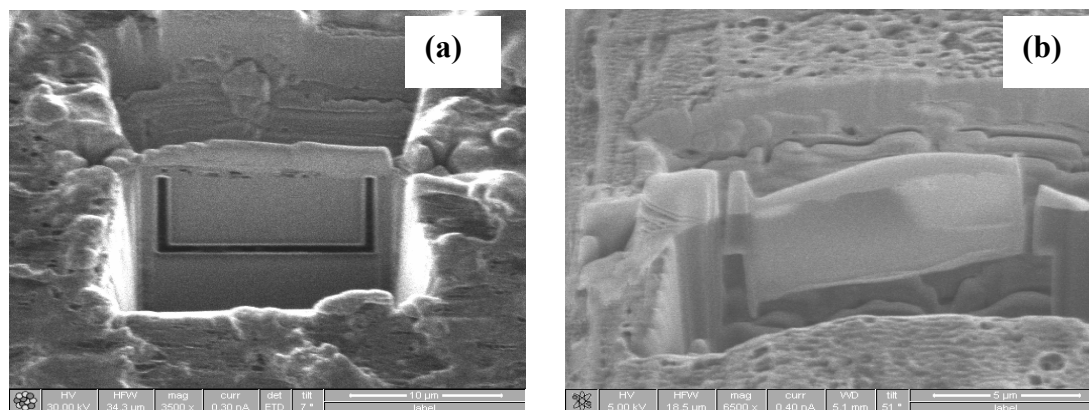


**Figure 5.4.** Fourth step of FIB milling: (a) Further thinning of the lamella and (b) cutting of holding edges



- 5) In the final step, the lamella is transferred to a TEM grid covered with a thin carbon film using a micro robot. The lamella is attracted by electrostatic forces and jumped onto the probe. Electrostatic forces ensured that the lamella adhered to the film ( Figure 5.5).

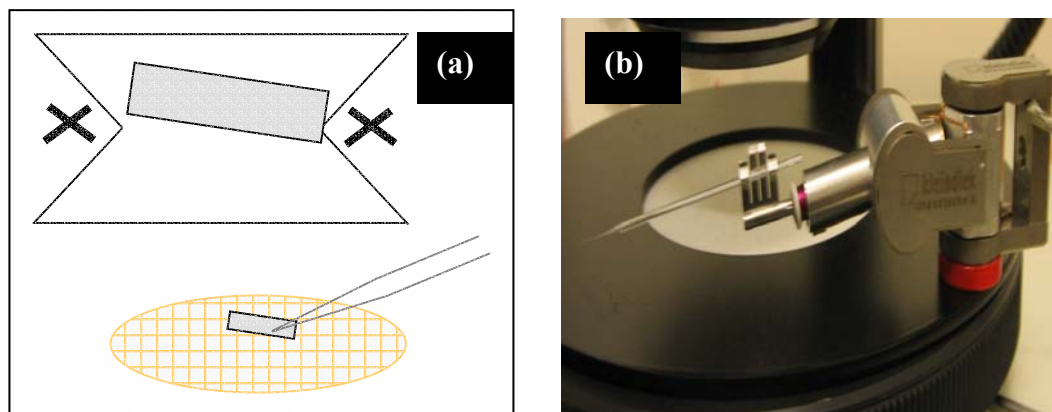


**Figure 5.5.** Final step of FIB milling: (a) transfer of the thin film on a TEM grid using a micro robot (b) Schematic indicating a micro robot machine.

### 5.2.3 Characterisation of SWNT dispersions

#### 5.2.3.1 DCAA versus DMPU as solvent

To investigate the effect of solvent, ~ 1mg of SWNTs was dispersed by continuous sonication in 10 g of DCAA for 30 min. The resultant dispersions (with and without AMPSA) were characterised by UV-Vis-NIR spectroscopy and the result compared with spectra obtained from SWNT-DMPU dispersion in section 4.3.2.1.

#### 5.2.3.2 Influence of AMPSA on degree of SWNT aggregation

To demonstrate the effect of AMPSA on the degree of SWNT aggregation, a range between, 0.0 - 0.4 g AMPSA was added to a SWNTs-DCAA (0.05 % w/w) mixture. The

resultant dispersions were characterised by dynamic light scattering (DLS) in order to illustrate the influence of AMPSA on the stability of SWNTs dispersions.

### 5.2.3.3 Ability of DCAA for to disperse higher concentration of SWNTs

SWNTs were sonicated in 20 g DCAA containing 0.4 g AMPSA for 30 min at 25 °C to produce dispersions with 0.03, 0.045, 0.06 and 0.09 % w/w SWNTs content regarding to the weight of solvent. Dynamic light scattering and viscometry were employed to characterise the resultant SWNTs dispersions.

### 5.2.4 Preparation of composite spinning solutions

A range of AMPSA and PAni concentrations were investigated in order to find the minimum amount of PAni needed for successful wet spinning (Table 5.1).

**Table 5.1.** Range of PAni and AMPSA contents used to prepare PAni-ES/AMPSA solutions in DCAA for fibre spinning. 20 g of DCAA was used for each.

sample	PAni (g)	AMPSA (g)	PAni:AMPSA (mole ratio)	% w/w PAni-ES/ AMPSA in DCAA
S1	0.4	0.52	1:0.6	4.6
S2	0.6	0.82	1:0.6	7.0
S3	0.8	1.09	1:0.6	9.5
S4	1.0	1.37	1:0.6	11.5

A two stage procedure was used to prepare the PAni spinning solutions. In all cases, the molar ratio of PAni (EB) to AMPSA was maintained at 1:0.6. This amount of AMPSA was in slight molar excess to ensure full protonation of the PAni (EB) to PAni-ES/AMPS (2-acrylamido-2-methyl-1-propane sulfonate). Four different solutions were prepared

(designated S1-S4 in Table 5.1) with each having different PAni-ES/AMPSA content in the DCAA solvent. In each case, AMPSA was ground with PAN (EB) (0.4-1.0 g) to produce a grey powder. The resultant PAni-ES/AMPSA powder was added to a previously prepared solution of AMPSA in DCAA by continuous stirring over a period of 30 min at 40 RPM and 10 °C under a N<sub>2</sub> atmosphere. The spinning solution was stirred for another 30 min at 2000 rpm and at 5 °C. Bubbles formed in the viscous solution were removed using a dynamic vacuum over a 1 hour period.

Each solution containing different amount of SWNTs were prepared, firstly by sonication of AMPSA (0.4 g) in DCAA (20 g). The same procedure was used to prepare the PAni-ES/AMPSA/SWNT dispersions in DCAA. The SWNTs (6-18 mg) were sonicated in a AMPSA-DCAA solution for 30 min. Next the ground PAni-ES/AMPSA powder was added and the process continued as described above. The weight percent of SWNTs in spinning solutions and in final fibres (whole solvent extracted or evaporated) are given in Table 5.2.

**Table 5.2.** Amount of PAni (EB), AMPSA and SWNTs used for the preparation of PAni-ES/AMPS/SWNTs spinning solution (each solution made up in 20 g DCAA solvent).

SWNT (mg)	PAni-EB (g)	AMPSA (g)	%(w/w) of SWNT in spinning solution	%(w/w) of SWNT in final fibre
0	1	1.37	0.000	0.00
6	1	1.37	0.030	0.25
9	1	1.37	0.045	0.38
12	1	1.37	0.060	0.50
18	1	1.37	0.090	0.76

The weight percent of SWNTs in the final fibre were calculated with respect to the total mass of PAni and AMPSA present. Only the S4 solution was used to prepare such composite fibres.

### **5.2.5 The fibre spinning process**

Viscous bubble free spinning solutions are transferred to a N<sub>2</sub> pressure vessel to drive the spinning solution through a filter (200µm, Millipore) then through a single hole spinneret with  $L/D = 4$  and  $D = 250 \mu\text{m}$ , and finally to an acetone coagulation bath at room temperature. It has been shown that acetone is the most useful coagulant material for PAni in the ES oxidation state and can produce smoothly cylindrical and dense fibres with high solidification rates even when using low viscosity spinning solutions ( $\sim 3000$  cP) [11]. Fast coagulation results in skin formation in shorter coagulation bath residence time and as a result, a higher take up velocity can be employed. A higher take-up velocity is desirable in that it usually improves the mechanical properties of the fibre due to a higher orientation of the polymer chains [25]. As a consequence of those previous findings, acetone was used in the coagulation for all fibre spinning investigations that follow. The N<sub>2</sub> pressure was adjusted to 50 - 125 psi to fix the injection rate for the spinning dopes having different rheological properties. In the coagulation bath, the solution solidified and the emerging fibre was taken up on the first bobbin ( $D = 2.5$  cm) with a linear velocity of 3 m/min. The semi-solid fibre was then passed through warm air created above a hot plate and was collected at a linear velocity of 6 m/min on a second bobbin ( $D = 5$  cm). Fibres were dried at room temperature at least for 30 min prior to hot drawing process. The drawing process involved stretching as-spun fibres 5 times of initial length, across a soldering iron wrapped with Teflon tape and heated to 100 °C.

The thermally stretched fibres were dried in room temperature for 48 hrs before characterisation.

### **5.3 Results and discussion**

In regards to reinforcing of PAni with SWNTs, it is first necessary to achieve a homogenous dispersion within PAni matrix at weight fractions sufficient enough to allow the percolation threshold to be exceeded. In this regard, a solvent system capable of stabilising SWNTs and dissolving the PAni is required. Thus, the first subsection of results considers Investigation. Beyond this the following considers the characterisation of spinning solutions before focusing mainly on the preparation and characterisation of wet spun PAni(ES)-AMPSA/SWNT composite fibres.

#### **5.3.1 SWNTs dispersions**

##### **5.3.1.1 UV-Vis– NIR spectroscopy of SWNT dispersions**

UV-Vis-NIR of SWNT dispersions in DCAA with or without AMPSA when compared to those in DMPU, showed less pronounced absorption bands suggesting a lower dispersability of SWNTs in DCAA compared to DMPU (Figure 5.6).

The sharper absorption band of SWNTs dispersion in DMPU compared to DCA may also attributed to the longer sonication time (2 hrs) in DMPU compared to DCAA (30 min). The use of a 30 min sonication time for SWNTs in DCAA here is discussed in section 5.3.1.3. The origin of labeled peaks was described in section 4.3.2.1.

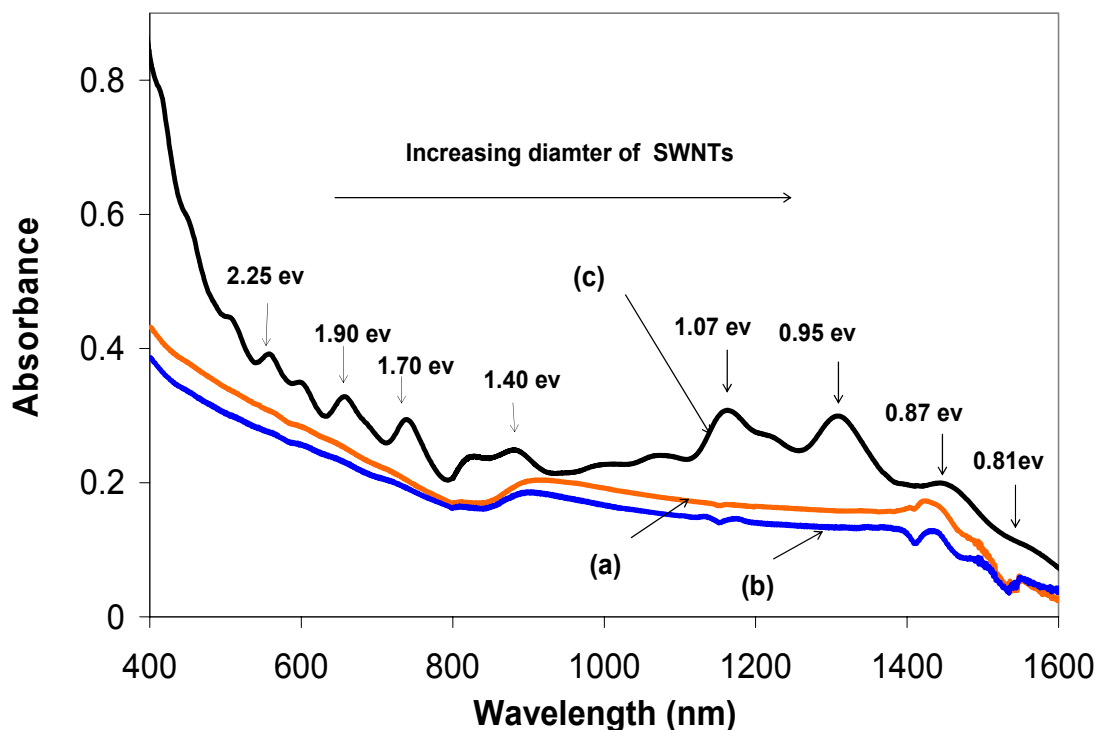


**Figure 5.6.** UV-Vis NIR spectra of SWNT (0.01 % w/w) in (a) DCAA after 30 min sonication (b) DCAA-AMPSA (2 % w/w) after 30 min sonication and (c) DMPU after 2 hrs sonication

### 5.3.1.2 Influence of AMPSA on degree of SWNT aggregation in DCAA

The combination of DCAA and AMPSA results in an efficient solvent for the dissolution of PAni in the salt form. The hydrodynamic diameter distribution for a SWNT- DCAA (0.05 % w/w) solution containing 0 % w/w- 2 %w/w AMPSA was determined (Figure 5.7) using the dynamic light scattering technique and results illustrated in Figure 5.7.

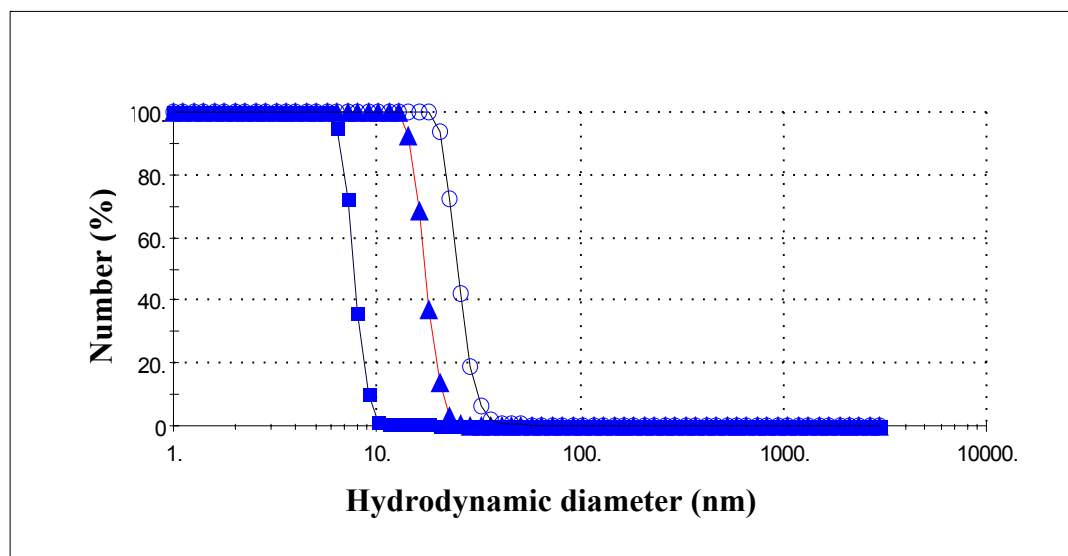


**Figure 5.7.** Influence of AMPSA concentration (% w/w) in DCAA on hydrodynamic diameter distribution of SWNT dispersions (0.05 % w/w). (○) 0 % w/w (▲) 1 % w/w (■) 2 % w/w. The results were obtained 30 min after samples preparation.

SWNT dispersions that contained AMPSA showed lower hydrodynamic diameters compared with the neat SWNTs dispersion in DCAA without AMPSA. In addition, the presence of more AMPSA increasing the concentration from 1 % w/w to 2 % w/w led to a smaller hydrodynamic diameter for SWNT dispersions. This smaller hydrodynamic diameter may reflect the effect of AMPSA in efficiently exfoliating of SWNT by overcoming the Van Der Waals forces between SWNTs. It is shown that the sonication of SWNTs in strong acidic solution oxidises [14] the surface of nanotubes and facilitates the dispersion process. It has also been found that the addition of AMPSA to DCAA assists in preventing sedimentation or aggregation of SWNTs dispersions over a short period of time (Figure 5.8).

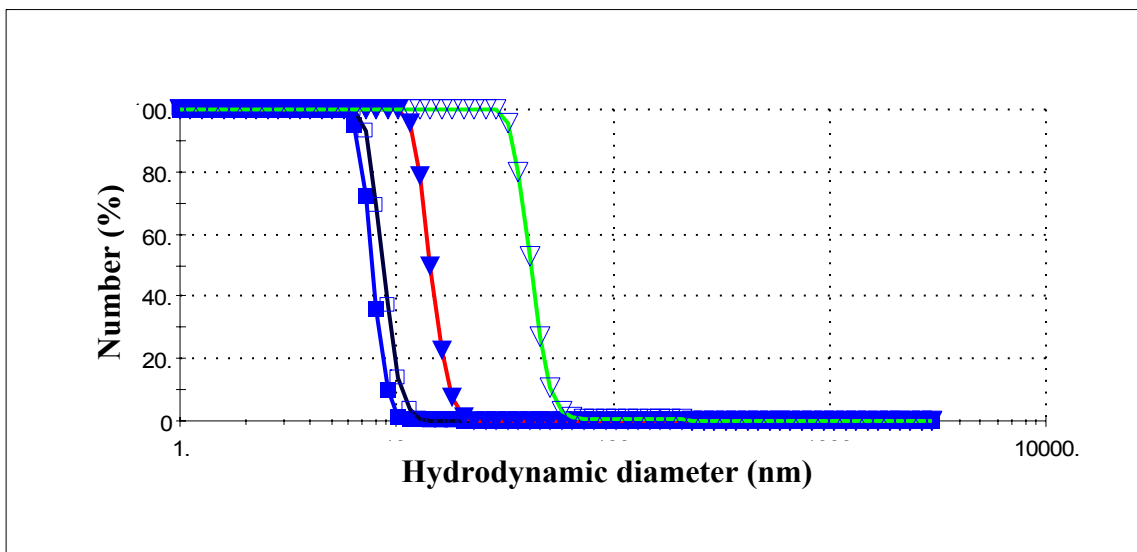


**Figure 5.8.** Hydrodynamic diameter of SWNTs (0.05 % w/w ) in DCAA with ( $\square$ ) and without ( $\nabla$ ) AMPSA (2 % w/w). Hydrodynamic diameters immediately after sonication are indicated by the filled symbols; while those measured 60 min after sonication was stopped are indicated by the unfilled symbols.

The higher stability of SWNTs after the addition of AMPSA can be attributed to the affinity of the alkyl chain groups to adsorb on SWNTs surface and simultaneous accommodation of the  $\text{SO}_3^-$  group [15]. This adsorption increases the charge on the surface of the tubes and consequently, generates electrostatic repulsion of  $\text{SO}_3^-$  group on neighboring tubes [16, 17] thus prevents aggregation. The superior dispersing capability of surfactants containing  $\text{SO}_3^-$  can be explained in terms of graphite-surfactant interactions, alkyl chain length, head group size, and charge [17].

### 5.3.1.3 Effect of sonication time on SWNTs agglomeration in DCAA

The dimensions of SWNTs and the homogeneity of dispersions containing them can be controlled through sonication. Determining of the minimum sonication time required to



obtain a homogenous dispersions is beneficial for maintaining the length of SWNTs bundles and, as a consequence, optimising mechanical and electrical properties. Zakri and co-workers [18] showed that increasing the sonication time significantly reduces the length of nanotubes and the conductivity of SWNT fibres. It has also been shown that the aspect ratio of nanotubes has a considerable impact on tensile strength of composites containing them [19] highlighting the importance of determining minimum sonication time. The homogeneity of SWNT dispersions was detected by viscometry. It was observed that the viscosity of a SWNTs/AMPSA/DCAA dispersion containing 0.06 % w/w SWNTs and 2 % w/w AMPSA fluctuates undesirably when a sonication time of less than 30 min was used (Figure 5.9). Therefore, a sonication time of 30 min was selected for further experiments using SWNTs dispersions in AMPSA/DCAA.

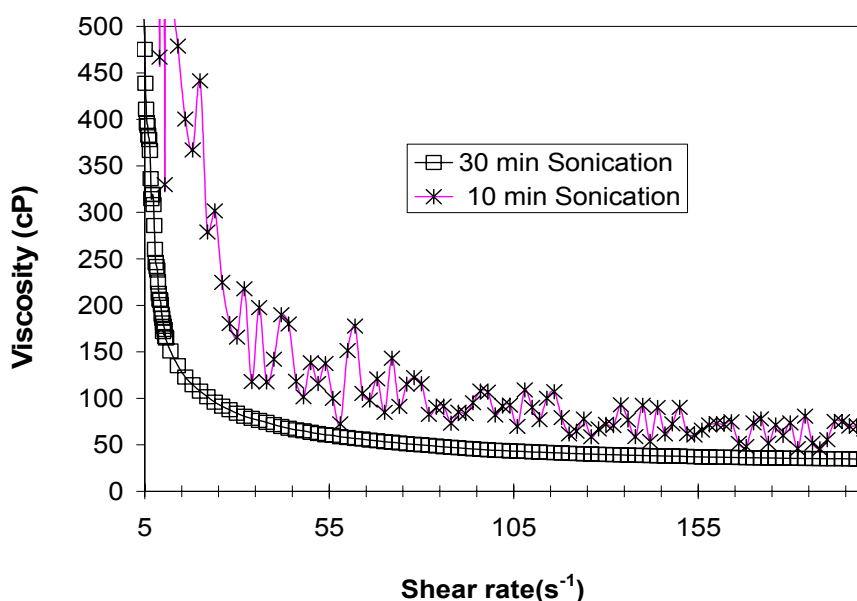


**Figure 5.9.** Influence of sonication time on homogeneity of SWNTs dispersion as gauged by fluctuation of viscosity versus shear rate. The dispersion contained 0.060 % w/w SWNT and 2 % w/w AMPSA relative to the DCAA solvent.

In addition to the viscometry measurements in Figure 5.9, the variation in average hydrodynamic diameter was observed to stabilise after 30 min sonication time compared with 10 min sonication time (Figure 5.10). These results confirmed that 30 min sonication can be sufficient for dispersing SWNTs in AMPSA-DCAA.

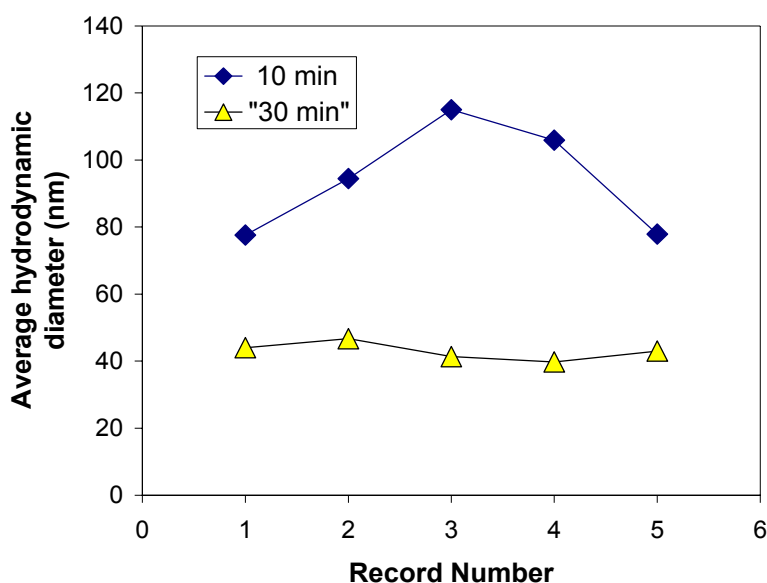


**Figure 5.10.** Average hydrodynamic diameter of SWNT dispersions for 5 repetitive experiments using either 10 min or 30 min sonication time. The dispersion contained 0.060 % w/w SWNT and 2 %w/w AMPSA relative to the DCAA solvent

#### 5.3.1.4 Effect of SWNT concentration on aggregation of SWNTs in DCAA

The hydrodynamic diameter of SWNTs dispersions in DCAA containing 2 % w/w and 0.030, 0.045, 0.06 or 0.09 % w/w SWNTs are shown in Figure 5.11. For dispersions containing 0.030, 0.045 and 0.060 % (w/w) SWNTs, hydrodynamic diameters ranged between 10-30 nm. However for the 0.090 % w/w dispersion, the hydrodynamic

diameter of SWNTs was between 100 nm and 1000 nm. Addition of SWNTs greater than 0.09 % w/w gave agglomerated lumps of unexfoliated SWNTs that were observed by the naked eye. The measurement of the size of these particles was not possible using the zeta sizer due to multiple scattering. From these finding, a SWNTs concentration of  $\leq 0.09$  % w/w was used for fibre spinning experiments.

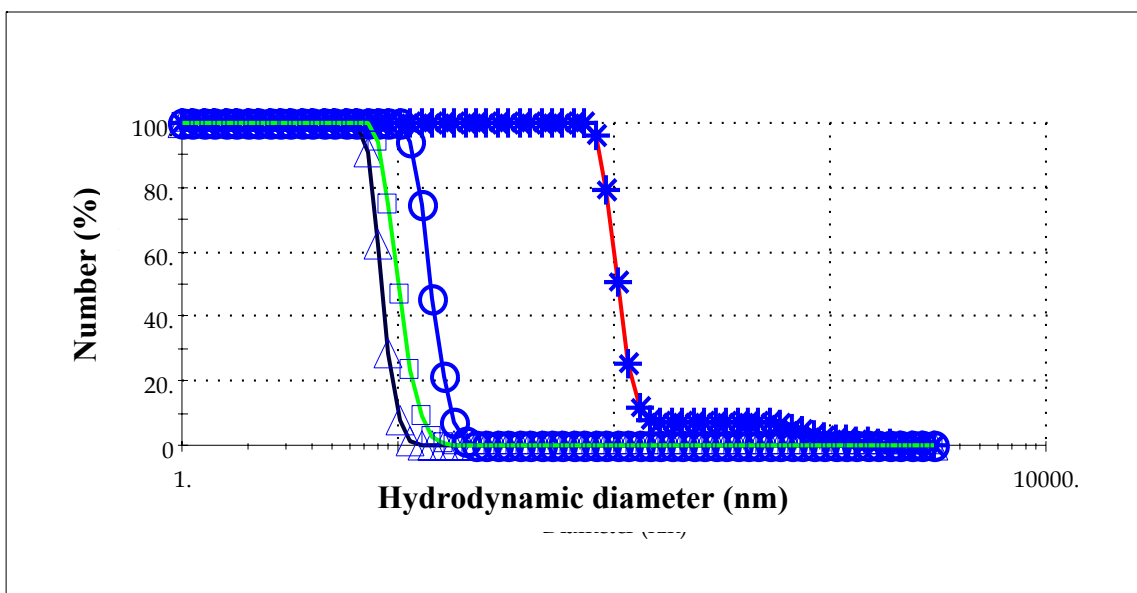


**Figure 5.11.** Influence of SWNTs concentration in DCAA/AMPSA solution on hydrodynamic diameter ( $\triangle$ ) 0.030 %w/w ( $\square$ ) 0.045 %w/w ( $\circ$ ) 0.060 %w/w ( $\ast$ ) 0.090 %w/w

The hydrodynamic diameter of SWNTs dispersion can not fully characterise or predict their behavior. Viscometry of the SWNT dispersions can produce a basic qualitative description of the degree of entanglement and intertube connections.

The shear viscosities of SWNT dispersions with different SWNTs loading were determined and illustrated in Figure 5.12. Generally, the rheology of networks containing

rod shaped particles depends on many factors, including the bonds between rods, rod concentration, and rod flexibility [20]. It was observed that the addition of small amounts of SWNTs to DCAA introduces a shear thinning, non Newtonian behavior suggesting that SWNTs form entangled networks. The higher the SWNTs loading, the higher viscosity at all shear rates tested.

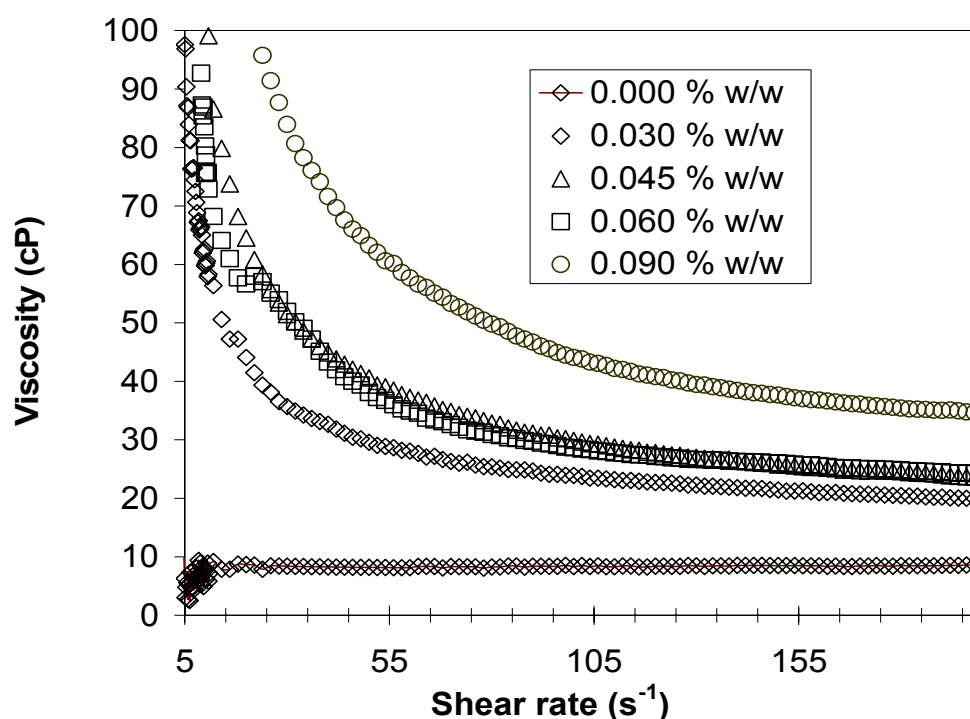


**Figure 5.12.** Viscosity vs. shear rate for SWNTs dispersion in DCAA containing 2 % w/w AMPSA for various SWNT loadings from 0.00 % w/w to 0.09 % w/w.

### 5.3.2 Characterisation of spinning solutions

#### 5.3.2.1 Determination of suitable PAni/AMPSA composition

A homogenous and viscous solution that does not gel during preparation is required for wet spinning. Various formulations were prepared here in order to find suitable viscosity,

and homogeneity, specifically an optimum PAni/AMPSA composition and proper mole ratio of PAni/AMPSA. A mole ratio of PAni / AMPSA of 1/0.6 [11, 21] has been reported in the literature to reach high conductivity in the PAni-ES/AMPSA fibres. Solutions with this mole ratio, but with different solid content (4.6-11.5 %w/w) were thus prepared and evaluated for their spinnability. The formulation of the mixture tested are described in Table 5.1(refer section 5.2.4). Observations made when attempting to spin fibres from mixtures “S1” to “S4” are summarised in Table 5.3.

**Table 5.3.** Summary of observations made during attempts to spin fibres from mixures “S1” to “S4”(refer Table 5.1).

<b>Sample</b>	<b>Observation</b>
<b>S1</b>	No fibres obtained
<b>S2</b>	short tread with many breakages
<b>S3</b>	Continues thread without proper take up
<b>S4</b>	Continuous thread with proper take up

Mixtures “S1” having the lowest PAni content was, unsuitable for fibre spinning due to its low viscosity (~1000 cP). All other solutions had higher viscosities (>2000 cP), however, continues lengths of fibre could only be obtained using mixture “S4”. The total content of PAni and AMPSA in this mixture was 11.5 % w/w.

### 5.3.2.2 Viscometry of PAni-ES/AMPSA/SWNTs-DCAA spinning solutions

Solutions of PAni/SWNTs were prepared based on formulation “S4” by addition of different amounts of SWNT (refer Table 5.2). Figure 5.13 shows the viscosity of PAni-ES/AMPSA/SWNT solutions in DCAA containing different amounts of SWNTs. As the SWNTs content increased, nanotube–nanotube interactions and/or nanotube-polymer interactions appeared to dominate and restrain the motion of polymer chains. However, at higher shear rates, the effect of nanotubes interactions appeared to diminish since all solutions shows similar viscosities.

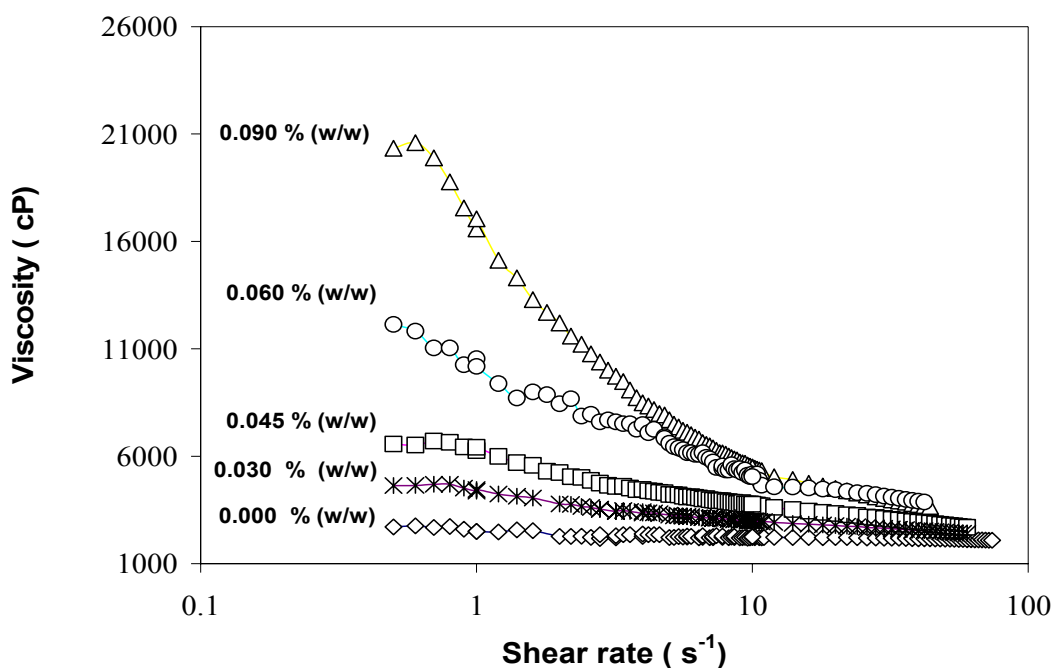


**Figure 5.13.** Influence of SWNTs content on viscosity of PAni-ES/AMPSA/SWNT solution versus shear rate. The total concentration of PAni and AMPSA was 11.5 % w/w.

The rheological behavior of the PAni-ES/AMPSA/SWNT- dispersions in DCAA closely resembled that reported in Chapter 4 for PAni-LEB/SWNT dispersions in DMPU. The

power law indices for the PAni-ES/AMPSA/SWNT dispersions in DCAA are given in Table 5.4 and are lower than the indices for PAni-LEB/SWNT dispersions in DMPU at the same concentration ( $n_{0.09\%} = 0.625$ ) of nanotubes (data obtained by interpolation of data given in Table 4.5). The smaller power law index ( $n$ ) shows a larger deviation from Newtonian behavior in solutions of PAni-ES/AMPSA/SWNT in DCAA solution compared with PAni-LEB/SWNT in DMPU. In addition  $K_{0.09\%}/K_{0\%}$  for PAni-ES/AMPSA/SWNT dispersions was  $\sim 5.9$  which was higher than  $K_{0.09\%}/K_{0\%}$  value for PAni-LEB/SWNT ( $\sim 5.45$ ). These observations suggest stronger physical interaction, between nanotubes and polymer chains in the PAni-ES/AMPSA/SWNT spinning solution compared to the PAni-LEB/SWNT spinning solution in Chapter 4 .

**Table 5.4.** The power law index and consistency index for samples containing different amounts of SWNTs

% w/w SWNT/ DCA	0	0.03	0.045	0.060	0.090
<b>K</b>	2653	4194	6260	10115	15663
<b>n</b>	0.93	0.86	0.78	0.72	0.58
<b>% confidence</b>	94	97	96	97	94.1

The measurement of the viscosity of spinning solutions versus time showed good stability against gelation. This was indicated by the relatively flat viscosity profile measured with time in Figure 5.14 between 5-15 hr after the start of spinning. This good stability of PAni-ES/AMPSA/SWNT solutions with and without SWNTs more than sufficient to allow wet spinning of fibre without concern of gelation.

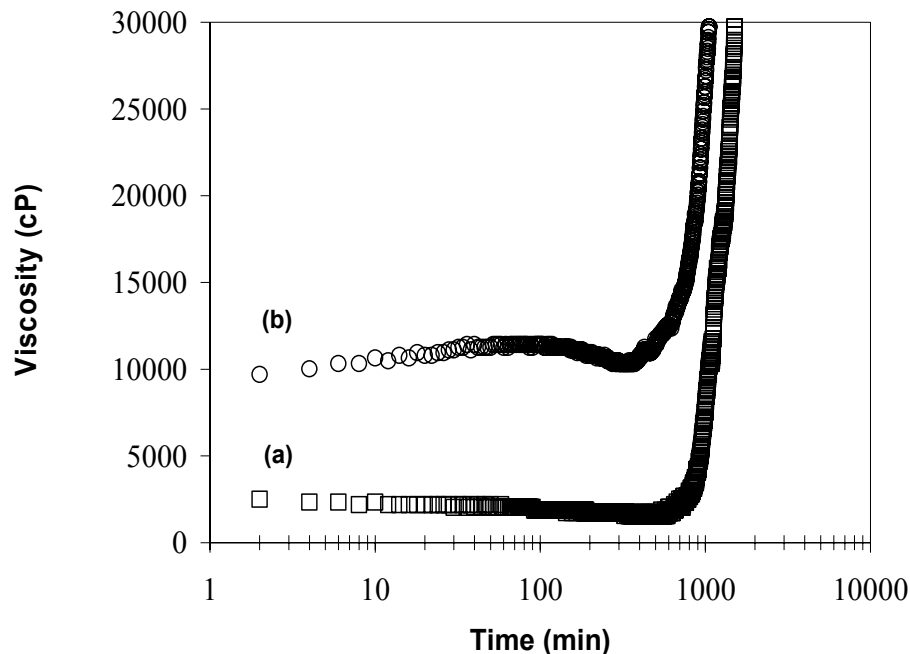


**Figure 5.14.** Time before gelation indicated by sharp rise in viscosity for (a) neat PAni-ES/AMPSA and (b) PAni-ES/AMPSA/SWNT (0.090 % w/w) SWNT spinning solutions. Shear rate =  $1 \text{ s}^{-1}$

### 5.3.3 Preparation and characterisation of composite fibres

The following subsection present findings in regards to the preparation and characterisation of PAni-ES/AMPSA/SWNT composite fibres. Particular emphasis is placed on the effect of the SWNTs concentration on morphological, mechanical, thermal, electrical, spectroscopic and electrochemical properties

#### 5.3.3.1 Morphological properties of PAni-ES/AMPSA/SWNT as spun fibres

Different amounts of pressure (50-125 psi) were applied to the spinning solutions to maintain a constant injection rate ( $1.3\text{-}1.40 \text{ cm}^3/\text{min}$ ) for solutions with different SWNTs



contents. All as-spun fibres were prepared at the same take up speed of 3 m/min and using spin draw ratio of  $\phi=2$ . SEM micrographs of typical as spun fibres of neat PAni-ES/AMPSA and PAni-ES/AMPSA/SWNT (0.76 % w/w) fibres are shown in Figure 5.15. Both samples show a non porous morphology, the sample containing SWNTs showed a rougher outer surface. The average diameter of 160-180  $\mu\text{m}$  for PAni-ES/AMPSA/SWNT fibres were smaller compared with PAni-LEB/SWNT fibres ( $\sim 210 \mu\text{m}$ ) due to higher take up rate used in this method (3 m/min as opposed to 2 m/min).

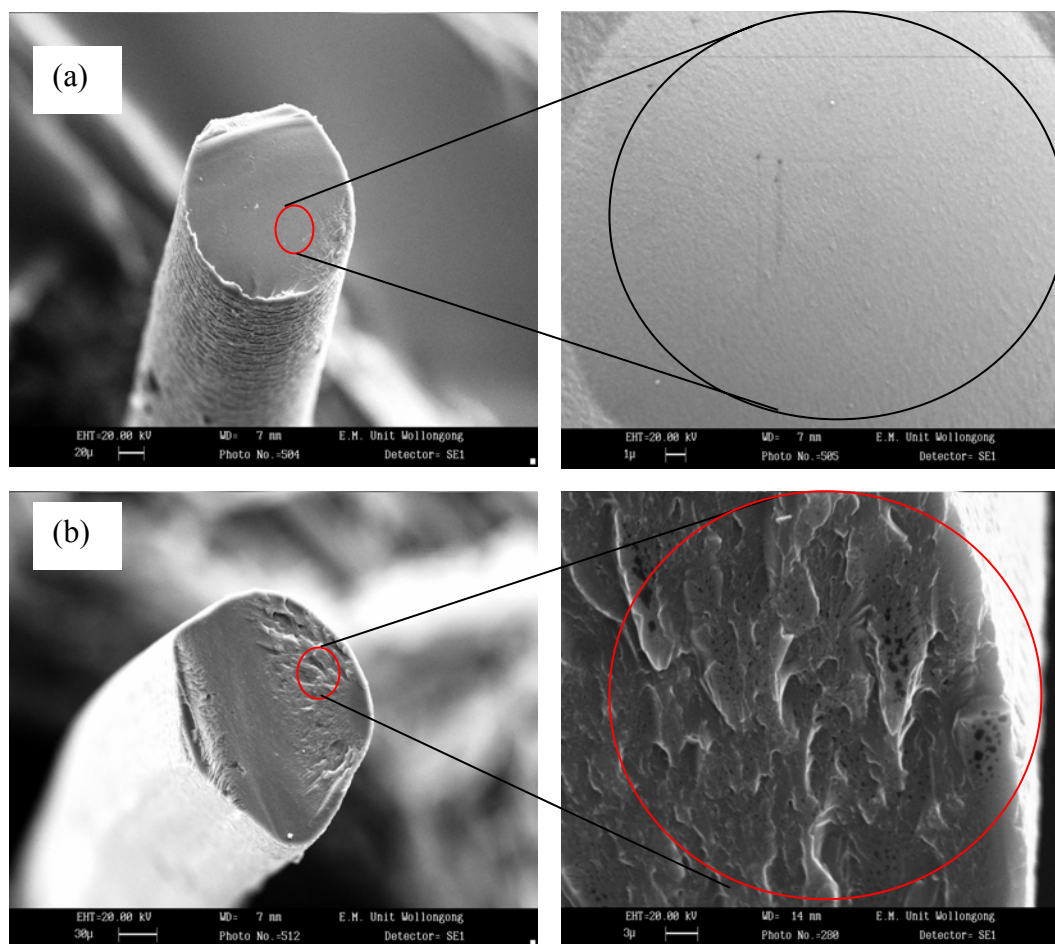


**Figure 5.15.** Typical SEM micrographs of as-spun fibres of (a) neat PAni-ES/AMPSA (b) PAni-ES/AMPSA/SWNT 0.76 % w/w

### 5.3.3.2 Morphological properties of thermally stretched PAni-ES/AMPSA/SWNT

The ability of PAni-ES/AMPSA fibre to be drawn at room temperature, unlike PAni fibre processed in the LEB form, which can only be drawn at  $\geq 398$  K (refer Chapter 4) has been demonstrated by Pomfret and co-workers [11]. The very low  $T_g$ , for PAni-ES/AMPSA/SWNT fibres can be attributed to the plasticising effect of both AMPSA and the residual solvent. As a result, as spun fibres of PAni-ES/AMPSA with and without SWNTs were able to be elongated 5-6 times compared to their initial length through a thermal stretching process at mild temperature ( $\sim 60$ - $70$  °C). Typical SEM micrograph of thermally drawn fibres is shown in Figure 5.16. Stretched fibres had diameters in the range of  $50 \pm 20$   $\mu\text{m}$ , deniers of  $60 \pm 10$  and densities of  $1.3 \pm 0.2$   $\text{g}/\text{cm}^3$ .

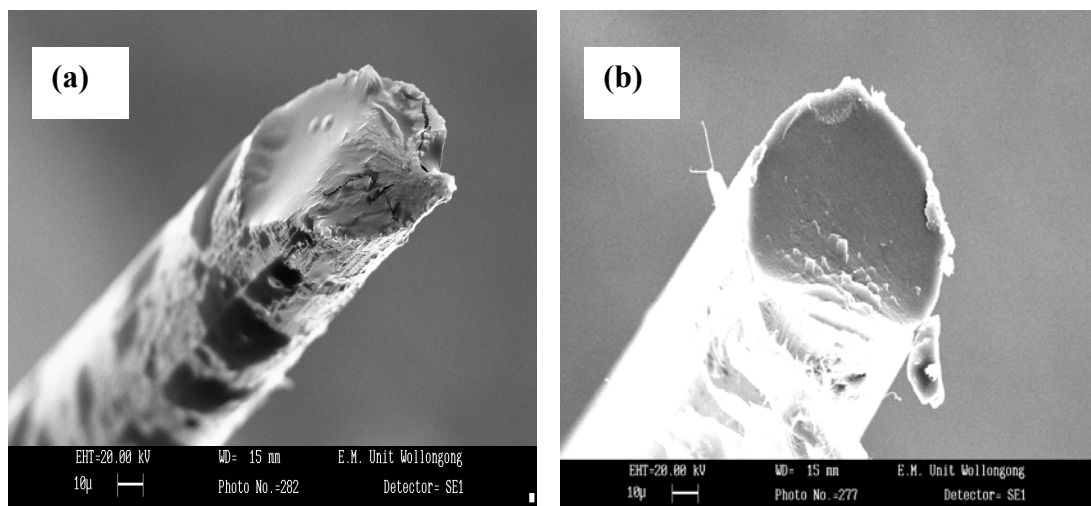


**Figure 5.16.** Typical SEM micrographs of 5x thermally stretched fibre of (a) PAni-ES/AMPSA (b) PAni-ES/AMPSA/SWNT (0.76 % w/w).scale bar is 10  $\mu\text{m}$

SEM micrographs of side wall including FIB milled cross section of the thermally stretched fibre of PAni-ES/AMPSA-SWNT were illustrated in Figure 5.17. The rough surface was a morphological characteristic of fibres containing SWNT. Sections were

milled at approximately  $90^\circ$  with respect to fibre axis. The even distributions of bright dots were observed on the surface which was assumed to be the cut ends of the SWNT bundles. These bright dots were not observed in the neat PAni-AMPS fibres (The TEM picture Figure 5.18 from thin film confirm this observation).

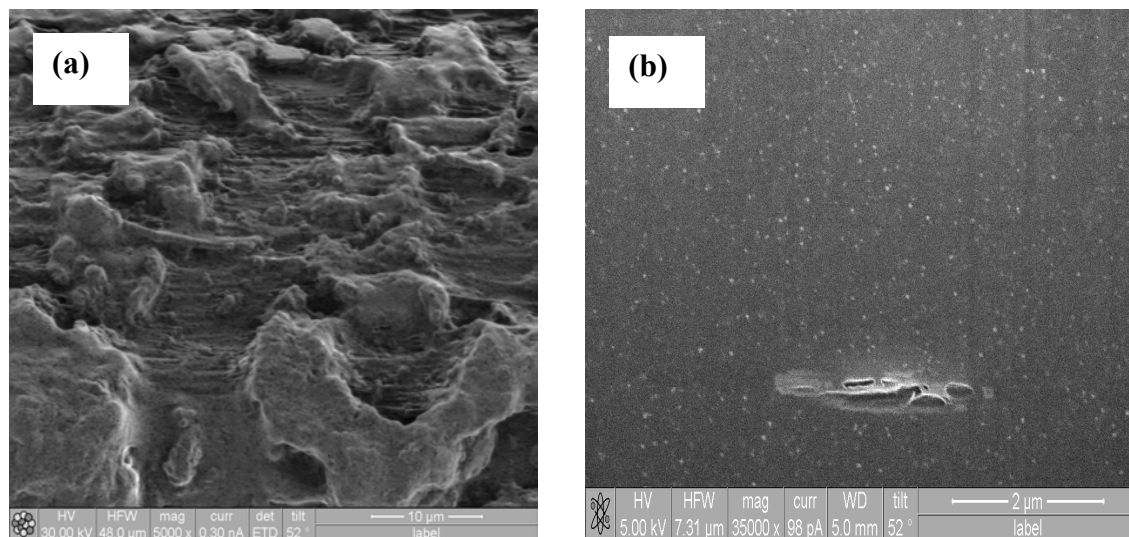


**Figure 5.17.** SEM micro graph of the PAni-ES/AMPSA/SWNT (0.76 %w/w)(a) side wall  
(b) cross section parallel to fibre axis.

Further characterisation of the morphology of PAni-ES/AMPSA/SWNTs fibres was carried out using TEM to determine the state of nanotubes in the PAni matrix. Examination of the ultrathin FIB milled cross section of the PAni-ES/AMPSA/SWNTs composite containing 0.76 %w/w SWNTs (Figure 5.18- b) shows a fairly homogeneous dispersion of SWNTs throughout the PAni matrix. The SWNTs particles showed diameters between 20-30 nm. It can be reasonably assumed that therefore expected that the black particles are cross section of SWNTs bundles that were aligned in the direction

of the fibre axis by thermal stretching of the matrix as observed by other researchers [26, 27], especially taking into account that cross section were taken at  $\sim 90^\circ$  to the fibre axis.

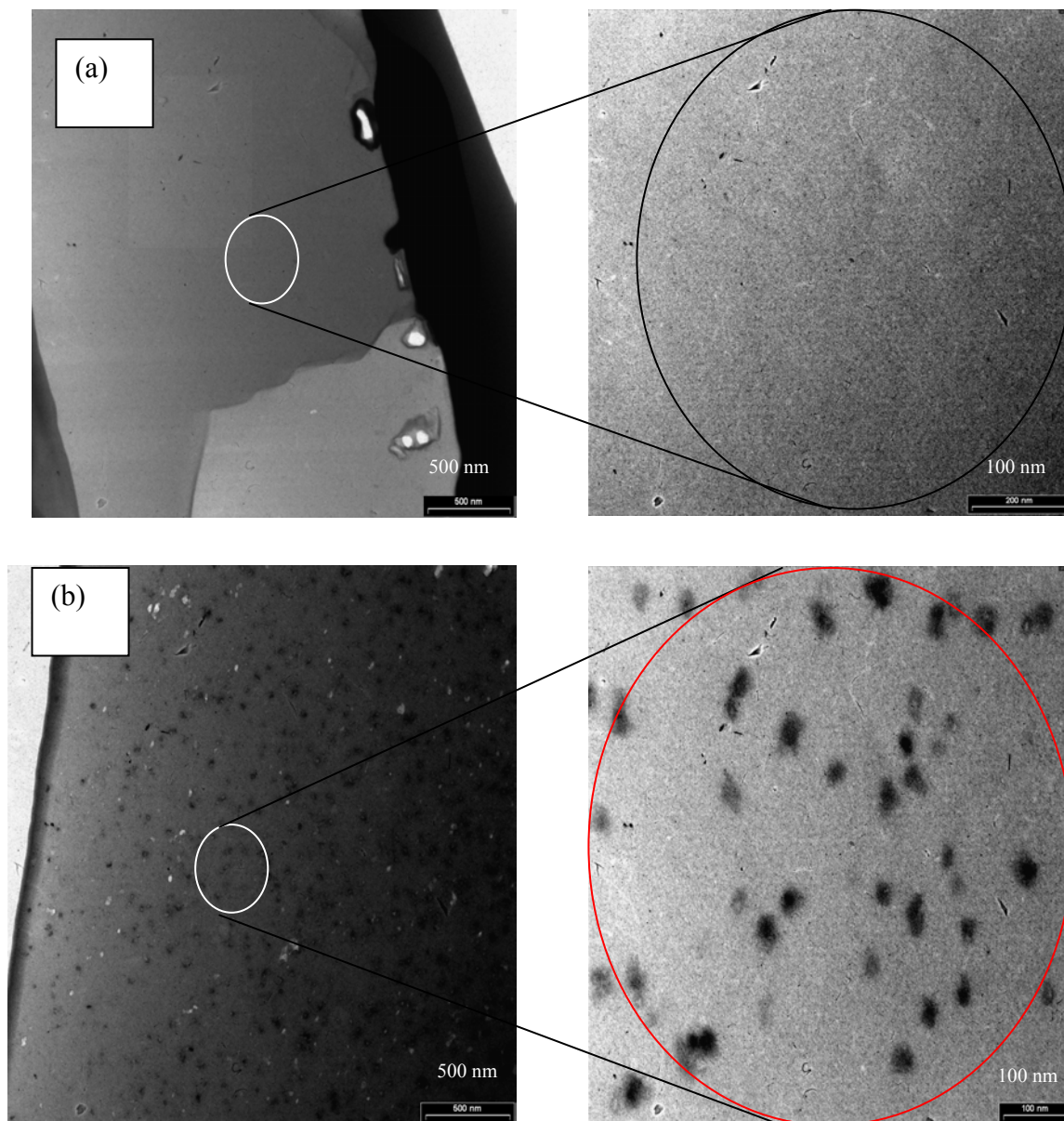


**Figure 5.18.** TEM micrographs of thin film obtained by FIB milling, showing SWNTs dispersion within an PAni-ES/AMPSA matrix for (a) neat PAni-ES/AMPSA (b) PAni-ES/AMPSA/SWNTs (0.76 %w/w SWNT).

### 5.3.4 The mechanical properties of composite fibres

Stress-strain curves for 5x drawn PAni-ES/AMPSA/SWNT composite fibres having different SWNTs contents are compared to those for neat PAni-ES/AMPSA in Figure 5.19. All fibres show linear deformation at low strain followed by plastic deformation above 2% strain. Table 5.5 lists the mechanical property data of PAni-ES/AMPSA/SWNT with different SWNT contents. Fibre containing 0.76 % w/w SWNT demonstrated a 50 % increase in tensile stress ( $\sigma_b$ ), 120 % increase in Young's Modulus (E) and a 40 % decrease in elongation at break ( $\epsilon_b$ ) compared with the fibres containing no SWNTs. The addition of SWNTs results in a decrease in the elongation at break which decreased steadily from  $\sim 9$  % to  $\sim 7$  % for fibres containing  $\leq 0.5$  % w/w SWNTs. However, above 0.5 % w/w SWNTs, the breaking point dramatically depressed. The trend of increasing of elastic modulus and tensile strength to some extent are similar. The modulus and strength showed a gentle increase up to 0.25 % w/w SWNTs content followed by sharper increases and then gentle increase, between 0.25 % w/w-0.5 % w/w SWNTs and between 0.5 % w/w-0.76 % w/w SWNTs, respectively. Specific tensile strength and elastic modulus based on gpd also were listed in Table 5.5 for fibres with and without SWNTs which show similar increasing trend. It can be seen from Table 5.5 that the efficiency of reinforcing performance (refer section 4.3.7) of SWNTs in low nanotubes content (0.25 %w/w) was minor. However, reinforcement efficiency sharply increases when the SWNTs content was increased and remained essentially constant at higher SWNTs content. This behavior may be attributed to the higher density of entanglements of rigid SWNTs bundles in the matrix at higher SWNTs content as shown by viscometry of the composite spinning solutions (refer section 5.3.2.2).

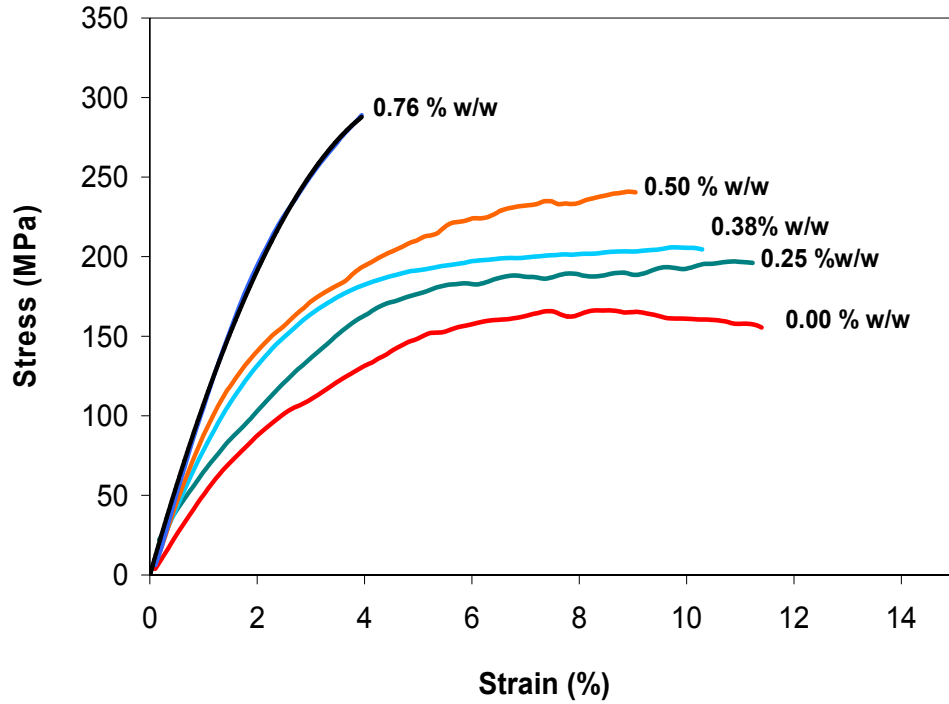


**Figure 5.19.** The typical stress – strain curve of PAni-ES/AMPSA fibre and its composites with different SWNT contents ( $D_{\text{fibre}}=50\pm 20\ \mu\text{m}$ , strain rate= 500  $\mu\text{m}/\text{min}$ ).

**Table 5.5.** The mechanical properties of PAni-ES/AMPSA fibre and its composites with different SWNT contents.

% w /w SWNT/ ES- AMPSA	$\delta_b$		E		$E_b(\%)$	$E_{\text{effNT}}$ (GPa)
	(MPa)	gpd	(Gpa)	gpd		
<b>0.00</b>	$170 \pm 22$	1.47	$3.4 \pm 0.4$	29.56	$9 \pm 3$	-----
<b>0.25</b>	$196 \pm 17$	1.70	$3.9 \pm 0.4$	33.90	$8 \pm 3.5$	204
<b>0.38</b>	$199 \pm 9$	1.73	$5.6 \pm 0.3$	48.67	$7 \pm 2$	580
<b>0.50</b>	$242 \pm 28$	2.10	$6.2 \pm 0.3$	53.89	$7 \pm 1.5$	560
<b>0.76</b>	$255 \pm 32$	2.21	$7.3 \pm 0.4$	63.45	$4 \pm 0.6$	520

The significant improvement in elastic modulus of PAni-ES/AMPSA fibres with the addition of nanotubes was confirmed by a creep test under a load of 40 mN ( Fig 5.20). The results showed that lower strains were produced in PAni-ES/AMPSA with SWNTs compared to fibres without SWNTs. In addition, the creep over time for fibres without SWNTs was not observed for fibres with SWNTs. The results above indicate that the motion of PAni chains under static load is likely to be more constrained when blended with SWNTs. This constraint may be attributed to physical or chemical interactions between the SWNTs and PAni matrix, and these will be discussed in the next section.

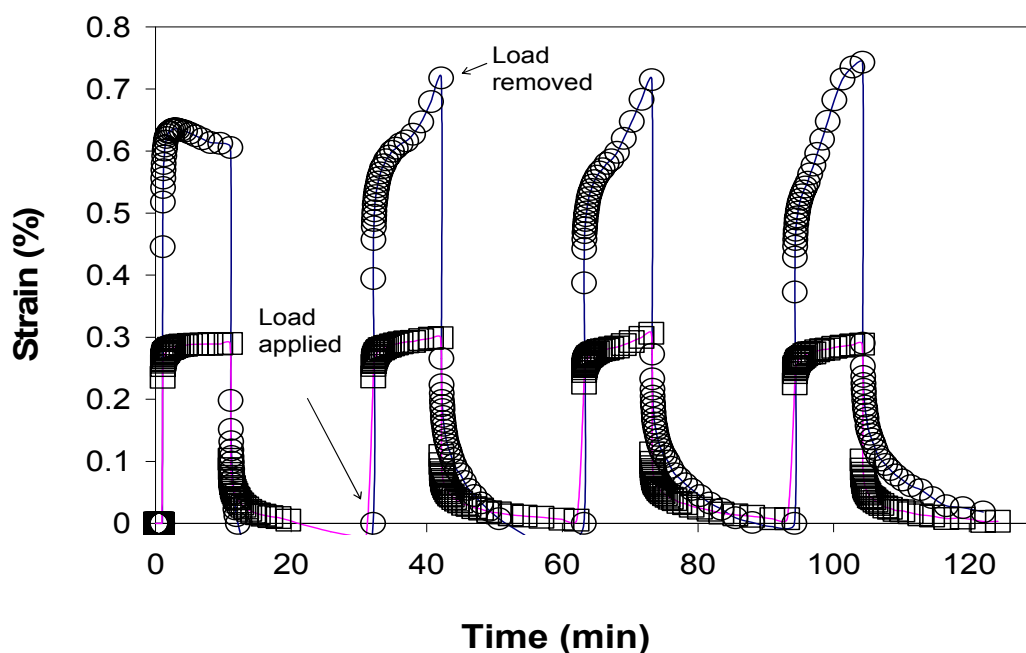


**Figure 5.20.** Strain recovery behavior of (○) neat PAni-ES/AMPSA fibre (□) PAni-ES/AMPSA/SWNT (0.76 % w/w) with cyclical application and removal of a 40 mN force.

Although it was shown above that the elongation at break decreases considerably with increasing SWNTs content in PAni-ES/AMPSA/SWNT fibres, the tight knot could be



formed even in fibres containing a high SWNT content (Figure 5.21 a,b). Fibres containing nanotubes also showed high level of twistability in the S (counter clock wise) and Z (clockwise) directions which is essential in order to enable fibres to form strong threads that can be woven into textiles at the industrial scale (Figure 5.21 c,d).

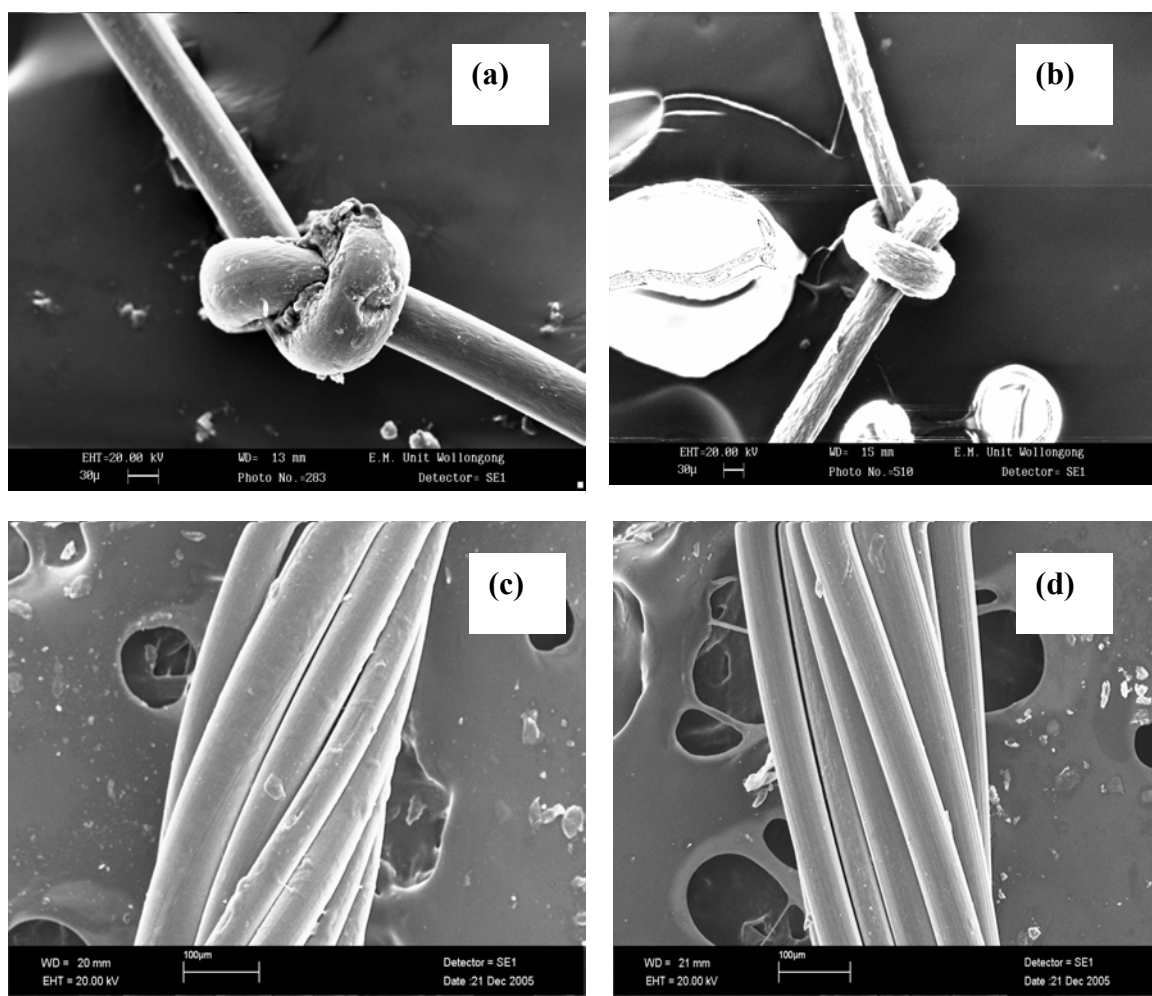


**Figure 5.21.** SEM micrographs of full knots of (a) PAni-ES/AMPSA (b) PAni-ES/AMPSA/SWNT (0.76% w/w). SEM micrographs of 16 ply twisted fibre of PAni-ES/AMPSA/SWNT (0.76 % w/w) fibre with (c) S shaped twisting (d) Z shaped twisting. The number of twist per inch was 36.



Since the processing parameters used to prepare fibres here including take-up rate, drawing and thermal stretching ratio are similar for all fibres, the improvement in mechanical properties of fibres can be attributed mainly to the role of SWNTs in reinforcing of PAni matrix through efficient load transfer to oriented nanotube ropes. Some preliminary evidence will be presented in next Chapter regarding the monitoring of load transfer to SWNTs using in-situ Raman spectroscopy.

### **5.3.5 Thermal analysis of the PAni-ES/AMPSA/SWNT composite fibres**

Fig 5.22(a) shows the DSC results for 5x drawn fibres of PAni-ES/AMPSAS/SWNT fibre with and without SWNTs. Both samples showed two sharp and one broad endothermic peaks and one exothermic peak over the temperature range investigated (25–425 °C). The first endothermic peaks occurred at ~100 °C can be attributed to the removal of moisture and residual DCAA solvent. This result is consistent with the TGA results in previously studies [28]. A small and broad endothermic shoulder at ~195 °C was probably associated with the melting of AMPSA or the complete boiling of DCAA. The second endothermic peak at ~315 °C is perhaps due to weight loss owing to the loss of decomposed fragments of AMPSA, and is not associated with the melting of PAni segment. Weight loss at ~ 300 °C has been observed previously using TGA [28]. The absence of any endothermic or exothermic peaks in the second heating cycle (Figure 5.22) revealed that the process that led to peaks observed on the first cycle were irreversible.

An exothermic peak at ~ 215 °C was observed for both fibres in Fig 5.22(a). It has been shown previously that this relatively large exothermic peak, accompanied by a weight loss transition on the TGA trace [28], could be attributed mainly to decomposition of AMPSA.

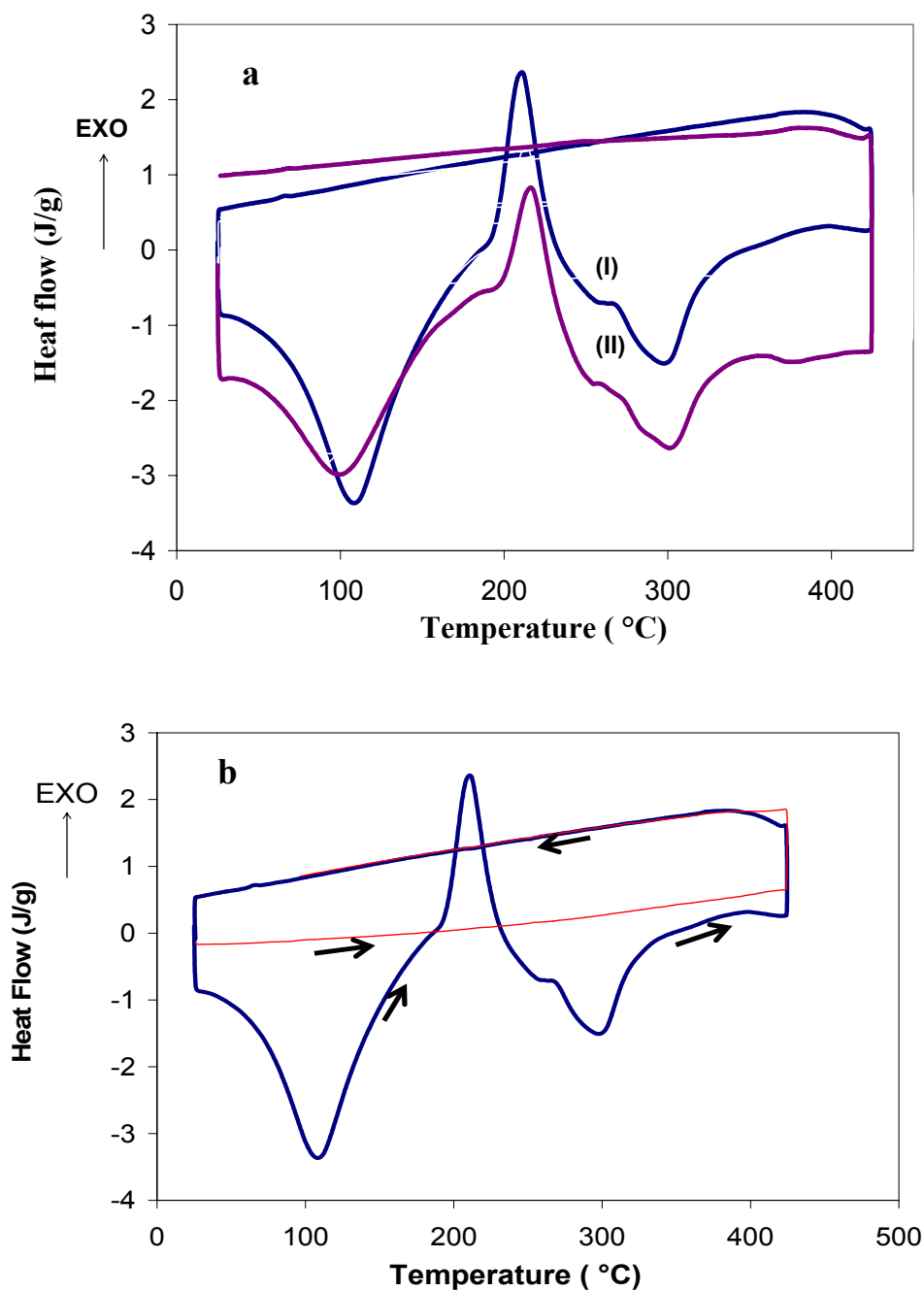


**Figure 5.22.** (a) DSC thermogram of 5x drawn fibre (I) PAni-ES/AMPSA (II) PAni-ES/AMPSA/SWNT (0.76 %w/w). (b) The DSC thermogram for the first and second cycles of 5X drawn PAni-ES/AMPSA/SWNT.

Significantly, the PAni- ES/AMPSA fibres did not show melting and crystallisation transitions that were observed for LEB fibres (Fig 4.13). It may be concluded that the PAni-ES/AMPS fibre shows low crystallinity. Figure 5.23 shows storage modulus and  $\tan\delta$  curves for neat fibres made from PAni-ES/AMPSA and PAni-ES/AMPSA/SWNTs containing 0.76 % w/w SWNTs as a function of temperature. It can be seen that with addition of SWNTs the storage modulus increases which is in agreement with results obtained by normal tensile testing (Figure 5.19). The storage modulus  $\sim 7$  GPa for the PAni-ES/AMPSA fibre containing 0.76 % w/w SWNTs was exhibited  $\sim 75$  % higher compared to neat PAni-ES/AMPSA fibre  $\sim 4$  GPa at room temperature. The significant improvement in the storage modulus of PAni-ES/AMPSA fibre with the addition of SWNTs is ascribed to interaction between SWNTs and the PAni matrix through physical adhesion. A steady decrease followed by a plateau was observed with increasing temperature in Figure 5.23-a, which may be attributed to a sub glass transition temperature ( $T_g$ ) known as  $\beta$  transition or secondary transition [29]. Breshtein [30] has reported that this transition may be attributed to the activation barriers for solid phase reactions regarding deformation, flow or creep [30]. This transition is correlated to first peak in Figure 5.23-b at  $\sim 100$  °C. The composite PAni-ES/AMPA fibre containing SWNTs showed a wider peak compared to the neat PAni-ES/AMPSA fibre, and this may be attributed to the low mobility of PAni chains that interact with the SWNTs. The sharp drop in storage modulus above 150 °C attributed to the transition between glassy to rubbery states  $T_g$ . This transition is manifested as a sharp peak in the curve of  $\tan \delta$  vs. temperature at  $\sim 220$  °C (Figure 5.23-b). As shown by the DSC results in Figure 5.22, this transition is also associated with the melting of AMPSA, which assists in the transition

between glassy to rubbery states.  $T_g$  shifted slightly to a higher temperature 225 °C upon addition of SWNTs. This is in agreement with other reported composites containing SWNTs [31]. The tails of the storage modulus curves in Figure 5.23-A for both types of fibre show another plateau, which is common to thermoset polymers without melting transition.

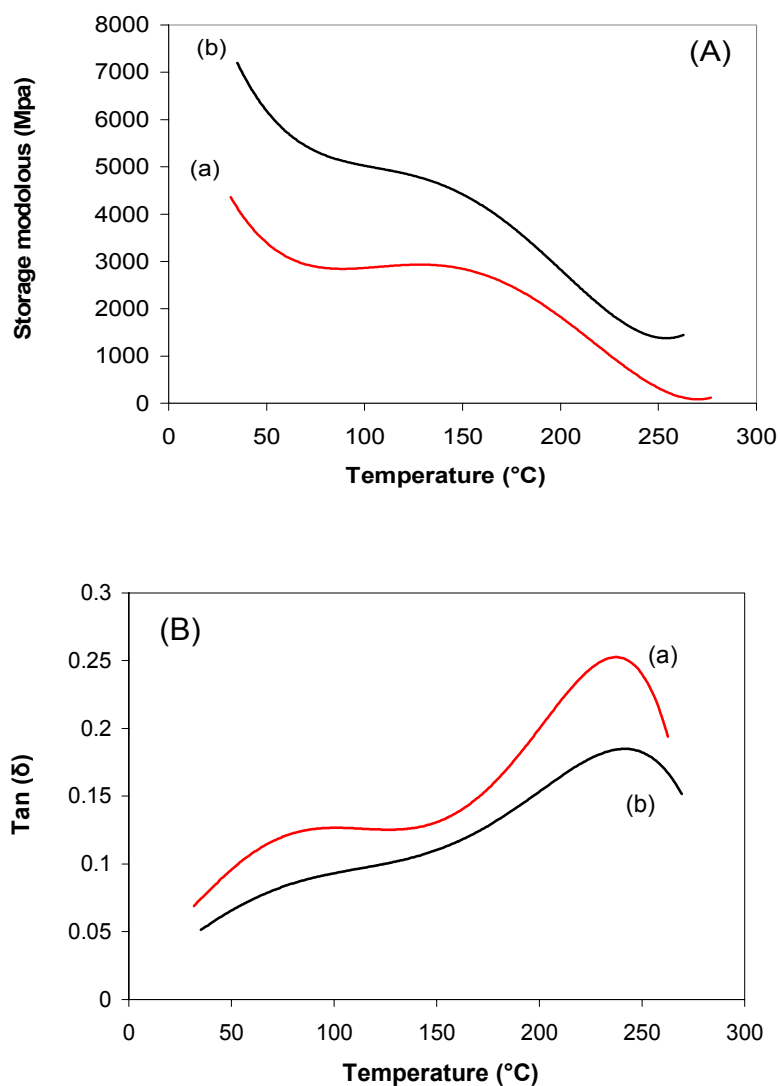


**Figure 5.23.** (A) Storage modulus (B) the Tan $\delta$  (Loss modulus/Storage modulus) vs temperature curves for (a) PAni-ES/AMPSA and (b) PAni-ES/AMPSA - SWNTs (0.76 % w/w).

### 5.3.6 Electrical conductivity of PAni-ES/AMPSA-SWNT composite fibres

Figure 5.25 shows the typical four point probe electrical conductivity of 5x drawn PAni-ES/AMPSA/SWNT fibres obtained as a function of the weight fraction of nanotubes after drying in room temperature for 24 hr. Table 5.6 also shows the average values of four probe electrical conductivity. Increases in electrical conductivity were observed in PAni-ES/AMPSA/SWNT fibres as the SWNT content was raised. A 45 % increase in electrical conductivity was observed in going from neat PAni-ES/AMPSA ( $497 \text{ S/cm}^{-1}$ ) To PAni-ES/AMPSA/SWNTs containing 0.76 % w/w of SWNTs ( $716 \text{ S/cm}^{-1}$ ). This increase in electrical conductivity can be attributed to interactions between PAni and SWNTs that increases the effective degree of electron delocalisation (refer Chapter 4) This interaction was verified using Raman spectroscopy (see next section).

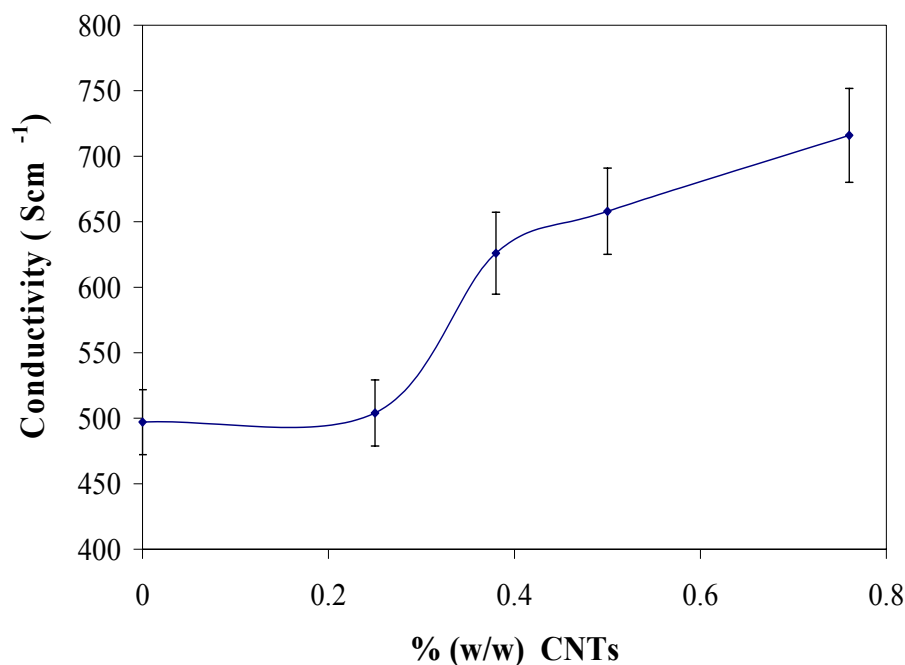


**Figure 5.24.** Influence of SWNTs content on the electrical conductivity of PAni-ES/AMPSA/SWNTs fibres

**Table 5.6.** The influence of SWNT loading on four point probe conductivity of 5xdrawn fibre of PAni/AMPSA

% w/w SWNTs in PAni-ES/AMPSA	Conductivity (S/cm)
0	$497 \pm 55$
0.25	$504 \pm 35$
0.38	$626 \pm 37$
0.5	$658 \pm 60$
0.76	$716 \pm 36$

The fitting of electrical conductivity data for PAni-ES/AMPSA/SWNTs fibres to the percolation power law (Equation 4.3) yields a low percolation threshold of  $\sim 0.35$  % w/w SWNTs (Figure 5.25). This value for the conductivity percolation threshold is in good agreement with other polymer-nanocomposite systems (e.g. 0.5 % w/w percolation level [24] and 0.4 %w/w) for PAni-LEB-SWNT fibres (refer Chapter 4).

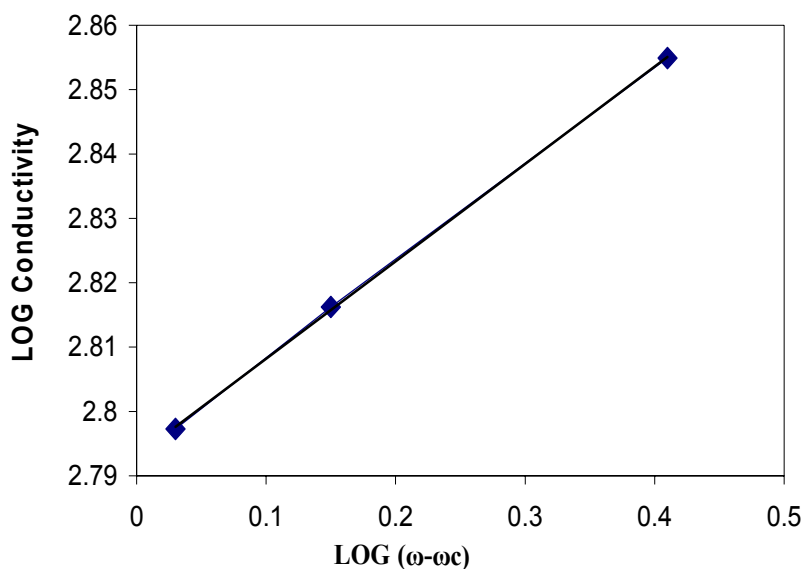


**Figure 5.25.** log–log plot of electrical conductivity vs reduced mass fraction.

### **5.3.7 Raman spectroscopy of PAni-ES/AMPSA/SWNTs fibres**

Raman spectroscopy was used to investigate the presence of carbon nanotubes (Figure 5.26) in PAni-ES/AMPSA-SWNT composite fibres (Figure 5.25). Table 5.6 also shows the Raman band frequency assignments for PAni-ES/AMPSA/SWNTs fibres. Raman peaks originating from SWNTs increase in intensity when more SWNTs were incorporated into the fibres. Similar observations have been made previously [32]. Raman spectra also revealed information regarding the interaction between SWNT and PAni. Raman spectra shows that the secondary doping of EB/AMPSA using DCAA results in ES form of PAni and gives rise to the bands at 1337, 1496 and 1592  $\text{cm}^{-1}$  as described previously [33, 34] (bands at 1337  $\text{cm}^{-1}$ , 1496  $\text{cm}^{-1}$ , 1592  $\text{cm}^{-1}$ ). The peak at 1337  $\text{cm}^{-1}$  corresponded to the formation of the (C-N<sup>+</sup>) band and this response was enhanced by addition of more SWNTs. This may be attributed to increasing levels of doping [35, 36]. With increased amounts of SWNTs a decrease in the ratio of intensity in the 1496  $\text{cm}^{-1}$  band (N-H in plane bending of benzoid ring) and the 1169  $\text{cm}^{-1}$  band (C-H stretching of benzoid ring) was observed. This can be attributed to the interaction of the bipolaronic structure of PAni and SWNTs [32, 36].

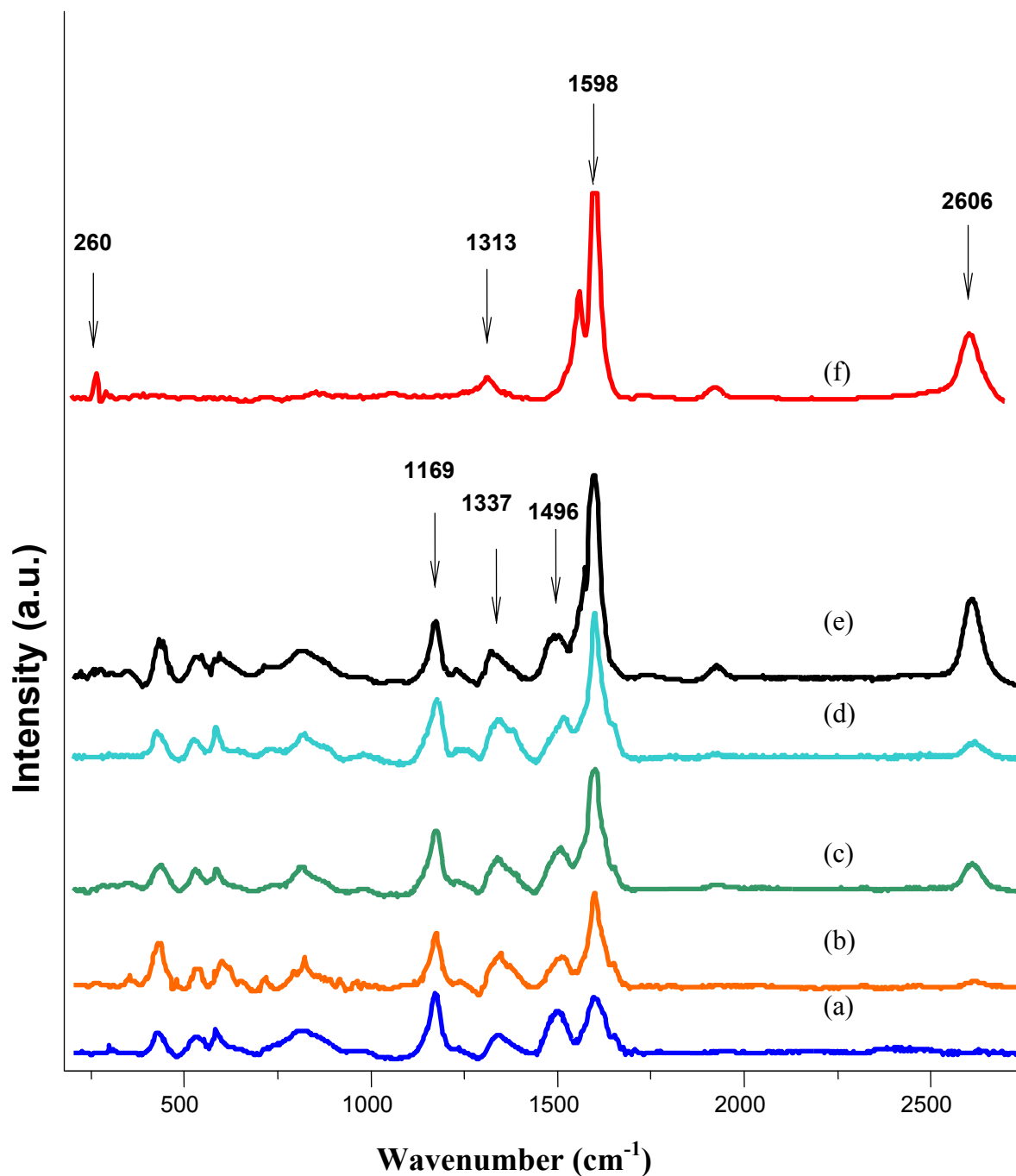


Figure 5.26. Enhanced Raman spectra ( $\lambda_{\text{exc}} = 632.8 \text{ nm}$ ) obtained for PAni-ES/AMPSA/SWNTs obtained containing various amounts of SWNTs (a) 0.00 % w/w (b) 0.26 % w/w (c) 0.38 % w/w (d) 0.5 %w/w (e) 0.76 % w/w and (f) SWNT bucky paper.



**Table 5.7.** The assigned frequencies originated from PAni-ES/AMPSA and its SWNTs composite

Raman shift( $\text{cm}^{-1}$ ) $\lambda_{\text{exc}}=632.8$				Description of vibration
Neat EB	PAni-ES /AMPSA	Pristine SWNTs	PAni-ES/AMPSA/SWNTs (0.76 %w/w)	
-----	-----	2606	2606	D* band of SWNTs
-----	-----	1598	1594	G band of SWNT
-----	1592	-----		C-C stretching( $B^*$ )
1580	-----	-----	-----	C=C stretching of( $Q^+$ )
-----	1496	-----	1496	N-H in plane bending (B)
1475	-----	-----	-----	C=N stretching of (Q)
-----	1337	-----	1337	C-N <sup>+</sup> stretching of bipolaron structure
-----	-----	1313	-----	D band SWNTs
1216	-----	-----	-----	C-N stretching (B)
-----	1169	-----	1169	C-H stretching (B)
1161	-----	-----	-----	C-H Bending (Q)
-----	-----	190-260	190-260	(RBM) SWNTs

To separate the influence of SWNTs and AMPSA on the Raman spectra of PAni-ES/AMPSA/SWNTs composite fibres, such fibres with and without nanotubes were deprotonated. Fig 5.26 shows the Raman spectra of a neat PAni-ES/AMPSA fibre after deprotonation by treatment with an  $\text{NH}_4\text{OH}$  (3 % w/w) solution for different periods of time between 3 to 24 hrs. Complete deprotonation was observed after 6 hrs of chemical treatment with the base solution as evidenced by the decrease in intensity of characteristics bands of PAni-ES/AMPSA at 1169, 1337, 1496 and  $1592\text{ cm}^{-1}$  assigned to semiquinoid structures [33]. After complete deprotonation, the characteristic bands of PAni-EB emerged with a corresponding increase in bands attributed to the quinoid structure at 1161, 1216, 1475, and  $1587\text{ cm}^{-1}$ . The mechanism of deprotonation and the emergence of semiquinoid polaron and quinoid structure are illustrated in Figure 5.27. After deprotonation, the delocalised bipolaron structure disappears and oxidised quinoid segment ring forms a localised non-conductive structure.

**Scheme 5.1.** Polaronic (semiquinoid), bipolaronic and oxidised unit of PAni[33].

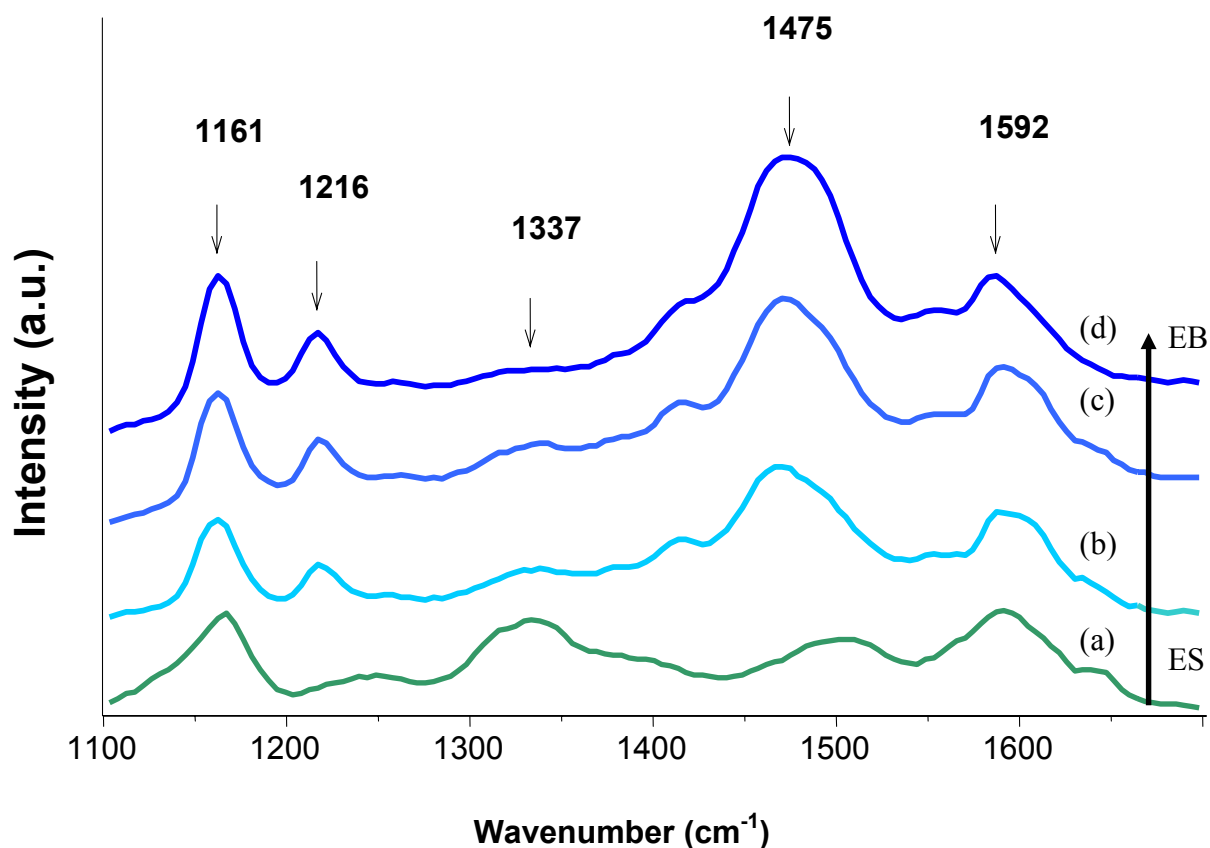


**Figure 5.27.** Enhanced Raman spectra ( $\lambda_{\text{exc}} = 632.8$ ) of neat PAni-ES/AMPSA (a) before deprotonation, (b) 3 hr after deprotonation and (c) 6 hr after deprotonation (d) Raman spectrum of PAni(EB). Arrow indicates the transition from the protonated ES form to the deprotonated EB form

Although PAni-ES/AMPSA fibres could be deprotonated in 6 hrs, the PAni-ES/AMPSA/SWNTs composite fibres showed a combination of EB/ES structure even after 24 hrs of deprotonation treatment. Therefore, it may be concluded that the chemical interaction between PAni and SWNTs significantly stabilises the conducting form of PAni (ES) which may become very important in any future possible application of PAni/SWNTs fibre

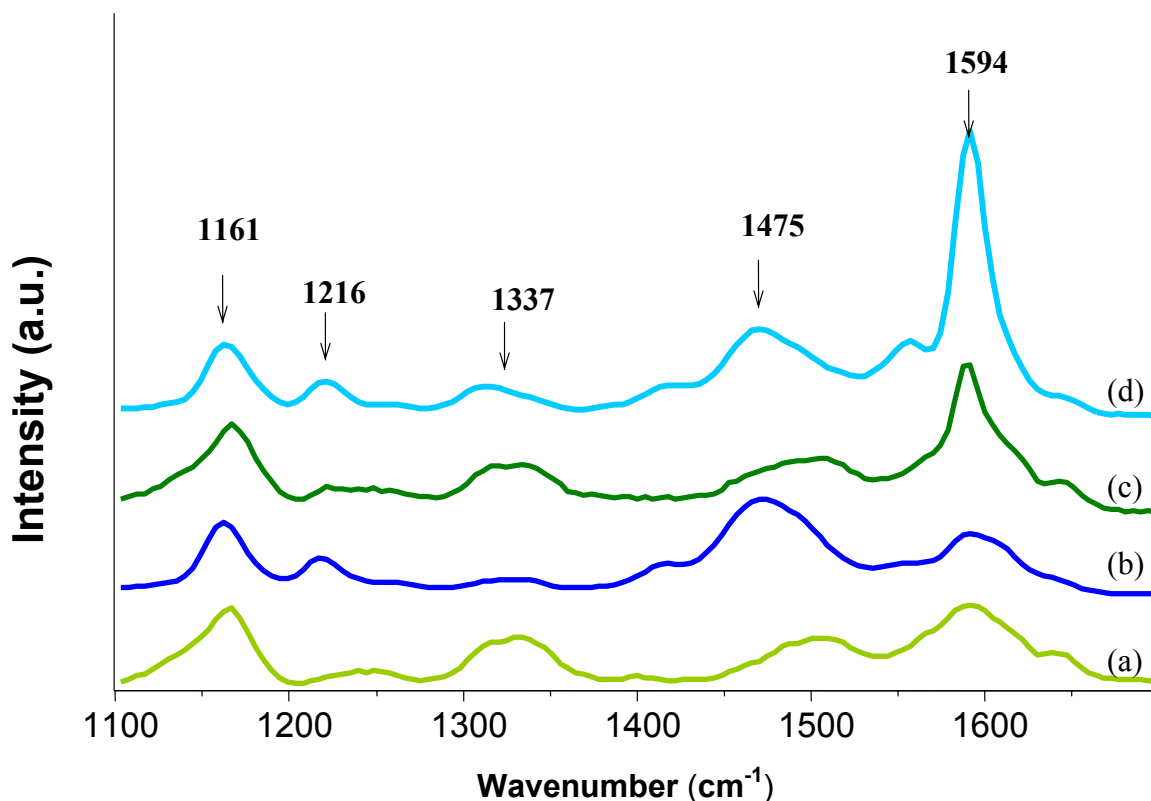


**Figure 5.28.** Enhanced Raman spectra ( $\lambda_{\text{exc}} = 632.8$ ) of (a) Neat PAni-ES/AMPSA fibre before deprotonation, (b) Neat PAni-ES/AMPSA after 6 hrs deprotonation (c) PAni-ES/AMPSA/SWNT (0.76 % w/w) before deprotonation and (d) PAni-ES/AMPSA/SWNT (0.76 % w/w) after 24 hrs deprotonation.

### 5.3.8 Cyclic Voltammetry

Cyclic voltamograms (CVs) were obtained using neat PAni-ES/AMPSA and PAni-ES/AMPSA/SWNT (0.76 % w/w) fibre, as the working electrodes, in HCl (aq) and EMI.TFSI ionic liquid electrolytes. Unlike the low electrical conductivities for PAni fibres prepared from LEB state in Chapter 4, the excellent electrical conductivity of PAni-ES/AMPSA fibres with or without SWNTs meant no Pt coating was required to obtain CVs.

**5.3.8.1 Cyclic voltammetry of PAni-ES/AMPSA/SWNTs composite fibres in HCl (aq)**

As described in Chapter 4 the potential range for the CV characterisation of PAni needs to be limited so as to prevent sample degradation. In order that the reversible redox chemistry of PAni could be observed, the potential range was limited between -0.2 V and 0.5 V. Over this potential range, PAni was cycled reversibly between the Leucoemeraldine salt (LES) and ES forms only. Figure 5.29 shows the oxidation and corresponding reduction peak potentials. The oxidation potential decreased from 0.39 V to 0.32 V and reduction peak increased from 0.09 V to 0.13 V when SWNT (0.76 % w/w) was added to PAni-ES/AMPSA. The current signal increased and the separation between oxidation and reduction peaks, reflect the higher conductivity of fibres containing SWNTs.

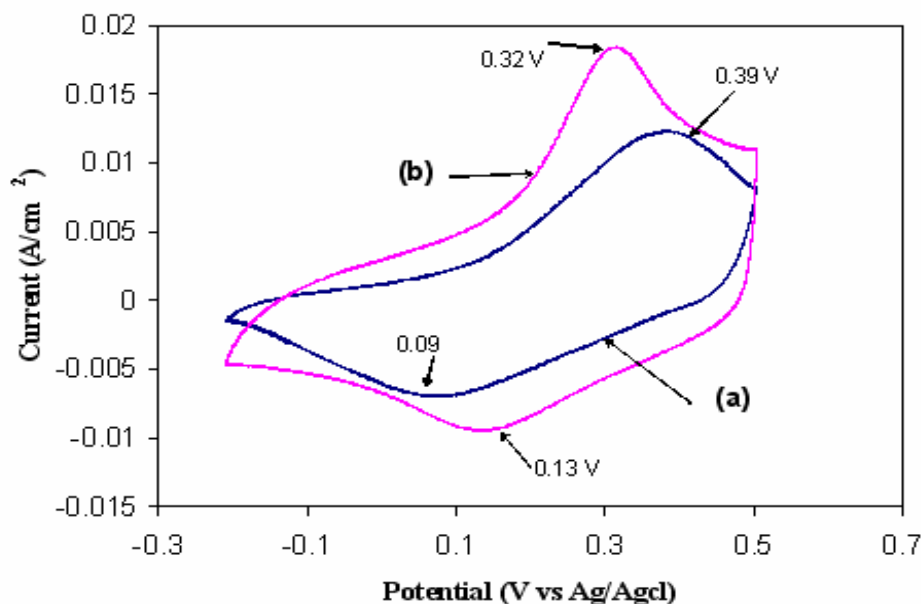


**Figure 5.29.** CV characterisation of (a) PAni-ES/AMPSA fibre (b) PAni-ES/AMPSA /SWNTs fibre 0.76 % w/w (b) in 1.0 M HCl (aq) electrolyte. 10 th cycle shown for each CV. Scan rate 10 mV/s. (L=10 mm, D= 70  $\mu$ m)

### **5.3.8.2 Cyclic voltammetry of PAni-ES/AMPSA/SWNTs composite fibres in ionic liquid electrolyte**

The use of conventional electrolytes creates some limitations in the practical application of PAni fibres. Narrow electrochemical windows and rapid evaporation rates life time and result in the degradation of PAni upon redox cycling [21, 38]. Even though, the use of other types of aqueous acids, such as methane sulfonic acid (MSA) in place of HCl can retain reversible electrochemical activity even when cycling into the pernigraniline state, They induce poor mechanical properties in PAni and thus limiting its effectiveness for application in electrochemical actuators or other electronic devices [39]. In contrast, ionic liquids have high ionic conductivities, large electrochemical windows, excellent thermal and electrochemical stability, and negligible evaporation rates. They can be employed as electrolytes in the development of stable and durable electrochemical devices [38, 40]. The majority of ionic liquids consist of an organic cation based on quaternary nitrogen, such as imidazolium and a very weakly basic anion such as  $\text{BF}_4^-$  or bis-trifluoromethanesulfono imide (TFSI). The chemical structures of two well known ionic liquids, 1-butyl-3-methyl imidazolium tetrafluoroborate (BMI. $\text{BF}_4$ ) and EMI.TFSI are presented in Table 5.8. Their electrochemical stability is usually in excess of +2V with respect to oxidation and - 2 V with respect to reduction (vs.  $\text{Ag}/\text{Ag}^+$ ) [41]. The conductivities of EMI.TFSI and BMI. $\text{BF}_4$  as reported in the literature are in the range of 400- 500  $\mu\text{S}/\text{cm}$  [42]. In addition, their decomposition temperature as measured by TGA is typically > 300 °C [43]. Recently, Mattes and co-workers reported that neat PAni-ES/AMPSA fibre in BMIBF<sub>4</sub> shows no electrochemical activity. The lack of an electrochemical response was explained by the insolubility of the AMPS- anion in BMI. $\text{BF}_4$  [42]. However, these

studies showed that if the PAni-ES/AMPSA was subjected to ion exchange using trifluoro-methane sulfonic acid ( $\text{CF}_3\text{SO}_3\text{H}$ ), sharp redox peaks were produced.

**Table 5.8.** The chemical structure of the ionic liquids 1-butyl-3-methyl imidazolium tetrafluoroborate (BMI.BF<sub>4</sub>) and ethyl methyl imidazolium bis (trifluoromethane sulfonyl) imide (EMI.TFSI)

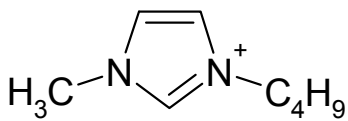
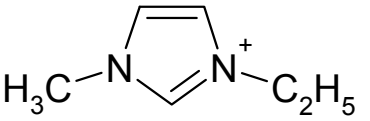
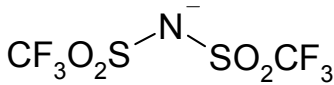
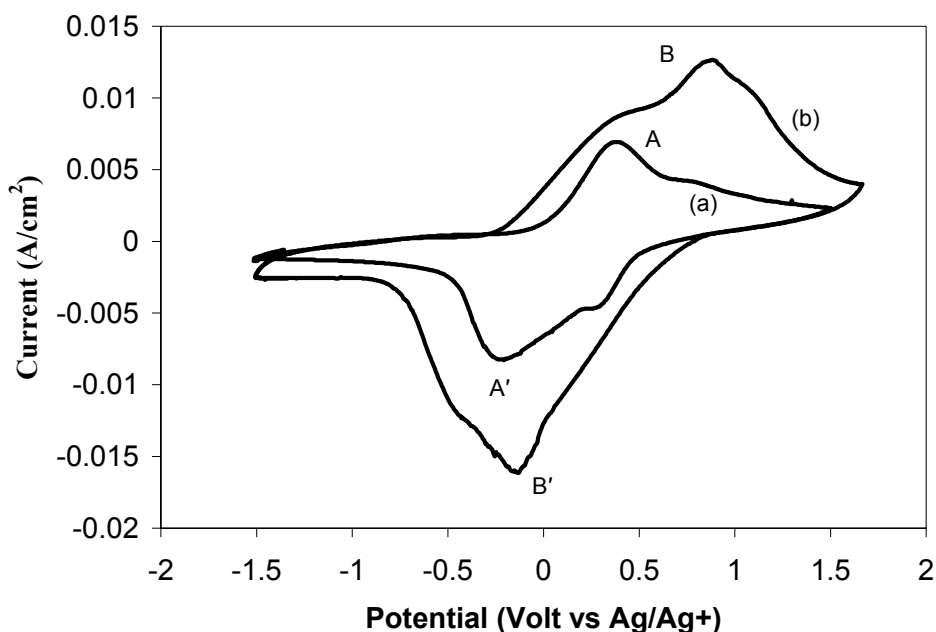
Ionic liquids	Cation	Anion
BMI-BF <sub>4</sub>		BF <sub>4</sub> <sup>-</sup>
EMI.TFSI		

Figure 5.30 shows the CVs obtained using either PAni-ES/AMPSA or PAni-ES/AMPSA/SWNT fibres as working electrodes in EMI.TFSI. The potential was cycled between +1.5 V and -1.5 V under a 10 mN tensile load to keep the fibre straight. Both samples showed very distinct redox peaks (without any prior dopant exchange treatment), which may be explained by the higher solubility of AMPSA in EMI.TFSI compared to BMI.BF<sub>4</sub>. Lu and colleagues[40] previously explained the mechanism of electrochemical switching of PAni fibre doped with  $\text{CF}_3\text{SO}_3\text{H}$  in BMI.BF<sub>4</sub>. A similar mechanism can be proposed for PAni fibre doped with AMPSA in EMI.TFSI as shown by Scheme 5.2.

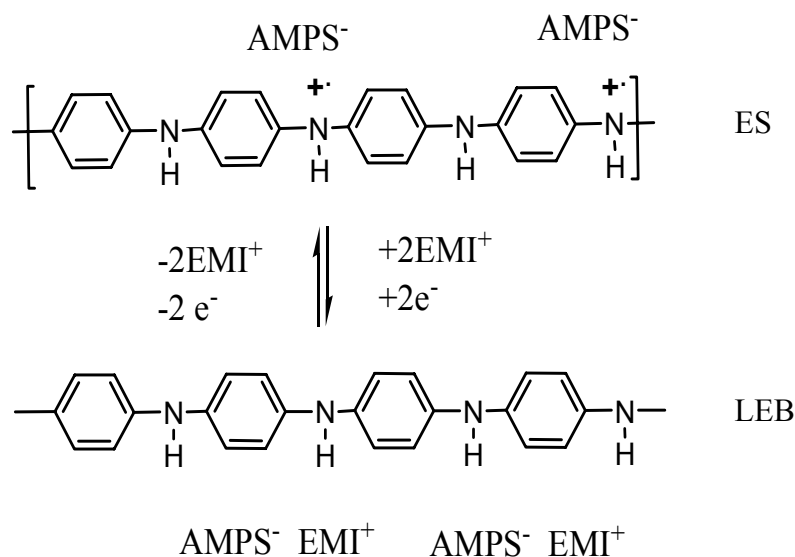
PAni (ES) is electrochemically reduced to the LEB form by gaining two electrons and two EMI cations per tetrameric repeat unit. This form of PAni then reversibly loses two electrons and two EMI cations to reform the ES structure when it is cycled to higher

positive potentials. The mechanism of maintaining electron neutrality in PAni fibres during charging/discharging processes has been explained by the intercalation/ de-intercalation of the cations between fibre and electrolyte [40]. Figure 5.30 indicated that the incorporation of SWNTs in PAni-ES/AMPSA resulted in higher anodic potential (See potentials at A and B), while the cathodic potential was lightly increased (See potentials at A', B'). The higher anodic potential of the fibre containing SWNTs indicated that oxidation was made more difficult, likely due to the intermolecular attraction of large  $\pi$  bonded surface of SWNTs and EMI cation. The much higher current signal observed for the PAni-ES/AMPSA/SWNTs fibre compared to the PAni-ES/AMPSA was likely due to the higher electrical conductivity of the former.



**Figure 5.30.** CV characterisation of fibres made of (a) PAni-ES/AMPSA/SWNT and (b) PAni-ES/AMPSA/SWNT (0.76 %w/w) in EMI.TFSI. potential cycled in range of ( $\pm 1.5$ ), scan rate 50 mV/s, under 10 mN Load. (L=10 mm, D=70  $\mu\text{m}$ )





**Scheme 5.2.** The mechanism of electrochemical switching of PAni-ES/AMPSA between ES-LEB oxidation states in EMI.TFSA.

The electrochemical stability of PAni-ES/AMPSA fibres with and without SWNT are compared over two different potential ranges namely  $\pm 1.5$  and  $\pm 2$  V (Figure 5.31). The PAni-ES/AMPSA fibre showed an anodic peak shifted to a higher potential when the potential scan range was widened. In contrast, for the PAni-ES/AMPSA/SWNTs fibre the anodic peak did not shift in potential while cathodic peak shifted to a lower potential. The greater stability of the PAni-ES/AMPSA/SWNTs fibre in terms of electrochemical signature with a widening of the potential range compared to the PAni-ES/AMPSA fibre illustrated an important advantage of SWNTs incorporation.

The high electrochemical reversibility of the PAni- AMPSA-SWNT fibre is illustrated in Figure 5.32 which shows its CV response over 30 cycles. No shift in peak potentials was observed after 30 successive cycles between  $\pm 2.0$  V.

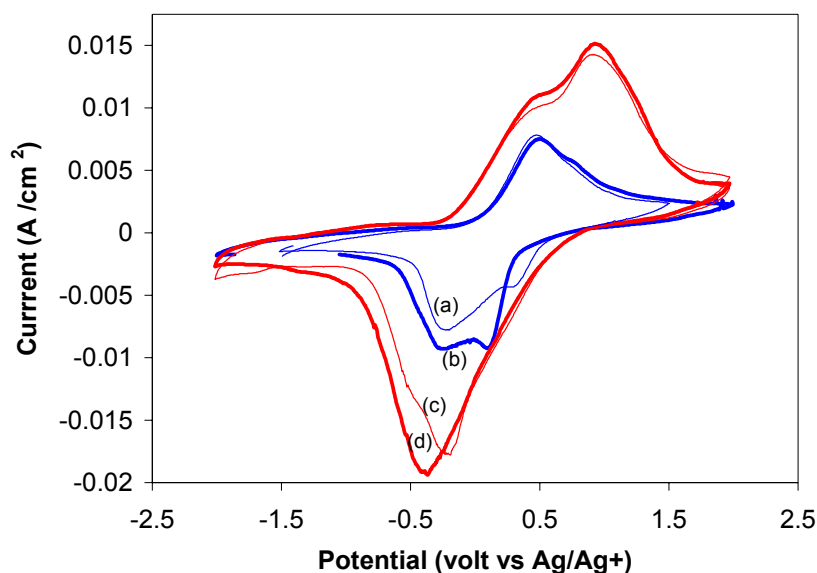


**Figure 5.31.** Comparison of the electrochemical stability of (a,b) PAni-ES/AMPSA and (c,d) PAni-ES/AMPSA/SWNT (0.76 % w/w) over potential ranges of (a,c)  $\pm 1.5$  and  $\pm 2$  V (b,d)

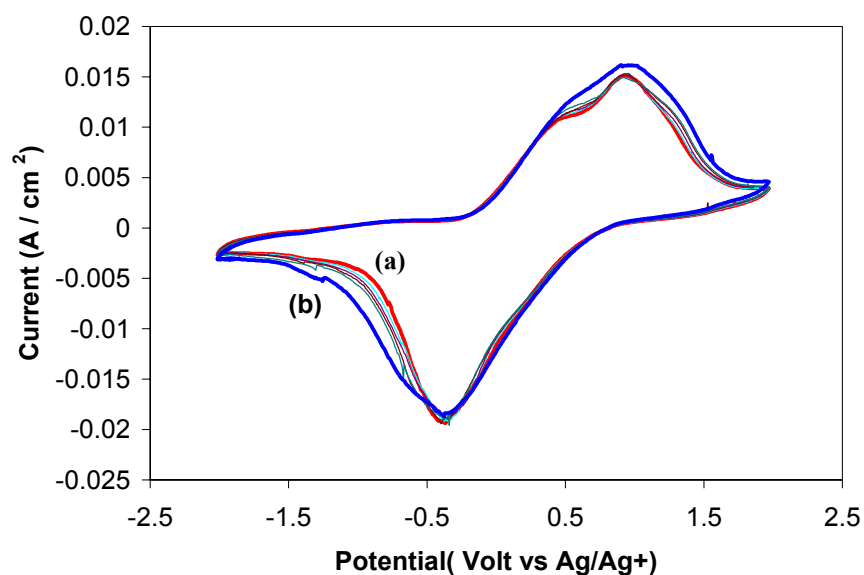


**Figure 5.32.** CV characterisation of the PAni-ES/AMPSA/SWNT fibre illustrating electrochemical stability over 30 successive cycles.(a) 1<sup>st</sup> cycle (b) 30<sup>th</sup> cycle scan rate 50 mV/s, under 10 mN Load. Potential cycled in range of ( $\pm 2.0$ ).

## 5.4 Conclusions

High strength, flexible and conductive PAni - SWNT composite fibres were produced in continuously spun fibres using wet spinning. PAni-ES/AMPSA-DCAA showed much better performance as a matrix for incorporation of SWNTs to form PAni-ES/AMPSA in PAni/SWNT composite fibres compared with PAni produced from the LEB oxidation state (refer Chapter 4). Superior conductivity, higher mechanical strength and sharper electrochemical redox peaks were achieved with the addition of SWNTs to the ES form of PAni. DCAA-AMPSA was shown to be a promising solvent for obtaining homogenous SWNTs dispersion. The addition of SWNTs changed the rheological behavior of the spinning solution from Newtonian to non-Newtonian fluid. This change could be related to the interconnection of SWNTs in suspension and adhesion of SWNTs to long PAni chain, which impede polymer chain mobility. The tensile strength and elastic modulus of PAni-ES/AMPSA fibres were increased by 50 % and 124 % respectively, upon the addition of 0.76% (w/w) nanotubes. In addition, the incorporation of SWNTs resulted in elongation at break decreased from 11% to 4% however fibres remained tough enough to be knotted. An electronic conductivity percolation threshold of 0.35 % w/w SWNTs was determined, and fibres showed electronic conductivities as high as  $750 \text{ Scm}^{-1}$ . The SWNTs also stabilise the conductivity of PAni fibres subjected to basic condition. Raman spectroscopy confirmed the presence of SWNTs in the PAni fibres and also the interaction of the quinoid ring with SWNTs to provide a doping effect. The results obtained from cyclic voltammetry of the fibres with and without SWNTs in aqueous solution and ionic liquid electrolytes reveals improved electrochemical stability with the incorporation of SWNTs. The high strength, robustness, high electrical

conductivity and good electroactivity make PAni-ES/AMPSA/SWNTs composite fibres potentially useful in many electronic textile applications. The evaluation of these fibres for artificial muscles, sensors, batteries and capacitors is investigated in Chapter 8.

## 5.5 References

- [1] A. P. Chacko, S. S. Hardaker and R. V. Gregory, Polymer Preprints. 37 (1996) 743-744.
- [2] A. P. Chacko, S. S. Hardaker and R. V. Gregory, Polymer Preprint. 38 (1997) 367-368.
- [3] R. V. Gregory ANTEC Conference Proceedings. 2 (1995) 1683-1687.
- [4] B. R. Mattes, H. L. Wang, D. Yang, Y. T. Zhou, W. R. Blumenthal and M. F. Hundeleys, Synth. Met. 84 (1997) 45-49.
- [5] B. R. Mattes, H.-L. Wang and D. Yang, ANTEC Conference Proceedings. 2 (1997) 1463-1467.
- [6] E. M. Scherr, A.G. MacDiarmid, S.K.Manohar, J.G.Masters, Y.Sun, X.Tang, M. A. Druy, P.J.Glatkowski, V. B. Cajipe, J. E. Fischer, K.R.Cromack, M. E. Jozefowicz, J. M. Ginder, R. P. McCall and A. J. Epstein, Synth. Met. 41-43 (1991) 735-738.
- [7] S. J. Pomfret, P. N. Adams, N. P. Comfort and A. P. Monkman, Adv. Mater. 10 (1998) 1351-1353.
- [8] Y. Cao, P. Smith and A. J. Heeger, Synth. Met. 48 (1992) 91-97.
- [9] E. R. Holland, S. Pomfret, P. N. Adams and A. P. Monkman, J Phys: Condens. Mater. 8 (1996) 2991-3003.
- [10] Y. Z. Wang, J. Joo, C. H. Hsu and A. J. Epstein, Synth. Met. 69 (1995) 267-268.
- [11] S. J. Pomfret, P. N. Adams, N. P. Comfort and A. P. Monkman, Polymer. 41 (2000) 2265-2269.
- [12] H. Matsumoto, H. Kageyama and Y. Miyazaki, Electrochemistry (Tokyo, Japan). 71 (2003) 1058-1060.

- [13] H. Randriamahazaka, C. Plesse, D. Teyssie and C. Chevrot, *Electrochimica Acta*. 50 (2005) 1515-1522.
- [14] C. Bower, A. Kleinhammes, Y. Wu and W. Zhou, *Chem. Phys. Lett.* 288 (1998) 481-486.
- [15] O. Matarredona, H. Rhoads, Z. Li, J. H. Harwell, L. Balzano and D. E. Resasco, *J. Phys. Chem. B*. 107 (2003) 13357-13367.
- [16] Y. Sabba and E. L. Thomas, *Macromolecules*. 37 (2004) 4815-4820.
- [17] M. F. Islam, E. Rojas, D. M. Bergey, A. T. Johnson and A. G. Yodh, *Nano. Lett.* 3 (2003) 269-273.
- [18] S. Badaire, P. Poulin, M. Maugey and C. Zakri, *Langmuir*. 20 (2004) 10367-10370.
- [19] J. N. Coleman, M. Cadek, R. Blake, V. Nicolosi, K. P. Ryan, C. Belton, A. Fonseca, J. B. Nagy, Y. K. Gun'ko and W. J. Blau, *Adv. Func. Mater.* 14 (2004) 791-798.
- [20] L. A. Hough, M. F. Islam, P. A. Janmey and A. G. Yodh, *Phys. Rev. Lett.* 93 (2004) 168102-168104.
- [21] W. Lu and B. R. Mattes, *J. Electrochem. Soc.* 150 (2003) E416-E422.
- [22] P. Potschke, T. D. Fornes and D. R. Paul, *Polymer*. 43 (2002) 3247-3255.
- [23] R. Wagener and T. J. G. Reisinger, *Polymer*. 44 (2003) 7513-7518.
- [24] F. Du, R. C. Scogna, W. Zhou, S. Brand, J. E. Fischer and K. I. Winey, *Macromolecules*. 37 (2004) 9048-9055.
- [25] A. P. Chacko, S. S. Hardaker, B. Huang and R. V. Gregory, *Mater. Res. Soc. Symp. Proc.* 413 (1996) 503-511.

- [26] P. M. Ajayan, O. Stephan, C. Colliex and D. Trauth, *Science*. 265 **(1994)** 1212-1214.
- [27] P. M. Ajayan, L. S. Schadler, C. Giannaris and A. Rubio, *Adv. Mater.* 12 **(2000)** 750-753.
- [28] J. Zhou, G. Tzamalís, N. A. Zaidi, N. P. Comfort and A. P. Monkman, *J. Appl. Polym. Sci.* 79 **(2001)** 2503-2508.
- [29] P. M. Kevin in *Dynamic Mechanical Analysis, "Time-Temperature scans: Transitions in polymers"*, CRC Press, Florida, **(1999)**, 96.
- [30] V. Bereshtein and V. Egorov, in *Physical chemistry of polymers, "Differential scanning calorimetry"*, Ellis Horwood, Chichester, UK, **(1993)**
- [31] T. V. Sreekumar, T. Liu, B. G. .Min, H. Guo, S. Kumar, R. H. Hauge and R. E. Smalley, *Adv. Mater.* 16 **(2004)** 58-61.
- [32] M. Baibarac, I. Baltog, S. Lefrant, J. Y. Mevellec and O. Chauvet, *Chem. Mater.* 15 **(2003)** 4149-4156.
- [33] J. E. Pereira da Silva, M. L. A. Temperini and S. I. Cordoba de Torresi, *Electrochimica Acta.* 44 **(1999)** 1887-1891.
- [34] J. E. Pereira da Silva, D. L. A. de Faria, S. I. Cordoba de Torresi and M. L. A. Temperini, *Macromolecules.* 33 **(2000)** 3077-3083.
- [35] V. Mottaghitalab, G. M. Spinks and G. G. Wallace, *Synth. Met.* 152 **(2005)** 77-80.
- [36] M. Cochet, W. K. Maser, A. M. Benito, M. A. Callejas, M. T. Martinez, J. M. Benoit, J. Schreiber and O. Chauvet, *Chem. Comm.* **(2001)** 1450-1451.
- [37] G. L. Louarn, M. Quillard, S. Pron, A. Buisson, J.P. and Lefrant, S., *J. Phys. Chem.* 100 **(1996)** 6998-7006.

- [38] W. Lu, I. D. Norris and B. R. Mattes, *Australian Journal of Chemistry*. 58 **(2005)** 263-269.
- [39] E. Smela and B. R. Mattes, *Synth. Met.* 151 **(2005)** 43–48.
- [40] W. Lu, A. G. Fadeev, B. Qi, E. Smela, B. R. Mattes, J. Ding, G. M. Spinks, J. Mazurkiewicz, D. Zhou, G. G. Wallace, D. R. MacFarlane, S. A. Forsyth and M. Forsyth, *Science*. 297 **(2002)** 983-987.
- [41] J. Golding, S. Forsyth, D. R. MacFarlane, M. Forsyth and G. B. Deacon, *Green Chemistry*. 4 **(2002)** 223-229.
- [42] A. Noda, K. Hayamizu and M. Watanabe, *J. Phys. Chem. B*. 105 **(2001)** 4603-4610.
- [43] H. L. Ngo, K. LeCompte, L. Hargens and A. B. McEwen, *Thermochimica Acta*. 357-358 **(2000)** 97-102.



# **CHAPTER SIX**

The Understanding of the Mechanism of  
Strength Increase in the PA<sub>ni</sub>-ES/AMPSA-  
SWNT Composite Fibre

### 6.1. Introduction

The efficient performance of SWNT filler in the composite is related to load transfer from the polymer matrix to homogeneously distributed and well oriented thin SWNT bundles. Moreover, the mechanical properties of the composite are influenced by the physical behavior of interface between the polymer matrix and SWNT bundles. Raman spectroscopy techniques are useful for understanding the orientation of nanotubes and the detection of load transfer to SWNTs in polymer composites. Unlike XRD methods, Raman spectroscopy can detect very low concentrations of SWNTs in a polymer matrix [1, 2]. The average orientation of aligned nanotubes can be estimated from the intensity of polarised Raman modes with respect to the direction of the excitation laser polarisation [3, 4]. Furthermore, the load transfer to the nanotubes within the composite can be detected from the shift in D\* band [5-7]. For example, thermal loading of a SWNT-epoxy composite gave a  $21\text{ cm}^{-1}$  shift per unit strain [8], while another study showed a  $2\text{ cm}^{-1}$  shift per unit strain for a SWNT- epoxy composite loaded in tension [5]. In addition, the band shift can be correlated to the change in bond length [7], which in turn is proportional to the overall tube deformation for SWNTs [9].

This study uses Raman techniques to investigate the origin of the reinforcing effect of SWNTs in a PANi matrix through evaluation of the degree of orientation of SWNTs, and clarifying of load transfer from PANi matrix to nanotube ropes. The orientation of SWNTs with respect to the fibre axis was investigated using polarised Raman spectroscopy with the analyzer parallel (VV) and perpendicular (VH) to the polariser. Intensities are correlated to orientation factors through the development of an orientation distribution

function. Finally the shift in the D\* band was determined when the fibre was stretched so as to evaluate the load transfer between PANi and SWNT reinforcement.

## **6.2. Experimental**

### **6.2.1. Materials**

The PANi-ES/AMPSA and PANi-ES/AMPSA-SWNT (0.76 % w/w) composite fibres (5x drawn and as-spun fibre) were prepared as described in chapter 5. They were subjected to orientation and load transfer tests.

### **6.2.2. Instrumentation**

Raman spectra were obtained with the JOBIN Yvon Horiba Raman spectrometer model HR800. The spectra were collected with a spectral resolution of  $1.5 \text{ cm}^{-1}$  in the backscattering mode, using the 632.8 nm line of a Helium/Neon laser. The nominal power of the laser, polarised 500:1, was 20 mW. A Gaussian/ Lorentzian-fitting function was used to obtain band position and intensity. The incident laser beam was focused onto the specimen surface through a  $100 \times$  objective lens, forming a laser spot of approximately  $1 \mu\text{m}$  in diameter, using a capture time of 50 s. The Raman signals was obtained with the half wave plate rotated at  $170^\circ$  with a confocal hole set at  $1100 \mu\text{m}$  and the slit set at  $300\mu$ . The orientation studies were performed when fibre was at  $0^\circ$ ,  $30^\circ$ ,  $45^\circ$ ,  $60^\circ$ ,  $75^\circ$  and  $90^\circ$  to the plane of polarisation of the incident laser. At each angle, the enhanced spectra at VV and VH configuration collected. In the VV configuration, the polarised laser and the analyzer are parallel to each other; and in the VH configuration, the polarised laser and the analyzer are perpendicular to each other.

For micro-Raman spectroscopy of composite fibres, a 10 mm fibre sample was fitted on the Raman stage and fixed at one end. The other end was attached to a movable clamp and micrometer mechanism allowing the fibre to be tensioned to a known strain. For each strain increment, the laser was focused and the Raman shift recorded around D\* band.

### 6.3. Results and discussion

#### 6.3.1. SWNTs orientation

The analysis of SWNTs orientation using polarised Raman spectroscopy was carried out based on a the coordination system defined in Fig 6.1. The fibre axis is defined as  $Z$  and SWNTs are oriented at angle  $\theta^\circ$  with respect to the  $Z$  axis. The fibre is mounted on the stage of the Raman microscope such that the incident laser comes in along the  $x'$  axis. The angle between the polarisation plane and the fibre axis is  $\psi$ .

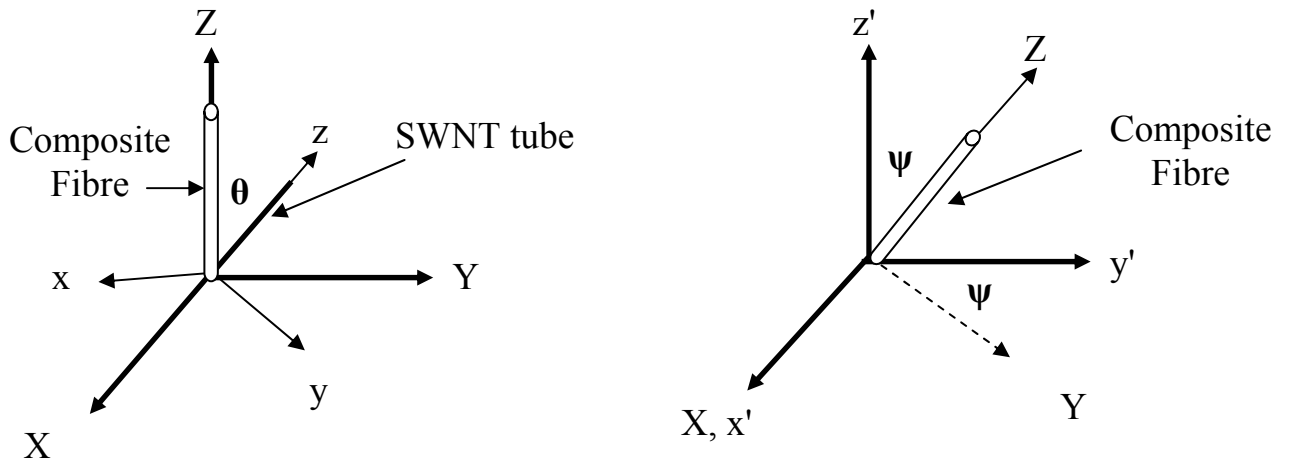


**Figure 6.1.** Demonstration of SWNTs coordination ( $xyz$ ) in PANi-ES/AMPSA-SWNTs composite fibre ( $XYZ$  coordinates) and the fibre arrangement in reference frame of the Raman sample stage ( $x'y'z'$  coordinates).

Figure 6.2 shows the Raman spectra of the neat PAni-ES/AMPSA and PAni-ES/AMPSA-SWNT (0.76 %w/w) fibres using VV and VH configuration for different amounts of  $\psi$ . For the neat PAni-ES/AMPSA (5x drawn) Raman spectra were obtained in two directions, parallel ( $\psi=0^\circ$ ) and vertical direction ( $\psi=90^\circ$ ) with respect to the polarisation plane (Figure 6.2-a). The origin of enhanced Raman peaks by SWNT and PAni and their composites were described in section 5.3.8.

According to literature SWNTs show high polarizability in all Raman modes, more specifically in G ( $1594\text{ cm}^{-1}$ ) and RBM (150-250) bands [10]. In contrast, smaller orientation dependence in Raman peaks was observed for neat PAni-ES/AMPSA.

A small increase in peak intensity of  $1592\text{ cm}^{-1}$  (the C-C stretching of benzoid ring[11]) was observed when the polarisation plane was parallel to the fiber axis ( $\psi=0^\circ$ ) compared with vertical configuration indicating some alignment of the PAni chain. Figure 6.2-c, however, demonstrates a much larger orientation effect in the 5x drawn fiber of PAni-ES/AMPSA-SWNT composite fiber (0.76 %w/w) at the same frequency band which is associated with G band (tangential mode: TM) of SWNT ropes. Compared to Peak enhanced in  $1169\text{ cm}^{-1}$  (C-H stretching of benzoid ring) with constant intensity in different polarisation angle, the intensity at  $1594\text{ cm}^{-1}$  monotonically decreases with increasing of  $\psi$ , which is in good agreement with previous studies that showed similar behavior for SWNT as fibre or isolated tube [8, 12-14]. Other peaks that enhanced between  $1594\text{ cm}^{-1}$  and  $1169\text{ cm}^{-1}$  did not decreased significantly, except the peak enhanced at  $1381\text{ cm}^{-1}$  and  $1654\text{ cm}^{-1}$ . It is worth noting that similar trend in peak intensity observed for neat PAni-ES/AMPSA at  $1381\text{ cm}^{-1}$  and  $1645\text{ cm}^{-1}$  (Fig 6.2-a). They can be attributed to moderate orientation dependence of mentioned peaks.

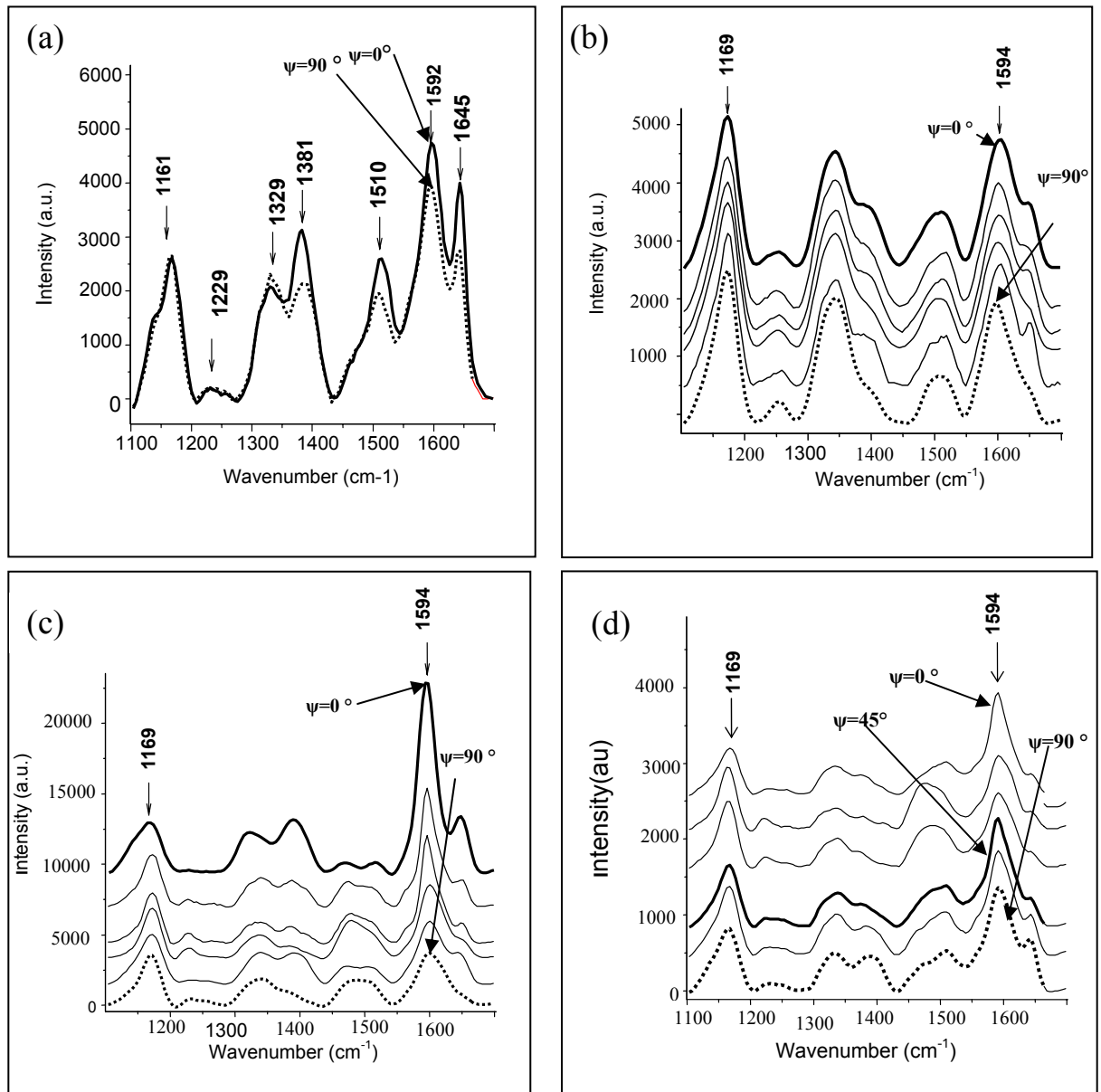


**Figure 6.2.** The Raman spectra under VV and VH configuration,  $\psi$  = the angle between fibre axis and polarisation plane (a) PANi-ES/AMPSA fibre (5x drawn fibre) for  $\psi = 0^\circ$  and  $90^\circ$ . VV configuration (b) PANi-ES/AMPSA-SWNT (0.76 % w/w) composite fibre (as spun) VV configuration (c) PANi-ES/AMPSA-SWNT (0.76 % w/w) composite fibre (5x drawn) VV configuration. (d) PANi-ES/AMPSA-SWNT (0.76 % w/w) composite fibre (5x) VH configuration. From top to bottom, the angle between fibre axis and polarisation plane is  $0^\circ$ ,  $30^\circ$ ,  $45^\circ$ ,  $60^\circ$ ,  $75^\circ$  and  $90^\circ$ .

The intensity ratio of  $I_{vv}(90^\circ)/I_{vv}(0^\circ)$  at  $1592\text{ cm}^{-1}$  (around G band) for neat PANi-ES/AMPSA fibre (5x drawn) is 0.85. However, this ratio shows a significant decrease to 0.19 after addition of SWNTs in the 5x drawn fibre. This difference shows the much lower sensitivity of the polarised Raman scattering intensity versus  $\psi$  for neat PANi-ES/AMPSA compared with composite fibre containing SWNTs.

In addition, Raman spectra show a much stronger orientation effect in the 5x drawn composite fibres compared with the as spun composite fibres (Figure 6.2-b and c). For the as spun fibres, the change in intensity of the peak at  $1592\text{ cm}^{-1}$  was insignificant with respect to  $\psi$  from the parallel to the perpendicular direction. It is clear that the drawing process is mostly responsible for the alignment of SWNTs in the fibre direction. Therefore, as expected, the low orientation dependence of Raman modes was observed in as spun fibres.

When the composite fibres were examined using the VH configuration, the intensity dependence on  $\psi$  showed a different trend for TM (Figure 6.2.d). The intensity increases with increasing  $\psi$  and goes through a maximum at  $45^\circ$  and then decrease symmetrically up to  $90^\circ$ . However the observed intensity ratios between maximum ( $45^\circ$ ) and minimum ( $0^\circ$  or  $90^\circ$ ) are quite small compared with the ratio of peak intensities in VV configuration.

The interference of the C-C peak of PANi and the G band may show a small effect on the analysis of the intensity of the G band for measurement of the degree of orientation of SWNTs and the distribution function.

Figure 6.3 demonstrates the intensity of RBM band in VV and VH configuration under different angle regards to polarisation plane. Compared to the TM band, lower RBM band intensity ratio was observed for  $I_{vv}(90)/I_{vv}(0)$  at  $224\text{ cm}^{-1}$  due to absence of polarised

peak of PANi in this region. Similar behavior was also observed for RBM band in VH configuration. The intensity increases with increasing  $\psi$  and reach to a maximum value at  $45^\circ$  and then decrease dramatically at  $90^\circ$ .

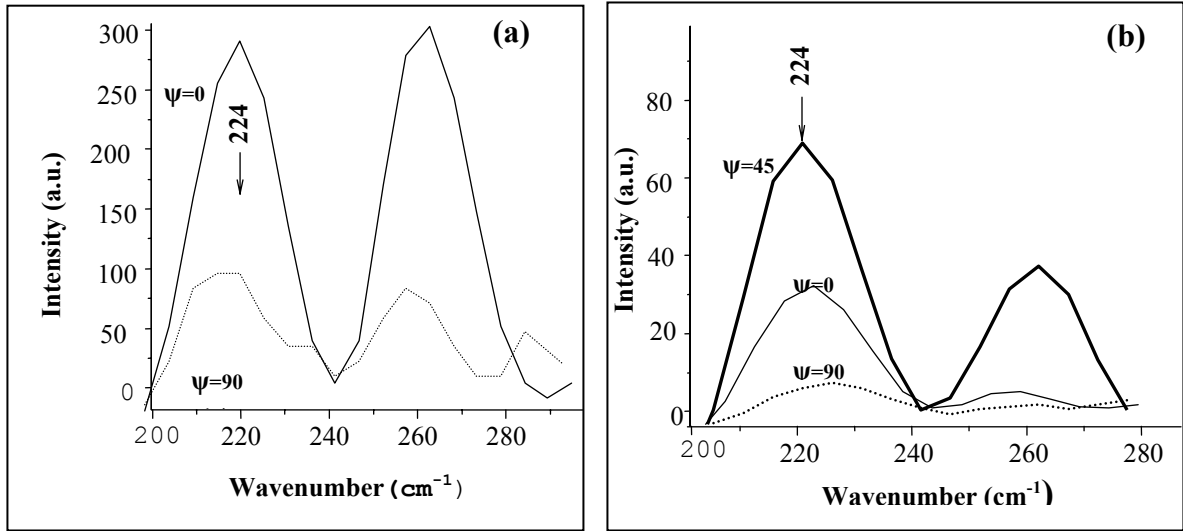


**Figure 6.3.** The Raman spectra under VV and VH configuration for RBM band,  $\psi$  is the angle between fibre axis and polarisation plane (a) PANi-ES/AMPSA fibre (5x drawn fibre) for  $\psi=0^\circ$  and  $90^\circ$ . VV configuration (b) PANi-ES/AMPSA-SWNT (0.76 % w/w) composite fibre (5x) VH configuration.

The intensity ratio data ( $I_{VV}(\psi^\circ)/I_{VV}(0^\circ)$ ) versus  $\psi$  represented in Figure 6.4, for TM and RBM bands. A small difference in intensity ratio at each  $\psi$  was observed for the TM and RBM bands in the PANi-ES/AMPSA-SWNT fibres. However, a comparison of data of TM and RBM intensity ratios extracted from references [10] and [15] for SWNT fibres exhibit a similar discrepancy. It can therefore, be assumed that the interference between the PANi C-C peak and the G band has little effect on the intensity ratio.



**Figure 6.4.** The comparison of  $I_{vv}(\psi^o)/I_{vv} 0^\circ$  versus  $\psi$  in tangential mode (TM) and resonance breathing mode (RBM) modes for this work and references [10, 15]

It can be seen from Figure 6.4 that the intensity ratio obtained in the present work closely follows the data from the published literature [10, 15]. The previous literature reported results from SWNT fibres containing a small amount of polymer (<40%). Qualitatively, the results shown in Figure 6.4 suggest that the degree of alignment achieved in the PAni-ES/AMPSA-SWNT fibres of the present study is similar to that reached in the SWNT fibres reported previously. In next following part, the polarised Raman scattering intensity will be correlated to the angle between the nanotube axis and the fibre axis ( $\theta$ ) and the angle between the fibre axis and the polarisation plane( $\psi$ ) [8]. The variation in polarised Raman band intensity can, therefore, be used to quantitatively

study the orientation of nanotube bundle along the composite fibre axis [13]. A simplified uniaxial model was used for quantitative evaluation of orientation distribution function (ODF) based on the formulation of Liu and his coworkers [8]. The mathematic formulation of Raman intensity in VV and VH modes are represented by the following expressions:

$$I^{VV}(\psi)\alpha\left(\cos^4\psi - \frac{6}{7}\cos^2\psi + \frac{3}{35}\right)\langle P_4(\cos\theta)\rangle + \left(\frac{6}{7}\cos^2\psi - \frac{2}{7}\right)\langle P_2(\cos\theta)\rangle + \frac{1}{5}$$

**Equation 6.1**

$$I^{VH}(\psi)\alpha\left(-\cos^4\psi + \cos^2\psi - \frac{4}{35}\right)\langle P_4(\cos\theta)\rangle + \frac{1}{21}\langle P_2(\cos\theta)\rangle + \frac{1}{15}$$

**Equation 6.2**

The orientation order parameters of  $\langle P_2(\cos\theta)\rangle$  and  $\langle P_4(\cos\theta)\rangle$  which are, respectively, the average values of  $P_2(\cos\theta)$  and  $P_4(\cos\theta)$  for the SWNTs bulk product. The  $P_i(\cos\theta)$  is the Legendre polynomial of degree  $i$  which is defined as  $P_2(\cos\theta) = (3\cos^2\theta - 1)/2$  and  $P_4(\cos\theta) = (35\cos^4\theta - 30\cos^2\theta + 3)/8$  for the second and fourth degree, respectively.

More specifically the  $\langle P_2(\cos\theta)\rangle$  is known as the Herman's orientation factor (**f**) which varies between values of 1 and 0 corresponding, respectively, to nanotubes fully oriented in the fibre direction and randomly distributed.

$$f = \frac{3 \langle \cos^2 \theta \rangle - 1}{2} \quad \text{Equation 6.3}$$

The orientation factors can be determined by solving of following simultaneous algebraic equations given in 6.4 and 6.5. These equations are obtained from equations 6.1 and 6.2 by dividing of both side of these equations and substitution of angles of 0 and 90 degrees for  $\psi$ .

$$\frac{I_{G,RBM}^{VV}(\psi = 0)}{I_{G,RBM}^{VH}(\psi = 0)} = -\frac{24 \langle P_4(\cos \theta) \rangle + 60 \langle P_2(\cos \theta) \rangle + 21}{12 \langle P_4(\cos \theta) \rangle - 5 \langle P_2(\cos \theta) \rangle - 7} \quad \text{Equation 6.4}$$

$$\frac{I_{G,RBM}^{VV}(\psi = 90)}{I_{G,RBM}^{VH}(\psi = 0)} = \frac{-9 \langle P_4(\cos \theta) \rangle + 30 \langle P_2(\cos \theta) \rangle - 21}{12 \langle P_4(\cos \theta) \rangle - 5 \langle P_2(\cos \theta) \rangle - 7} \quad \text{Equation 6.5}$$

The left hand side terms of equations of 6.4 and 6.5 are the depolarisation ratios that can be experimentally determined. As it can be seen only the intensity at 0° and 90 ° are required to determine the  $\langle P_2(\cos \theta) \rangle$  and  $\langle P_4(\cos \theta) \rangle$  for a uniaxially oriented SWNTs in the PANi matrix. The numerical amount of orientation order parameters are given in Table 6.1 for as spun and 5x drawn fibres based on both TM and RBM intensity ratios.

A complete orientation distribution function (ODF) can be formed as given in equation 6.6 from information of  $\langle P_2(\cos \theta) \rangle$  and  $\langle P_4(\cos \theta) \rangle$  [16]:

$$f(\theta) = A \exp \left[ - \left( \lambda_2 P_2(\cos \theta) \right) + \lambda_4 P_4(\cos \theta) \right] \quad \text{Equation 6.6}$$

The coefficients of  $A$ ,  $\lambda_2$  and  $\lambda_4$  are determined by solving of following simultaneous equations:

$$\int_{\theta=0}^{\theta=\pi} f(\theta) \sin \theta d\theta = \frac{1}{4\pi^2} \quad \text{Equation 6.7}$$

$$\int_{\theta=0}^{\theta=\pi} P_2(\cos(\theta)) f(\theta) \sin \theta d\theta = \frac{\langle P_2 \cos(\theta) \rangle}{4\pi^2} \quad \text{Equation 6.8}$$

$$\int_{\theta=0}^{\theta=\pi} P_4(\cos(\theta)) f(\theta) \sin \theta d\theta = \frac{\langle P_4 \cos(\theta) \rangle}{4\pi^2} \quad \text{Equation 6.9}$$

The presented simultaneous equations were simplified to three polynomial equations using the Legendre polynomial multiplication rules and Taylor's expansion for  $\exp[x]$  [17]. The polynomial equations were solved simultaneously using Mathcad for three unknown parameters of  $A$ ,  $\lambda_2$  and  $\lambda_4$  by knowing the amount of  $\langle P_2(\cos\theta) \rangle$  and  $\langle P_4(\cos\theta) \rangle$ . The orientation distribution coefficients for as spun and 5x drawn fibres of PAni-ES/AMPSA-SWNT(0.76 %w/w) (results listed in Table 6.1). Based on these coefficients, the ODF of PAni-ES/AMPSA-SWNT composite fibre before and after stretching were plotted for a range of angles between nanotubes and the fibre axis (Figure 6.5).

**Table 6.1.** The polarised Raman scattering intensity ratio of TM and RBM bands in VV configuration ( $\theta=0^\circ, 90^\circ$ ) versus VH configuration at  $\theta=0^\circ$  for as-spun and 5x drawn fibres of PAni-Es/AMPSA-SWNT (0.76 % w/w). Orientation order parameters are listed for construction of orientation distribution function.

	$\psi$ /peak	$I_{VV}(\psi)/I_{VH}(0)$	
		TM	RBM
<b>5x drawn</b>	<b>0</b>	10.5	9
	<b>90</b>	2.5	2
	$\langle P_2(\cos\theta) \rangle$	0.42	0.4
	$\langle P_4(\cos\theta) \rangle$	0.32	0.27
	<b>A</b>	0.0042	0.0044
	$\lambda_2$	-1.223	-1.483
	$\lambda_4$	-3.496	-2.747
<b>As spun fibre</b>	<b>0</b>	3.2	NA
	<b>90</b>	2.9	
	$\langle P_2(\cos\theta) \rangle$	0.022	NA
	$\langle P_4(\cos\theta) \rangle$	0.006	NA
	<b>A</b>	0.0063	NA
	$\lambda_2$	-0.206	NA
	$\lambda_4$	-0.135	NA

It can be seen that in the 5x drawn fibre of PAni-ES/AMPSA-SWNT, the most of nanotubes were oriented between  $-30^\circ$  and  $+30^\circ$  and only small portion of them lies

between 30° and 150°. However, in the as spun fibre, the majority of SWNTs shows a distribution between 60° and 120 and a small portion oriented between -60° and +60°. For simplification, the data has been normalised to the numerical amount of ODF at  $\theta=0^\circ$ .

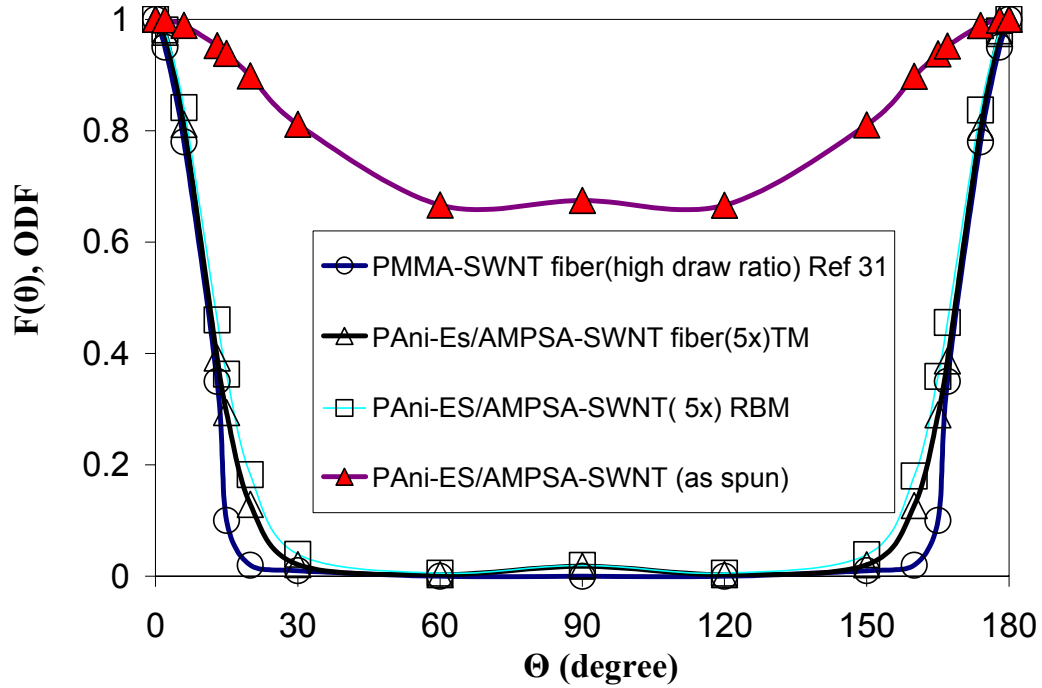


**Figure 6.5.** The orientation distribution function of SWNT in PAni-ES/AMPSA-SWNT (0.76 %w/w) composite fibres constructed with the orientation parameters,  $\langle P_2(\cos\theta) \rangle$  and  $\langle P_4\cos(\theta) \rangle$  listed in Table 6.1

The ODF of highly stretched fibre of PMMA/SWNT reported in the literature [8] was compared with PAni-ES/AMPSA-SWNT fibre in Figure 6.5. The previously reported results show that the majority of SWNTs were oriented with an angle of less than 30° respect to the fibre axis. In addition the ODF function for PAni-Es/AMPSA-SWNT fiber

compared to PMMA-SWNT shows a similar mirror symmetry. Therefore fiber sample is symmetric with respect to the plane perpendicular to the fibre axis.

The similar order of orientation of PAni-ES/AMPSA-SWNT (5X drawn) fibre and the highly oriented fibre of PMMA-SWNT suggests a similar adhesion for PAni matrix to SWNT bundles compared with PMMA-SWNT composite. The strong adhesion may result in simultaneous orientation of SWNT and matrix during the thermal stretching process.

The quantitative comparison also shows a good agreement between the SWNT orientation in SWNT fibre produced previously [12] and the PAni-ES/AMPSA-SWNT fibres produced in the present study. Poulin and coworkers [12] have shown that the 50% of nanotubes were oriented between  $0^\circ$  and  $50^\circ$  and 75% of SWNT lies between  $0^\circ$  and  $70^\circ$  for SWNT fibre developed by Vigolo [15]. These wet spun fibres contained more than 60 % SWNT in a PVA matrix. Moreover, Gommans, et.al [14] developed SWNT fibre in another study and reported that 86% of the nanotubes lies within  $\pm 31^\circ$  of the fibre axis.

Based on the knowledge of the orientation of SWNT in the PAni, it is possible to predict the elastic modulus of the composite fibre based on the fibre composite theory[18]. One approach that has been successfully applied to composite with a high loading of SWNT (>60%) has highlighted the importance of shear modulus of the nanotube bundles [8] and therefore nanotube bundle diameter, as well as nanotube orientation.

However, the influence of the matrix has been ignored and the elastic modulus of composite was assumed to be due only to the nanotubes. The composites described in the present study have less than 1% CNTs, so it is not appropriate to ignore the effect of the matrix on the composite modulus.

The Krenchel's rule of mixtures can be used to estimate the elastic modulus of composite fibres based on the known elastic modulus and volume fraction of matrix and nanotubes and by assuming perfect orientation of the nanotubes in the fibre direction. From the previous discussion, it is known that the SWNTs are not fully aligned in the fibre direction so it is expected that the rule of mixtures would slightly over-estimate the composite modulus. Table 6.2 shows the predicted elastic modulus for PAni-ES/AMPSA-SWNT composite containing 0.76 wt % SWNTs. In this simple analysis using a value of 640 GPa for the elastic modulus of fully oriented nanotubes, the elastic modulus of composite was calculated as 8.6 GPa, which is slightly higher than the experimental value of 7.3 GPa.

**Table 6.2.** The comparison of predicted elastic modulus from rule of mixture and experimental value

	<b>PAni-ES/AMPSA-SWNT (0.76 %w/w)</b>
$v_{\text{SWNT}}^{[i]}$	0.008
$E_c[\text{GPa}](E_{\text{eff SWNT}}=640 \text{ GPa})$	8.6 <sup>ii</sup>
$E_{\text{exp}}[\text{GPa}]$	7.3

However, as can be seen from Fig 6.4 the nanotubes ropes were not fully aligned, therefore we expect a lower effective modulus. The rule of mixtures predicts an effective modulus of 520 GPa for the SWNTs based on the measured composite modulus. This

<sup>i</sup> Volume fraction of SWNTs calculated based on density of 1.4 g/cm<sup>3</sup> for PAni and 1.3 g/cm<sup>3</sup> for SWNT

<sup>ii</sup> calculated from mixing rule for fully aligned CNT



value is 81% of the modulus expected for fully aligned SWNTs. These results confirm a high degree of alignment of the SWNTs in the PANi matrix.

### 6.3.2. Load transfer Mechanism

When a strain is applied to a material, the interatomic distances change, and thus the vibrational frequencies of some of the normal modes change, causing a Raman peak shift [5, 6]. Amongst specific enhanced peaks in SWNTs, the D\* band is more sensitive to applied strain. Figure 6.6 shows a typical Raman peak shift in tension for two extreme strains (i.e. 0 % and 3%). The frequency peak number were identified by a Gaussian /Lorentzian function. It can be clearly seen that approximately a 5 cm<sup>-1</sup> shift was occurred after applying 3 % strain.

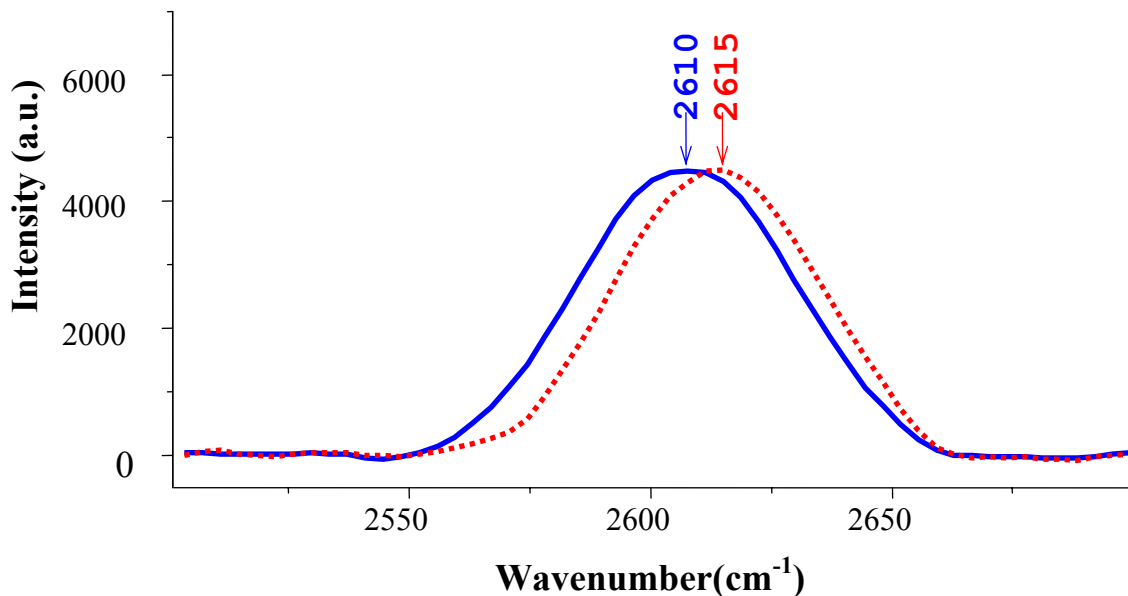


**Figure 6.6.** Effect of mechanical strain on the frequency shift of D\* band of SWNTs incorporated in PANi-Es/AMPSA matrix. (dashed line) before applying strain (solid line) after applying 3 % strain

The reproducibility of data was examined by several tests carried out in same experimental condition. Figure 6.6 shows the results of Raman peak shift in tension for PANi fibre containing 0.76% SWNTs as a function of applied strain for three sample.

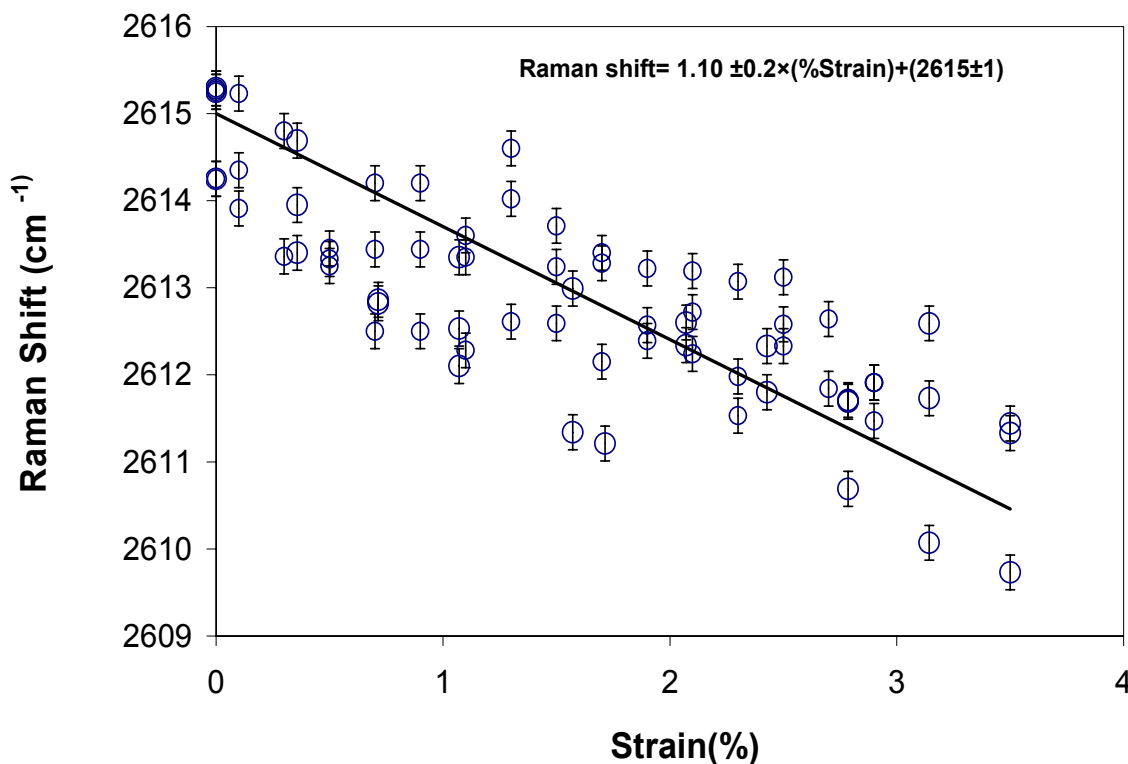


**Figure 6.7.** The Raman shift of D\* peak of nanotube under axial tension for two sample of SWNT (0.76 %w/w) in the PANi.

The shift in the Raman peak position with strain in tension is negative about 90-130 wave numbers/ applied strain. Under increasing tension, the Raman wave number decreases linearly down to about 2610 cm<sup>-1</sup> (corresponding to a strain of about 3.5%).

As can be seen at the same strain some points show a higher Raman shift than other points. Wood and coworkers [2] were able to show that samples with transversely aligned SWNTs had a lower Raman shift compared with the sample having longitudinal

orientation of SWNTs. As a consequence, more load is transferred in case of longitudinal orientation. Therefore, the observed difference in Raman shift reflects the different level of load transfer to SWNT in the composite which aligned within  $\pm 30^\circ$  of the fibre axis.

In the elastic regime, the spectroscopic stress- strain curve can be developed using the slope of the curve ( $m_1$ ) of Raman shift versus strain and numerical amount of Raman shift:

$$\sigma = \left( \frac{\text{Raman shift}}{m_1} \right) E_m \quad \text{Equation 6.10}$$

Where  $E_m$  is the Elastic modulus of the composite fibre containing 0.76 wt % SWNT (7.3 GPa). In Figure 6.8 the stress- strain from a mechanical test has been compared with the spectroscopic stress-strain data calculated from equation 6.10.

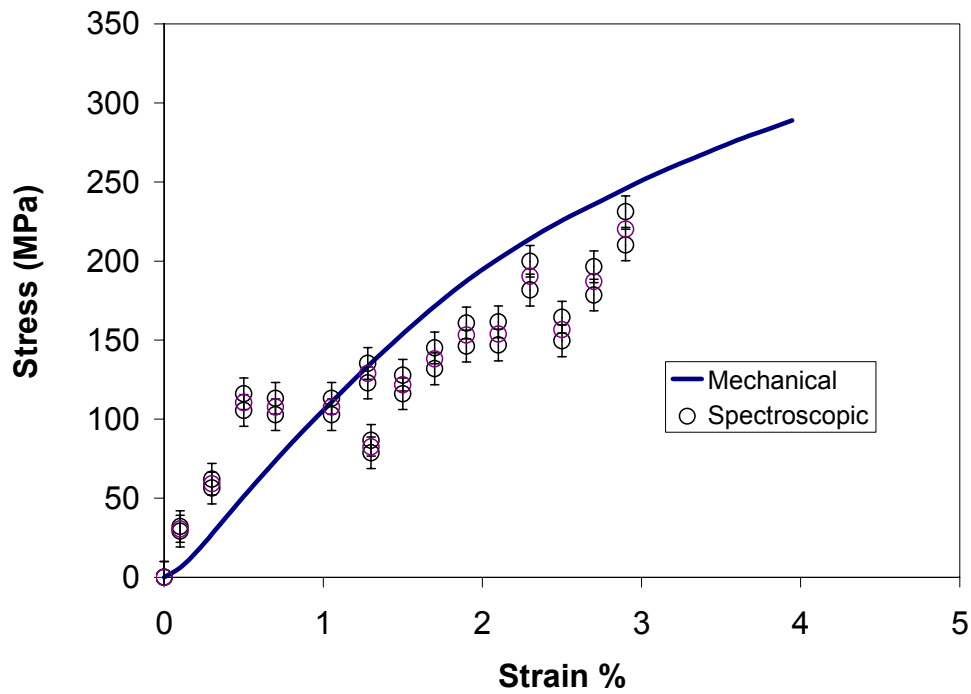


**Figure 6.8**-Mechanical versus spectroscopic stress – strain curve

The spectroscopic stress- stress data based on the average amount of Raman shift in any specified strain fits well with the results of mechanical stress– strain test. This suggests a good adhesion between PANi matrix and SWNTs which results in a strong nanotube-polymer interface.

Two possibilities can be considered for the nature of interaction between PANi and SWNTs. The formation of crystalline coating around bundles of nanotubes which is quite strong and restricts deformation. Another possibility offers a non-crystalline covalent bond between nanotubes and PANi.

The DSC results presented in section 5.3.6 showed that introducing of nanotube do not appreciably increase the melting peak of the composite and it is likely attributed to formation of a noncrystalline morphology for interfacial layer between PANi and SWNT .

## **6.4. Conclusion**

In summary it has been shown that the Raman spectroscopy can be employed as a powerful technique for characterisation of the mechanical behavior of PANi–SWNT composite. The intensity of G band and RBM band significantly increase by decreasing of angle between fibre axis and polarisation plane in VV configuration of polariser and analyzer. This functionality was correlated to the orientation of nanotubes through measurement of average angle between nanotubes and fibre axis. It has been found that thermal stretching of as spun fibre orients more than 80% of nanotubes in a range of about 30° versus fibre axis. Moreover, the Herman's orientation factor increased from 0.02 to 0.43 respectively, for as spun and 5x drawn fibre. Micro Raman spectroscopy has been

used to show the load transfer from matrix to nanotubes. A significant shift between 90-130  $\text{cm}^{-1}$ /strain in D\* band has been observed. The comparison of mechanical and spectroscopic results elucidates the mechanism of load transfer from bulk polymer to interfacial area and nanotubes. It was proposed the small discrepancy between the observed value of the elastic modulus and the predicted amount by rule of mixtures originated from imperfect adhesion between the nanotubes and the polymer and /or through non complete alignment of the nanotubes.

**6.5. References**

- [1] J. R. Wood, M. D. Frogley, E. R. Meurs, A. D. Prins, T. Peijs, D. J. Dunstan and H. D. Wagner, *J.Phys. Chem. B.* 103 **(1999)** 388-392.
- [2] J. R. Wood, Q. Zhao and H. D. Wagner, *Composites - Part A: Appl.Sci & Manufac.* 32 **(2001)** 391-399.
- [3] A. Launois, B. Marucci, P. Vigolo, A. D. Bernier, P. Poulin and J. Nanoscience Nanotech. 1, *J. Nanosci. Nanotech.* 1 **(2001)** 125.
- [4] P. Poulin, B. Vigolo and P. Launois, *Carbon.* 40 **(2002)** 1741-1749.
- [5] P. M. Ajayan, L. S. Schadler, C. Giannaris and A. Rubio, *Adv. Mater.* 12 (2000) 750-753.
- [6] J. Gou, S. Jiang, B. Minaie, K.-T. Hsiao, Z. Liang, C. Zhang and B. Wang, *International SAMPE Technical Conference.* **(2004)** 2287-2298.
- [7] O. Lourie and H. D. Wagner, *J. Mater. Res.* 13 **(1998)** 2418-2422.
- [8] T. Liu and S. Kumar, *Chem.Phys.Lett.* 378 **(2003)** 257-262.
- [9] O. Lourie, H. D. Wagner, Y. Zhang and S. Iijima, *Adv. Mater.* 11 **(1999)** 931-933.
- [10] G. S. Duesberg, I. Loa, M. Burghard, K. Syassen and S. Roth, *Phys. Rev.Lett.* 85 **(2000)** 5436-5439.
- [11] V. Mottaghitalab, G. M. Spinks and G. G. Wallace, *Synth. Met.* 152 **(2005)** 77-80.
- [12] E. Anglaret, A. Righi, J. L. Sauvajol, P. Bernier, B. Vigolo and P. Poulin, *Physica B: Condensed Matter.* 323 **(2002)** 38-43.
- [13] A. R. Bhattacharyya, T. Liu, S. Kumar, L. M. Ericson, R. H. Hauge, R. E. Smalley and T. V. Sreekumar, *Polymer.* 44 **(2003)** 2373-2377.
- [14] H. H. Gommans, J. W. Alldredge, H. Tashiro, J. Park, J. Magnuson and A. G. Rinzler, *J. Appl. Phys.* 88 **(2000)** 2509-2514.
- [15] B. Vigolo, P. Poulin, M. Lucas, P. Launois and P. Bernier, *Appl. Phys.Lett.* 81 **(2002)** 1210-1212.
- [16] M. v. Gorp, *colloid .Polym.Sci.* 273 **(1995)** 607.
- [17] M. L. Abell and J. P. Braselton, *The Mathematica handbook*, Acedemic press, Boston, **(1992)** .

- [18] I. M. Ward and D. W. Hadley, in *An Introduction to the mechanical Properties of Solid Polymers*", John Wiley & Sons: New York, New York, **(1995)**, 300.

# **CHAPTER SEVEN**

Charge Transport Regime in the PAni-  
ES/AMPSA/SWNTs Composite Fibre  
System



## 7.1. Introduction

The transport regime and magnitude of conductivity in doped  $\pi$ -conjugated polymers is determined by the degree of structural disorder. In general, as the disorder increases, more localisation is induced and the material becomes more insulating upon decreasing the temperature [1]. It has been widely shown [2-6] that the measurement of macroscopic (DC) electrical conductivity over a wide range of temperatures can provide a comprehensive insight into nanoscale polymer morphology and the extent of disorder.

Several studies have indicated that the PANi-ES/AMPSA [7-10] cast from DCAA is in the metallic regime toward the insulator-metal transition. The metallic behavior was attributed to the criterion of finite conductivity when  $T \rightarrow 0$  K, the positive slope of the temperature dependent reduced activation energy (i.e:  $W(T) = d[\log \sigma(T)]/d[\log(T)]$ ), and delocalised electronic states at the Fermi level that allow conduction without thermal activation. However, this polymer does not show metallic behavior over the whole range of temperatures. They exhibit semiconducting ( $d\sigma/dT > 0$ ) and metal-like behaviours ( $d\sigma/dT < 0$ ) respectively at temperatures lower and higher than room temperature.

The linear metallic and a crossover to nonmetallic behaviours at lower temperature has also been observed in the temperature dependence resistivity of ropes and mats of single walled carbon nanotubes [11, 12].

It has been already shown that either quasi-one-dimensional variable range hopping (quasi-1D VRH) or 3-dimensional VRH models [1, 13] do not apply across the entire temperature range studied, showing both metallic and non metallic regime (5 K -340 K)[10]. This complex temperature dependence in both PANi-ES/AMPSA and SWNTs suggest that the heterogeneous model proposed by Kaiser [2] may be suitable for the

quantitative determination of electronic transport parameters in both the metallic islands with highly ordered domain and the disordered amorphous regions. As emphasized in the literature the electrical transport occurs through metallic islands of oriented crystalline polymer chains (subscript c) that are interconnected by amorphous regions [14-16]. By taking into account that metallic-semiconducting transitions may occur in the amorphous region with both non metallic (subscript n) and metallic disorder (subscript d), the heterogeneous transport model assumes that the metallic and amorphous regions act as resistors in series. A simplified view of the oriented polymer microstructure is shown in Fig 7.1

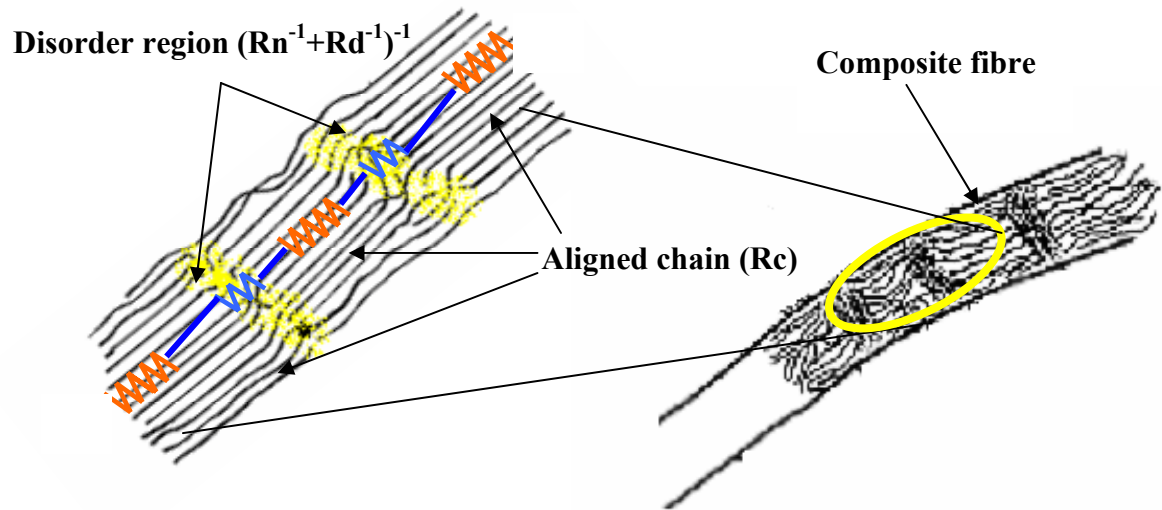


**Figure 7.1.** Crystalline regions separated by disordered regions constitutes the heterogeneous morphology in composite fibre

The resistivity of the composite, therefore, is determined by the contribution of metallic (crystalline) and non metallic (amorphous) resistivity. The role of each portion in the determination of DC conductivity is described by temperature functions which identify the contribution of each part in the total electrical transport mechanism. The metallic part is

described by the quasi VRH one dimensional exponential model [2, 17, 18] and an expression describing the amorphous part of the resistivity which is based on the fluctuation-induced tunneling between metallic islands [3].

The measurement of electrical transport over a very broad range of temperatures from 5 K to 340 K has been carried out. This data has been used to understand the influence of carbon nanotubes addition on morphological disorder and the metallic properties of a PAni-ES/AMPSA fibre through extraction of conductivity data, such as reduced activation energy, and by fitting of the obtained data to a range of functions integrated into the heterogeneous model.

## **7.2. Experimental**

### **7.2.1. Material**

The 5X drawn fibres of PAni-ES/AMPSA( described in chapter 5) containing different amount of SWNTs (0.00 %w/w, 0.25 % w/w, 0.76 %w/w) were dried at 50 °C for 24 hr in vacuum. High purity silver paint (SPI) for connecting metallic wires to fibre samples, cigarette paper as an electrical insulating substrate and a specific type of varnish (known as “G” varnish) have been used for preparation of sample for transport measurement.

### **7.2.2. Sample preparation**

The sample holder equipped with 12 ports was designed for 3 samples to measure resistance through the 4 point probe method. It should be completely cleaned using acetone to remove all particles left from previous experiments. Then a piece of cigarette paper which can properly conduct thermal energy is attached to surface using “G” varnish which is thermally conductive and electrically non-conductive. Next, a 1 cm length of 3

fibre samples having different nanotube content was located on the paper and fixed using silver paste. A small needle was used to apply a very small amount of silver paste on each junction. The four point probe apparatus is designed in each port to pass current from the outer connections and to measure the voltage from the inner connections. The distance between inner points should be as far apart as possible (0.5-0.7 cm). Four wires contact from each channel were connected to the four measurement points using silver paste. One hour vacuum drying at 50 °C is required to ensure that the silver paste was fully dried. Finally “G” varnish is used to completely connect the fibre to the surface of the sample holder for efficient heat transfer.

### **7.2.3. Instrumentation**

The physical characterisation equipment of PPMS (Physical Properties Measurement System, Oxford, UK) were used in the range of temperature of 5 °K to 340 °K. The sequence was defined for the experiment based on increasing or decreasing of temperature using the lowest possible scan rate. In this experiment the temperature starts at 300 K and then goes up to 340 K and back to 5 K using a scan rate 3 K/min.

The data fitting module of MATLAB was used for experimental data fitting on proposed models.

## **7.3. Results and discussion**

### **7.3.1. Electrical transport Analysis**

Conductivity ( $\sigma$ ) versus temperature (T) plots for neat PANi-ES/AMPSA fibre and fibres containing 0.25 and 0.76 % w/w SWNT (5X thermally stretched) were illustrated in

Figure 7.2 . The conductivity parameters for these different samples were also listed in Table 7.1. For all samples a strong dependence of conductivity and temperature can be seen over the whole temperature range investigated. At higher temperatures, a turnover temperature ( $260\text{ K} < T_{\sigma_{\max}} < 320\text{ K}$ ) corresponding to the temperature of maximum conductivity and a change in slope of the curve from nonmetallic ( $d\sigma/dT > 0$ ) to metallic ( $d\sigma/dT < 0$ ) was observed for all samples.

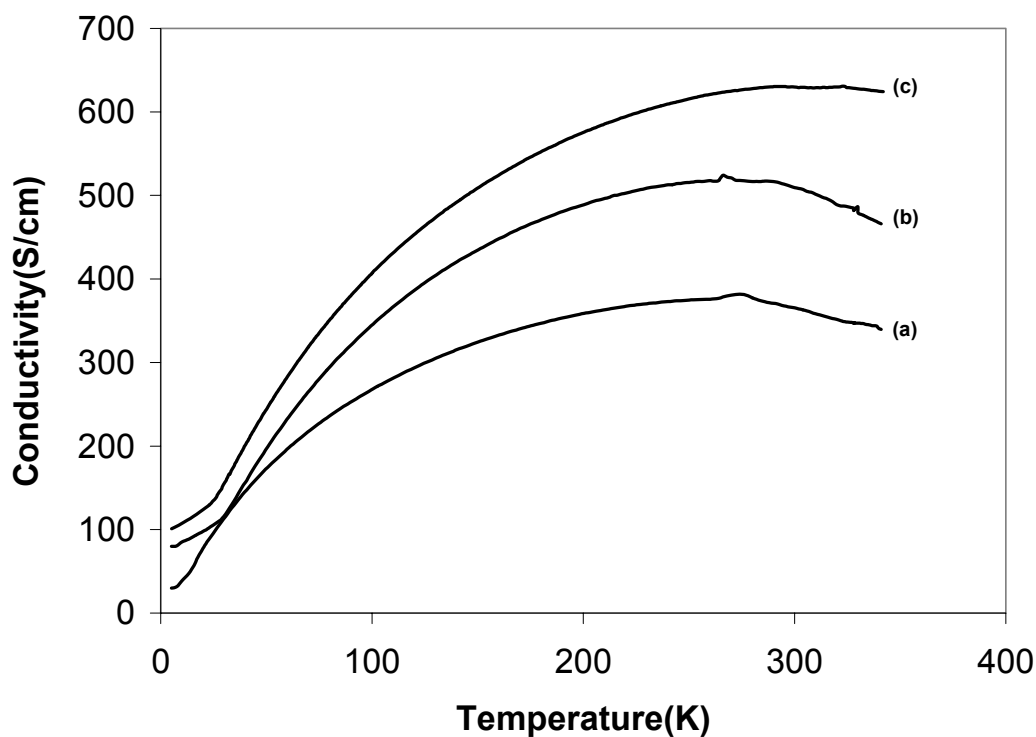


**Figure 7.2** The temperature dependence conductivity for (a) PANi-ES/AMPSA fibre and their composite containing (b) 0.25% w/w and (c) 0.76 %w/w SWNT.

This transition occurs when sufficient thermal motion of the AMPSA counter ion and the polymer chain [7] eliminates the disorder induced in the amorphous regions between metallic islands [16, 19]. The higher  $T_{\sigma_{\max}}$  suggests that the SWNTs restrict the degree of

motion of polymer chains so that higher energy must be absorbed to cross the transition temperature. The lower mobility of the polymer chains in the PAni-ES/AMPSA-SWNT composite fibre compared with neat PAni-ES/AMPSA has already been shown by DSC and DMA data (see section 5.3.5).

In addition, the extraction of temperature dependent reduced activation energy data from conductivity data helps to recognise the location of the metal- insulator phase boundary. Figure 7.3 shows a log-log plot of reduced activation energy versus temperature,  $W(T)$ , for the different samples.

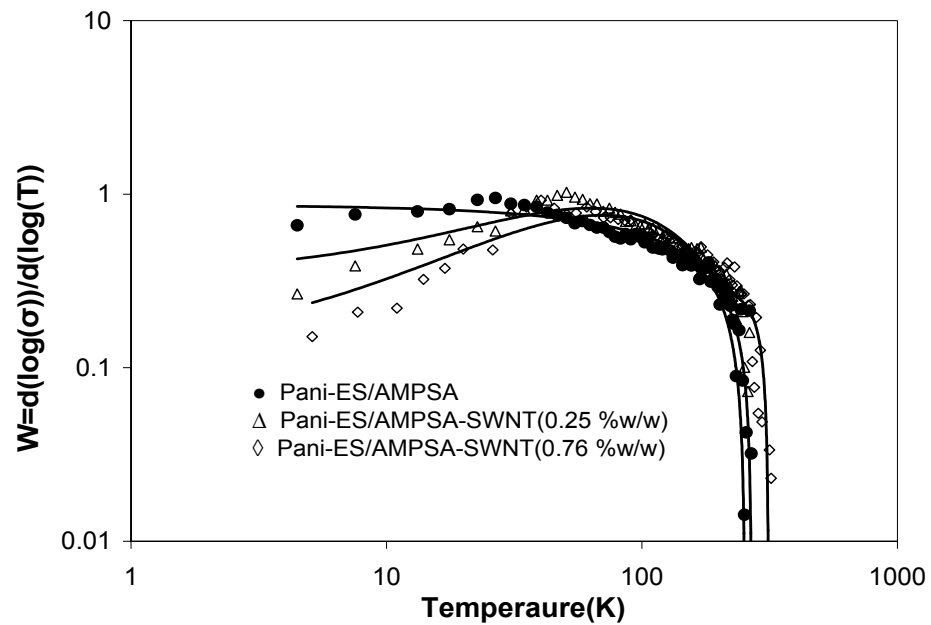


**Figure 7.3.** Log-Log plot of reduced activation energy ( $W$ ) vs. temperature (●) PAni-Es-AMPSA (Δ) PAni-Es-AMPSA-SWNT (0.25 % w/w) (◇) PAni-Es-AMPSA-SWNT (0.76 % w/w).

As a general rule the plot of  $W(T)$  for the metallic, critical and insulator regime respectively show positive, zero and negative slope. It can be observed that at low

temperatures the PAni-ES/AMPSA fibre exhibits a metallic profile (i.e. the temperature below which metallic transport is present) less than 10 K. Addition of carbon nanotubes shifts the metallic-insulator boundary towards higher temperatures ( $\sim 50$  K). In addition, the neat PAni-ES/AMPSA fibre compared with those fibres containing SWNT sustain a smaller positive slope region in proximity of the critical region or the insulator –metal boundary (zero slope at M-I boundary) at low temperature. The low metallic transport regime for neat PAni-ES/AMPSA is in good agreement with literature [9], [20] for PAni film and fibres doped with AMPSA. This phenomena was explained by simultaneous improvement of the metallic properties of the highly ordered domains (HOD) and increasing of disorder in amorphous regions which separates the metallic islands in thermally stretched fibres [20].

The PAni-ES/AMPSA-SWNT composite fibres, however, show a well defined metallic behavior (positive slope of  $W$  vs  $T$ ). Presumably, the nanotubes act by interlinking the metallic regions of the fibre ensuring a smaller coulomb gap in the density of states near the Fermi level [21, 22]. Table 7.1 lists conductivity parameters for different fibre samples extracted from the experimental temperature dependent conductivity data.

**Table 7.1.** The conductivity parameters for PAni-ES/AMPSA fibre and its SWNT composite fibres.

<b>% w/w SWNT in PAni-ES/AMPSA matrix</b>	<b><math>\sigma_{(298\text{ K})}</math> (S/cm)</b>	<b><math>\sigma_{\text{max}}</math> (S/cm)</b>	<b><math>T_{\sigma \text{ max}}</math> (K)</b>	<b><math>T_{\text{M-I}}</math></b>
<b>0.00</b>	360	378	260	<10 K
<b>0.25</b>	480	483	290	40
<b>0.76</b>	620	620	320	50

### 7.3.2. Heterogeneous model

The qualitative explanation of temperature dependence on conductivity can be verified by fitting of the conductivity data to the heterogeneous model described above. The resistance in a heterogeneous model can be formulated as the sum of the resistances of the crystalline parts (subscript c) and barrier parts of the conduction path along the fibre (Figure 7.4). It was considered that the M-I transition may happen in the barrier region, with both non-metallic (subscript n) and disordered metallic (subscript d) portions present in parallel resistance form[2, 23-27]. The behaviour of this system can be represented by Equation 7.1 [2].

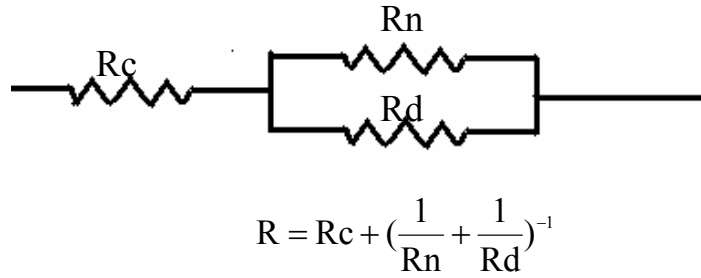


**Figure 7.4.** Schematic of the resistance arrangement in the proposed model of charge transport described in equation 7.1.

$$\sigma^{-1} = f_c \rho_c + \left[ (f_n \rho_n)^{-1} + (f_d \rho_d)^{-1} \right]^{-1} \quad \text{Equation 7.1}$$

Where  $f_c, f_n, f_d$  are the ratio of effective length and cross section area of each region with resistivity  $\rho_c, \rho_n, \rho_d$  respectively for metallic, nonmetallic and metallic disorder regions. Based on earlier work [28], Kaiser [2] proposed that the model of Sheng [3] for fluctuation-induced tunneling between extended metallic regions can be employed to



describe the mechanism of non-metallic temperature dependence for the barrier resistance including a constant parameter for the disordered metal resistance denoted by  $\rho_d$  (the second term in equation 7.1. Using this term, the influence of electron scattering on impurities and lattice perfection is considered leading to temperature independent residual resistivity ( $f_d\rho_d$ ). In addition, a quasi-one dimensional exponential model has been inserted for describing the crystalline conductivity in the metallic regions (first term of equation 7.1). Based on these proposed terms for metallic and non metallic resistivity, the following comprehensive equation can be fitted on the temperature dependence conductivity data:

$$\sigma^{-1} = f_c \rho_m \exp\left(\frac{-T_m}{T}\right) + \left( \left[ f_n \rho_t \exp\left(\frac{T_t}{T+T_s}\right) \right]^{-1} + (f_d \rho_d)^{-1} \right)^{-1} \quad \text{Equation 7.2}$$

The MATLAB software equipped with a powerful curve fitting tool based on least square algorithm was employed for data fitting on Equation of 7.2. The equation comprise six parameters ( i.e.  $T_m$ ,  $T_t$ ,  $T_s$ ,  $f_{cpm}$ ,  $f_{dpd}$ ,  $f_{npt}$ ) that can be fitted on imported data based on initial starting value and domain of variation for each parameter. The sensitivity of best fit with respect to variation of starting value while the other parameters keep constant were demonstrated in Table 7.2. Table divided to six parts that each part shows the influence of individual parameter. For example, in first column of part 1 , different value of  $T_m$  was selected between 1 and 500 while the value of other parameters are equal to 1. In each measurement based on these initial values, fitting parameters were calculated and also the amount of R-square was presented in last column. This should be obvious, as R-squared approaches unity as a regression approaches a perfect fit. The comparison among the value of fitting parameter in all part reveals their sensitivity versus initial values. Even

in part six it can be seen that for some initial value the calculation do not converge to any consistent result. However, some other initial values although converges appropriately but it was not best fit compared to those data shown as bold. It worth noting that fitting parameters in same R- square show very low discrepancy and also very low sensitivity versus initial values.

**Table 7.2.** The sensitivity of the model to the initial starting values for the fitting

Variable starting value $T_m$		$T_m$	$T_s$	$T_t$	$f_c\rho_m$	$f_d\rho_d$	$f_n\rho_t$	$R^2$
<i>Part one</i>	1	2077	9.759	67.5	0.2071	0.04197	0.002155	0.9972
	<b>5</b>	<b>2342</b>	<b>5.287</b>	<b>55.96</b>	<b>0.3176</b>	<b>0.0363</b>	<b>0.00237</b>	<b>0.9984</b>
	<b>10</b>	<b>2335</b>	<b>4.627</b>	<b>54.11</b>	<b>0.2428</b>	<b>0.035</b>	<b>0.0024</b>	<b>0.9984</b>
	20	1813	23.61	97.82	0.1799	0.107	0.001708	0.9916
	40	2298	10.98	69.82	0.458	0.044	0.00211	0.9968
	50	2371	10.23	67.19	0.489	0.0426	0.00218	0.9969
	100	2310	25.76	92.67	0.6461	30.21	0.00178	0.9906
	500	2338	26.03	93.88	0.6901	142.5	0.00176	0.9906
Variable starting value $T_s$		$T_m$	$T_s$	$T_t$	$f_{cpm}$	$f_{dpd}$	$f_{npt}$	$R^2$
<i>Part Two</i>	1	2077	9.759	67.5	0.2071	0.04197	0.002155	0.9972
	<b>5</b>	<b>2186</b>	<b>4.87</b>	<b>54.77</b>	<b>0.1653</b>	<b>0.036</b>	<b>0.0024</b>	<b>0.9984</b>
	<b>10</b>	<b>2199</b>	<b>4.39</b>	<b>53.41</b>	<b>0.1387</b>	<b>0.035</b>	<b>0.0024</b>	<b>0.9984</b>
	20	2377	5.85	57.45	0.3285	0.036	0.0023	0.9983
	40	2377	4.24	53.1	0.2512	0.035	0.0024	0.9984
	50	2380	4.3	53.25	0.2597	0.035	0.0024	0.9984
	100	2148	9.03	63.51	0.2274	0.04	0.00219	0.9975
	<b>500</b>	<b>2324</b>	<b>3.59</b>	<b>51.22</b>	<b>0.1296</b>	<b>0.034</b>	<b>0.0025</b>	<b>0.9982</b>
variable starting value $T_t$		$T_m$	$T_s$	$T_t$	$f_c\rho_m$	$f_d\rho_d$	$f_n\rho_t$	$R^2$
<i>Part Three</i>	1	2077	9.759	67.5	0.2071	0.04197	0.002155	0.9972
	<b>5</b>	<b>2391</b>	<b>3.887</b>	<b>52.16</b>	<b>0.249</b>	<b>0.035</b>	<b>0.0024</b>	<b>0.9983</b>
	<b>10</b>	<b>2342</b>	<b>3.716</b>	<b>51.77</b>	<b>0.2516</b>	<b>0.035</b>	<b>0.0024</b>	<b>0.9983</b>
	<b>20</b>	<b>2254</b>	<b>4.92</b>	<b>54.91</b>	<b>0.2066</b>	<b>0.036</b>	<b>0.0024</b>	<b>0.9984</b>
	40	2038	25.3	91.39	0.2344	2.713	0.0018	0.9906
	50	2379	0.02	48.38	0.128	0.0317	0.0026	0.9946
	<b>100</b>	<b>2398</b>	<b>4.693</b>	<b>54.28</b>	<b>0.305</b>	<b>0.0358</b>	<b>0.0024</b>	<b>0.9984</b>
	<b>500</b>	<b>2324</b>	<b>3.599</b>	<b>51.22</b>	<b>0.1296</b>	<b>0.034</b>	<b>0.0025</b>	<b>0.9982</b>

Variable starting value fcpm		$T_m$	$T_s$	$T_t$	$f_c\rho_m$	$f_d\rho_d$	$f_n\rho_t$	$R^2$
Part Four	1	2077	9.759	67.5	0.2071	0.04197	0.002155	0.9972
	5	2371	6.898	60.1	0.3914	0.0376	0.0023	0.9981
	10	2397	1.293	44.53	0.00635	0.03359	0.0026	0.9968
	20	2336	7.046	60.31	0.3695	0.03829	0.00228	0.9980
	40	2293	10.29	68.13	0.4291	0.0426	0.00214	0.9750
	50	2320	17.23	74.11	0.3148	0.08867	0.002136	0.9916
	100	2214	8.934	65.06	0.3058	0.0407	0.00219	0.9976
	500	2324	3.599	51.22	0.1296	0.03483	0.0025	0.9982
Variable starting value fdpd		$T_m$	$T_s$	$T_t$	$f_c\rho_m$	$f_d\rho_d$	$f_n\rho_t$	$R^2$
Part Five	1	2077	9.759	67.5	0.2071	0.04197	0.002155	0.9972
	5	1864	26.14	94.3	0.1546	9.26	0.001756	0.9907
	10	989.7	26.57	96.57	0.01268	73.07	0.001714	0.991
	20	1979	22.85	81.95	0.1544	0.8071	0.001992	0.9893
	40	2347	25.88	92.94	0.8636	40.51	0.00178	0.9905
	50	2246	24.36	87.47	0.4929	142.5	0.001863	0.9903
	100	1800	25.96	93.79	0.1323	12.7	0.001764	0.9907
	500	2324	3.599	51.29	0.1296	0.03483	0.0025	0.9982
Variable starting point fnpt		$T_m$	$T_s$	$T_t$	$f_c\rho_m$	$f_d\rho_d$	$f_n\rho_t$	$R^2$
Part Six	1	2077	9.759	67.5	0.2071	0.04197	0.002155	0.9972
	5	2284	4.806	54.69	0.2261	0.03958	0.002405	0.9984
	10	2394	8.353	63.65	0.4874	0.03942	0.002232	0.9977
	20	No convergence						
	40							
	50							
	100							
	500	2324	3.599	51.22	0.1296	0.0328	0.0025	0.9982

The curve fitting precedes using best initial values to reach nearly same closest  $R$ -square to unity in each set of data of temperature dependent conductivity for different fibers. Good fitting of the prescribed model according to fitting parameter on experimental data is shown for neat PANi-ES/ AMPSA and PANi –ES/AMPSA-SWNT (0.76 %w/w) fibres in Figure 7.5. The precision of the data in Figure 7.5 shows a residual amount of nearly zero in temperature range between 50 -300 K, however the scattered residual data

beyond this temperature range even is in the order of  $1 \times 10^{-3}$ . The data given in Table 7.3 shows the fitting parameter of conductivity data for PANi-ES/AMPSA fibre and its composites with carbon nanotube.

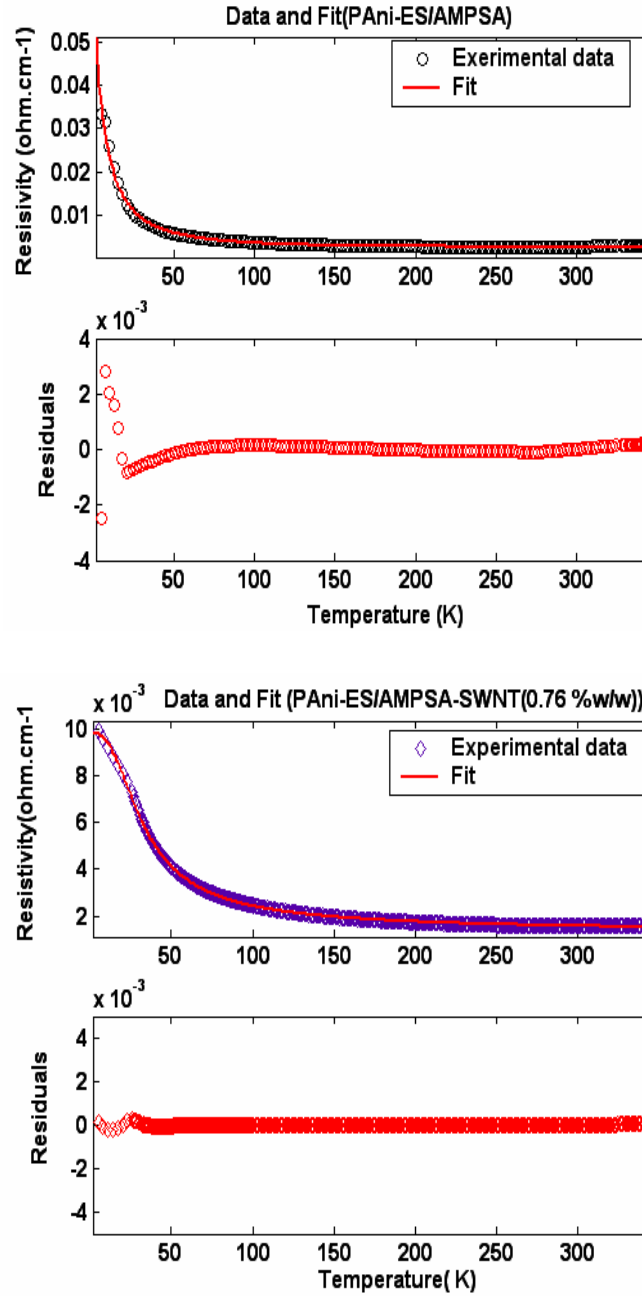


**Figure 7.5.** The fitting quality of experimental data and proposed model and residual amount of least square of fitting calculation.

**Table 7.3.** The fitting parameters presented in equation 7.2 for different samples.

% w /w SWNT/PAni- ES/AMPSA	$f_c\rho_m$	Tm	$f_n\rho_t$	Tt	Ts	$f_d\rho_d$	R <sup>2</sup>
<b>0.00</b>	0.2071	2077	0.0021	127.05	9.75	0.0095	0.9984
<b>0.25</b>	0.3134	2244	0.0015	97.74	4.82	0.012	0.9982
<b>0.76</b>	0.0540	2276	0.0009	87.84	3.92	0.14	0.9978

Tm set the energy of phonons that can backscatter charge carriers, Tt and Ts are the tunnelling parameters which shows the magnitude of electrical barriers [3]. Highly conductive samples show lower Tt. Also Lower Ts values are obtained for high conductive samples. It can be seen that the numerical amount of Tt and Ts significantly decrease by addition of SWNTs that suggests a lower morphological barrier in the amorphous region for electrical transport. The data given in Table 7.3 can be employed to deduce the relative size of the temperature-dependent metallic term ( $\omega_1$ ) and the relative size of the constant metallic disorder ( $f_d\rho_d$ ) in the amorphous term ( $\omega_2$ ).

$\omega_1$ = The contribution of metallic resistivity in bulk resistivity at room temperature is

given by

$$\omega_1 = \frac{f_c \rho_m \exp\left(\frac{-T_m}{T}\right)}{\sigma^{-1}} \quad \text{Equation 7.3}$$

$\omega_2$  = The contribution of metallic disorder in amorphous resistivity at room temperature is given by

$$\omega_2 = \frac{f_d \rho_d}{\left( \left[ f_n \rho_t \exp\left( \frac{T_t}{T + T_s} \right) \right]^{-1} + (f_d \rho_d)^{-1} \right)^{-1}} \quad \text{Equation 7.4}$$

Table 7.3 shows the numerical amounts of  $\omega_1$  and  $\omega_2$  based on the equation 6.15 and 6.16. Both of these terms shows that, the fraction of the quasi-1D metallic transport in crystalline region (at room temperature) and the fraction of metallic disorder in amorphous area of  $\omega_2$  is increased by addition of SWNTs to PAni-ES/AMPSA.

**Table 7.4.** The contribution of metallic resistivity in bulk resistivity and the metallic disorder in amorphous resistivity

% w /w SWNT in PAni-ES/AMPSA	$\omega_1(\%)$	$\omega_2(\%)$
0%	5.4	0.83
0.25 %	12	0.84
0.76 wt %	14	1.01

Thermal induced alignment during fiber formation aligns the metallic phase of the highly ordered domain(HOD), while simultaneously partially orients the amorphous regions, which separate the “metallic islands”[29-31]. The increasing of  $\omega_1$ ,  $\omega_2$ , and decreasing of

Tt and Ts after addition of SWNT, suggests the formation of an interconnected network of metallic SWNTs in barriers of the amorphous area between crystalline PANi islands. It may result in a higher extended structure and higher metallic transport of PANi-ES/AMPSA after addition of SWNTs.

#### 7.4. Conclusion

In summary, the temperature dependent conductivity of PANi-ES/AMPSA fibre with and without SWNTs was evaluated. The results of experimental data were fitted on a model that proposes a heterogeneous structure comprising crystalline and amorphous resistivities in series for conducting polymer and SWNTs which are used to identify the conductivity parameters and/ or transport regime.

Metallic behaviour accompanied with a peak in the conductivity and a turn over to non-metallic behaviour was observed for highly conducting PANi and its SWNT composites. The temperature corresponding to maximum conductivity is increased by addition of SWNTs suggesting a change in morphological disorder. In addition, the reduced activation energy indicates greater metallic behaviour in PANi-ES-AMPSA containing SWNT compared with neat PANi-ES/AMPSA.

The qualitative analysis of the metallic behavior of composite fibres was further investigated using a quantitative approach. It was shown that the higher metallic transport of PANi-ES/AMPSA-SWNT composite fibre compared to neat PANi-ES/AMPSA fibre is based on the numerical amount of the fraction of metallic resistivity to the total resistivity and the contribution of metallic disorder in resistivity of amorphous regions ( i.e.  $\omega_1$ ,  $\omega_2$ ).

These parameters indicated that the addition of SWNTs improves the metallic property in the crystalline areas and boosts the metallic disorder contribution in amorphous areas.

In the PANi fibre without SWNTs, the induced separation in highly ordered domains (HOD) of metallic islands during the stretching process is filled by nonmetallic disorder of the amorphous regions. Meanwhile the addition of SWNTs may produce a network including a mixture of metallic and nonmetallic ropes interacting with PANi in the crystalline and amorphous areas. It is therefore expected that the gap between metallic regions is filled by metallic ropes which are well distributed and aligned in the composite.



## 7.5. References

- [1] R. Menon, C. O. Yoon, D. Moses and A. J. Heeger, in Handbook of conducting polymers,"Metal-Insulator transition in doped conducting polymers", Marcel Dekker, New York, (1997), 27.
- [2] A. B. Kaiser, Adv.Mater. 13 (2001) 927-941.
- [3] P. Sheng, Phys. Rev. B. 21 (1980) 2180.
- [4] W. W. Focke and G. E. Wnek, J. Elec. Anal. Chem. 256 (1988) 343-352.
- [5] R. Menon, C. O. Yoon, D. Moses and A. J. Heeger, in Handbook of Organic Conductive Molecules and Polymers,"" the erlatinship conductivity ratio and M-I transition"", Wiley, New York, (1996), 27.
- [6] P. K. Kahol, H. Guan, B. J. McCormick and P. R. 10393., Phys. Rev.B. 44 (1991) 10393.
- [7] P. N. Adams, S. J. Pomfret and A. P. Monkman, Synth. Met. 101 (1999) 776-777.
- [8] P. N. Adams, S. J. Pomfret and A. P. Monkman, Synth. Met. 101 (1999) 685-689.
- [9] M. F. Hundley, P. N. Adams and B. R. Mattes, Synth. Met. 129 (2002) 291-297.
- [10] W. P. Lee, K. R. Brenneman, A. D. Gudmundsdottir, M. S. Platz, P. K. Kahol, A. P. Monkman and A. J. Epstein, Synth. Met. 101 (1999) 819-820.
- [11] J. E. Fisher, Phys.Rev.B. 55 (1997) R4921.
- [12] A. B. Kaiser, Y. W. Park, G. T. Kim, E. S. Ghoi, G. Dusberg and S. Roth, Synth. Met. 103 (1999) 2547-2550.
- [13] Z. H. Wang, E. M. Scherr and A. G. M. Diarmid, Phys. Rev.B. 45 (1992) 4190-4202.
- [14] A. J. Epstein, J. Joo, R. S. Kohlman, G. Du, A. G. MacDiarmid, E.J.Oh, Y. Min, J. Tsukamoto, H. Kaneko and J. P. Pouget, Synth. Met. 65 (1994) 149.
- [15] J. Joo, S. M. Long, J. P. Pouget, E. J. Oh, A.G. MacDiarmid and A.J.Epstein, Phys. Rev. B. 9567 (1998) 157-160.
- [16] R. S. Kohlman, J. Joo, Y. G. Min, A. G. Macdiarmid and A. J. Epstein, Phys. Rev. Lett. 77 (1996) 2766.
- [17] L. Pietronero, Synth. Met. 8 (1983) 225.
- [18] S. Kivelson and A. J. Heeger, Synth. Met. 22 (1988) 371.

- [19] J. Joo, V. N. Prigodin, Y. G. Min, A. G. MacDiarmid and A.J. Epstein, Phys. Rev. B. 50 (**1994**) 12226.
- [20] D. Bowman and B. R. Mattes, Synthetic Metals. 154 (**2005**) 29-32.
- [21] A. L. Efros and B. I. Shklovskii, J.Phys. C: Solid State Phys. 8 (**1975**) L49-L51.
- [22] J. Adkins, J. Phys: Condens. Matter. 1 (**1989**) 1253.
- [23] A. B. Kaiser, Phys. Rev. B. 40 (**1989**) 2806.
- [24] A. B. Kaiser, Synth. Met. 45 (**1991**) 183.
- [25] A. B. Kaiser, G. U. Flanagan, D. M. Stewart and D. Beaglehole, Synth.Met. 117 (**2001**) 67.
- [26] A. B. Kaiser and S. C. Graham, Synth. Met. 367 (**1990**) 367.
- [27] A. B. Kaiser, C. K. Subramaniam, P. W. Gilberd and B. Wessling, Synth.Met. 69 (**1995**) 197.
- [28] Y. W. Park, A. J. Heeger, M. A. Druy and A. G. MacDiarmid, J. Chem. Phys. 73 (**1980**) 946-57.
- [29] E. R. Holland, S. J. Pomfret, P.N.Adams, L. Abell and A. P. Monkman, Synth. Met. 84 (**1997**) 777-778.
- [30] A. L. Efros and B. I. Shklovskii, J. Phys. C: Solid State Phys. (**1975**) L49-L51.
- [31] J. Adkins, J Phys: Condens Matter. 1 (**1989**) 1253.

# ***CHAPTER EIGHT***

**The Preliminary Studies into  
Applications of  
PAni-ES/AMPSA/SWNT Composite  
Fibres**

## 8.1. Introduction

As described in Chapter one, there are many applications in E-textiles for conductive, electroactive fibre. In this Chapter, just three example applications are considered: mechanical actuators, rechargeable batteries and humidity, temperature sensors. Although stand alone devices embedded in textile matrix were not constructed, the PAni composite fibres described in Chapter five were considered in each of these areas. The aim of the current study was to determine whether the composite fibres are viable candidates to be further developed into fully functioning standalone devices.

### 8.1.1. Actuators: recent development and general requirement

Actuating materials capable of producing useful movement and forces are recognised as the “missing link” in the development of a wide range of frontier technologies including haptic devices [1, 2], microelectromechanical systems (MEMS) [3] and even molecular machines [4]. Immediate uses for these materials include an electronic Braille screen [5], a rehabilitation glove [6], tremor suppression [7] and a variable camber propeller [8]. Most of these applications could be realised with actuators that have equivalent performance to natural skeletal muscle. Although many actuator materials are available, none have the same mix of speed, movement and force as skeletal muscle. Indeed the actuator community was challenged to produce a material capable of beating a human in an arm wrestle[9]. This challenge remains to be met.

One class of actuator material that has received considerable attention is low DC voltage electrochemical systems utilising conducting polymers [10-12] and carbon nanotubes [13, 14] . One deficiency of conducting polymers and nanotubes compared with skeletal

muscle is their low actuation strains: less than 15% for conducting polymers and less than 1% for nanotubes. It has been argued that the low strains can be mechanically amplified (levers, bellows, hinges etc.) to produce useful movements [8], but higher forces are needed to operate these amplifiers.

In recent studies of the forces and displacements generated from conducting polymer actuators, it has become obvious that force generation is limited by the breaking strength of the actuator material [15-17]. Baughman [18] has predicted that the maximum stress generated by an actuator can be estimated as 50 % of the breaking stress so that for highly drawn PANi (PANi) fibres stresses of the order of 100 MPa should be achievable. However, in practice the breaking stresses of conducting polymer fibres when immersed in electrolyte and operated electromechanically are significantly lower than their dry-state strengths [15, 17, 19]. The reasons for the loss of strength are not well known, but the limitations on actuator performance are severe. The highest reported stress that can be sustained by conducting polymers during actuator work cycles is in the range 20 MPa – 34 MPa [17, 20] for polypyrrole (PPy) films. However, the maximum stress that can be sustained by PPy during actuation appears very sensitive to the dopant ion used and the preparation conditions [17], with many studies showing maximum stress values of less than 10 MPa [5, 15-17, 21].

The low stress generation from conducting polymers, limited by the low breaking strengths, mean that the application of mechanical amplifiers is also very limited. To improve the mechanical performance, we have investigated the use of carbon nanotubes as reinforcing fibres in a PANi matrix. Previous work has shown that the addition of single wall nanotubes (SWNTs) and multi-wall nanotubes (MWNTs) to various polymer

matrices have produced significant improvements in strength and stiffness [22-25]. It has been shown that the modulus of PANi can be increased by up to 4 times with the addition of small (<2%) amounts of nanotubes ( see Chapter 4 and 5 and reference [26] ). Similar improvements in the modulus of actuating polymers may lead to significant increases in the stress generated and work per cycle. Other previous studies have shown that wet spun PANi fibre may be used as actuators [27, 28]. Isotonic strains of 0.3 % and isometric stresses of 2 MPa were obtained from these fibres when operated in ionic liquid electrolytes.

The aim of the present study in actuation part is to determine the actuator performance of PANi-ES/AMPSA fibre containing SWNTs.

### **8.1.2. PANi fibre electrode for application in rechargeable battery**

Among the family of conducting polymers, PANi has been extensively studied as battery material due to its conductive electroactive properties [29-38]. PANi has a good redox reversibility and high stability, and it is neither soluble nor passive during the oxidation process. PANi has usually been employed as the cathode material with Zn as the anode electrode. The electrolyte contains inorganic acids such as  $\text{HClO}_4$  or  $\text{H}_2\text{SO}_4$  [33, 38]. Battery voltages of 2 V and discharge capacity of  $121 \text{ mAh g}^{-1}$  have been reported [33]. There have also been a few reports about the application of PANi in all polymer batteries. Rehan [39] , described a battery composed of a doped PANi anode and a poly-1-naphthol cathode with methyl cyanide containing lithium perchlorate and perchloric acid as electrolyte. It has been claimed that this battery system exhibited a discharge capacity of  $150 \text{ mAh g}^{-1}$ . The charging /discharging tests showed a gradual decrease in capacity up to

15 % after 100 cycles. A discharge capacity of  $79 \text{ mAh g}^{-1}$  was also reported for a cell composed of a PANi cathode and a polyindole anode using sulfuric acid electrolyte [40].

The aim of this part of the thesis was to evaluate the performance of PANi fibres as an electrode for wearable power source. Such batteries may be useful for embedding in a wearable diagnostic system to provide enough power for monitoring of vital signs using a sensor network in medical and military applications. The fibre shaping of electrochemical cells may ensure a superior grade of integration into textiles and a higher working surface and is preferable to the flat thin film batteries [41].

PANi fibres and its composite containing SWNTs were investigated in ionic liquid EMITFSI in this work. High ionic conductivity, large electrochemical windows, excellent thermal and electrochemical stability and negligible evaporation make ionic liquids an ideal electrolyte for such system compared to mineral aqueous acids (i.e.  $\text{H}_2\text{SO}_4$ ) [42-44].

The charge discharge capacity was obtained in this part for PANi-ES/AMPSA and fibre containing SWNT.

### 8.1.3. Sensitivity to temperature and humidity

The realisation of the all “organic” wearable smart and interactive textile may require the integration of conducting electroactive polymers into skin-adherent clothes as wearable sensors for several biomedical applications. In this regards sensing device (e.x. thermoelectric and piezoelectric sensors) have been fabricated by deposition of polypyrrole (PPy) on Lycra/Cotton fabric [45, 46]. Similarly, Researchers in CSIRO (Canberra, Australia) and the University of Wollongong (Wollongong, Australia) correspondingly have integrated this kind of fabric-based sensors into a smart knee sleeve [47]. The conducting electroactive fibre composed of PANi and SWNT due to low weight,

flexibility, ease of processing and several miniature geometries can be considered as another promising candidate for embedded knitted sensors in textile substrate. They are mechanically strong and showed conductivity in the range of metallic material. However, Prerequisites of an efficient performance for a sensor is generally related to linear sensitivity, high stability, reversibility and low response time.

Two simple common physical properties like temperature and humidity were selected in this part to investigate the effectiveness of conducting fibres as a passive sensors to respond linear or step stimulators.

The achievement of similar performance of diverse conventional sensors integrated in a typical smart T-Shirt ( composed of wearable fabric embedded with metallic fibre and woven optical fibre developed by Sensatex [48]) used to monitor several vital signs n human body, such as heart rate, respiration rate, electrocardiogram (ECG) and skin temperature [49-51], can be possibly addressed in further study.

## **8.2. Experimental**

### **8.2.1. The actuation tests**

#### **8.2.1.1. Materials and reagents**

Neat PANi-ES/AMPSA fibre (5x thermally stretched) and PANi-ES/AMPSA/SWNT (0.76 % w/w) were employed for characterisation of actuation performance.

HCl (32 % w/w) was purchased from Sigma Aldrich and diluted with Milli-Q water to obtain the required concentration (1M).



**8.2.1.2. Instrumentation**

15 mm fibre samples were cut from a length of thermally drawn fibre with a diameter  $\sim$  50-60  $\mu\text{m}$ . One end of fibre was attached to a Pt wire (100  $\mu\text{m}$ ) with silver paint and then covered completely by epoxy glue to prohibit leakage of silver paint components into electrolyte. The other end was connected to an insulated copper wire with epoxy glue.

The instrumental set up used for characterisation of actuation performance is similar to the set up used for cyclic voltammetry test described in section 3.5.2. The test has been conducted in the isotonic (constant force) mode (Fig 8.1).

**Figure 8.1.** Experimental set-up for actuation test in isotonic mode [52]

Measurement of mechanical parameters (i.e force and displacement) was carried out using an Aurora Scientific force/strain transducer, the dual mode lever system model 300B, which has an upper force limit of 50 g (0.5 N) . This system is able to measure both the force on, and the displacement of, a lever arm using an electromagnet. In order to provide a given force for isotonic measurements a constant current can be applied to the

electromagnet, and the displacement in the lever arm position applied by the actuator is detected for measurement of active stroke[52].

### 8.2.1.3. Actuator work per cycle

The calculation of the work performed by the actuator depends upon the definition of the work cycle. The net change in length of the actuator or the actuator stroke ( $\Delta L_f$ ) when stimulated under a constant (isotonic) load ( $f$ ) is then given by equation 8.1 and the work done is given by equation 8.2 [53].

$$\Delta L_f = \Delta L_0 + \frac{fL_0}{A} \left( \frac{1}{Y'} - \frac{1}{Y} \right) \quad \text{Equation 8.1}$$

$$W = f\Delta L_f \quad \text{Equation 8.2}$$

Where  $Y$  the elastic modulus when no voltage is applied,  $Y'$  the elastic modulus after the voltage has been applied,  $A$  the cross-sectional area of the actuator (assumed not to change during the actuation process) and  $\Delta L_0$  the “free stroke” of the actuator, or the length change that occurs when the actuator operates against no external force.

## 8.2.2. Electrode material for rechargeable battery

### 8.2.2.1. Materials and reagents

Neat PANi-ES/AMPSA fibre (5X thermally stretched) and Neat PANi-ES/AMPSA/SWNT (0.76 % w/w) were employed for characterisation of electrode performance for application in rechargeable battery. The ionic liquid ethylmethyl imidazolium bis(trifluoro methane sulfonyl) imide (EMI.TFSI) was synthesised in our laboratories according to methods described elsewhere [54, 55].

#### 8.2.2.2. Fabrication of polymer electrode

The thermally stretched (5X) PANi-ES/AMPSA fibres or PANi AMPSA fibres containing SWNT (0.76 %w/w) were cut into small segments, each was 3 cm length ( $D=60-80\text{ }\mu\text{m}$ ). Three such segments were bound together with platinum wire ( $\phi = 0.125\text{ mm}$ ), and Pt wire was also used as current lead. The electrodes were soaked in ionic liquids (EMI.TFSI) for 2 hours to penetrate into the inner part of the fibres before electrochemical measurements.

#### 8.2.2.3. Electrochemical characterisation

All the electrochemical evaluation of PANi-ES/AMPSA or its SWNT composite fibres were performed in a standard one compartment three-electrode cell with a stainless steel mesh counter electrode,  $\text{Ag}/\text{Ag}^+$  (EMI.TFSI) reference electrode, and ionic liquid EMI.TFSI electrolyte. The charge/discharge investigation were carried out using an EG&G PAR 363 Potentiostat/Galvanostat, a MacLab 400, and EChem v 1.5.2 software (ADI Instruments). In the charge/discharge test, the cells were charged galvanostatically at a current density of 0.1 mA to a cell voltage of 2.0 V, and then discharged at the same current to a cut-off voltage of -1.2 V.

### 8.2.3. Test for sensitivity to temperature and humidity

#### 8.2.3.1. Material and reagents

The thermally stretched (5X) PANi-ES/AMPSA fibres or PANi -AMPSA fibres containing SWNT (0.76 %w/w) were used for measurement of resistivity at different

temperatures and humidities. Different solution were employed to prepare a suitable environment for different relative humidity (RH %).

**Table 8.1** The description of aqueous solution required for preparation of different relative humidity in the conductivity chamber

RH%	The description of humid environment
3	Blue silica gel
11	Saturated LiCl aqueous solution
51	Saturated $\text{Ca}(\text{NO}_3)_2$ aqueous solution
74	Saturated $\text{NaNO}_3$ aqueous solution

#### 8.2.3.2. Instrumentation

The sensitivity of both samples versus temperature in constant humidity was evaluated by measurement of resistance using the PPMS (physical properties measurement system) instrument as described in Chapter 7 with scan rate of 3 °C/min.

A multi-channel multi-meter data acquisition system of Agilent model 34970 using a four probe technique has been used to measure the resistance in different humidity at constant room temperature. A 10 mm fibre sample was fixed on the two-point probes using silver paint (SPI) The sample holder was connected to a two probe socket which was fixed in a stopper using long metallic rods (Figure 8.2).

The whole sample holder including the sample was placed in a resistivity chamber containing different material to create different relative humidity.

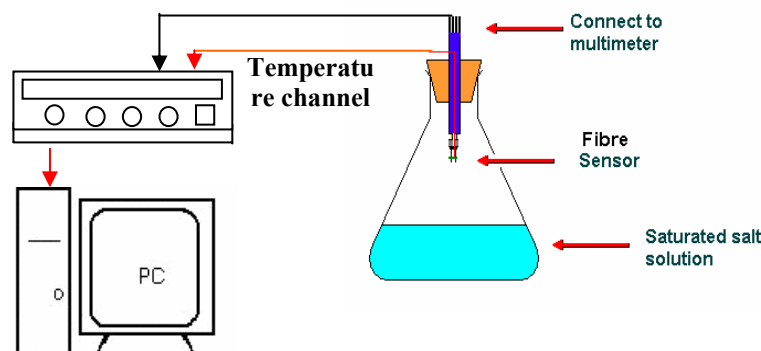


**Figure 8.2.** Schematic shows the experimental set up used for measurement of resistance across the fibres for measurement of resistance in different humidity

### 8.3. Results and discussion

#### 8.3.1. Actuation behavior

The reinforcing effect afforded by small additions of SWNTs to the PANi-ES/AMPSA was demonstrated by dry-state tensile testing, as shown in Fig 5.19 and summarised in Table 5.5. A very large increase in the breaking strength from 170 MPa for neat PANi-ES/AMPSA to 255 MPa was produced with the addition of 0.76 % w/w SWNTs. Similarly, the modulus of the composite fibres was nearly doubled from 3.4 GPa to 7.3 GPa. It has been shown that the measured modulus is in good agreement with the calculated value based on the principal of the rule of mixture (see Chapter 6), suggesting a high degree of separation, alignment and bonding of the nanotubes to the PANi matrix. Typical isotonic actuation data obtained during cyclic voltammetry at low stress is shown in Figure 8.3. Such simultaneous measurements by cycling of voltage provide valuable information regarding the actuation mechanism through correlation of actuation strain with potential and charge, and therefore the oxidation level.

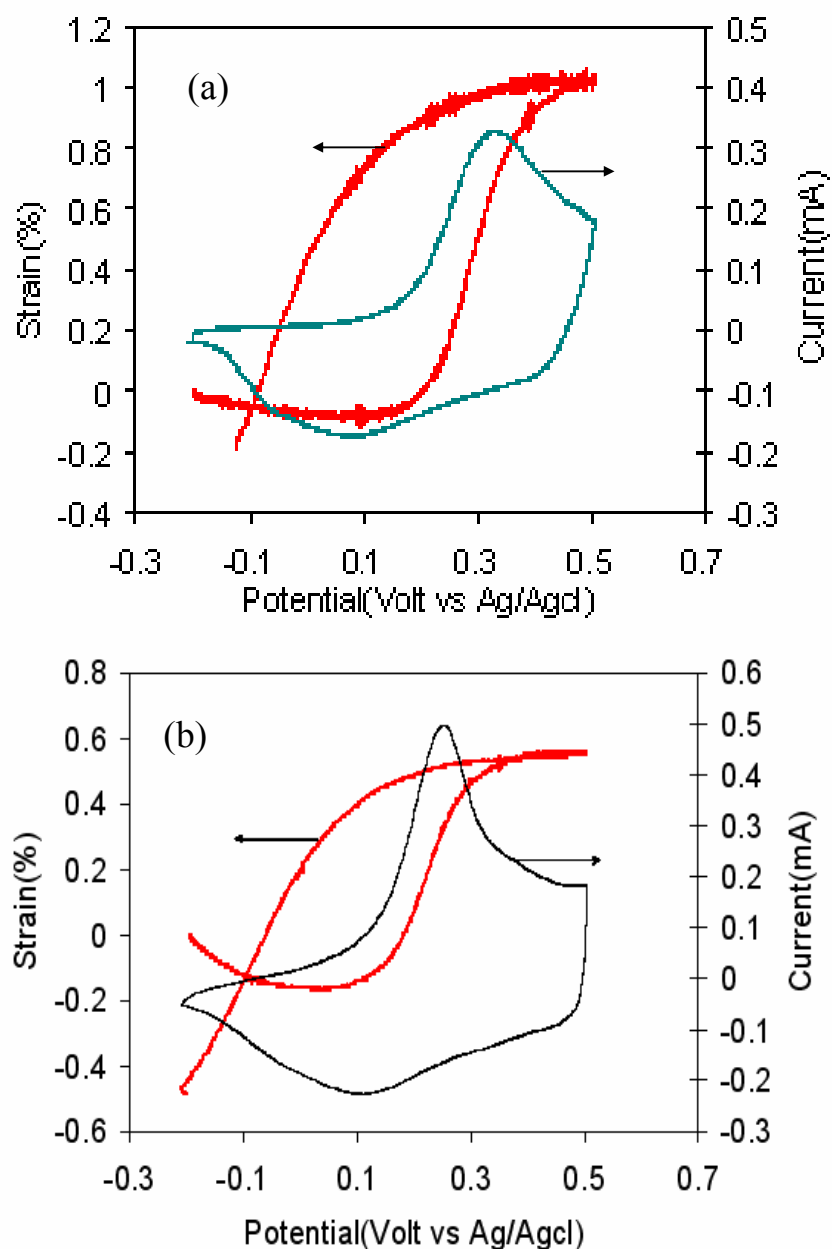


**Figure 8.3.** The typical isotonic actuation data as a function of scanning potential in 1.0 M HCl at scan rate of 5 mV/s. Simultaneous demonstration of linear strain and cyclic voltammogram in one cycle for (a) Neat PANi-ES/AMPSA (b) PANi – ES/AMPSA/SWNT (0.76 % w/w) under 10 mN load

Potentials were limited to between -0.2 V and +0.5 V versus Ag/AgCl to avoid the pernigraniline state and thus prevent degradation in the HCl. Oxidation and reduction between the leucoemeraldine and emeraldine states was stable, as evidenced by consistent cyclic voltammograms. The isotonic actuation strains also were determined at different (constant) stresses as shown in Figure 8.4 for the neat PANi-ES/AMPSA and PANi-ES/AMPSA-SWNT (0.76 %w/w) composite fibre. During isotonic actuation testing, each sample was tested at increasing loads until rupture occurred. Note that the addition of nanotubes greatly increases the breaking strength of the composite fibres under actuation conditions. The nanotube reinforced fibres could sustain stresses up to 120 MPa without failure during electrochemical cycling. Even the neat PANi-ES/AMPSA could sustain stresses up to 90 MPa during work cycles.

The results in Figure 8.4 also show that the addition of nanotubes to the PANi matrix affects the actuation strain at low stress levels. The “free stroke” (strain at zero external load) for the PANi-ES/AMPSA/SWNT (0.76 % w/w) was approximately 60% of the neat PANi-ES/AMPSA free stroke. In this case the higher modulus nanotubes restrict the volume changes occurring within the PANi matrix.

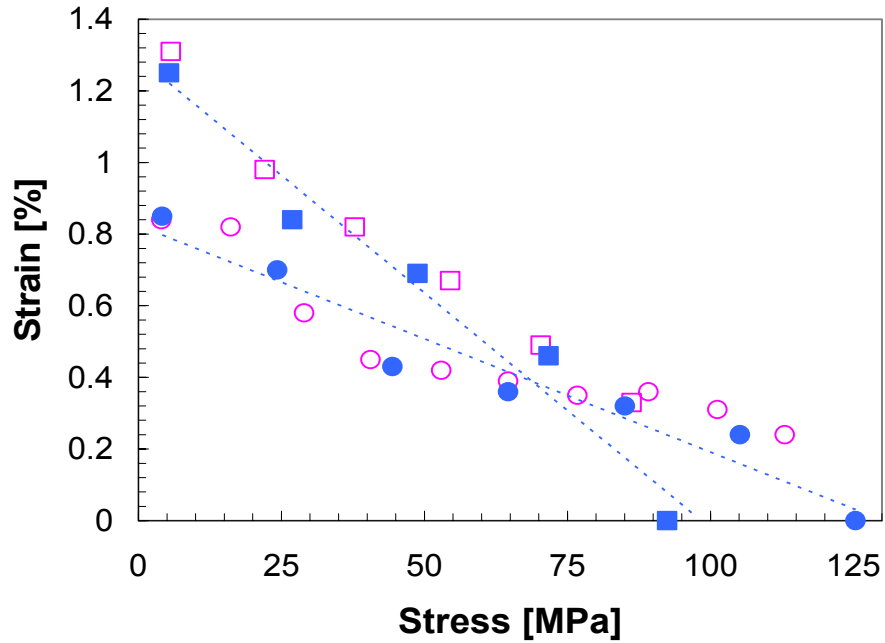


**Figure 8.4.** Isotonic strains measured during cyclic voltammetry in 1M HCl at 5 mV/s between -0.2 and 0.5V (vs. Ag/AgCl reference). Open and filled symbols show the results from two separate samples. Square symbols are for neat PANi-ES/AMPSA fibres and circles are for SWNT-reinforced fibre

The actuator strains of the composite fibres may be calculated using the same iso-strain assumption inherent in the rule-of-mixtures approach. The expected actuator strain ( $\epsilon_c^*$ ) in the composite materials is estimated from:

$$\epsilon_c^* = \frac{\nu_m \epsilon_m^* E_m + \nu_f \epsilon_f^* E_f}{E_c} \quad \text{Equation 8.1}$$

Where subscripts  $c$ ,  $m$  and  $f$  refer to the composite, PANi matrix and SWNT fibres and  $E$  and  $\nu$  are the Young's Modulus and volume fraction for each phase. Actuation in both the matrix ( $\epsilon_m^*$ ) and the SWNT fibres ( $\epsilon_f^*$ ) are considered in the analysis, since it is known that the SWNTs also produce appreciable strains when electrochemically charged



[14]. In previous work on SWNT/PAni composites, where unaligned mats of SWNTs were dip coated with PAni to give composites of 75 % w/w SWNTs, it has been shown that both the nanotubes and the polymer contribute to the actuation strain.

The calculated composite actuation strain (at zero applied stress) was found to be 0.57 % where the matrix actuation strain ( $\epsilon_m^*$ ) was taken as 1.3 % and a SWNT actuation strain ( $\epsilon_f^*$ ) was assumed to be -0.06 % for an anodic current pulse [56]. The measured actuation strain (0.85 %) was appreciably larger than the calculated strain. Clearly, the stiffening effect caused by the nanotubes cannot on its own account for the observed actuation behaviour.

The larger than expected actuation in the composite fibres suggest that the nanotubes increase the efficiency of the actuation mechanism, perhaps through improved charge transfer. The magnitude of the increase in efficiency is demonstrated by calculating the matrix strain needed to account for the measured composite actuation strain. Thus, a matrix strain of 1.8 % would be required to generate a composite strain of 0.85 %. The higher matrix strains that occur in the SWNT composites compared with the neat PAni fibres, suggest a higher charge transfer efficiency possibly due to the higher conductivity of the SWNT-PAni composites (Table 8.2). For comparison, neat PAni fibres were also sputter coated with platinum to improve their conductivity and these samples showed actuation strains of 2 % compared with 1.3 % for uncoated PAni fibres[57]. Improved electrical conductivity has previously been shown to increase actuation performance by reducing  $iR$  losses along the fibre length and so increasing the active portion of the fibre [5].

**Table 8.2.** Measured and calculated properties of PAni-ES/AMPSA/SWNT fibre composites.

	<b>0% SWNT</b>	<b>0.76% SWNT</b>
<b>Elastic Modulus (GPa)</b>	$3.4 \pm 0.4$	$7.3 \pm 0.4$
<b>Tensile Strength (MPa)</b>	$170 \pm 22$	$255 \pm 32$
<b>Elongation at Break (%)</b>	$9 \pm 3$	$4 \pm 0.6$
<b>Max. Work Per Cycle (<math>\text{kJ/m}^3</math>)</b>	365	320
<b>Adjusted PAni matrix actuation (%)</b>	NA	2%
<b>4-probe conductivity (S/cm)</b>	$497 \pm 55$	$716 \pm 36$

Furthermore, the strong interactions between the PAni and SWNTs has been previously shown to enhance electroactivity [58]. As shown in Figure 8.4, the electroactivity of the composites is improved by the addition of only 0.76% SWNTs. The more pronounced redox processes occurring in the composite fibres indicate an improved electrochemical efficiency that leads to an increase in the PAni matrix actuation.

Enhancement of the electroactivity of PAni/SWNT composite fibres has been attributed to a possible increase in the degree of protonation of the PAni due to strong  $\pi$ -stacking interactions between the SWNTs and the PAni. Clearly the improved electroactivity of the composite fibres will induce larger actuation strains in the PAni matrix, as described above. The higher load capacity of the PAni/SWNT fibres also translates into higher work-per-cycle (Table 8.2). The maximum work-per-cycle of the neat PAni was  $365 \text{ kJ/m}^3$  compared with other reported values of up to  $83 \text{ kJ/m}^3$  for polypyrrole[59] [60]. With the addition of 0.76% NTs the work-per-cycle decreases slightly to  $325 \text{ kJ/m}^3$ , which is still more than 10 times higher than the work capacity of skeletal muscle [8, 61]. The

dramatic increase in work per cycle compared with previous results from conducting polymers is a consequence of the higher strains at much higher stresses that are produced by the PANi and composite fibres. In addition, the high cycling stability was observed after more than 100 cycle under applied load. This observation implies that high diffusivity of counter ions through fiber skin is achievable even for fibers under extensional load.

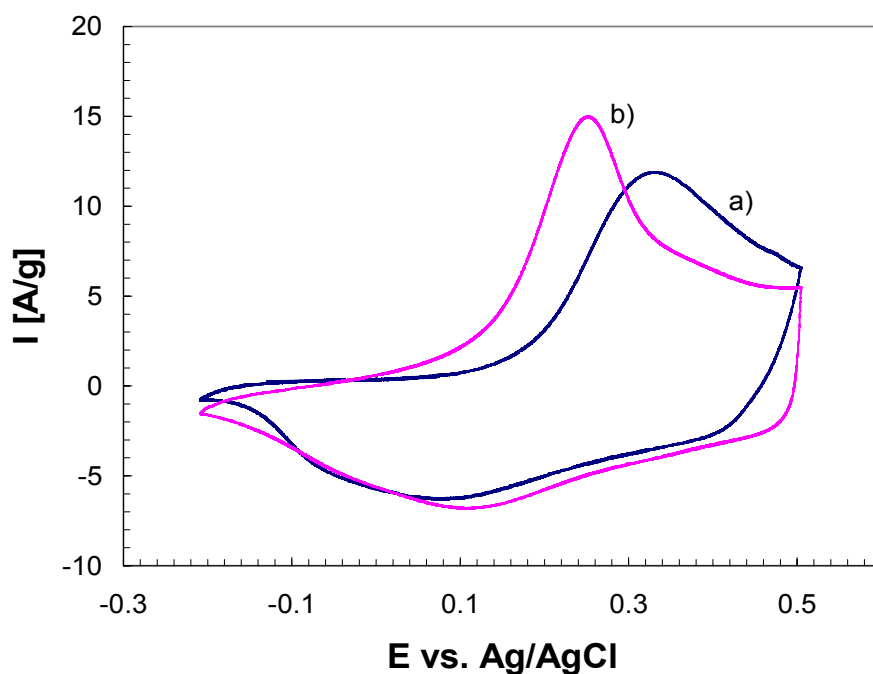


Figure 8.5. Cyclic voltammograms showing current density ( $I$ ) for potential ( $E$ ) scans between -0.2V and +0.5V (vs. Ag/AgCl) in 1M HCl at 5 mV/s: a) neat PANi-ES/AMPSA and b) PANi-ES/AMPSA-SWNT fibres.

### **8.3.2. Performance of PAni-ES/AMPSA and its composite containing SWNTs fibres as electrode material in rechargeable battery**

Cyclic voltammetry of PAni-ES/AMPSA fibre and its SWNT composite in EMI.TFSI as Ionic liquid electrolyte were shown in section 5.3.8.2. The redox reaction appeared to occur more reversibly after the addition of carbon nanotubes. It has also been noted that the redox peaks for PAni-ES/AMPSA-SWNT fibre became sharper. All these results indicate that the oxidation and reduction reactions occur more easily after carbon nanotubes incorporation, a higher charge and discharge capacity are expected.

#### **8.3.2.1. Charge/discharge characteristics**

The charge/discharge characteristics of the PAni-ES/AMPSA and its SWNT composite fibres were evaluated galvanostatically, and the charge/discharge curves are shown in Figure 8.6. The charge/discharge capacity was calculated from the amount of the PAni fibres. It can be seen that the charging potential increases and discharging potential decreases as the depth of the charge/discharge process is increased. This response is characteristic of electrode materials used in rechargeable batteries and indicates that PAni-ES/AMPSA fibres can be used as an electrode material in ionic liquid. A discharge capacity of  $11.2 \text{ mAh g}^{-1}$  and charge capacity of  $12.4 \text{ mAh g}^{-1}$  were obtained for PAni-ES/AMPSA with 0.76 % w/w SWNT. These results were 2-3 times higher than those obtained for pure PAni-ES/AMPSA. PAni-ES/AMPSA exhibited a discharge capacity of  $4.1 \text{ mAh g}^{-1}$  and charge capacity of  $4.5 \text{ mAh g}^{-1}$ . It has also been noted that the charge voltage became lower and discharge voltage became higher after SWNT were incorporated into the PAni-ES/AMPSA, which indicates that energy consumed for (IR)

was reduced and effective energy was improved. The reason for this could be that the higher conductivity reduces the internal resistance of the electrode after the carbon nanotubes were incorporated. However, the charge and discharge capacity obtained in this work is lower than that for PANi reported in electrolyte containing inorganic acid [33]. The significance of this work is that solid PANi fibre can be used as electrode material in ionic liquid EMITFSA, and it is promising electrode for wearable diagnostics system in wider electrochemical window compared to aqueous acids.

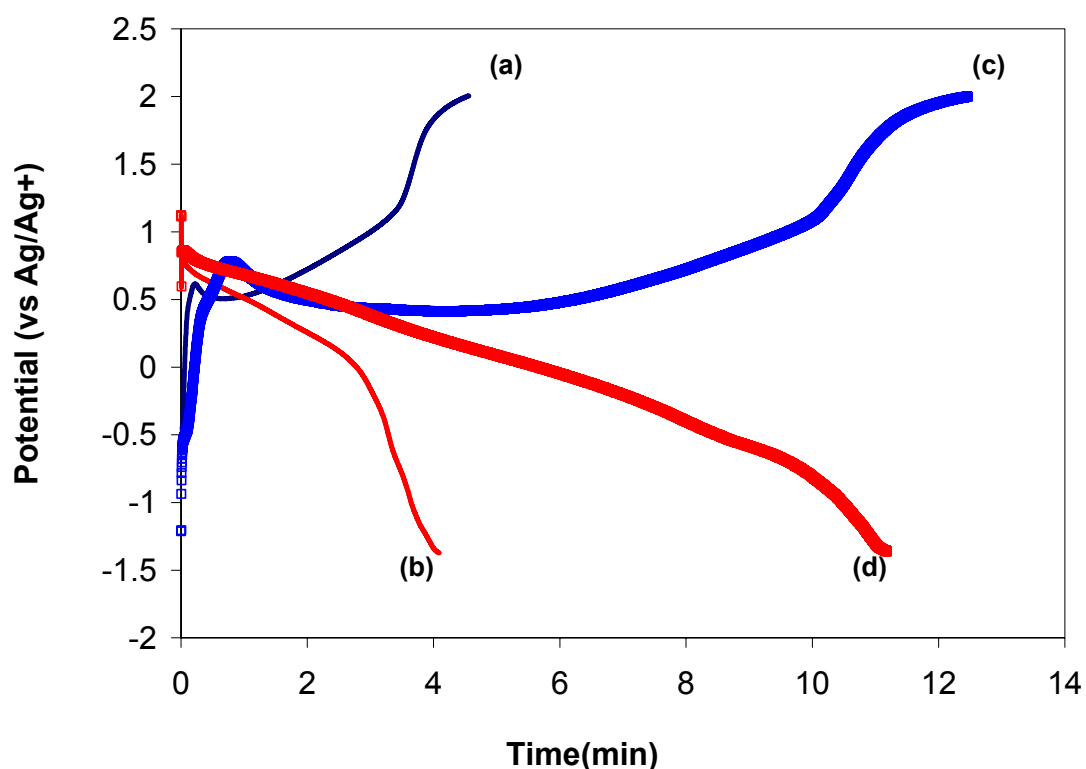


**Figure 8.6.** Charge/discharge curves of PANi –ES/AMPSA or PANi-ES/AMPSA/SWNT (0.76 % w/w) fibres (a) PANi-ES/AMPSA fibre charges (b) PANi-ES/AMPSA fibre discharges (c) PANi –AMPSA-SWNT (0.76 % w/w) charges (d) PANi –ES/AMPSA-SWNT (0.76 % w/w) discharges

### 8.3.2.2. Cycle life

Discharge capacity as a function of the cycle number is shown in Fig.5 for PAni-ES/AMPSA fibre with and without SWNT ( 0.76 % w/w) . The discharge capacities of PAni-ES/AMPSA fibre increased with the cycle number, and it attained  $9.7 \text{ mAh g}^{-1}$  after 10 cycles from the initial capacity of  $3.9 \text{ mAh g}^{-1}$ .

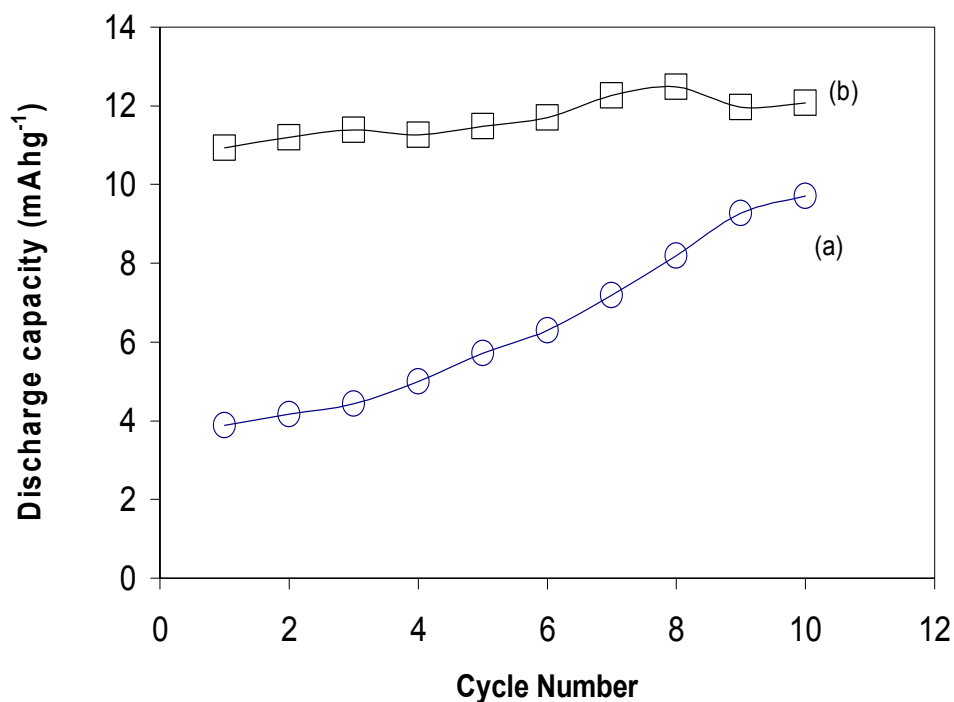


**Figure 8.7.** Cycle life of (a) PAni-ES/AMPSA (b) PAni-ES/AMPSA/SWNT fibres

These results suggest that a slow activation process occurred during the charge/discharge process. An initial discharge capacity of  $10.9 \text{ mAh g}^{-1}$  was obtained for PAni-ES/AMPSA /SWNT fibre, and it attained  $12.1 \text{ mAh g}^{-1}$  after 10 cycles. No obvious activation process was shown for PAni-ES/AMPSA/SWNT fibre. Conclusions can be made that the incorporation of SWNTs into PAni-ES/AMPSA fibre increased the electrochemical activation surface area and made it easier to activate the fibre electrodes.

### **8.3.3. Performance of PANi-ES/AMPSA fibres with and without SWNTs as humidity and temperature sensors**

#### **8.3.3.1. Sensitivity to temperature**

Figure 8.8 demonstrates the response of PANi fibre sensors (with and without SWNTs) to a change in temperature. Both fibres showed definite response to temperature. In general, both fibres show an increase in the resistance with an increase in temperature. A nonlinear response was observed with increasing temperature while a more linear response was found during a temperature decrease. A 8 % change in normalised resistance was observed in the neat PANi-ES/AMPSA compared to 7 % in the PANi-ES/AMPSA-SWNT fibre. After first cycles a 2.5 % drift in the sensor response of  $R/R_0$  was observed respectively in PANi fibre and its SWNT composite at the reference temperature.

The non linear behavior of the PANi fibres suggest a complex mechanism in charge transport that is not favored for sensor applications. The PANi fibre without SWNTs gave a more reliable response and may be further developed for use as a temperature sensor.

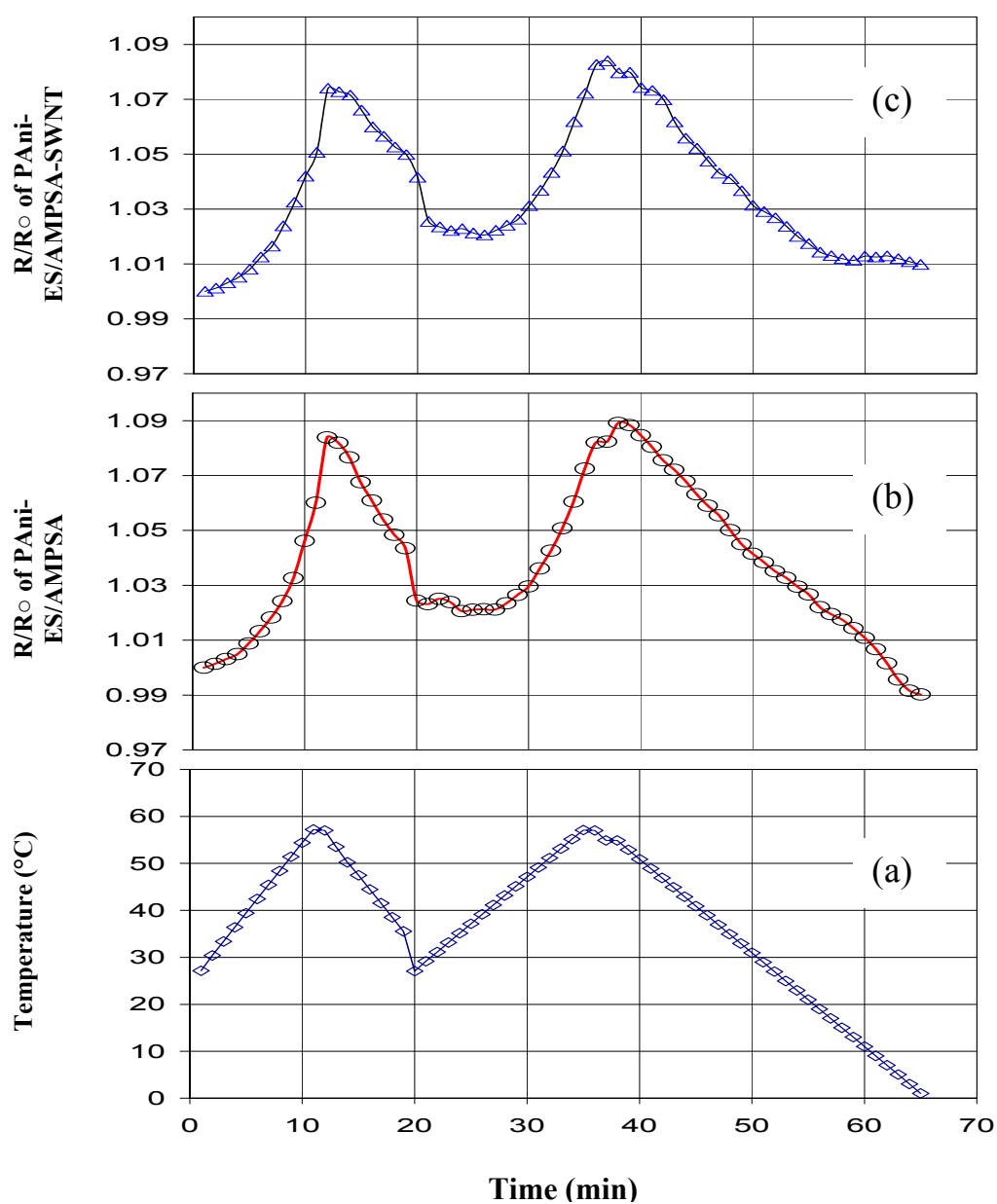


**Figure 8.8.** The sensitivity of normalised resistivity versus (a) temperature changes by scan rate ( 3 °C/min) at constant humidity.  $R/R_0$  response of (b) Neat PAni-ES/AMPSA versus temperature change (c) PAni-ES/ AMPSA-SWNT versus temperature change



### 8.3.3.2. Sensitivity to relative humidity (% R.H.)

Figure 8.9 shows the change in the normalised resistivity versus humidity at constant room temperature for the PANi fibres. A step change in relative humidity resulted in a non linear fast response in low % R.H when the neat PANi-ES/AMPSA fibre was exposed to a moist environment.

A 10 %, 22 % and 24 % decrease in  $R/R_0$  was observed after changing of % R.H. of the test chamber respectively from 3% RH to 11%, 51 % and 74 %. Thus these fibres are more accurate for determination of the water content in low RH environments. A much slower response was observed upon drying of samples.

The PANi-ES/AMPSA /SWNTs showed no predictable change in the results of  $R/R_0$  with changing humidity. There was a small drift during the drying phase, but no response in the humidifying phase. The low sensitivity to humidity for PANi-SWNT fibre is useful for applications in needs the lowest variability in conductivity for transferring of electrical signal, but clearly is not favored for sensing of humidity

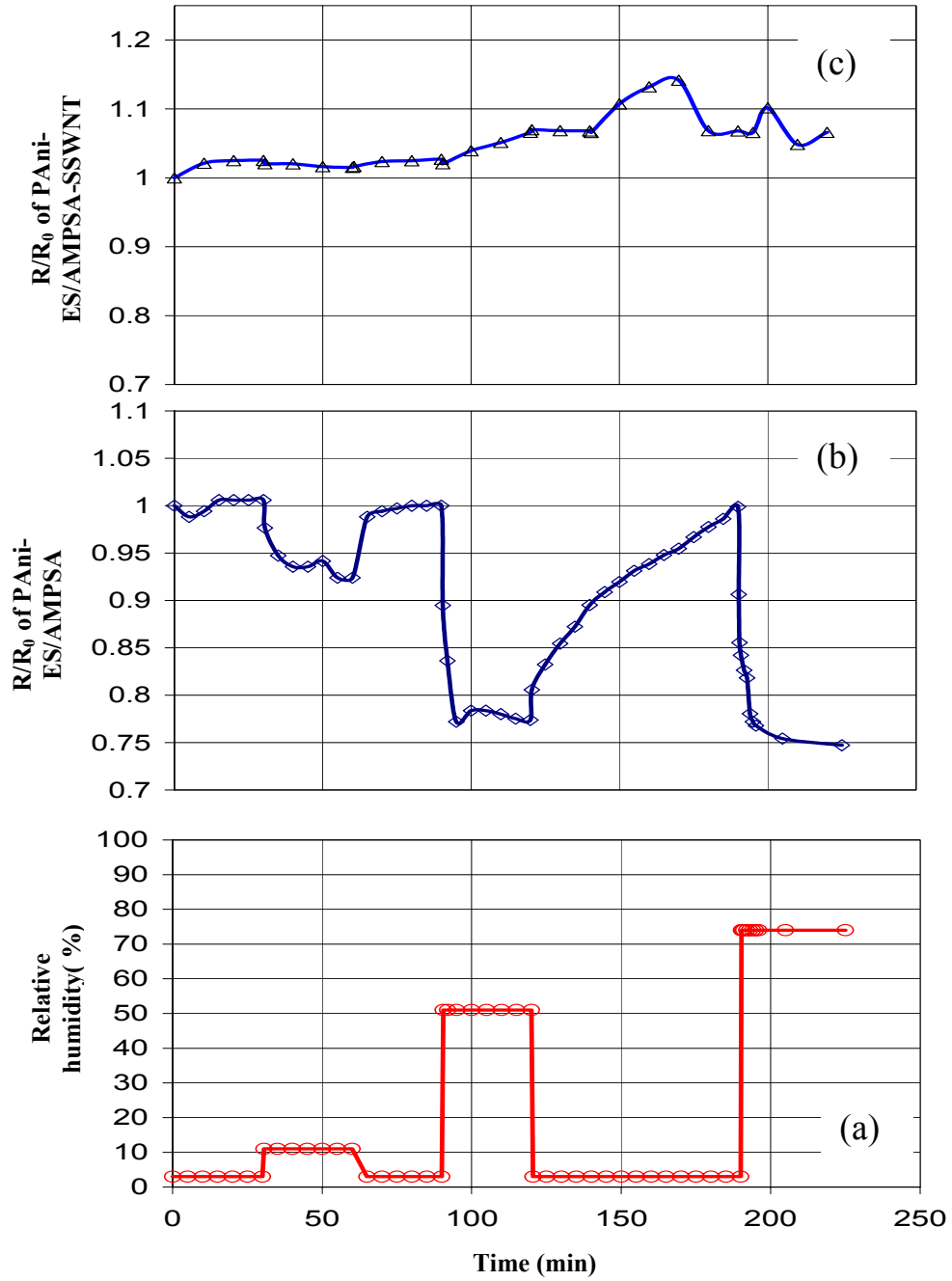


**Figure 8.9** (a) Pulse in relative humidity at constant temperature. The variation of normalised resistance( $R/R_0$ ) for (b) PANi-ES/AMPSA fibre and (c) PANi-ES/AMPSA /SWNT composite versus humidity pulse change.

#### 8.4. Conclusions

The possible application of PAni-ES/AMPSA with and without SWNTs fibres as actuators, energy storage and sensors were examined here. While the fibres showed great promise as actuators, their response as batteries and temperature/ humidity sensors was still well below conventional products. Only preliminary studies were conducted for the battery and sensor application. Further optimisation of the fibre (e.g. different dopants, different electrolyte and /or controlled porosity) may improve their performance. These further studies were beyond the scope of the current thesis.

It has been shown that the addition of small amounts of carbon nanotubes to PAni-ES/AMPSA fibres produces significant improvements in their electroactivity which translates to enhanced actuation performance. While the neat PAni-ES/AMPSA produced an actuation strain of 1.3 % at near zero loads, the presence of the SWNTs decreased this actuation to 0.85 %. The resultant actuation strain of the composite fibres was determined by a balance between the increased electroactivity leading to higher strains in the PAni matrix (up to 1.8 %) and the increased modulus, restricting matrix deformation and producing lower strains. The most significant effect of nanotube additions was, however, the much improved breaking strength and much higher operating stress levels. A 5-fold increase in work-per-cycle of compared with other conducting polymer actuators were achieved with the composite fibres. Useful actuation strains could be obtained at up to 100 MPa applied stress, which is 3 times higher than other conducting polymer actuators and 300 times higher than skeletal muscle. The improved strength and stiffness of the composite fibres can be utilised in various applications where high force

operation is required, such as in strain amplification systems or biomimetic musculoskeletal systems.

In addition, PAni-ES/AMPSA fibre with 0.76 % SWNT exhibited a higher charge/discharge capacity, lower charge voltage and higher discharge voltage compared with the neat PAni-ES/AMPSA. Results show that solid PAni fibre can be used directly as electrode in ionic liquid of EMI.TFSI, and the electrochemical properties of the fibre as an electrode material have been improved after the carbon nanotube incorporation. PAni-ES/AMPSA/SWNT fibre is a promising electrode material for wearable diagnostics system. However its current performance is still well below conventional rechargeable battery systems

PAni-ES/AMPSA fibre and its SWNT composite showed a nonlinear response with some delay to temperature signals. The addition of SWNT in PAni-ES/AMPSA fibre for temperature sensing also increased the variability in the sensor response.

The PAni-ES/AMPSA fibre incorporated with nanotubes showed much lower sensitivity to changes in humidity compared with the neat PAni-ES/AMPSA fibre. This behavior has good opportunities for application in conducting yarn that needs the lowest variability in conductivity for transferring of electrical signal but clearly is not favored for sensing of humidity. Time did not allow the development of fully packaged, stand –alone devices. If promising, their further development could be considered in future work.

## 8.5. References

- [1] J. Thilmany, Mechanical Engineering. Nov (2003) 30-32.
- [2] J. Thilmany, Mechanical Engineering. Nov (2003) 30-32.
- [3] E. W. H. Jager, E. Smela and O. Inganas, Science. 290 (2000) 1540-1545.
- [4] J. P. Collin, C. Dietrich-Buchecker, P. Gavina, M. Jimenez-Molero and J. P. Sauvage, Accounts of Chemical Research. 34 (2001) 477-487.
- [5] J. Ding, L. Liu, G. M. Spinks, D. Zhou and G. G. Wallace, Synthetic Metals. 138 (2003) 391-398.
- [6] G. M. Spinks, G. G. Wallace, L. Liu and D. Zhou, Materials Research Society Symposium Proceedings - (2002) 5-16.
- [7] M. Manto, M. Topping, M. Soede, J. Sanchez-Lacuesta, W. Harwin, J. Pons, J. Williams, S. Skaarup and L. Normie, IEEE Engineering In Medicine And Biology Magazine. 22 (2003) 120-132.
- [8] J. Madden, N. Vandesteeg, P. A. Anquetil, P. G. Madden, A. Takshi, R. Z. Pytel, S. R. Lafontaine, P. A. Wieringa and I. W. Hunter, IEEE J. of Oceanic Engineering. 29 (2004) 706-729.
- [9] Y. Bar-Cohen, SPIE - The International Society for Optical Engineering - Bellingham, Washington, USA. (2001) 3-44.
- [10] E. Smela, Adv. Mater. 15 (2003) 481-494.
- [11] T. F. Otero and J. M. Sansinena, Bioelectrochemistry & Bioenergetics. , 38 (1995) 411-414.
- [12] J.-M. Sansinena and V. Olazabal, SPIE - The International Society for Optical Engineering - Bellingham, Washington, USA. (2001) 193-221.
- [13] G. M. Spinks, G. G. Wallace, R. H. Baughman and L. Dai, SPIE - The International Society for Optical Engineering, - Bellingham, Washington, USA. (2001).
- [14] R. H. Baughman, C. Cui, A. A. Zakhidov, Z. Iqbal, J. N. Barisci, G. M. Spinks, G. G. Wallace, A. Mazzoldi, D. D. Rossi, A. G. Rinzler, O. Jaschinski, S. Roth and M. Kertesz, Science. 284 (1999) 1340-1344.

- 
- [15] G. M. Spinks, L. Liu, D. Zhou and G. G. Wallace, *Advanced Functional Materials*. 12 (2002) 437-440.
- [16] Y. Sonoda, W. Takashima and K. Kaneto, *Synth. Met.* 119 (2001) 267-268.
- [17] S. Hara, T. Zama, W. Takashima and K. Kaneto, *Polymer Journal*. 36 (2004) 151-161.
- [18] R. H. Baughman, *Synth. Met.* 78 (1996) 339-353.
- [19] P. Murray, G. M. Spinks, G. G. Wallace and R. P. Burford, *Synth. Met.* 84 (1997) 847-848.
- [20] J. D. Madden, P. G. Madden, P. A. Anquetil and I. W. Hunter, in *Materials Research Society Symposium(MRS)* - (2002) 137-144.
- [21] A. S. Hutchison, T. W. Lewis, S. E. Moulton, G. M. Spinks and G. G. Wallace, *Synthetic Metals*. 113 (2000) 121-127.
- [22] X. Gong, J. Liu, S. Baskaran, R. D. Voise and J. S. Young, *Chemistry of Materials*. 12 (2000) 1049.
- [23] L. S. Schadler, S. C. Giannaris and P. M. Ajayan, *Applied Physics Letters*. 73 (1998) 3842.
- [24] M. S. P. Shaffer and A. H. Windle, *Advanced Materials*. 11 (1999) 937-941.
- [25] D. Qian, E. C. Dickey, R. Andrews and T. Rantell, *Applied Physics Letters*. 76 (2000) 2868.
- [26] V. Mottaghitalab, G. M. Spinks and G. G. Wallace, *Synthetic Metals*. 152 (2005) 77-80.
- [27] W. Lu, I. D. Norris, B. R. Mattes and . *Australian Journal Of Chemistry*. 58 (2005) 263-269.
- [28] W. Lu, A. G. Fadeev, B. Qi, E. Smela, B. R. Mattes, J. Ding, G. M. Spinks, J. Mazurkiewicz, D. Zhou, G. G. Wallace, D. R. MacFarlane, S. A. Forsyth and M. Forsyth, *Science*. 297 (2002) 983-987.
- [29] E. M. Genies, P. Hany and C. Santier, *J. Appl. Electrochem.* 18 (1988) 751-756.
- [30] F. Goto, K. Abe, K. Okabayashi, T. Yoshida and H. Morimoto, *Journal of Power Sources*. 20 (1987) 243-248.
- [31] H. Karami, M. F. Mousavi and M. Shamsipur, *Journal of Power Sources*. 117 (2003) 255-259.

- 
- [32] Y. Ling-Sheng, S. Zhong-qiang, H. Pei-min, C. Wei-xiang and L. Li, *Journal of Power Sources*. 44 (1993) 499-503.
- [33] A. Mirmohseni and R. Solhjo, *Europ. Poly. J.* 39 (2003) 219-223.
- [34] M. Mizumoto, M. Namba, S. Nishimura, H. Miyadera, M. Koseki and Y. Kobayashi, *Synth. Met.* 28 (1989) 639-646.
- [35] T. Nakajima and T. Kawagoe, *Synth. Met.* 28 (1989) 629-638.
- [36] M. Shaolin, Y. Jinhai and W. Yuhua, *Journal of Power Sources*. 45 (1993) 153-159.
- [37] S. Taguchi and T. Tanaka, *Journal of Power Sources*. 20 (1987) 249-252.
- [38] K. S. Ryu, K. M. Kim, S. G. Kang, J. Joo and S. H. Chang, *Journal of Power Sources*. 88 (2000) 197-201.
- [39] H. H. Rehan, *Journal of Power Sources*. 113 (2003) 57-61.
- [40] Z. J. Cai, M. M. Geng and Z. Y. Tang, *J. Mater. Sci.* 39 (2004) 4001-4003.
- [41] F. Carpi and D. D. Rossi, *IEEE TRANSACTIONS ON INFORMATION TECHNOLOGY IN BIOMEDICINE*. 9 (2005) 295-316.
- [42] P. Koelle and R. Dronskowski, *European Journal of Inorganic Chemistry*. (2004) 2313-2320.
- [43] D. R. McFarlane, J. Sun, J. Golding, P. Meakin and M. Forsyth, *Electrochimica Acta*. 45 (2000) 1271-1278.
- [44] J. Sun, D. R. MacFarlane and M. Forsyth, *Solid State Ionics*. 148 (2002) 145-151.
- [45] E. P. Scilingo, F. Lorussi, A. Mazzoldi and D. D. Rossi, *IEEE Sensors J.* 3 (2003) 460-467.
- [46] D. D. Rossi, F. Lorussi, A. Mazzoldi, P. Orsini and E. P. Scilingo, *Proc. 1st Annu. Int. IEEE-EMBS Special Topic Conf. Microtechnol. Med. Biol - Lyon, France*. (2000) 587-592.
- [47] B. J. Muro, J. R. Steele, T. E. Campbell and G. G. Wallace, *Proc. Int. Workshop New Generation Wearable Syst. for e-Health: Toward Revolution of Citizens' Health, Life Style Management? - Lucca, Italy*. (2003) 87-193.
- [48] Sensatex, SmartShirt [Online]. Available: <http://www.sensatex.com>.
- [49] S. Park, C. Gopalsamy, R. Rajamanickam and S. Jayaraman, *Stud. Health Technol. Informatics*,. 62 (1999) 252-258.

- [50] S. Park and S. Jayaraman, IEEE Trans. Eng. Med. Biol. 22 **(2003)** 41-48.
- [51] D. Marculescu, Proc. IEEE. Vol. 91 **(2003)** 1995-2018.
- [52] E. Smela, W. Lu and B. R. Mattes, Synth. Met. 151 **(2005)** 25-42.
- [53] G. M. Spinks and V.-T. Truong, Sensors & Actuators A-Physical. 119 **(2005)** 455-461.
- [54] H. Matsumoto, H. Kageyama and Y. Miyazaki, Electrochemistry (Tokyo, Japan). 71 **(2003)** 1058-1060.
- [55] H. Randriamahazaka, C. Plesse, D. Teyssie and C. Chevrot, Electrochimica Acta. 50 **(2005)** 1515-1522.
- [56] M. Tahhan, V.-T. Truong, G. M. Spinks and G. G. Wallace, Smart Mater. Struct. 12 **(2003)** 626-632.
- [57] V. Mottaghitalab, B. Xi, G. M. Spinks and G. G. Wallace, Synth met. **(2005)** Submitted.
- [58] J. E. Huang, X.-H. Li, J.-C. Xu and H.-L. Li, Carbon . 41 **(2003)** 2731-2736.
- [59] G. M. Spinks, D. Zhou, L. Liu and G. G. Wallace, Smart Materials and Structures. 12 **(2003)** 468-472.
- [60] G. M. Spinks, A. J. Dominis and G. G. Wallace, Corrosion. 59 **(2003)** 22-31.
- [61] I. Hunter and S. LaFontaine, Technical Digest IEEE Solid-State Sensor Actuator Workshop. **(1992)** 178-185.



# ***CHAPTER NINE***

General Conclusion

The development, characterisation and introducing of potential applications of composite fibers consisting of polyaniline reinforced with SWNTs were the main objectives of the present study. Several strategies using ex-situ blending of components were investigated to obtain suitable approaches for processing of conducting fibers. Studies into the electrical, mechanical and electrochemical properties of the fiber were conducted to assess their usefulness in different applications.

Two approaches including “two step” (acid doping after fiber preparation) and “one step” (doping during preparation of spinning solution) have been employed to investigate the ease of formation of PANi-SWNT composite fiber. In addition the effectiveness of nanotube inclusion for improvement of mechanical, electrical and electrochemical properties was studied in each method.

In the two step method, a reduced form of polyaniline (EB reduced by phenyl hydrazine to form LEB) and in the one step process, the salt form (EB doped with AMPSA to form ES) were employed as the polymer phase during fiber spinning.

From a processing point of view, using DLS and UV-Vis-NIR, it has been shown that the DMPU and DCA as solvents, respectively, for PANi in base and salt form are able to effectively disperse the pristine SWNTs. This property has been used to prepare a highly stable spinning solution containing PANi and SWNTs. It has been also shown that the presence of small amounts of PANi and AMPSA, respectively, in DMPU and DCA delay the agglomeration of nanotube bundles.

The size distribution of SWNTs was found to depend on their concentration in both solvents. The DLS results showed that the range of the hydrodynamic diameter was

between 100-200 nm for a 0.2 % w/w SWNT/ DMPU dispersion. However, this range of hydrodynamic diameter for SWNT/ DCAA was observed for 0.09 % w/w dispersion. Beyond these concentrations, both dispersions showed a high level of nonhomogeneity and agglomerated lumps which can be observed by the naked eye. For concentrations of lower than 0.2 %w/w in SWNT/DMPU dispersion and 0.09 % w/w in SWNT/DCAA dispersion the hydrodynamic diameter was below 100 nm.

Using DLS it has been shown that the sonication time decrease the hydrodynamic diameter. Simple viscometry was used to find the lowest sonication time to obtain homogenous dispersions. Based on that, respectively a 2 hr and 30 min sonication was found as appropriate time for SWNT/DMPU and SWNT/DCAA dispersions.

The viscometry was also employed to investigate the degree of physical entanglement between nanotubes bundles and polymer chains. The rheological behavior of the PAni-ES/AMPSA/SWNT in DCAA dispersions closely resembles that reported for PAni-LEB/SWNTs dispersions in DMPU. The addition of nanotubes changes the rheological behavior of spinning solution from a Pseudo-Newtonian to non-Newtonian fluid based on power law regime. The larger deviation from Newtonian behavior was observed for the PAni-ES/AMPSA/SWNT dispersions compared with PAni-LEB/SWNT at the same concentration of nanotubes by comparing of power law indices and ratio of consistency index. These observations suggest stronger physical interaction between nanotubes and the polymer chain in PAni-ES/AMPSA-SWNT spinning solution. In addition, the measurement of viscosity versus time revealed a high level of stability in a range of 5 hr and 24 hr ,respectively, for PAni-ES/AMPSA /SWNT (0.09 % w/w)- and PAni-LEB/SWNT (0.2 % w/w) solutions.

The formation of solid fiber from these spinning solutions was carried out by coagulation in a 10 % w/w NMP/water solution for PAni-LEB/SWNT and pure acetone for PAni-ES/AMPSA/SWNT. The faster coagulation was observed for PAni-ES/AMPSA/ SWNT in acetone compared with PAni (LEB)/SWNT in NMP/water solution thus allowing a nonporous fiber to be produced at a higher take-up velocity in same coagulation length.

In addition, the as spun fiber produced from the one step process (PAni-ES/AMPSA/SWNT) showed a tendency to high thermal stretching ratio (even seven times of initial length) in lower temperature( 60-80 °C) compared with 2-3 times for PAni-LEB/SWNT in higher temperature( 100-120 °C).

The mechanical, electrical and electrochemical properties of stretched fiber of PAni-LEB/SWNT fiber (before and after doping) and PAni-ES/AMPSA/SWNT were characterised respectively by using DMA (strain rate), four probe conductivity and CV. In addition the morphological study was carried out using SEM and TEM. Raman spectroscopy and thermal analysis including (DSC and DMA) were employed to identify the chemical and/or physical interaction between Polyaniline chain and nanotube bundles.

In both the one step and two steps methods, fibres containing SWNTs have superior mechanical, electrical and electrochemical properties compared with neat polyaniline fiber. The non porous morphology and a fairly homogeneous dispersion of SWNTs throughout the PAni matrix were evidenced by SEM and TEM. In addition, the thermal study confirms the influence of nanotube on reducing of mobility of PAni chains which reflect the good physical adhesion. These effects at the nano/microscale directly influenced the macroscopic mechanical properties of PAni fiber after addition of nanotubes.

For PANi-LEB/SWNT composite, the fibre containing 2 % SWNT demonstrated a 100% increase in yield stress, 50% increase in tensile stress, 240% increase in Young's modulus and 30% decrease in elongation at break compared with the neat PANi fibre. The dramatic increase in mechanical strength and elastic modulus revealed an efficient interfacial interaction between PANi and SWNTs. In spite of the superior mechanical strength for the composite fibers containing SWNTs, the low flexibility under bending stress was a major disadvantage of the fiber produced by this method. In contrast, the ultimate tensile strength and elastic modulus of PANi-ES/AMPSA/SWNT fibres were increased by 50% and 124% upon addition of 0.76% (w/w) nanotubes. The elongation at break decreased from 11% to 4% upon addition of nanotubes however fibers remained tough enough to be knotted.

Tenacity and elastic modulus versus elongation at break of fibers produced in present study and commercial fibers have been compared in Figures 9.1 and 9.2. It can be seen that for PANi-ES/AMPSA/SWNT fiber the tenacity occurs at higher elongation compared with PANi-LEB/ SWNT. It reveals that, although the tenacity varies in the range of fibers such as Acrylic, triacetate and Nylon-6, however, the lower elongation at break may produce a challenge for application in textile fabric.

The elastic modulus of PANi-LEB/ SWNT fiber is approximately 150% more than PANi-ES/AMPSA/SWNT. In contrast the elastic modulus of PANi-ES/AMPSA/SWNT is very close to polyester, cotton or polyethylene, however commercial fibers still shows higher strain at break compared to fibers produced in this work.

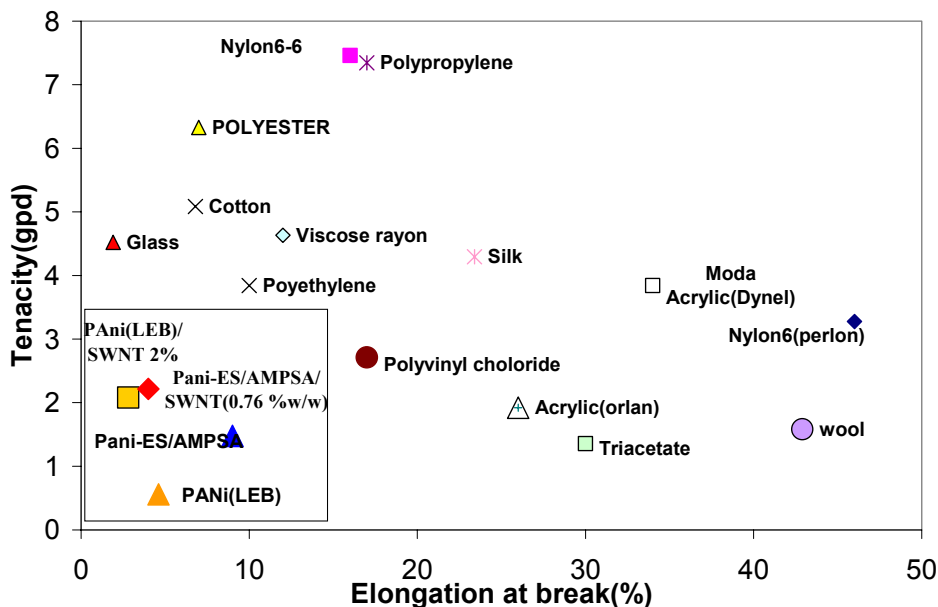


**Figure 9.1.** The comparison of tensile strength versus elongation at break of PANi –CNT fiber produced from one step and two step methods with commercial yarns

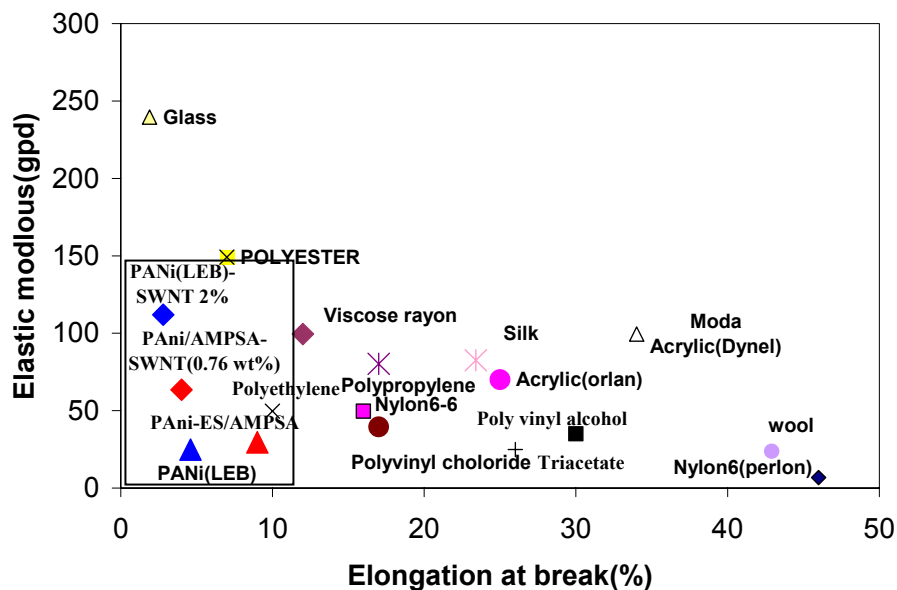


**Figure 9.2.** The comparison of elastic modulus versus elongation at break of PANi –CNT fiber produced from one step and two step methods with commercial yarns.

The fibers containing SWNTs showed higher electrical conductivity over neat polyaniline for both approaches. However, the fiber produced from salt form inherently is more conductive ( $\approx 450$  S/cm) than fiber produced from base form doped with acid dopant ( $\approx 90$  S/cm). The conductivity of PANi-ES/AMPSA/SWNT fiber at percolation level of 0.35 % w/w SWNTs increased to  $\approx 600$  Scm<sup>-1</sup>. In contrast the PANi -LEB/SWNT showed a conductivity of about 120 Scm<sup>-1</sup> at percolation level of 0.4 % w/w SWNTs.

The improvement of electrical conductivity was evidenced by the peak corresponding to the formation of (C-N<sup>+</sup>) band in the Raman spectrum and this response was enhanced by addition of carbon nanotubes. The formation of a new passage way for charge transport was indicated also by Raman spectroscopy which detected the interaction between quinoid ring of PANi and SWNTs through  $\pi$ - $\pi$  stacking. In addition, using EPR it has been shown that the presence of nanotubes in PANi matrix increases the density of free radicals.

The impact of higher conductivity was apparent in cyclic voltammetry test where the fiber was used directly as the working electrode. The cyclic voltammetry test revealed that the use of metal backing was necessary to obtain well defined redox peaks for LEB-DMPU-SWNT fibers even after acid doping. The employment of metal backing adds an additional processing step and expense for fabrication of fibers for different electronic devices. However, the results obtained from cyclic voltammetry of the PANi-ES/AMPSA/SWNT fibers without any metal backing either in aqueous solution or ionic liquid reveals a promotion in the degree of oxidation/reduction with a doping effect of SWNTs through  $\pi$ - $\pi$  stacking of SWNT fragment and PANi molecule.

In summary, although in the two step fiber spinning process, the negative impact of acid doping on mechanical properties can be compensated and the electrical properties can be

improved by addition of nanotubes, there are still major problems with fibers formed using this process. These problems include low spinning rate, low flexibility and low conductivity and insufficient charge transfer along uncoated fiber. These disadvantages can be removed by processing of PAni-SWNT in emeraldine salt form through a one step process.

The quantitative analysis of nanotube orientation and detection of load transfer from matrix to nanotubes were investigated in PAni-ES/AMPSA/SWNT composite fiber using Raman spectroscopy. It has been shown that the significant change in intensity of G band and RBM band by changing of angle between fiber axis and polarisation plane in VV and VH configuration of polariser and analyzer can be correlated to orientation of nanotubes through measurement of average angle between nanotubes and fiber axis. It has been found that thermal stretching of as spun fiber orients majority of nanotubes in a range of about  $\pm 30^\circ$  versus fiber axis. Moreover, the Herman's orientation factor increased from 0.02 to 0.43 respectively, for as spun and 5x drawn fiber.

Micro Raman spectroscopy has been used to show the load transfer from matrix to nanotubes. A significant shift between 90-130  $\text{cm}^{-1}$ /strain in D\* band has been observed. The comparison of mechanical and spectroscopic results elucidates the mechanism of load transfer from bulk polymer to interfacial area and nanotubes. It was proposed the small discrepancy between the observed value of the elastic modulus and the predicted amount by the rule of mixtures originated from imperfect adhesion between the nanotubes and the polymer and /or through non complete alignment of the nanotubes.

In addition using a PPMS instrument, the results of temperature dependent electrical conductivity experimental data has been fitted on a heterogeneous model comprising



crystalline and amorphous resistivities in series for conducting polymer and CNTs to identify the conductivity parameters. Metallic sign accompanied with a peak in the conductivity and a turn over to non metallic sign at lower temperature was observed for the temperature dependence conductivity around room temperature for highly conducting PANi and its SWNT composite fibers. The temperature corresponds to maximum conductivity is increased by addition of SWNTs suggest that the SWNTs restrict the degree of motion of polymer chains so that higher energy must be absorbed to cross the M-I transition. It was shown that the higher conductivity of PANi-ES/AMPSA/SWNT composite fiber compared to neat PANi-ES/AMPSA fiber also can be described by improvement of the metallic property in the crystalline areas and boosting of the metallic disorder contribution in amorphous area.

The benefit of applying PANi-ES/AMPSA fiber and its composite having SWNT in applications as actuator, power source and sensor was examined using some preliminary tests. While the fibers showed great promise as actuators, their response as batteries and temperature/ humidity sensors was competitive with existing materials.

Low voltage actuating materials (“artificial muscles”) are required for many applications in robotics, medical devices and machines. One of the biggest limitations to date for the application of conducting polymers, such as polyaniline, is their low breaking strength—typically less than 10 MPa during an electrochemical actuation cycle under external load.

Significant improvements in actuator strength, stress generation and work-per-cycle have been achieved through the incorporation of small amounts (up to 0.76% w/w) of carbon nanotubes as reinforcement in the polyaniline matrix. As actuators, these composites fibres continue to operate at applied stresses in excess of 100 MPa producing a maximum

work per cycle of over 300 kJ/m<sup>3</sup>. This performance is 3 times higher than previously produced conducting polymer actuators and exceeds skeletal muscle in terms of stress generation by 300 times. The improved strength and stiffness of the composite fibres can be utilised in various applications where high force operation is required, such as in strain amplification systems or biomimetic musculoskeletal systems.

New battery material was constructed consisting of either a solid PAni-ES/AMPSA fiber or a similar fibre containing SWNTs. An ionic liquid (EMI.TFSI) was used as electrolyte with wide electrochemical window in a range of  $\pm 2$  V. PAni-ES/AMPSA fiber with 0.76 % SWNT exhibited a discharge capacity of 11.2 mAh g<sup>-1</sup> and charge capacity of 12.4 mAh g<sup>-1</sup>. These values are higher than those obtained for neat PAni-ES/AMPSA fibre which exhibited a discharge capacity of 4.1 mAh g<sup>-1</sup> and charge capacity of 4.5 mAh g<sup>-1</sup>. In addition lower charge voltage and higher discharge voltage was observed for PAni-ES/AMPSA/SWNT fiber compared with the neat PAni-ES/AMPSA fiber. PAni-ES/AMPSA/SWNT fiber can be a promising electrode material for wearable diagnostics system. However, its current performance is still well below conventional rechargeable battery systems.

PAni fiber and its SWNT composite showed a nonlinear response with some delay to temperature signals. The addition of SWNT in PAni-ES/AMPSA fiber for temperature sensing also increased the variability in the sensor response.

The PAni fiber incorporated with nanotubes showed much lower sensitivity to change in humidity pulse compared with neat PAni fiber. This behavior has good opportunity for application in conducting yarn that needs the lowest variability in conductivity for transferring of electrical signal but clearly is not favored for sensing of humidity.

Only preliminary studies were conducted for the battery and sensor application. Further optimisation of the fiber (e.g. different dopants, different electrolyte and /or controlled porosity) may improve their performance. These further studies were beyond the scope of the current thesis. If promising, their further development could be considered in future work.

Table 9.1 and 9.2 compares processing characteristics and includes brief economical and safety information that needs to be considered for further development. As can be seen from economical point of view the total cost required for preparation of 1 gram of spinning solution in two step method is nearly twice that of the one step method. In this calculation, the equal cost has been considered for energy during solution preparation and fiber processing steps.

**Table 9.1.** The comparison of one step and two steps methods by considering economical and safety issues

Characteristic	PAni-ES/AMPSA/SWNT		PAni-LEB/SWNT
	One step process		Two steps process
The price of consumable material based on 20 g of solvent	solvent	2.06 AUD/20 g DCAA	7.52 AUD/20 g DMPU
	PAni	10 AUD/1g of PAni	20 AUD/2 g of PAni
	Additive	0.26 AUD/1.3 g AMPSA	0.09 AUD/0.66g phenyl hydrazine
	SWNTs	12.24 AUD/18 mg SWNT	27.2 AUD/40 mg SWNT
Total price / g of spinning solution	1.1 AUD		2.41 AUD
Total price / gram of solid fiber	10.59 AUD		26.86 AUD

The hazardous identification of materials which used for fiber spinning in both methods show disadvantages those are dangerous for human and environmental safety. (Table 9.2)

**Table 9.2.** The hazardous identification of solvents, additive and coagulants used in one step and two steps methods

	<b>PAni-ES/AMPSA/SWNT</b> <b>One step process</b>	<b>PAni -LEB/SWNT</b> <b>Two steps process</b>
<b>Solvent</b>	Causes severe burns .Very toxic for aquatic organism <b>(DCAA)</b>	May cause sensitisation by skin contact. Harmful if swallowed. Irritating to eyes <b>(DMPU)</b>
<b>Additive</b>	Causes burns <b>(AMPSA)</b>	May cause cancer. Also toxic by inhalation, in contact with skin and if swallowed. Irritating to eyes and skin <b>(Phenyl hydrazine)</b>
<b>Coagulant</b>	Highly flammable. irritating to eye .Vapor may cause drowsiness and dizziness <b>(Acetone)</b>	Irritating to eyes and skin <b>( NMP/water)</b>